GRK 1640

UNIVERSITÄT BAYREUTH

Protons, Electrons, and States: A way to simulate charge transfers in complex (protein) systems

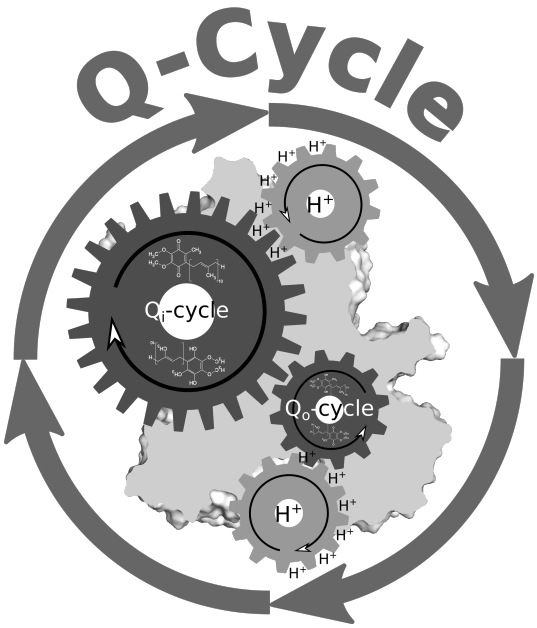

Von der Universität Bayreuth

zur Erlangung des Grades eines

DOKTORS DER NATURWISSENSCHAFTEN (Dr. rer. nat.)

im Promotionsprogramm

FOTOPHYSIK SYNTHETISCHER UND BIOLOGISCHER MULTICHROMOPHORER SYSTEME

genehmigten Abhandlung

vorgelegt von

Jan Zoller
geboren in Heidenheim an der Brenz

1. Gutachter Universitätsprofessor Dr. G. Matthias Ullmann
2. Gutachter Universitätsprofessor Dr. Andreas Möglich

Tag der Einreichung: 08.08.2023

Tag des Kolloquiums: 16.01.2024

Bayreuth, 2024

Die vorliegende Arbeit wurde in der Zeit von 01.04.2016 bis 31.03.2023 in Bayreuth am Lehrstuhl Biochemie V unter Betreuung von Herrn Professor Dr. G. Matthias Ullmann angefertigt.

Vollständiger Ausdruck der von der Bayreuther Graduiertenschule für Mathematik und Naturwissenschaften der Universität Bayreuth genehmigten Dissertation zur Erlangung des akademischen Grades eines Doktor der Naturwissenschaften (Dr. rer. nat.).

Dissertation eingereicht am: 08.08.2023

Wissenschaftliches Kolloquium: 16.01.2024

Amtierender Direktor der Graduiertenschule: Universitätsprofessor Dr. Jürgen Köhler

PRÜFUNGSAUSSCHUSS:

Universitätsprofessor Dr. G. Matthias Ullmann (1. Gutachter)
Universitätsprofessor Dr. Andreas Möglich (2. Gutachter)
Universitätsprofessor Dr. Birte Höcker (Vorsitzende)
Universitätsprofessor Dr. Stephan Gekle

Jan Zoller: *Protons, Electrons, and States: A way to simulate charge transfers in complex (protein) systems*, PhD thesis, January 25, 2024

This was a triumph!
I'm making a note here:
Huge success!
It's hard to overstate
My satisfaction.
...
We do what we must
Because we can
For the good of all of us.
Except the ones who are dead.
But there's no sense crying
Over every mistake.
You just keep on trying
'Til you run out of cake.
And the science gets done.
...
There is research to be done.
...
Still alive.
Portal: "Still Alive" written by Jonathan Coulton and performed by Ellen McLain (Part)

ZUSAMMENFASSUNG

Der bc_1-Komplex, der auch Komplex III genannt wird, ist ein Schlüsseltransmembranprotein bei der Energiegewinnung sowohl bei der Photosynthese als auch bei der Atmungskette. Durch eine spezifische Abfolge von Redoxreaktion ist dieser Komplex in der Lage, einen Protonengradienten über eine Membran hinweg zu erzeugen. Dieses perfekt ineinandergreifendes Räderwerk verschiedener Einzelreaktionen, das als Q-Zyklus bezeichnet wird, stellt in ihrer Gesamtheit einen Quinon-Quinol-Kreislauf innerhalb der Membran sowie eine Protonenpumpe (H^+-Pumpe) über die Membran hinweg dar. Die Kenntnis dieser Einzelreaktionen ist entscheidend für das Verständnis des gesamten Q-Zyklus und seiner Kinetik. Die Betrachtung der verschiedenen Einzelreaktionen erfordert einen tieferen Einblick in das Verhalten der Kofaktoren innerhalb des bc_1-Komplexes. Zu diesen Kofaktoren zählen das Rieskezentrum, die Hämgruppen b_L, b_H und c_1 sowie die Quinone bzw. Quinole an den Q_o- und Q_i-Bindestellen. Für ein besseres Verständnis dieser Kofaktoren sind pK_a-Werte und Redoxpotenziale erforderlich. Eine Methode der Wahl zur Bestimmung dieser Werte ist die Berechnung mit Hilfe der Poisson-Boltzmann-Gleichung. Hierfür sind jedoch sogenannte G_{model}-Werte für die einzelnen Kofaktoren erforderlich, die bisher nur teilweise vorlagen. Die G_{model}-Werte werden normalerweise auf Basis von Modellverbindungen bestimmt und sind ein für die Berechnung notwendiger Energieterm. Eine Modellverbindung ist dabei ein vereinfachtes Modell eines Kofaktors, um experimentelle Messungen oder theoretische Berechnungen zu vereinfachen. Durch die Etablierung verschiedener Methoden konnte das Problem der fehlenden G_{model}-Werte gelöst und die G_{model}-Werte bestimmt werden. Die entwickelten Methoden lassen sich dabei in zwei unterschiedliche Vorgehensweisen unterteilen. Sie basieren entweder auf experimentellen und theoretischen Werten oder rein auf theoretischen Berechnungen.

- *Ab initio* Berechnungen (Kapitel 3):
  Bei diesem Ansatz werden die G_{model}-Werte mit Hilfe von quantenmechanischen Berechnungen und thermodynamischen Zyklen berechnet. Für diese Methode sind im Prinzip keine experimentellen Werte erforderlich. Experimentelle Werte können jedoch zur Verbesserung der theoretischen Berechnungen beitragen.
- Virtueller Modellverbindungsansatz (Kapitel 4):
  Bei dieser Methode wird keine klassische Modellverbindung verwendet, sondern ein ganzes Makromolekül, das einen einzelnen gesuchten Kofaktor enthält. Stark vereinfacht ausgedrückt müssen experimentelle und theoretische Werte für den gesuchten Kofaktor im Makromolekül auf einer Geraden mit der Gleichung $f(x) = x$ liegen. Fehlt nun der entsprechende G_{model}-Wert für den Kofaktor, so kann nur die Gleichung $f(x) = x + b$ erfüllt werden und der b-Wert stellt somit den gesuchten G_{model}-Wert dar. Wird der gefundene G_{model}-Wert für den Kofaktor verwendet, kann die Gleichung $f(x) = x$ erfüllt werden.
- Erweitertes Mikro- und Makrozustandsmodell (Kapitel 5):
  Diese Methode verwendet pH-abhängige Redoxpotenzialtitrationskurven, um die gesuchten G_{model}-Werte mittels „Curve-Fitting“ zu bestimmen. Dabei wird ausgenutzt, dass in solchen Titrationskurven theoretisch alle möglichen Zustände enthalten sind, die z.B. eine Modellverbindung oder auch eine virtuelle Modellverbindung annehmen können, auch wenn diese nur sehr gering populiert sind. Zusätzlich wird das makromolekulare Mikrozustandsmodell um einen Supermakrozustand erweitert, um ein „Curve-Fitting“ zu ermöglichen. Die G_{model}-Werte ergeben sich schließlich aus dem „Curve-Fitting“.

Nach der Bestimmung aller erforderlichen G_{model}-Werte konnten der bc_1-Komplex und der Q-Zyklus untersucht werden. Es ist jedoch anzumerken, dass die Semiquinonzustände noch nicht optimal durch die G_{model}-Werte repräsentiert werden. Aufgrund der experimentellen Ergebnisse und der hier durchgeführten theoretischen Betrachtungen konnte geschlussfolgert werden, dass an der Q_i-Bindestelle das Glu295 an der Deprotonierung des Quinols beteiligt ist. Ebenso konnte gezeigt werden, dass an der Q_o-Bindestelle Lys251, Asp252, His217 und ein Kristallwasser an der Protonierung des Quinols beteiligt sind. Darüber hinaus zeigen die berechneten Werte eine gute Übereinstimmung mit den vorhandenen experimentellen Daten.

Im nächsten Schritt konnte die Kinetik des Q-Zyklus berechnet werden. Hierzu wurden auf Basis der genannten Kofaktoren und ausgewählter Aminosäuren elementare Reaktionsnetzwerke aufgebaut und analysiert. Eine Elementarreaktion ist dabei z.B. die Aufnahme eines H^+-Atoms durch das Glu295 oder ein Elektronentransfer von der Hämgruppe b_L zur Hämgruppe b_H. Ein solches Netzwerk kann mehr als 130.000 Knoten/Zustände besitzen und ist nicht mehr händisch zu analysieren. Aus diesem Grund wurde ein spezieller Pfadsuchalgorithmus entwickelt, der in der Lage ist, einen Hauptzyklus sowie Nebenzyklen bzw. parallele Pfade zu finden. Eine genaue Beschreibung des Algorithmus findet sich im Anhang in Kapitel B. Mit Hilfe des Algorithmus konnten schließlich Netzwerke identifiziert werden, die in der Lage sind, einen Protonengradienten zu erzeugen. Die gefundenen Netzwerke wurden schließlich als Q_o- und Q_i-Zyklen, aber noch nicht als vollständiger Q-Zyklus identifiziert. Sowohl der Q_o-Zyklus als auch der Q_i-Zyklus sind in der Lage, unter Energieaufwand einen Protonengradienten zu erzeugen. Die Elementarreaktionen, die einen geschwindigkeitsbestimmenden Schritt innerhalb der gefundenen Netzwerke darstellen, konnten ebenfalls gefunden werden. Eine dieser Reaktionen ist die Reduktion des Quinons an der Q_i-Bindestelle durch die Hämgruppe b_H.

ABSTRACT

The bc_1-complex, also called complex III, is a key transmembrane protein in energy production in both photosynthesis and the respiratory chain. By a specific sequence of redox reaction, this complex is able to generate a proton gradient across a membrane. This perfectly interlocking gear system of various individual reactions, known as the Q-cycle, forms as a whole a quinone-quinol cycle within the membrane as well as a proton pump (H^+-pump) across the membrane. Understanding these individual reactions is critical to understand the overall Q-cycle and its kinetics. Consideration of various individual reactions requires a more detailed insight into the behavior of the cofactors within the bc_1-complex. These cofactors include the Rieske center, the heme groups b_L, b_H, and c_1, and the quinones or quinols at the Q_o and Q_i binding sites. For a better understanding of these cofactors pK_a-values and redox potentials are necessary. A method of choice for determining these values is to calculate them using the Poisson-Boltzmann equation. However, that requires the so-called G_{model}-values for the individual cofactors, which were only partially available until now. The G_{model}-values are normally determined on the basis of model compounds and are a necessary energy term for the calculation. A model compound is a simplified model of a cofactor to simplify experimental measurements or theoretical calculations. With the implementation of different methods, the lack of G_{model}-values could be eliminated and the G_{model}-values could be determined. The developed methods can be divided into two different approaches. They are based either on experimental and theoretical values or purely on theoretical calculations.

- *ab initio* calculations (chapter 3):
  In this approach, the G_{model}-values are calculated using quantum mechanical calculations and thermodynamic cycles. In principle, no experimental values are necessary in this method. However, experimental values can help to improve the theoretical calculations.
- virtual model compound approach (chapter 4):
  This method does not use a classical model compound. Instead, it uses a whole macromolecule that contains a single and searched cofactor. In very simplified terms, experimental and theoretical values for the searched cofactor in the macromolecule must be on a straight line with equation $f(x) = x$. If the corresponding G_{model}-value for the cofactor is now missing, only the equation $f(x) = x + b$ can be satisfied and the b value thus represents the searched G_{model}-value. If the found G_{model}-value is used for the cofactor, the equation $f(x) = x$ can be satisfied.
- extended micro and macro state model (chapter 5):
  This method uses pH-dependent redox potential titration curves to determine the searched G_{model}-values using curve fitting. It takes advantage of the fact that such titration curves theoretically contain all possible states that, for example, a model compound or even virtual model compound can assume, even if they are very less populated. In addition, the macromolecular microstate model is extended to allow curve fitting by a super macrostate. Finally, the G_{model}-values are obtained from the curve fitting.

After determination of all required G_{model}-values, the bc_1-complex and the Q-cycle could be studied. However, it should be noted that the semiquinone states are not yet optimally represented by the G_{model}-values. Based on experimental results and the theoretical considerations carried out here, it could be concluded that at the Q_i-binding site Glu295 is involved in the deprotonation of the quinol. Also it could be shown that at the Q_o-binding site Lys251, Asp252, His217 and a crystal water play a

role in the protonation of the quinone. In addition, the calculated values showed good agreement with the available experimental data.

In the next step, it was now possible to start looking at the kinetics of the Q-cycle. For this purpose, elementary reaction networks based on the cofactors mentioned and selected amino acids were constructed and analyzed. An elementary reaction here is, for example, the uptake of an H^+ atom by the Glu295 or an electron transfer from the heme group b_L to the heme group b_H. Such a network can have more than 130,000 nodes/states and cannot be analyzed by hand. For this reason, a special path finding algorithm was developed that can find a major cycle as well as side cycles or parallel paths. A detailed description of the algorithm can be found in the appendix B. Finally, the algorithm was used to identify networks capable of generating a proton gradient. The networks found were finally identified as Q_o and Q_i-cycles and not yet full Q-cycles. The Q_o-cycle as well as the Q_i-cycle are capable of generating a proton gradient with the expenditure of energy. The elementary reactions, which are rate-determining steps within the found networks, could also be found. Among these reactions is the reduction of the quinone in the Q_i-binding site by the heme group b_H.

CONTENTS

ACRONYMS

Amino acids:

Ala (A) alanine
Arg (R) arginine
Asn (N) asparagine
Asp (D) aspartate
Cys (C) cysteine
Gln (Q) glutamine
Glu (E) glutamate
Gly (G) glycine
His (H) histidine
Ile (I) isoleucine
Leu (L) leucine
Lys (K) lysine
Met (M) methionine
Phe (F) phenylalanine
Pro (P) proline
Ser (S) serine
Thr (T) threonine
Trp (W) tryptophane
Tyr (Y) tyrosine
Val (V) valine

Ubiquinone/Ubiquinol:

u2pp double reduced, double protonated
u2dp double reduced, protonated at O1
u2pd double reduced, protonated at O4
u2dd double reduced, deprotonated
u1pp single reduced, double protonated
u1dp single reduced, single protonated at O1
u1pd single reduced, single protonated at O4
u1dd single reduced, unprotonated
u0pp oxidized, double protonated
u0dp oxidized, protonated at O1
u0pd oxidized, protonated at O4
u0dd oxidized, deprotonated

Benzoquinone/Benzoquinol:

b2pp double reduced, double protonated
b2dp double reduced, protonated at O1
b2pd double reduced, protonated at O4
b2dd double reduced, deprotonated
b1pp single reduced, double protonated
b1dp single reduced, single protonated at O1
b1pd single reduced, single protonated at O4
b1dd single reduced, unprotonated
b0pp oxidized, double protonated
b0dp oxidized, protonated at O1
b0pd oxidized, protonated at O4
b0dd oxidized, deprotonated

Rieske center:

riop oxidized, fully protonated Rieske center
rrcp reduced (Cys 1), fully protonated Rieske center
rrhp reduced (His 2), fully protonated Rieske center
rio1 oxidized, deprotonated His1 Rieske center
rrc1 reduced (Cys 1), deprotonated His1 Rieske center
rrh1 reduced (His 2), deprotonated His1 Rieske center
rio2 oxidized, deprotonated His2 Rieske center
rrc2 reduced (Cys 1), deprotonated His2 Rieske center
rrh2 reduced (His 2), deprotonated His2 Rieske center
riot oxidized, totally deprotonated Rieske center
rrct reduced (Cys 1), totally deprotonated Rieske center
rrht reduced (His 2), totally deprotonated Rieske center

Others:

NAD nicotinamide adenine dinucleotide
NADP nicotinamide adenine dinucleotide phosphate
ETC electron Transport Chain

CTC carbon Transport Chain
PCET proton-coupled electron transfer
RC reaction center
FeS iron sulfur cluster
LH light harvesting (complex)
PS photo system
MiS microstate
MaS macrostate
ZPE zero point energy
DMF dimethylformamide
CPCM/C-PCM conductor-like polarizable continuum model
SHE standard hydrogen electrode
SSE sum of squares explained
SST sum of squares total
SSR sum of squares residual
FMN flavin mononucleotide
ox oxidized
semi radical state
red reduced
PDB Protein Data Bank
MAE mean absolute error
RPM reaction path matrix
DGM differential equation matrix
SCF self-consistent field
QMMM quantum mechanics molecular mechanics
NEB nudged elastic band
MEP minimum energy path
PES potential energy surface
CHARMM chemistry harvard macromolekular mechanics
CHELPG charges from electrostatic potentials using a grid based method
mead/my_mead macrosopic electrostatics with atomic detail
gmct general monte carlo titration

1 INTRODUCTION

1.1 The bc_1complex and the Q-cycle

1.1.1 Brief history

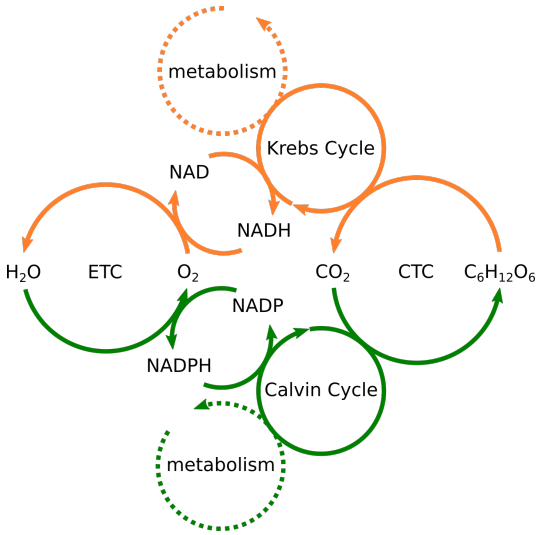

Figure 1.1: Connection between photosynthesis (green) and respiratory chain (orange). The complex III is a part of the ETC.
ETC: Electron Transport Chain; CTC: Carbon Transport Chain

The discovery and characterization of the complex III started already in the 1920s by D. Keilin *et al.* (*1*). Figure 1.1 illustrates that the Electron Transport Chain (ETC) and Carbon Transport Chain (CTC) are at the interface of anabolic and catabolic pathways. As shown in figure 1.1 complex III is part of the ETC and therefore occupies a key position in both metabolic pathways. Due to this fact, the complex III occurs in different forms in animals, yeasts and plants. Because of this very general occurrence, complex III has many names. For example, the complex is also known as cytochrome c oxidoreductase or bc_1-complex (used in this thesis). The bc_1-complex may also be relatively old in evolutionary terms. Dibrova *et al.* (*2*) suggested that the bc_1-complex may have descended from a very early oxidoreductase. The review also shows that the bc_1-complex has structural and functional similarities to the bf_6-complex. The bf_6-complex is embedded in the thylakoid membrane of plants, algae, and cyanobacteria and performs a similar function to the bc_1-complex. The bc_1-complex and the bf_6-complex appear to have a common ancestor, which is thought to be more similar to the bf_6-complex. The further divergence and spread of the bc_1-complex may be due to gene transfers and atmospheric oxygenation. For further details, the review by Dibrova *et al.* is recommended. The bc_1-complex was first extracted from bovine hearts in 1962 by Hatefi *et al.* (*3*). A structure determination of the bovine bc_1-complex with its eleven subunits did not occur for another 35 years and was reported in 1997 by Xia D *et al.* (*4*). After this first crystal structure, other bc_1-complexes could be solved. All studies of the bc_1-complex have shown that it is part of photosynthesis or the respiratory chain.

1.1.2 Structure and Function

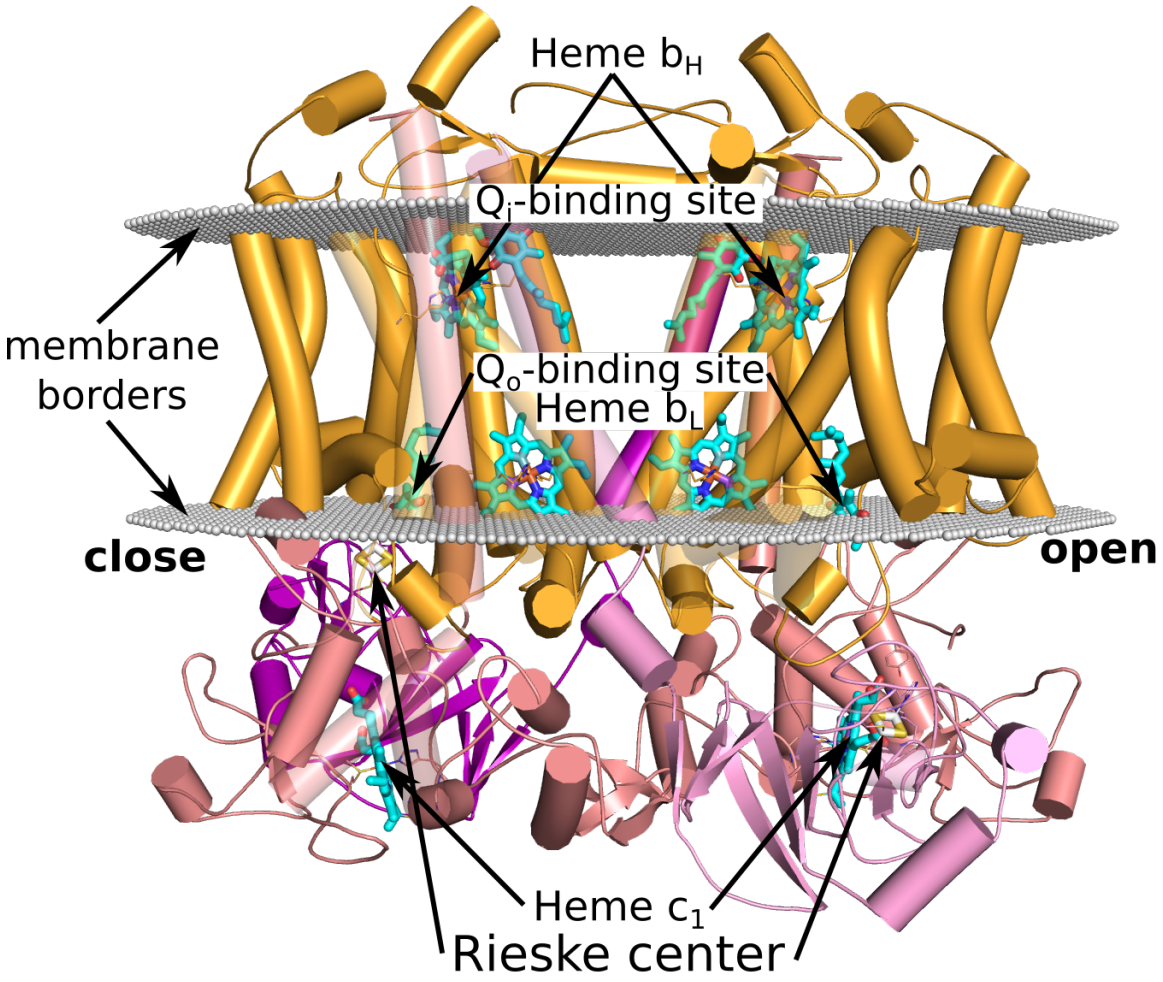

Figure 1.2: A: Cartoon representation of bc_1 complex in its open (right) and closed (left) forms. In the open form, the Rieske protein subunit is located near cytochrome c1, whereas in the closed form, the Rieske protein subunit is located near the Q_o-binding site. In orange are the cytochrome b subunits and in salmon are the cytochrome c_1 subunits. The Rieske protein subunit is colored in pink in the open position and purple in the closed position. The whole complex is embedded in a symbolic membrane (gray).

The bc_1-complex *per se* is a multifunctional oligomeric membrane protein located in the inner membrane of the mitochondria in eukaryotes or in the cytoplasmic membrane of prokaryotes. The complexes of different species differ mainly in their number of subunits and in their structure. For example, the bc_1-complex in human or bovine mitochondria has eleven subunits while in purple bacteria it has only three subunits. In eukaryotes, more subunits can be found that contribute to the stability of the complex or have another metabolic function, as in plants (*5–7*). However, all complexes contain at least three redox-active subunits in each monomer, *namely*:

- Cytochrome b (cyt_b) with the two b-hemes
- Cytochrome c (cyt_{c_1}) with one c-heme
- iron-sulfur protein with one Rieske center

In addition to the different subunits, the two binding sites Q_i and Q_o should also be mentioned. The Q_i-binding site is the inner binding site, as it is oriented to the periplasm. An important amino acid residue for this binding site is Glu295, among others. The Q_o-binding site is the outer binding site, as it is oriented to the cytoplasm. Important amino acid residues for this binding site are His217, Lys251, and Asp252, among others.

In photosynthesis and in the respiratory chain the bc_1-complex has the same function as part of the electron transport chain (ETC, figure 1.1). In both cases, a proton gradient (seen in the figure 1.3 as red and blue potential) is established using quinone/quinol (figure 1.3). In the respiratory chain, the energy to convert quinone to quinol comes from the oxidative degradation of food. In contrast, photosynthesis uses the energy of light to convert quinone to quinol. This light is collected in the light-harvesting complexes (LH2 or/and LH1-RC) and converted into energy by several further steps (figure 1.3). In both cases, the oxidation and deprotonation of quinol to quinone in the bc_1-complex is used to generate a proton gradient and later to build up energy-containing structures, e.g. by an ATP-synthase.

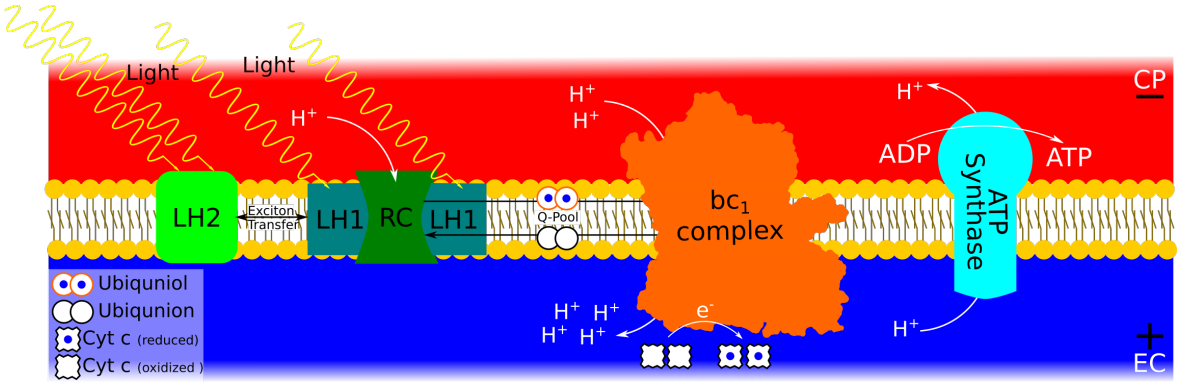

Figure 1.3: Position of the LH2, LH1-RC, bc_1-Complex (Complex III) and ATP-Synthase in the membrane and the corresponding chemical potential (red: negative potential and cytoplasm (CP); blue: positive potential and periplasm (EC)).

In this study, the bc_1-complex of the already mentioned purple bacteria *Rhodobacter sphaeroides* was chosen since it represents the smallest possible configuration of the bc1-complex with a know protein structure (*8*, *9*). This bacterium is a Gram-negative proteobacteria and was reclassified as *Cereibacter sphaeroides* in 2020. It uses anaerobic phototrophy with LH2 and LH1-RC (quinone (PSII-type)) or aerobic chemoheterotrophy as energy source. In purple bacteria, the bc_1-complex is located in the chromatophore, which also contains the light-harvesting complexes and the reaction center. The chromatophore consists of a lipid double membrane of different lipids including carotenoids. The carotenoids protect against photodamage and absorb excess light energy. A chromatophore by itself is approximately 700 Å in diameter and contains a variety of LH2, LH1-RC, bc_1-complexes and ATP synthases. A minimal combination of these proteins that would be functional has three LH2, one LH1-RC, one bc_1-complexes and one ATP synthases.

As mentioned previously, the bc_1-complex is a membrane protein. Isolated complexes often contain ubiquinols and phospholipids, which are also seen in the crystallization of the proteins. Some of the bound lipids appear to be necessary for the function and stabilization of the protein. There is a

possibility that the polar lipid heads affect heme B in their properties (*10–15*). However, a precise function of the lipid for the bc_1-complex is yet unknown.

1.1.3 The Q cycle

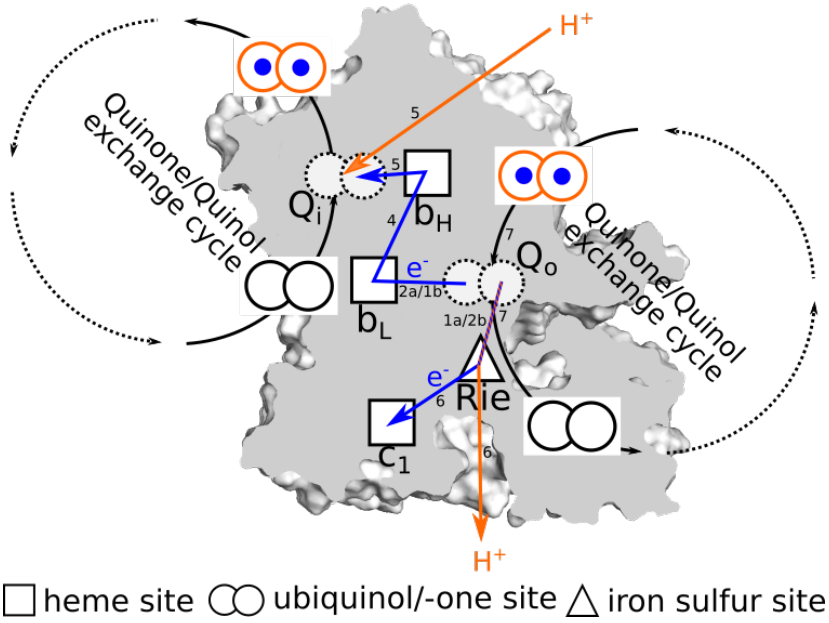

Figure 1.4: A detailed view on the Q-cycle for one monomer of the bc_1-complex. The blue circles represent the electrons and the orange frames are protonated sites. The small numbers at the arrows are the numbered steps of the Q-cycle in the text.

After a closer look at the bc_1-complex, now the Q-cycle will be discussed in more detail. The Q-cycle was first proposed by Peter D. Mitchell *et al.* in the 1960s (*16*, *17*). It has been followed by a large number of other studies in the last decades (*18–44*). The basis for many experimental studies of the function of the bc_1-complex or the Q-cycle have been various inhibitors so that the cycle can be interrupted at different points. The inhibitors can be divided into three groups. The first group binds at the Q_i position and the second group binds at the Q_o position. The third group of inhibitors binds at both the Q_i and Q_o positions (*45*, *46*). Although, the researchers have been trying to understand different aspects of Q-cycle with experimental and computational methods. The main focus was very often on the Q_o-binding site, as this is where the first steps of the Q-cycle are carried out (*18*, *21*, *25*, *30–32*, *47*). Important questions were, among others, what is the rate-determining step, in which order does the oxidation and deprotonation of the quinol take place in the binding site, how is the possible semiquinone stabilized, which amino acids play a role in the reaction. The Q_i-binding site was also studied on the basis of similar questions (*33*). All of these questions are also studied, discussed, and expanded in chapter 7.

On the basis of these investigations, a general reaction equation (1.1) can be established for the Q-cycle. The equation (1.1) clarifies that the complex does not act as a channel that moves protons from one side of the membrane to the other, but that the protonation of the quinone or deprotonation of the quinol is responsible for the shift of protons. In fact, two quinols are needed in a cycle-run to protonate and reduce a quinone, creating two quinones and a quinol, which can be shortened in the equation (1.1).

$$Q\text{-cycle: } QH_2 + 2c_1^{3+} + 2H_{CP}^{+} \xrightarrow{bc_1} Q + 2c_1^{2+} + 4H_{EC}^{+} \tag{1.1}$$

with

Q: quinone	H_{CP}^{+}: Proton from the cytoplasm
QH_2: quinol	H_{EC}^{+}: Proton from the periplasm

It has also be shown that, in addition to the task of the phospholipids, which has not yet been fully clarified, the dimeric structure of the complex is also important (*48*). Due to the dimeric structure, the Q-cycle can not only take place within a monomer as shown in figure 1.4, but also between the homodimer. This exchange between the two monomers, or more precisely between their cofactors, can also be described as a cross-reaction and complicates the investigation of the Q-cycle process.

Figure 1.4 shows a summary of the sequence of the Q-cycle of one monomer of the bc_1-complex as it can be described on the basis of the various publications. These first reaction steps (1a, 1b, 2a, 2b), especially their order, are still under discussion (*19–21*, *24*, *25*). The steps one and two are a bifurcation, whereby the two emitted electrons from the oxidation of the quinol describe different pathways.

(1a) A proton-coupled electron transfer (PCET) from the quinol at the binding site Q_o to the nearby Rieske center takes place.

(2a) The other electron from the quinol at the binding site Q_o is transferred to the heme b_L.

(3a) The proton still remaining at the quinol can be transferred to the Glu295.

(1b) An electron transfer from the quinol at the binding site Q_o to the heme b_L takes place.

(2b) The proton still remaining at the quinol can be transferred to the Glu295.

(3b) A proton-coupled electron transfer (PCET) from the quinol at the binding site Q_o to the nearby Rieske center takes place.

(4) The electron at the heme b_L is transferred to the heme b_H.

(5) Transferring the electron from b_H heme to the quinone in the Q_i binding site, this quinone can be protonated by a H^+ from the cytoplasm.

(6) The electron that has been transferred to the Rieske center is further transferred to cytochrome c_1 by means of a conformational change (*23*, *49*) and from there to cytochrome c. The proton at the Rieske center can be transferred to the periplasm.

(7) Due to the conformational change, the quinone can now also be released from the active site of the Q_o-binding site and a new quinol originating from the reaction center (LH1-RC) can be incorporated into the active site. The Glu295 is also delivered to the periplasm

(8) The reaction [(1)-(7)] takes place again and thus the semiquinone in the Q_i-binding site can be reduced to a quinol.

(9) Another reduction and protonation of a quinone to a quinol at the Q_i-binding site follows by repeating the steps one to eight.

In the description of the Q-cycle above, a bifurcation is mentioned. In a bifurcation, a pair of electrons is split or transferred to acceptors such that one electron has a more positive reduction potential than the second electron (figure 1.5). In other words, the reduction power of the first electron is transferred to the second electron. The concept of a bifurcation was first mentioned by Peter Mitchell in the context of the description of the Q-cycle (*16*, *50*). Another well-known example is flavin. A detailed description of a bifurcation can be found in the reviews by Buckel and Thauer (*51*, *52*), who were also the first to describe bifurcation (*53*, *54*).

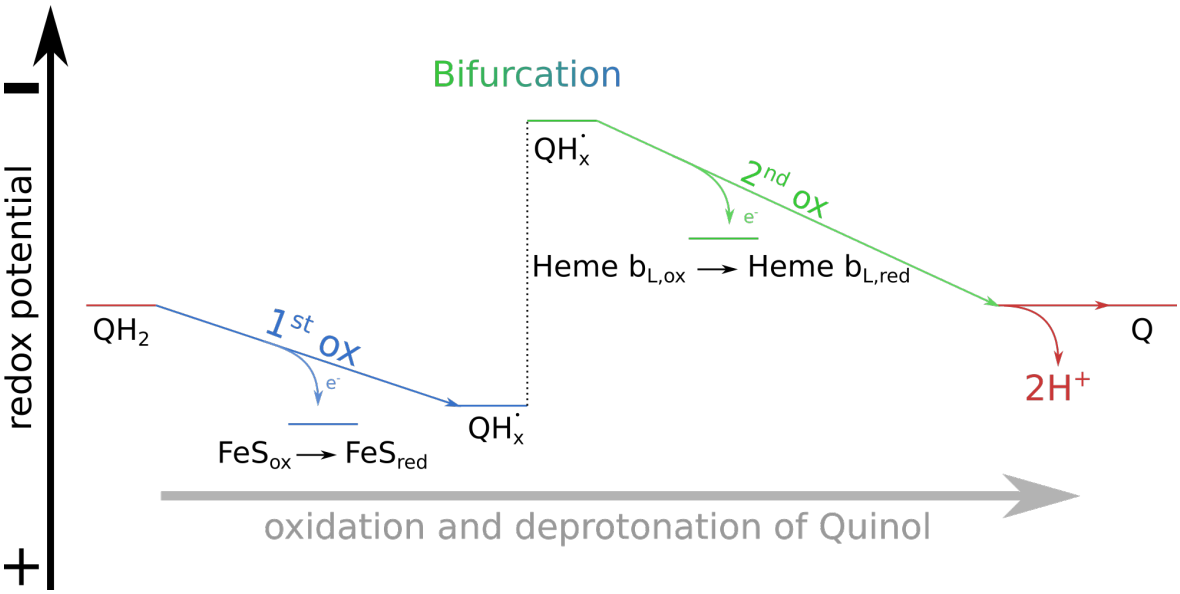

Figure 1.5: The figure shows schematically how bifurcation can occur in the bc_1-complex. In general, that is an oxidation and deprotonation of quinol to quinone (red). The steps of the bifurcation are shown in blue (first step) and green (second step). The figure was inspired by illustrations from various publication (*51*, *52*, *55*).

In this thesis, using electrostatic and kinetic investigations of the bc_1-complex, a contribution will be made to the considerations published up to now on the function of the Q-cycle. The calculations are based on the microstate and macrostate model and the resulting considerations of state energies and model energies (chapter 3). Another application of the state model in connection with the Poisson-Boltzmann equation is described in chapter 4. An extension of the state model for the determination of the model energy is introduced in chapter 5. The extension there was necessary to enable the determination of the model energy by fitting experimental values. This chapter describes another method for determining the model energy. After all the model energies for the different cofactors of the bc_1-complex have been determined via the methods described above, it is possible to determine the electrostatics of the protein complex and derive redox potentials, pK_a-values and kinetics. Similar considerations and calculations have already been described in publications (*56*, *57*) from our group and in publications (*21–23*, *25*, *37*, *47*, *58–66*) from other groups. In this thesis, these findings are extended and continued, with the main focus on determining the required theory and model energies, the application of which is at the end of the thesis.

References

(*1*) Keilin, D. (1925). On cytochrome, a respiratory pigment, common to animals, yeast, and higher plants. *P R Soc Lond B-Conta 98*, 312–339, DOI: 10.1098/rspb.1925.0039.

(*2*) Dibrova, D. V., Cherepanov, D. A., Galperin, M. Y., Skulachev, V. P., and Mulkidjanian, A. Y. (2013). Evolution of cytochrome bc complexes: From membrane-anchored dehydrogenases of ancient bacteria to triggers of apoptosis in vertebrates. *BBA-Bioenergetics 1827*, 1407–1427, DOI: 10.1016/j.bbabio.2013.07.006.

(*3*) Hatefi, Y., Haavik, A. G., and Griffiths, D. E. (1962). Studies on the electron transfer system. XLI. Reduced coenzyme Q (QH2)-cytochrome c reductase. *J Biol Chem 237*, 1681–1685.

(*4*) Xia, D., Yu, C. A., Kim, H., Xia, J. Z., Kachurin, A. M., Zhang, L., Yu, L., and Deisenhofer, J. (1997). Crystal structure of the cytochrome bc1 complex from bovine heart mitochondria. *Science (New York, N.Y.) 277*, 60–66, DOI: 10.1126/science.277.5322.60.

(*5*) Gennis, R. B., Barquera, B., Hacker, B., van Doren, S. R., Arnaud, S., Crofts, A. R., Davidson, E., Gray, K. A., and Daldal, F. (1993). The bc1 complexes of Rhodobacter sphaeroides and Rhodobacter capsulatus. *J Bioenerg Biomembr 25*, 195–209.

(*6*) Geyer, T., and Helms, V. (2006). A spatial model of the chromatophore vesicles of Rhodobacter sphaeroides and the position of the Cytochrome bc1 complex. *Biophys J 91*, 921–926, DOI: 10.1529/biophysj.105.078501.

(*7*) Iwata, S., Lee, J. W., Okada, K., Lee, J. K., Iwata, M., Rasmussen, B., Link, T. A., Ramaswamy, S., and Jap, B. K. (1998). Complete structure of the 11-subunit bovine mitochondrial cytochrome bc1 complex. *Science (New York, N.Y.) 281*, 64–71, DOI: 10.1126/science.281.5373.64.

(*8*) Hördt, A., Lopez, M. G., Meier-Kolthoff, J. P., Schleuning, M., Weinhold, L.-M., Tindall, B. J., Gronow, S., Kyrpides, N. C., Woyke, T., and Göker, M. (2020). Analysis of 1,000+ Type-Strain Genomes Substantially Improves Taxonomic Classification of Alphaproteobacteria. *Front Microbiol 11*, 468, DOI: 10.3389/fmicb.2020.00468.

(*9*) Nereng, K. S., and Kaplan, S. (1999). Genomic complexity among strains of the facultative photoheterotrophic bacterium Rhodobacter sphaeroides. *J Bacteriol 181*, 1684–1688, DOI: 10.1128/JB.181.5.1684-1688.1999.

(*10*) Yu, C. A., and Yu, L. (1980). Structural role of phospholipids in ubiquinol-cytochrome c reductase. *Biochemistry-Us 19*, 5715–5720, DOI: 10.1021/bi00566a008.

(*11*) Gomez, B., JR, and Robinson, N. C. (1999). Phospholipase digestion of bound cardiolipin reversibly inactivates bovine cytochrome bc1. *Biochemistry-Us 38*, 9031–9038, DOI: 10.1021/bi990603r.

(*12*) Lange, C., Nett, J. H., Trumpower, B. L., and Hunte, C. (2001). Specific roles of protein–phospholipid interactions in the yeast cytochrome bc1 complex structure. *Embo J 20*, 6591–6600, DOI: 10.1093/emboj/20.23.6591.

(*13*) Palsdottir, H., and Hunte, C. (2004). Lipids in membrane protein structures. *Biochim Biophys Acta 1666*, 2–18, DOI: 10.1016/j.bbamem.2004.06.012.

(*14*) Wenz, T., Hielscher, R., Hellwig, P., Schagger, H., Richers, S., and Hunte, C. (2009). Role of phospholipids in respiratory cytochrome bc(1) complex catalysis and supercomplex formation. *Biochim Biophys Acta 1787*, 609–616, DOI: 10.1016/j.bbabio.2009.02.012.

(*15*) Hunter, C. N., Tucker, J. D., and Niederman, R. A. (2005). The assembly and organisation of photosynthetic membranes in Rhodobacter sphaeroides. *Photochem Photobio S 4*, 1023–1027, DOI: 10.1039/b506099k.

(*16*) Mitchell, P. (1976). Possible molecular mechanisms of the protonmotive function of cytochrome systems. *J Theor Biol 62*, 327–367, DOI: 10.1016/0022-5193(76)90124-7.

(*17*) Mitchell, P. (1979). Keilin's respiratory chain concept and its chemiosmotic consequences. *Science (New York, N.Y.) 206*, 1148–1159, DOI: 10.1126/science.388618.

(*18*) Barragan, A. M., Crofts, A. R., Schulten, K., and Solov'yov, I. A. (2015). Identification of ubiquinol binding motifs at the Qo-site of the cytochrome bc1 complex. *J Phys Chem B 119*, 433–447, DOI: 10.1021/jp510022w.

(*19*) Crofts, A. R., Guergova-Kuras, M., Kuras, R., Ugulava, N., Li, J., and Hong, S. (2000). Proton-coupled electron transfer at the Q(o) site: what type of mechanism can account for the high activation barrier? *Biochim Biophys Acta 1459*, 456–466.

(*20*) Crofts, A. R., Shinkarev, V. P., Kolling, D. R. J., and Hong, S. (2003). The modified Q-cycle explains the apparent mismatch between the kinetics of reduction of cytochromes c1 and bH in the bc1 complex. *J Biol Chem 278*, 36191–36201, DOI: 10.1074/jbc.M305461200.

(*21*) Crofts, A. R. (2004). Proton-coupled electron transfer at the Qo-site of the bc1 complex controls the rate of ubihydroquinone oxidation. *Biochim Biophys Acta 1655*, 77–92, DOI: 10.1016/j.bbabio.2003.10.012.

(*22*) Crofts, A. R., Lhee, S., Crofts, S. B., Cheng, J., and Rose, S. (2006). Proton pumping in the bc1 complex: a new gating mechanism that prevents short circuits. *Biochim Biophys Acta 1757*, 1019–1034, DOI: 10.1016/j.bbabio.2006.02.009.

(*23*) Crofts, A. R., Guergova-Kuras, M., Huang, L., Kuras, R., Zhang, Z., and Berry, E. A. (1999). Mechanism of Ubiquinol Oxidation by the bc1 Complex: Role of the Iron Sulfur Protein and Its Mobility. *Biochemistry-Us 38*, 15791–15806, DOI: 10.1021/bi990961u.

(*24*) Crofts, A. R., Holland, J. T., Victoria, D., Kolling, Dikanov, S. A., Gilbreth, R., Lhee, S., Kuras, R., and Kuras, M. G. (2008). The Q-cycle reviewed: How well does a monomeric mechanism of the bc(1) complex account for the function of a dimeric complex? *Biochim Biophys Acta 1777*, 1001–1019, DOI: 10.1016/j.bbabio.2008.04.037.

(*25*) Crofts, A. R., Hong, S., Wilson, C., Burton, R., Victoria, D., Harrison, C., and Schulten, K. (2013). The mechanism of ubihydroquinone oxidation at the Qo-site of the cytochrome bc1 complex. *Respiratory Complex III And Related Bc Complexes 1827*, 1362–1377, DOI: 10.1016/j.bbabio.2013.01.009.

(*26*) Crofts, A. R., Rose, S. W., Burton, R. L., Desai, A. V., Kenis, P. J. A., and Dikanov, S. A. (2017). The Q-Cycle Mechanism of the bc1 Complex: A Biologist's Perspective on Atomistic Studies. *J Phys Chem B 121*, 3701–3717, DOI: 10.1021/acs.jpcb.6b10524.

(*27*) Kaszuba, K., Postila, P. A., Cramariuc, O., Sarewicz, M., Osyczka, A., Vattulainen, I., and Róg, T. (2013). Parameterization of the prosthetic redox centers of the bacterial cytochrome bc 1 complex for atomistic molecular dynamics simulations. *Theor Chem Acc 132*, 1370, DOI: 10.1007/s00214-013-1370-8.

(*28*) Osyczka, A., Moser, C. C., Daldal, F., and Dutton, P. L. (2004). Reversible redox energy coupling in electron transfer chains. *Nature 427*, 607–612, DOI: 10.1038/NATURE02242.

(*29*) Osyczka, A., Moser, C. C., and Dutton, P. L. (2005). Fixing the Q cycle. *Trends Biochem Sci 30*, 176–182, DOI: 10.1016/j.tibs.2005.02.001.

(*30*) Osyczka, A., Zhang, H., Mathé, C., Rich, P. R., Moser, C. C., and Dutton, P. L. (2006). Role of the PEWY glutamate in hydroquinone-quinone oxidation-reduction catalysis in the Qo Site of cytochrome bc1. *Biochemistry-Us 45*, 10492–10503, DOI: 10.1021/bi060013a.

(*31*) Pietras, R., Sarewicz, M., and Osyczka, A. (2016). Distinct properties of semiquinone species detected at the ubiquinol oxidation Qo site of cytochrome bc1 and their mechanistic implications. *J R Soc Interface 13*, 20160133.

(*32*) Postila, P. A., Kaszuba, K., Sarewicz, M., Osyczka, A., Vattulainen, I., and Rog, T. (2013). Key role of water in proton transfer at the Qo-site of the cytochrome bc1 complex predicted by atomistic molecular dynamics simulations. *Biochim Biophys Acta 1827*, 761–768, DOI: 10.1016/j.bbabio.2013.02.005.

(*33*) Postila, P. A., Kaszuba, K., Kuleta, P., Vattulainen, I., Sarewicz, M., Osyczka, A., and Róg, T. (2016). Atomistic determinants of co-enzyme Q reduction at the Qi-site of the cytochrome bc1 complex. *Sci Rep-Uk 6*, 33607.

(*34*) Sarewicz, M., Dutka, M., Froncisz, W., and Osyczka, A. (2009). Magnetic interactions sense changes in distance between heme b(L) and the iron-sulfur cluster in cytochrome bc(1). *Biochemistry-Us 48*, 5708–5720, DOI: 10.1021/bi900511b.

(*35*) Sarewicz, M., Dutka, M., Pintscher, S., and Osyczka, A. (2013). Triplet state of the semiquinone-Rieske cluster as an intermediate of electronic bifurcation catalyzed by cytochrome bc1. *Biochemistry-Us 52*, 6388–6395, DOI: 10.1021/bi400624m.

(*36*) Sarewicz, M., and Osyczka, A. (2015). Electronic connection between the quinone and cytochrome C redox pools and its role in regulation of mitochondrial electron transport and redox signaling. *Physiol Rev 95*, 219–243, DOI: 10.1152/physrev.00006.2014.

(*37*) Hunte, C., Palsdottir, H., and Trumpower, B. L. (2003). Protonmotive pathways and mechanisms in the cytochrome bc1 complex. *Febs Letters 545*, 39–46.

(*38*) Bergdoll, L., ten Brink, F., Nitschke, W., Picot, D., and Baymann, F. (2016). From low- to high-potential bioenergetic chains: Thermodynamic constraints of Q-cycle function. *Biochim Biophys Acta 1857*, 1569–1579, DOI: 10.1016/j.bbabio.2016.06.006.

(*39*) Cramer, W. A., Hasan, S. S., and Yamashita, E. (2011). The Q cycle of cytochrome bc complexes: a structure perspective. *Biochim Biophys Acta 1807*, 788–802, DOI: 10.1016/j.bbabio.2011.02.006.

(*40*) Weinberg, D. R., Gagliardi, C. J., Hull, J. F., Murphy, C. F., Kent, C. A., Westlake, B. C., Paul, A., Ess, D. H., McCafferty, D. G., and Meyer, T. J. (2012). Proton-coupled electron transfer. *Chem Rev 112*, 4016–4093, DOI: 10.1021/cr200177j.

(*41*) Cape, J. L., Bowman, M. K., and Kramer, D. M. (2006). Understanding the cytochrome bc complexes by what they don't do. The Q-cycle at 30. *Trends Plant Sci 11*, 46–55, DOI: 10.1016/j.tplants.2005.11.007.

(*42*) Trumpower, B. L. (1990). The protonmotive Q cycle. Energy transduction by coupling of proton translocation to electron transfer by the cytochrome bc1 complex. *J Biol Chem 265*, 11409–11412.

(*43*) Crofts, A. R. (2021). The modified Q-cycle: A look back at its development and forward to a functional model. *Biochim Biophys Acta. Bioenergetics 1862*, 148417, DOI: 10.1016/j.bbabio.2021.148417.

(*44*) Geiss, A. F., Khandelwal, R., Baurecht, D., Bliem, C., Reiner-Rozman, C., Boersch, M., Ullmann, G. M., Loew, L. M., and Naumann, R. L. C. (2017). pH and Potential Transients of the bc1 Complex Co-Reconstituted in Proteo-Lipobeads with the Reaction Center from Rb. sphaeroides. *J Phys Chem B 121*, 143–152, DOI: 10.1021/acs.jpcb.6b11116.

(*45*) Esser, L., Elberry, M., Zhou, F., Yu, C.-A., Yu, L., and Di Xia (2008). Inhibitor-complexed structures of the cytochrome bc1 from the photosynthetic bacterium Rhodobacter sphaeroides. *J Biol Chem 283*, 2846–2857, DOI: 10.1074/jbc.M708608200.

(*46*) Kokhan, O., Shinkarev, V. P., and Wraight, C. A. (2010). Binding of imidazole to the heme of cytochrome c1 and inhibition of the bc1 complex from Rhodobacter sphaeroides: II. Kinetics and mechanism of binding. *J Biol Chem 285*, 22522–22531.

(*47*) Ding, H., Robertson, D. E., Daldal, F., and Dutton, P. L. (1992). Cytochrome bc1 complex [2Fe-2S] cluster and its interaction with ubiquinone and ubihydroquinone at the Qo site: A double-occupancy Qo site model. *Biochemistry-Us 31*, 3144–3158, DOI: 10.1021/bi00127a015.

(*48*) Covian, R., and Trumpower, B. L. (2008). Regulatory interactions in the dimeric cytochrome bc1 complex: The advantages of being a twin. *BBA-Bioenergetics 1777*, 1079–1091, DOI: 10.1016/j.bbabio.2008.04.022.

(*49*) Darrouzet, E., Moser, C. C., Dutton, P., and Daldal, F. (2001). Large scale domain movement in cytochrome bc1: a new device for electron transfer in proteins. *Trends Biochem Sci 26*, 445–451, DOI: 10.1016/s0968-0004(01)01897-7.

(*50*) Peters, J. W., Beratan, D. N., Bothner, B., Dyer, R. B., Harwood, C. S., Heiden, Z. M., Hille, R., Jones, A. K., King, P. W., Lu, Y., Lubner, C. E., Minteer, S. D., Mulder, D. W., Raugei, S., Schut, G. J., Seefeldt, L. C., Tokmina-Lukaszewska, M., Zadvornyy, O. A., Zhang, P., and Adams, M. W. (2018). A new era for electron bifurcation. *Curr Opin Chem Biol 47*, 32–38, DOI: 10.1016/j.cbpa.2018.07.026.

(*51*) Buckel, W., and Thauer, R. K. (2018). Flavin-Based Electron Bifurcation, A New Mechanism of Biological Energy Coupling. *Chem Rev 118*, 3862–3886, DOI: 10.1021/acs.chemrev.7b00707.

(*52*) Buckel, W., and Thauer, R. K. (2018). Flavin-Based Electron Bifurcation, Ferredoxin, Flavodoxin, and Anaerobic Respiration With Protons (Ech) or NAD (Rnf) as Electron Acceptors: A Historical Review. *Front Microbiol 9*, DOI: 10.3389/fmicb.2018.00401.

(*53*) Herrmann, G., Jayamani, E., Mai, G., and Buckel, W. (2008). Energy Conservation via Electron-Transferring Flavoprotein in Anaerobic Bacteria. *J Bacteriol 190*, 784–791, DOI: 10.1128/jb.01422-07.

(*54*) Li, F., Hinderberger, J., Seedorf, H., Zhang, J., Buckel, W., and Thauer, R. K. (2008). Coupled Ferredoxin and Crotonyl Coenzyme A (CoA) Reduction with NADH Catalyzed by the Butyryl-CoA Dehydrogenase/Etf Complex from Clostridium kluyver. *J Bacteriol 190*, 843–850, DOI: 10.1128/jb.01417-07.

(*55*) Baymann, F., Schoepp-Cothenet, B., Duval, S., Guiral, M., Brugna, M., Baffert, C., Russell, M. J., and Nitschke, W. (2018). On the Natural History of Flavin-Based Electron Bifurcation. *Front Microbiol 9*, DOI: 10.3389/fmicb.2018.01357.

(*56*) Klingen, A. R., Palsdottir, H., Hunte, C., and Ullmann, G. M. (2007). Redox-linked protonation state changes in cytochrome bc1 identified by Poisson-Boltzmann electrostatics calculations. *Biochim Biophys Acta 1767*, 204–221, DOI: 10.1016/j.bbabio.2007.01.016.

(*57*) Koepke, J., Krammer, E.-M., Klingen, A. R., Sebban, P., Ullmann, G. M., and Fritzsch, G. (2007). pH Modulates the Quinone Position in the Photosynthetic Reaction Center from Rhodobacter sphaeroides in the Neutral and Charge Separated States. *J Mol Biol 371*, 396–409, DOI: 10.1016/j.jmb.2007.04.082.

(*58*) Cartron, M. L., Olsen, J. D., Sener, M., Jackson, P. J., Brindley, A. A., Qian, P., Dickman, M. J., Leggett, G. J., Schulten, K., and Neil Hunter, C. (2014). Integration of energy and electron transfer processes in the photosynthetic membrane of Rhodobacter sphaeroides. *BBA-Bioenergetics 1837*, 1769–1780, DOI: 10.1016/j.bbabio.2014.02.003.

(*59*) Crofts, A. R., Hong, S., Ugulava, N., Barquera, B., Gennis, R., Guergova-Kuras, M., and Berry, E. A. (1999). Pathways for proton release during ubihydroquinone oxidation by the bc1 complex. *P Natl Acad Sci Usa 96*, 10021–10026.

(*60*) Crofts, A. R., Barquera, B., Gennis, R. B., Kuras, R., Guergova-Kuras, M., and Berry, E. A. (1999). Mechanism of ubiquinol oxidation by the bc(1) complex: different domains of the quinol binding pocket and their role in the mechanism and binding of inhibitors. *Biochemistry-Us 38*, 15807–15826.

(*61*) Di Xia, Esser, L., Tang, W.-K., Zhang, M., Yu, L., and Yu, C.-A. (2012). Redox Coupled Conformational Changes in Cytochrome BC1 Complex: Implication to the Bifurcated Electron Transfer at the Quinol Oxidation Site. *Biophys J 102*, 3a, DOI: 10.1016/j.bpj.2011.11.030.

(*62*) Di Xia, Esser, L., Tang, W.-K., Zhou, F., Zhou, Y., Yu, L., and Yu, C.-A. (2013). Structural analysis of cytochrome bc1 complexes: implications to the mechanism of function. *Biochim Biophys Acta 1827*, 1278–1294, DOI: 10.1016/j.bbabio.2012.11.008.

(*63*) Martin, D. R., LeBard, D. N., and Matyushov, D. V. (2013). Coulomb Soup of Bioenergetics: Electron Transfer in a Bacterial bc1 Complex. *J Phys Chem Lett 4*, 3602–3606.

(*64*) Shimizu, M., Katsuda, N., Katsurada, T., Mitani, M., and Yoshioka, Y. (2008). Mechanism on two-electron oxidation of ubiquinol at the Qp site in cytochrome bc1 complex: B3LYP study with broken symmetry. *J Phys Chem B 112*, 15116–15126, DOI: 10.1021/jp804387g.

(*65*) Zu, Y., Fee, J. A., and Hirst, J. (2001). Complete Thermodynamic Characterization of Reduction and Protonation of the bc1 -type Rieske [2Fe-2S] Center of Thermus thermophilus. *J Am Chem Soc 123*, 9906–9907.

(*66*) Bazil, J. N., Vinnakota, K. C., Wu, F., and Beard, D. A. (2013). Analysis of the Kinetics and Bistability of Ubiquinol:Cytochrome c Oxidoreductase. *Biophys J 105*, 343–355, DOI: 10.1016/j.bpj.2013.05.033.

2

MACRO MOLECULAR MICROSTATE MODEL

2.1 Conceptual background

According to the publications of Ullmann *et al.* (*1–4*), the conceptual idea of this model is to describe a molecule as a rigid quasi-macroscopic object with a defined dielectric permittivity and linked point charges. Based on the point charges, an electric field can be calculated. In this model consideration, the electrostatic continuum is divided into two "zones". One zone includes the molecule and another zone represents the solvent for this molecule. These two zones differ in their relative permittivities. The relative permittivity within the structure is lower than in the solvent. The permittivity, or dielectric conductivity, describes the polarizability of a material and how well an electric field can propagate in this material. The relative permittivity, on the other hand, describes the ability to weaken an electric field. The distribution of relative permittivities shown here indicates that the molecule weakens the electric field less than the solvent. The continuum electrostatic is determined using the Poisson-Boltzmann equation (2.1). The Poisson-Boltzmann equation describes the electrostatic interaction between molecules and liquids in which ions are dissolved.

$$\nabla[\epsilon(r)\nabla\phi(r)] = -4\pi\left(\rho_P(r) + \sum_{i=1}^{K} c_i^{bulk} Z_i e_o e^{-\frac{Z_i e_o \phi(r)}{RT}}\right) \tag{2.1}$$

with

- $\phi(r)$: electrostatic potential
- $\epsilon(r)$: relative permittivity (position dependent "dielectric constant")
- $\rho_P(r)$: charge density due to the protein
- c_i^{bulk}: ion concentration in the bulk solution
- Z_i: charge number
- e_o: elementary charge
- r: position
- R: ideal gas constant
- T: temperature
- K: number of ionic species

Equation (2.1) can be linearized to equation (2.2). A program is used to solve this linearized Poisson-Boltzmann equation (2.2) and to calculate the potential of a protein. The surrounding solvent is not explicitly but implicitly defined by a solvation permittivity ($\varepsilon(r)$).

$$\nabla[\varepsilon(r)\nabla\phi(r)] = -\rho_f(r) + \varepsilon(r)\bar{\kappa}^2(r)\phi(r) \tag{2.2}$$

- $\varepsilon(r)$: solvation permittivity
- $\phi(r)$: electrostatic potential
- $\rho_f(r)$: fixed charge distribution
- $\bar{\kappa}^2(r)$: modified inverse Debye-Hückel parameter
- r: position

Based on the continuum electrostatics, not only the electrostatics of macromolecules can be determined, e.g. to consider the interaction between different macromolecules. It is also possible to calculate pK_a-values or redox potentials for the individual components of a macromolecule.

2.2 Continuum electrostatics - pK_a-values and redox potentials

The previously mentioned components of a macromolecular system will now be defined in more detail. In principle, such a component can be called site or group. The component usually comprises two different parts. One part is called titratable, while the other part can be called non-charge-changeable. This distinction has to be made because during the calculations shown below, the point charges of the non-charge-changeable part is invariant and the titratable part can occur in several charge states or in other words they are able to accept or donate protons or/and electrons. The components that do not have a titratable part and do not change their charge state are called non-titratable. So, there are titratable (with non-charge-changeable part) and non-titratable site or groups. On the basis of N components ($\mathfrak{c}'s$) a system state in a specific conformation (s_c) can be built, which is described by the vector

$$\vec{s_c} = \left(\ldots, \mathfrak{c}_k^{(a)}, \ldots, \mathfrak{c}_l^{(b)}, \ldots \right), 0 < k < l < N \text{ with } k, l \in \mathbb{N} \tag{2.3}$$

A component ($\mathfrak{c}_k$ or $\mathfrak{c}_l$) can assume different states (a, b) on the basis of the titratable parts. That is possible because titratable parts have binding sites ($bisi$) for e.g. protons or electrons. The states can be called macrostate (MaS) or microstate (MiS). A MaS can contain several MiS, more details about this context are described in chapter 3. As an example to illustrate of the theory the known amino acid residues lysine and histidine are chosen as sites (figure 2.1 right side). Lysine residues have a $bisi$ for one proton. This bisi can be protonated or deprotonated and lysine residues therefore occur in two states or MiS. Because each MaS is a set of MiS, they coincide in this case and each MiS is at the same time a MaS. So lysine residues are a special case, because each MiS is a MaS at the same time (MiS = MaS).

Histidine residues on the other hand have one more $bisi$ for protons than lysine residues. It results in four MiS. The possibility of distributing the MiS to different MaS will be now discussed. The system histidine can assume three MaS in relation to the number of bound protons. So the four MiS must be distributed to three MaS. This results in two MaS containing only one MiS, which is the deprotonated and the doubly protonated state. The singly protonated MaS contains two MiS, because there are two positions (nitrogens) for the single proton (figure 2.1 right side).
Using these two systems, lysine and histidine residues, the interactions of two sites can also be explained.

Table 2.1: Possible nature of bisi interactions depending on the respective charge states of lysine and histidine residues.

		histidine residue		
	charge	-1	0	1
lysine residue	1	attractive	-	repulsive
	0	-	-	-

Table 2.1 shows the possible bisi interactions depending on the respective charge states of lysine and histidine residues. Two positive or negative charges show an interaction of repulsive nature. One positive and one negative charge show an interaction with attractive nature.

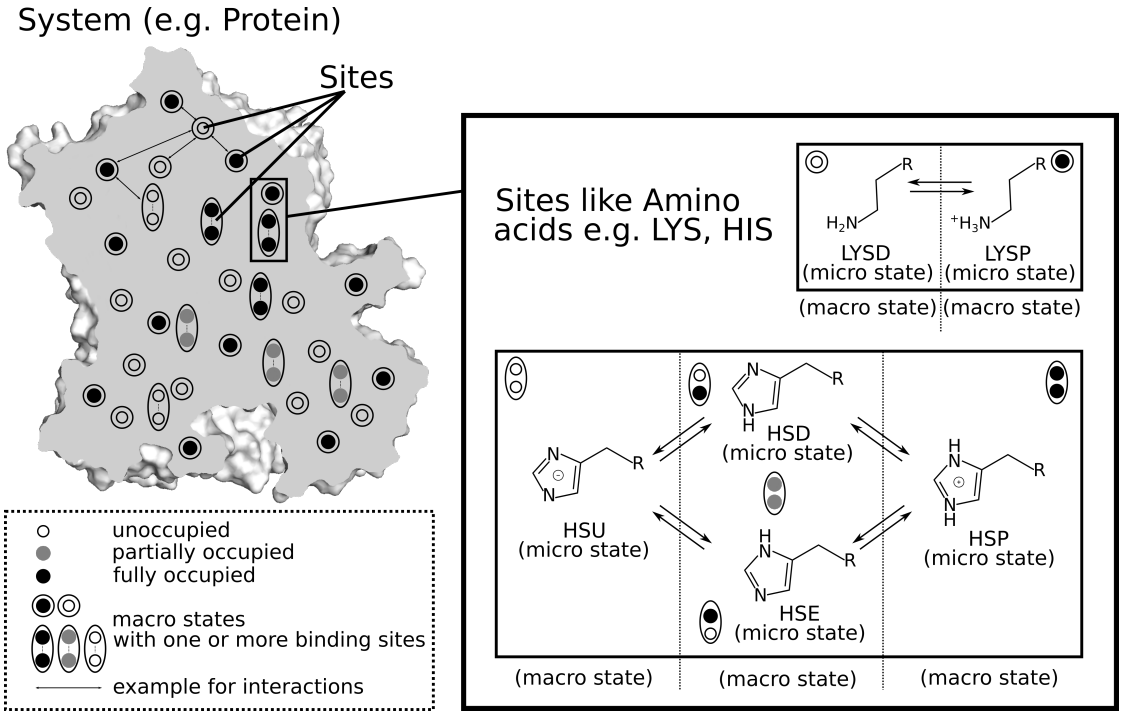

Figure 2.1: Macro and microstate model: The figure describes the individual levels of the micro and macrostate model. It is a system (e.g. protein) that contains different macrostates (sites). The single macrostates are shown in different states in the left figure. The right figure shows a detailed view of the different states of two sites, which are exemplified here by histidine and lysine residues.

In the later calculation of various energies to get pK_a-values or redox potentials, the classification into titratable (with non-charge-changeable part) and non-titratable sites or groups play an important role. At the end the equation (2.4) is to be calculated.

$$E\left(\vec{s_c}\right) = \sum_{k=1}^{N} \underbrace{\left[G_{model}\left(\mathfrak{c}_k^{(a)}\right) + G_{solv,c}\left(\mathfrak{c}_k^{(a)}\right) + G_{back,c}\left(\mathfrak{c}_k^{(a)}\right)\right]}_{E_{inter,c}} + \frac{1}{2}\sum_{k=1}^{N}\sum_{l=1}^{N} W_c\left(\mathfrak{c}_k^{(a)}, \mathfrak{c}_l^{(b)}\right) + \Delta G_{conf,c} \tag{2.4}$$

with

- $\mathfrak{c}_k^{(a)}, \mathfrak{c}_l^{(b)} \in \vec{s_c}$
- N: number of elements in $\vec{s_c}$
- c: configuration
- G_{model}: free energy for small molecular model for a configuration c
- $G_{solv,c}$: solvation energy for a configuration c
- $G_{back,c}$: background energy for a configuration c
- $E_{inter,c}$: intrinsic energy of part k in the state n for a configuration c
- W_c: interaction energy for a configuration c
- $\Delta G_{conf,c}$: conformational energy for a configuration c

After solving the Poisson-Boltzmann equation (equation (2.2)), the used program can determine the energies $G_{solv,c}$ and $G_{back,c}$ for a titratable part (equations (2.5) and (2.6)).

$$\Delta G_{solv,c}\left(\mathfrak{c}_k^{(a)}\right) = \frac{1}{2}\sum_{o=1}^{N_k} Q_o\left(\mathfrak{c}_k^{(a)}\right)\left(\phi_p\left(r_o;\left\{Q\left(\mathfrak{c}_k^{(a)}\right)\right\}\right) - \phi_m\left(r_o;\left\{Q\left(\mathfrak{c}_k^{(a)}\right)\right\}\right)\right) \tag{2.5}$$

with

- N_k: number of charges for part k
- $Q_o\left(\mathfrak{c}_k^{(a)}\right)$: one charge of the part k in state a
- $\left\{Q\left(\mathfrak{c}_k^{(a)}\right)\right\}$: set of charges for part k in state a
- r_o: position of electrostatic potential
- ϕ_p: protein potential
- ϕ_m: model compound potential

$$\Delta G_{back,c}(\mathfrak{c}_k^{(a)}) = \sum_{o=1}^{N_p} q_o\phi_p\left(r_k;\left\{Q\left(\mathfrak{c}_k^{(a)}\right)\right\}\right) - \sum_{t=1}^{N_{k,m}^a} q_t\phi_m\left(r_k;\left\{Q\left(\mathfrak{c}_k^{(a)}\right)\right\}\right) \tag{2.6}$$

with

- N_p: number of background charges q_o for protein
- $N_{k,m}^a$: number of background charges q_t for model compound for $\mathfrak{c}_k^{(a)}$

Based on the two energies G_{solv} and G_{back} (equations (2.5) and (2.6)), the intrinsic pK_a-values and the redox potential can be determined on the basis of equation (2.7).

$$E_{inter,c} = G_{model}\left(\mathfrak{c}_k^{(a)}\right) + G_{solv,c}\left(\mathfrak{c}_k^{(a)}\right) + G_{back,c}\left(\mathfrak{c}_k^{(a)}\right) \tag{2.7}$$

Important for solving the equation (2.7) is the G_{model}-value. The G_{model}-value cannot be derived directly from continuum electrostatics or the Poisson-Boltzmann equation, but must be determined separately. The G_{model}-value belongs to a model compound. A model compound is a model for a chemical compound such as an amino acid residue in a protein. Such an amino acid residue does not exist as a zwitterion because the amino and acid groups are involved in a peptide bond. For this

reason, a model compound for such an amino acid residue would be blocked at these termini to best represent the "natural" situation. Methods for determining the G_{model}-value would be, for example, a measurement of a model compound in aqueous ionic solution, as this represents the standard conditions or a quantum mechanical calculation with a thermodynamic cycle with a model compound.

Figure 2.2 illustrates the influence of the G_{model}-value on the calculations. The sketched plot of two titration curves of a glutamate in aqueous ionic solution with a G_{model}-value of zero and a G_{model}-value of 6.57 $\frac{kcal}{mol}$ clearly shows the shift of the curves. The pK_a-value can also be read from the respective titration curves. Only using the G_{model}-value results in a pK_a-value that agrees with the experimentally determined value.

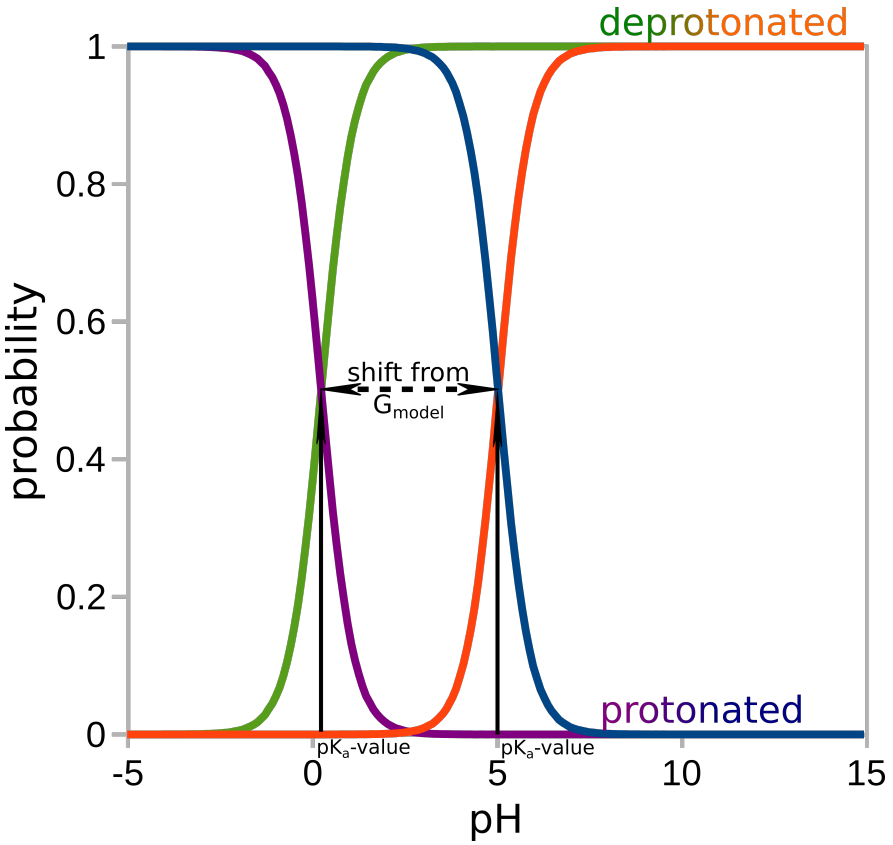

Figure 2.2: Sketch of two titration curves of a glutamate in aqueous ionic solution with a G_{model}-value of zero (purple and green) and a G_{model} of 6.57 $\frac{kcal}{mol}$ (blue and orange) clearly shows the shift of the curves. The blue and purple curves represent the titration curve of the probability of protonation over the pH scale. The green and orange curves represent the titration curve of the probability of deprotonation over the pH scale.

In addition to the two energies $G_{solv,c}$ and $G_{back,c}$ (equations (2.5) and (2.6)), the program also calculates the interaction energy between two parts $(\mathfrak{c}_k, \mathfrak{c}_l)$ in different states (a, b).

$$\begin{aligned} W_c\left(\mathfrak{c}_k^{(a)}, \mathfrak{c}_l^{(b)}\right) &= \sum_{o=1}^{N_k^a} Q_o\left(\mathfrak{c}_k^{(a)}\right) \phi_p\left(r_o; \left\{Q\left(\mathfrak{c}_k^{(n)}\right)\right\}\right) \\ &= \sum_{o=1}^{N_l^b} Q_o\left(\mathfrak{c}_l^{(b)}\right) \phi_p\left(r_o; \left\{Q\left(\mathfrak{c}_l^{(b)}\right)\right\}\right) \end{aligned} \tag{2.8}$$

with

- N_k^a: number of charges for part k in state a
- N_l^b: number of charges for part l in state b
- $Q_o\left(\mathfrak{c}_k^{(a)}\right)$ or $Q_o\left(\mathfrak{c}_l^{(b)}\right)$: one charge of the part k in state a or one charge of the part l in state b
- $\left\{Q\left(\mathfrak{c}_k^{(a)}\right)\right\}$ or $\left\{Q\left(\mathfrak{c}_l^{(b)}\right)\right\}$: set of charges for part k in state a or set of charges for part l in state b
- r_o: position of electrostatic potential
- ϕ_p: protein potential

The last energy $\Delta G_{conf,c}$ of the equation (2.4) was set to fixed values in this work, and the calculation of this energy is described in Ullmann *et al.* (*4*).
Based on the intrinsic energy and the interaction energies W_c determined in `preptitra`, a titration over all titratable groups is performed in `gmct` (*5–7*) using a Monte Carlo simulation with utilization of a Metropolis algorithm (*8*, *9*). In such a titration, simulations are performed for the individual sites for various pH-values (pH), redox potential (E) or both. By varying the pH or redox potential as mentioned above, the probability for the occurrence of such a specific state can be determined using a Boltzmann distribution. That creates the titration curve.

References

(*1*) Ullmann, G. M., and Knapp, E.-W. (1999). Electrostatic models for computing protonation and redox equilibria in proteins. *Eur Biophys J 28*, 533–551, DOI: 10.1007/s002490050236.

(*2*) Ullmann, G. M., Noodleman, L., and Case, D. A. (2002). Density functional calculation of pK a values and redox potentials in the bovine Rieske iron-sulfur protein. *JBIC 7*, 632–639, DOI: 10.1007/s00775-002-0342-6.

(*3*) Ullmann, G. M., and Bombarda, E. (2014). Continuum Electrostatic Analysis of Proteins. 135–163, DOI: 10.1007/978-3-319-09976-7_6.

(*4*) Ullmann, G. M. (2023). GMCT@UBT Manual - Version 2.0.

(*5*) Ullmann, R. T., and Ullmann, G. M. (2011). A generalized free energy perturbation theory accounting for end states with differing configuration space volume. *J Phys Chem B 115*, 507–521, DOI: 10.1021/jp1093838.

(*6*) Ullmann, R. T., and Ullmann, G. M. (2012). GMCT : a Monte Carlo simulation package for macromolecular receptors. *J Comput Chem 33*, 887–900, DOI: 10.1002/jcc.22919.

(*7*) Ullmann, G. M., and Ullmann, R. T. (2007-2014). GMCT Manual: A Monte Carlo simulation package for complex ligand binding phenomena: Version 1.2.3. ed. by Bioinformatics/Structural Biology Group.

(*8*) Metropolis, N., Rosenbluth, A. W., Rosenbluth, M. N., Teller, A. H., and Teller, E. (1953). Equation of State Calculations by Fast Computing Machines. *J Phys Chem 21*, 1087–1092, DOI: 10.1063/1.1699114.

(*9*) Hastings, W. K. (1970). Monte Carlo sampling methods using Markov chains and their applications. *Biometrika 57*, 97–109, DOI: 10.1093/biomet/57.1.97.

3

AB INITIO CALCULATION OF G_{model} WITH APPLICATIONS TO UBIQUINONE/UBIQUINOL

The theory of the micro/macrostate model (see also chapter 2) offers the possibility of an accurate description of pK_a-values, redox potentials or kinetics also in terms of the symmetry or asymmetry of a molecule. The pK_a-value describes the potential ability to transfer a proton (H^+) to a reactant. The smaller the value the greater the potential to donate a proton. In principle, for redox potentials the same theory is valid just for electrons. Micro/macrostate model theory is also known from statistical physics and thermodynamics. As a very simple example, consider the coin toss with two distinguishable coins with heads and tails. That results in four different microstates (TT, HT, TH, HH). A sum of microstates with the same properties describes a macrostate, often known as the experimentally observable state. Thus, in this example, there are three macrostates (TT, HT/TH, HH) possible. With this brief excursus into macro and microstates, it is easy to understand the basic idea of the macro and microstate model that will be used (section 3.2.1).

As an example of application, imidazole and its analogues were chosen because they describe the influence of symmetry on the pK_a-value very well. Imidazole *per se* was synthesized around 1858 in the Debus-Radziszewski synthesis by Radziszewski (*1*) and Debus (*2*). This synthetic route can also be used to prepare the methylated imidazoles. Figure 3.1 shows the numbering of the imidazole ring as used in this work. In addition, the symmetry of the imidazole and the asymmetry of the analog 5-methylimidazole can be clearly seen, as well as the nitrogen atoms N(1) and N(3), which serve as binding sites for protons. Due to the asymmetry in 5-methylimidazole, the nitrogen atoms N(1) and N(3) are distinguishable and different pK_a-values are obtained for these two nitrogen atoms.

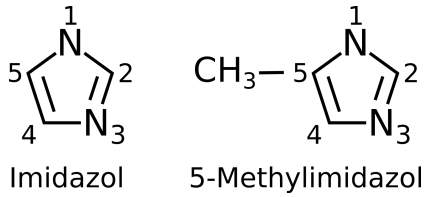

Figure 3.1: Atom numbering of imidazole and 5-methylimidazole

Experimental determination of the pK_a-value for the nitrogen atoms N(1) and N(3) is only possible by methylating one of the two nitrogen atoms, otherwise it cannot be determined which nitrogen atom is protonated or deprotonated. The theoretical analysis of the pK_a-values by quantum chemical calculation and a thermodynamic cycle is simpler in this respect, because no complex experimental methylation has to take place. In a thermodynamic cycle the final state is the same as the initial state. An example of such a circular process is the Carnot process (*3*). Such a circular process can now also be set up for the pK_a-value calculation, as it is described in the following theory section. The section further details how to derive the pK_a-values from quantum chemical calculations.

3.2 Theory

3.2.1 Macro and microstates

A system, for example a molecule, has so-called binding sites ($bisi$) to which protons or electrons can bind. There can be several $bisi$ per system. These $bisi$ can be used to uniquely describe the system. To describe the micro and macrostate (MiS/MaS) model, a system S (e.g. a protein) is defined that contains different sites (e.g. amino acid residues, iron-sulfur centers, heme, ...). These sites can occur in different states called MaS. A system consists of one or more sites and thus also of a set of different MaS.

$$S := \{MaS_i \mid i \in [0, \dots]\} \tag{3.1}$$

These MaS can interconvert into each other. A MaS can be realized as one (special case: MaS equal to MiS) or more MiS and is therefore a set of matching MiS.

$$MaS_i := \{MiS_j \mid j \in [0, \dots]\} \tag{3.2}$$

A MiS is a discrete state due to the exact description of the occupancy state of the $bisi$. Based on the number of $bisi$ ($\#bisi$), the possible number of MiS ($\#MiS$) can be determined by the equation (3.3). It can be seen from the equation (3.3) that the number of MiS increases almost exponentially with the increase of the $bisi$. However, MiS can be ambiguous due to symmetries and thus no longer distinguishable.

$$\#MiS = \prod^{\#bisi} \text{states per site} \tag{3.3}$$

Since the $bisi$ of MaS can interact, the $bisi$ of MiS can also interact. The different MaS and MiS are related and can transition to each other. Because of that, a state of equilibrium can be established. In the case of a molecule these are pK_a-values and/or redox potentials, i.e. there is an energetic relationship between the individual states and it is possible to assign an energy to each MiS and MaS. The meaning of these definitions is most easily explained by examples figure 3.2.

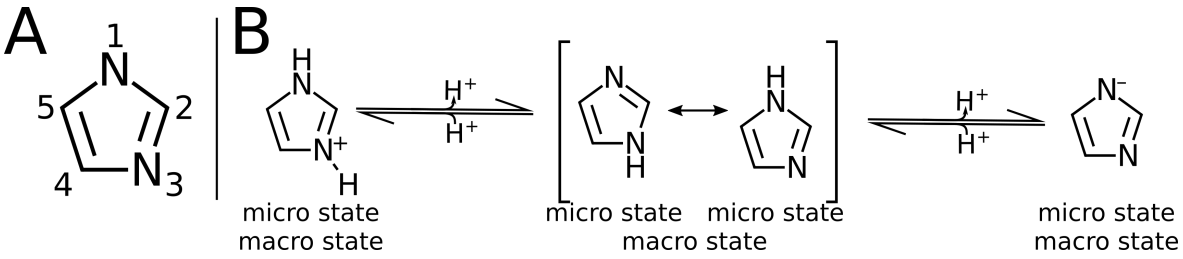

Figure 3.2: Overview of the example described here. Subfigure A shows the imidazole used and subfigure B shows the various protonation states and tautomers of the imidazole.

Imidazole has two binding sites for one proton each in the form of a H^+ atom at the nitrogen atoms N(1) and N(3). Four MiS result from the equation (3.3). These four MiS can be divided into two singly (de)protonated states, one doubly deprotonated state, and one doubly protonated state. Thus, the four MiS can be divided into three groups with respect to the protonation state, the so-called MaS. It is important to note that the two singly (de)protonated MiS are indistinguishable if only the MaS is considered. This indistinguishability of the MaS is important later, because it will also be reflected in the experimental values.

3.2.2 Definition of the pK_a-value and the redox potential with the micro and macrostates model[1]

Based on the MiS and MaS model, redox potential and pK_a-value can now be described. The MaS was defined as a set of MiS. The definition of the state model is now set into the definition of the equilibrium constant (K). For an acid-base reaction the equation (3.4) can be defined. Based on this general equilibrium constant the pK_a-values (equation (3.6)) can be determined. In the case of indistinguishable, the equation is much simpler because the MiS are no longer distinguished. Only the number of MiS is now relevant. In addition to the pK_avalue, the redox potential is now also defined. For this purpose, the equilibrium constant is again described in equation (3.5). Based on this general equilibrium constant the redox potential (E) can be determined. The equations (3.7) and (3.9) can also be derived from the normalized Boltzmann distribution.
For the determination of the pH-dependent redox potential, the transformations and considerations are the same. Only the term $\frac{1}{log(e)} \cdot pH$ must be added to get equation (3.10).

$$K = \frac{\left(\sum_{i}^{\#MiS} [MiS_i]\right)[H^+]}{\sum_{i}^{\#MiS'} MiS'_i} \tag{3.4}$$

$$K = \frac{\left(\sum_{i}^{\#MiS} MiS_i\right)[e^-]}{\sum_{i}^{\#MiS'} MiS'_i} \tag{3.5}$$

with

$\#MiS$: all microstates of the macrostate MaS

$\#MiS'$: all microstates of the macrostate MaS'

In order to make the following equations simpler and clearer, the two variables $C := 1 + \frac{\sum_{i=1}^{\#MiS} [MiS_i]}{[MiS_1]}$ and $C' := 1 + \frac{\sum_{i=1}^{\#MiS'} [MiS'_i]}{[MiS'_1]}$ are defined.

$$\begin{aligned} pK_a &= -log_{10}\left(\frac{\left([MiS_1] + \sum_{i=1}^{\#MiS}[MiS_i]\right)[H^+]}{[MiS'_1] + \sum_{i=1}^{\#MiS'}[MiS'_i]}\right) \\ &= -log_{10}\left(\frac{([MiS_1]\cdot C)\,[H^+]}{[MiS'_1]\cdot C'}\right) \\ &= -log_{10}\left(\frac{[MiS_1][H^+]}{[MiS'_1]}\right) - log_{10}\left(\frac{C}{C'}\right) \end{aligned} \tag{3.6}$$

indistinguishable MiS:

$$\begin{aligned} pK_a &= -log_{10}\left(\frac{[MiS_1][H^+]}{[MiS'_1]}\right) - log_{10}\left(\frac{1+(\#MiS-1)}{1+(\#MiS'-1)}\right) \\ &= -log_{10}\left(\frac{[MiS_1][H^+]}{[MiS'_1]}\right) - log_{10}\left(\frac{\#MiS}{\#MiS'}\right) \end{aligned} \tag{3.7}$$

1 In this chapter, as in the following chapters, the line represents a separation between formulas and text.

$$E = E^{\circ} - \frac{RT}{F \cdot z} \cdot ln\left(\frac{[MiS_1][e^-]}{[MiS_1']}\right) - \frac{RT}{F \cdot z} \cdot ln\left(\frac{C}{C'}\right) \tag{3.8}$$

E°: standard redox potential

T: temperature

z: number of electrons transferred

R: universal gas constant

F: Faraday constant

indistinguishable MiS:

$$\begin{aligned} E &= E^{\circ} - \frac{RT}{F \cdot z} \cdot ln\left(\frac{[MiS_1][H^+]}{[MiS_1']}\right) - \frac{RT}{F \cdot z} \cdot ln\left(\frac{1 + (\#MiS - 1)}{1 + (\#MiS' - 1)}\right) \\ &= E^{\circ} - \frac{RT}{F \cdot z} \cdot ln\left(\frac{[MiS_1][H^+]}{[MiS_1']}\right) - \frac{RT}{F \cdot z} \cdot ln\left(\frac{\#MiS}{\#MiS'}\right) \end{aligned} \tag{3.9}$$

$$E = E^{\circ} - \frac{RT}{F \cdot z} \cdot \left[ln\left(\frac{[MiS_1][e^-]}{[MiS_1']}\right) - ln\left(\frac{C}{C'}\right) - \frac{1}{log(e)} \cdot pH\right] \tag{3.10}$$

indistinguishable MiS:

$$\begin{aligned} &= E^{\circ} - \frac{RT}{F \cdot z} \cdot \left[ln\left(\frac{[MiS_1][H^+]}{[MiS_1']}\right) - ln\left(\frac{1 + (\#MiS - 1)}{1 + (\#MiS' - 1)}\right) - \frac{1}{log(e)} \cdot pH\right] \\ &= E^{\circ} - \frac{RT}{F \cdot z} \cdot \left[ln\left(\frac{[MiS_1][H^+]}{[MiS_1']}\right) - ln\left(\frac{\#MiS}{\#MiS'}\right) - \frac{1}{log(e)} \cdot pH\right] \end{aligned} \tag{3.11}$$

3.2.3 Calculation of absolute and relative pK_a-values and redox potentials

Based on the theory from the publication of Casasnovas *et al.* (*4*, *5*), the absolute and relative pK_a-values were calculated. The necessary energy (electronic energy E_{elec} or Gibbs free energy G) were determined by quantum mechanical calculations. The electronic energy can be defined by equation (3.12). A more accurate pK_a-value can be obtained by using Gibbs free energy (equation (3.13)). To calculate the Gibbs free energy the enthalpy H and entropy S are needed. The enthalpy is composed of the inner energy U, pressure p and volume V of the system. In this special case of one mole $pV = RT$ the enthalpy can be written like in equation (3.14). On the basis of enthalpy (H), the inner energy (U) can be divided into different parts. Thus the inner energy is defined as sum (equation (3.15)). Now only the entropy is needed to calculate the Gibbs free energy. Entropy can also be divided into different terms (equation (3.16)). Now all the quantities are available to calculate the Gibbs free energy.

Two thermodynamic cycles were performed to calculate pK_a-values. In both cases the energies ΔG_{gas}, $\Delta\Delta G_{solv}$ and ΔG_{aq} are required. These energies depend directly on the calculated values from quantum chemistry. However, because energies differences (ΔG_{gas}, $\Delta\Delta G_{solv}$, ΔG_{aq}) are always used, some terms are dropped. By using equations (3.17) and (3.27) it can easily be shown that the energies U_{rot}, U_{trans} and $k_B \cdot T$ have no influence on the pK_a-values and can be dropped.

$$U_{elec} = U_{kin,e} + U_{e,N} + U_{e,e} + U_{N,N} \tag{3.12}$$

with

U_{elec}: electronic energy
$U_{kin,e}$: kinetic energy of electron
$U_{e,N}$: attractions of nuclei and electron
$U_{e,e}$: electron-electron repulsion
$U_{N,N}$: nucleus-nucleus repulsion

$$G = H - T \cdot S \tag{3.13}$$

with

G: Gibbs free energy
H: enthalpy
T: temperature
S: entropy

$$H = U + p \cdot V = U + R \cdot T = U + N \cdot k_B \cdot T \tag{3.14}$$

with

U: inner energy
p: pressure
V: volume
T: temperature
R: gas constant
N: number of particles
k_B: Boltzmann constant

$$U_{tot} = U_{elec} + ZPE + U_{vib} + \underbrace{U_{rot}}_{=\frac{3}{2}\cdot R\cdot T} + \underbrace{U_{trans}}_{=\frac{3}{2}\cdot R\cdot T} \tag{3.15}$$

with

U_{elec}: electronic energy

ZPE: zero point energy

U_{vib}: vibrational thermal energy

U_{rot}: rotational thermal energy ($\frac{3}{2} \cdot R \cdot T$, because of a nonlinear polyatomic molecule)

U_{trans}: translational thermal energy ($\frac{3}{2} \cdot R \cdot T$)

$$S_{tot} = S_{elec} + S_{vib} + S_{rot} + S_{trans} \tag{3.16}$$

with

S_{elec}: electronic entropy

S_{vib}: vibrational entropy

S_{rot}: rotational entropy

S_{trans}: translational entropy (It depends just on system's volume and molecular mass)

Absolute pK_a-values

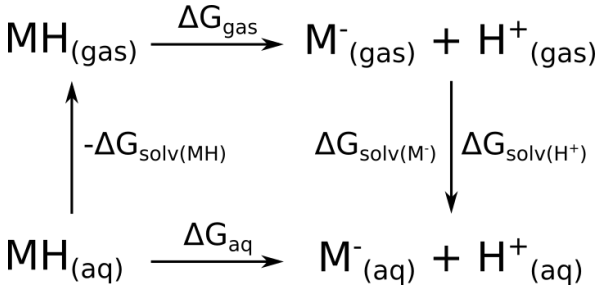

Figure 3.3: Thermodynamic cycle for absolute pK_a-value of an example molecule M.

To determine pK_a-values of a molecule M, first the ΔG_{gas} has to be calculated (equation (3.17) and equation (C.1) in the appendix C.1 which contains all intermediate steps of the calculation), which corresponds to the free energy in the vacuum (figure 3.3). For the correct calculation the free energy of a proton in a vacuum is needed. That can be determined from the Sackur-Tetrode equation (*6*) and is $-6.28\ \frac{kcal}{mol}$ (*7–9*). The next step is to determine the free solvation energy (ΔG_{solv}, equation (3.18)). That depends on the chosen solvent and has to be considered when calculating $\Delta\Delta G_{solv}$. $\Delta\Delta G_{solv}$ can be determined by using the equation (3.19), whereby the ΔG_{solv} of the proton has to be considered. This ΔG_{solv} of the proton was determined experimentally and is solvent dependent. In water, the value is $-265.6\ \frac{kcal}{mol}$ (*10*) and in DMF $-264.2\ \frac{kcal}{mol}$ (*11*). As second last step the aqueous free deprotonation energy (equations (3.20) and (C.2) in the appendix C.1) is determined. As last step the pK_a-value (equation (3.21)) is calculated.

$$\begin{aligned}\Delta G_{gas} =& G_{gas}(MH) - G_{gas}(M^-) + (G_{gas}(H^+) + RTln(24.46)) \\ =& E^{MH}_{elec,gas} - E^{M^-}_{elec,gas} + ZPE^{MH}_{gas} - ZPE^{M^-}_{gas} + U^{MH}_{vib,gas} - U^{M^-}_{vib,gas} \\ & -T(S^{MH}_{elec,gas} - S^{M^-}_{elec,gas} + S^{MH}_{vib,gas} - S^{M^-}_{vib,gas} + S^{MH}_{rot,gas} - S^{M^-}_{rot,gas} + S^{MH}_{trans,gas} - S^{M^-}_{trans,gas}) \\ & +\Delta G_{gas}(H^+)\end{aligned} \tag{3.17}$$

with

ΔG_{gas}: gas-phase free energy of reaction

$G_{gas}(MH)$:free energy of a molecule MH in a vacuum

$G_{gas}(M^-)$:free energy of a molecule M^- in a vacuum

T: temperature

$RTln(24.46)$: conversion factor from 1atm to 1M (*12*)

$\Delta G_{gas}(H^+)$: free energy of a proton in a vacuum

In order to make the following equations simpler and non-repetitive, a wildcard $*$ was introduced. This wildcard represents the protonated, deprotonated, reduced and oxidized form of the molecule M depending on whether a pK_a-value or a redox potential is calculated.

$$\begin{aligned}\Delta G_{solv}(M*) =& G_{gas}(M*) - G_{aq}(M*) \\ =& G_{gas}(M*) - (G_{aq}(M*)) \\ =& E^{M*}_{elec,gas} - E^{M*}_{elec,aq} + ZPE^{M*}_{gas} - ZPE^{M*}_{aq} + U^{M*}_{vib,gas} - U^{M*}_{vib,aq} \\ & -T(S^{M*}_{elec,gas} - S^{M*}_{elec,aq} + S^{M*}_{vib,gas} - S^{M*}_{vib,aq} + S^{M*}_{rot,gas} - S^{M*}_{rot,aq} + S^{M*}_{trans,gas} - S^{M*}_{trans,aq})\end{aligned} \tag{3.18}$$

with

$\Delta G_{solv}(M*)$: free solvation energy of a molecule $M*$

$G_{gas}(M*)$: free energy of a molecule $M*$ in a vacuum

$G_{aq}(M*)$: free energy of a molecule $M*$ in a solvent

$$\begin{aligned}\Delta\Delta G_{solv} =& \Delta G_{solv}(M^-) - \Delta G_{solv}(MH) + \Delta G_{solv}(H^+) \\ =& E^{M^-}_{elec,gas} - E^{M^-}_{elec,aq} + ZPE^{M^-}_{gas} - ZPE^{M^-}_{aq} + U^{M^-}_{vib,gas} - U^{M^-}_{vib,aq} \\ & -T(S^{M^-}_{elec,gas} - S^{M^-}_{elec,aq} + S^{M^-}_{vib,gas} - S^{M^-}_{vib,aq} + S^{M^-}_{rot,gas} - S^{M^-}_{rot,aq} + S^{M^-}_{trans,gas} - S^{M^-}_{trans,aq}) \\ & -(E^{MH}_{elec,gas} - E^{MH}_{elec,aq} + ZPE^{MH}_{gas} - ZPE^{MH}_{aq} + U^{MH}_{vib,gas} - U^{MH}_{vib,aq} \\ & -T(S^{MH}_{elec,gas} - S^{MH}_{elec,aq} + S^{MH}_{vib,gas} - S^{MH}_{vib,aq} + S^{MH}_{rot,gas} - S^{MH}_{rot,aq} + S^{MH}_{trans,gas} - S^{MH}_{trans,aq})) \\ & +\Delta G_{solv}(H^+)\end{aligned} \tag{3.19}$$

with

$\Delta\Delta G_{solv}$: change of free solvation energy

$\Delta G_{solv}(M^-)$: free solvation energy of a molecule M^-

$\Delta G_{solv}(MH)$: free solvation energy of a molecule MH

$\Delta G_{solv}(H^+)$: free solvation energy of a proton

$$\begin{aligned}\Delta G_{aq} =& \Delta G_{gas} + \Delta\Delta G_{solv} \\ =& \Delta\Delta E_{elec} + \Delta\Delta ZPE + \Delta\Delta U_{vib} - \Delta\Delta S_{elec} - \Delta\Delta S_{vib} - \Delta\Delta S_{rot} - \Delta\Delta S_{trans} \\ & +\Delta G_{solv}(H^+) + \Delta G_{gas}(H^+)\end{aligned} \tag{3.20}$$

with

ΔG_{aq}: reaction free energy of deprotonation in solution

$\Delta\Delta E_{elec} = \left(E^{M^-}_{elec,gas} - E^{M^-}_{elec,aq}\right) - \left(E^{MH}_{elec,gas} - E^{MH}_{elec,aq}\right)$

$\Delta\Delta ZPE = \left(ZPE^{M^-}_{gas} - ZPE^{M^-}_{aq}\right) - \left(ZPE^{MH}_{gas} - ZPE^{MH}_{aq}\right)$

$\Delta\Delta U_{vib} = \left(U^{M^-}_{vib,gas} - U^{M^-}_{vib,aq}\right) - \left(U^{MH}_{vib,gas} - U^{MH}_{vib,aq}\right)$

$$\Delta\Delta S_{elec} = \left(S^{M^-}_{elec,gas} - S^{M^-}_{elec,aq}\right) - \left(S^{MH}_{elec,gas} - S^{MH}_{elec,aq}\right)$$
$$\Delta\Delta S_{vib} = \left(S^{M^-}_{vib,gas} - S^{M^-}_{vib,aq}\right) - \left(S^{MH}_{vib,gas} - S^{MH}_{vib,aq}\right)$$
$$\Delta\Delta S_{rot} = \left(S^{M^-}_{rot,gas} - S^{M^-}_{rot,aq}\right) - \left(S^{MH}_{rot,gas} - S^{MH}_{rot,aq}\right)$$
$$\Delta\Delta S_{trans} = \left(S^{M^-}_{trans,gas} - S^{M^-}_{trans,aq}\right) - \left(S^{MH}_{trans,gas} - S^{MH}_{trans,aq}\right)$$

$$\begin{aligned} pK_a =& \frac{\Delta G_{aq}}{ln(10.0)\cdot R\cdot T} \\ =& \frac{\Delta\Delta E_{elec} + \Delta\Delta ZPE + \Delta\Delta U_{vib} - \Delta\Delta S_{elec} - \Delta\Delta S_{vib} - \Delta\Delta S_{rot} - \Delta\Delta S_{trans}}{ln(10.0)\cdot R\cdot T} \\ &+ \frac{\overbrace{\Delta G_{solv}(H^+) + \Delta G_{gas}(H^+)}^{const}}{ln(10.0)\cdot R\cdot T} \end{aligned} \tag{3.21}$$

Absolute redox potentials

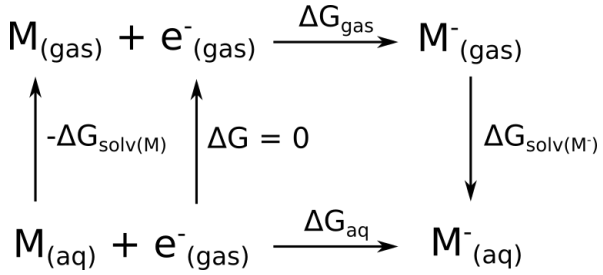

Figure 3.4: Thermodynamic cycle for absolute redox potential of an example molecule M.

To determine redox potentials of a molecule M, first the ΔG_{gas} (equation (3.22) and equation (C.4) in the appendix C.1 which contains all intermediate steps of the calculation) has to be calculated, which corresponds to the Gibbs free energy in the vacuum (figure 3.4). The next step is to determine the free solvation energy (equation (3.23)). That depends on the chosen solvent and has to be taken into account when calculating $\Delta\Delta G_{solv}$. $\Delta\Delta G_{solv}$ can be determined by solving the equation (3.24), whereby the ΔG_{solv} of the proton has to be considered. As second last step the free energy of deprotonation in aqueous solution (equations (3.25) and (C.6) in the appendix C.1) is determined. As last step the redox potential (equation (3.26)) is calculated.

$$\begin{aligned}\Delta G_{gas} =& G_{gas}(MH) - G_{gas}(M^-) \\ =& E^{MH}_{elec,gas} - E^{M^-}_{elec,gas} + ZPE^{MH}_{gas} - ZPE^{M^-}_{gas} + \\ & U^{MH}_{elec,gas} - U^{M^-}_{elec,gas} + U^{MH}_{vib,gas} - U^{M^-}_{vib,gas} \\ & -T(S^{MH}_{elec,gas} - S^{M^-}_{elec,gas} + S^{MH}_{vib,gas} - S^{M^-}_{vib,gas} + \\ & S^{MH}_{rot,gas} - S^{M^-}_{rot,gas} + S^{MH}_{trans,gas} - S^{M^-}_{trans,gas})\end{aligned} \tag{3.22}$$

$$\begin{aligned}\Delta G_{solv}(M*) =& G_{gas}(M*) - G_{aq}(M*) \\ =& E^{M*}_{elec,gas} - E^{M*}_{elec,aq} + ZPE^{M*}_{gas} - ZPE^{M*}_{aq} + \\ & U^{M*}_{elec,gas} - U^{M*}_{elec,aq} + U^{M*}_{vib,gas} - U^{M*}_{vib,aq} \\ & -T(S^{M*}_{elec,gas} - S^{M*}_{elec,aq} + S^{M*}_{vib,gas} - S^{M*}_{vib,aq} + \\ & S^{M*}_{rot,gas} - S^{M*}_{rot,aq} + S^{M*}_{trans,gas} - S^{M*}_{trans,aq})\end{aligned} \tag{3.23}$$

$$\begin{aligned}\Delta\Delta G_{solv} =& \Delta G_{solv}(M^-) - \Delta G_{solv}(M) \\ =& E^{M^-}_{elec,gas} - E^{M^-}_{elec,aq} + ZPE^{M^-}_{gas} - ZPE^{M^-}_{aq} + \\ & U^{M^-}_{elec,gas} - U^{M^-}_{elec,aq} + U^{M^-}_{vib,gas} - U^{M^-}_{vib,aq} \\ & -T(S^{M^-}_{elec,gas} - S^{M^-}_{elec,aq} + S^{M^-}_{vib,gas} - S^{M^-}_{vib,aq} + \\ & S^{M^-}_{rot,gas} - S^{M^-}_{rot,aq} + S^{M^-}_{trans,gas} - S^{M^-}_{trans,aq}) \\ & -(E^{M}_{elec,gas} - E^{M}_{elec,aq} + ZPE^{M}_{gas} - ZPE^{M}_{aq} + \\ & U^{M}_{elec,gas} - U^{M}_{elec,aq} + U^{M}_{vib,gas} - U^{M}_{vib,aq} \\ & -T(S^{M}_{elec,gas} - S^{M}_{elec,aq} + S^{M}_{vib,gas} - S^{M}_{vib,aq} + \\ & S^{M}_{rot,gas} - S^{M}_{rot,aq} + S^{M}_{trans,gas} - S^{M}_{trans,aq}))\end{aligned} \tag{3.24}$$

$$\begin{aligned}\Delta G_{aq} =& \Delta G_{gas} + \Delta\Delta G_{solv} \\ =& \Delta\Delta E_{elec} - \Delta\Delta ZPE + \Delta\Delta U_{elec} + \Delta\Delta U_{vib} - \\ & \Delta\Delta S_{elec} - \Delta\Delta S_{vib} - \Delta\Delta S_{rot} - \Delta\Delta S_{trans}\end{aligned} \tag{3.25}$$

$$E = \frac{-\Delta G_{aq}}{n \cdot F} + E_{SHE} \tag{3.26}$$

with

F: Faraday constant

n: number of electrons transferred

E_{SHE}:standard hydrogen redox potential

Calculation of relative pK_a-values

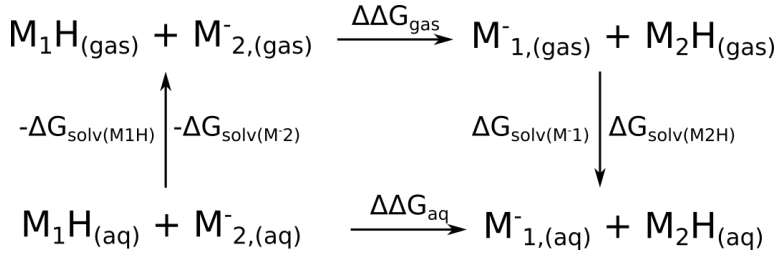

Figure 3.5: Thermodynamic cycle for relative pK_a of the example molecules M_1 and M_2.

Determining relative pK_a-values is very similar to determining absolute pK_a-values (figure 3.5). However, two molecules M_1, M_2 are now required, and a pK_a-value must be known for one of these molecules. The determination of the energy ΔG_{solv} is described in equation (3.18). The other necessary energy is determined in the equations (3.27) to (3.29). The pK_a-values now result from the equation (3.30).

$$\begin{aligned}\Delta\Delta G_{gas} =&(G_{gas}(M_1H) - G_{gas}(M_1^-) + (G_{gas}(H^+) + RTln(24.46))- \\ &(G_{gas}(M_2H) - G_{gas}(M_2^-) + (G_{gas}(H^+) + RTln(24.46)) \\ =&(G_{gas}(M_1H) - G_{gas}(M_1^-)) + (G_{gas}(M_2^-) - G_{gas}(M_2H))\end{aligned} \tag{3.27}$$

$$\begin{aligned}\Delta\Delta G_{solv} =&(\Delta G_{solv}(M_1H) - \Delta G_{solv}(M_1^-) + \Delta G_{solv}(H^+))- \\ &(\Delta G_{solv}(M_2H) - \Delta G_{solv}(M_2^-) + \Delta G_{solv}(H^+)) \\ =&(\Delta G_{solv}(M_1H) - \Delta G_{solv}(M_1^-)) + (\Delta G_{solv}(M_2^-) - \Delta G_{solv}(M_2H))\end{aligned} \tag{3.28}$$

$$\begin{aligned}\Delta\Delta G_{aq} =&\Delta G_{gas} + \Delta\Delta G_{solv} \\ =&(G_{gas}(M_1H) - G_{gas}(M_1^-)) + (G_{gas}(M_2^-) - G_{gas}(M_2H))+ \\ &(\Delta G_{solv}(M_1H) - \Delta G_{solv}(M_1^-)) + (\Delta G_{solv}(M_2^-) - \Delta G_{solv}(M_2H)) \\ =&\Delta G_{M_1,aq} - \Delta G_{M_2,aq}\end{aligned} \tag{3.29}$$

$$pK_a = \frac{\Delta\Delta G_{aq}}{ln(10.0) \cdot R \cdot T} + pK_a(M_2) \tag{3.30}$$

3.3 Methods

Structure modeling

The application example imidazole and its analogues were created with the program `bkchem 0.13.0` (*13*) and then saved as xyz files. These files contain the coordinates for the `orca` (*14*) calculations.

Geometry optimization

The geometry optimization was performed in two steps in `orca-5.0.1`. Two optimizations were performed in vacuum, increasing the basis set from Def2-SVPD (pre-optimization) to Def2-TZVPPD (optimization) from the first to the second run. Def2-SVPD was chosen because this basis set is sufficient for the first structural optimization and then Def2-TZVPPD is used to optimize the structure. For both optimization runs, the B3LYP functional and the SlowConv options were used for the SCF cycle. (explanation see appendix A.1.1)

Frequency calculation

The frequency calculation was performed in `orca-5.0.1`. The calculation of the frequencies was also done with the functional B3LYP and the base set Def2-TZVPPD. Furthermore, the options SlowConv, TightOpt and TightSCF were set for the SCF cycle. Additionally the option NumFreq was set to determine the frequencies (explanation see appendix A.1.1).

pK_a*-value und redox potential calculation*

For all structures, calculations were performed with and without explicit waters near the proton binding site. In both cases, however, an implicit solvent environment representing either DMF, acetonitrile, or water was set (settings see appendix A.1.1).
The energies calculated by `orca` were used to calculate the pK_a-values. The pK_a-values are calculated as described in the section 3.2.3.

python3-scripts

Because of the large number of states, a python script was written for the calculations, which is divided into several modules:

- read_orca_output: This module contains the methods for reading and processing the output from orca.
- thermodynamic_cycle: This module defines the individual methods for the application of the thermodynamic cycle.
- calc_pkvalues: This module inherits from the previous two modules and contains the methods for calculating the pK_a-values based on the orca output.

3.4 Imidazole and analogues

Figure 3.6 includes the various protonation and deprotonation reactions of imidazole and its analogues. Figure 3.6 A and C represent the reaction pathways for imidazole and 5-methylimidazole, respectively. However, these reactions do not allow experimental discrimination of the nitrogen atoms N(1) and N(3). For experimental differentiation, the structures of figure 3.6 B, D, and E were used. However, that is not necessary for the quantum mechanical calculations, because it is possible to define which nitrogen atom is deprotonated.

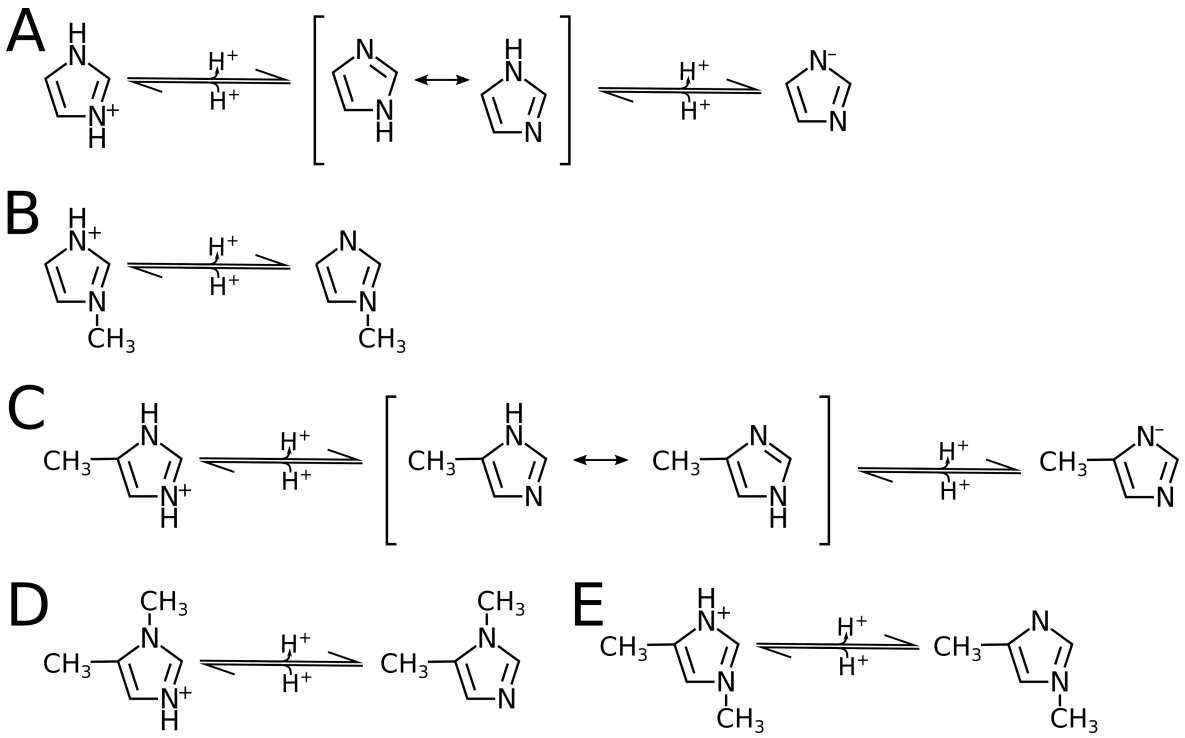

Figure 3.6: Deprotonation/Protonation reactions of imidazole and his analogues. Also shown are all isomers, which in this context are referred to as microstates.
A: Deprotonation/Protonation of imidazole
B: Deprotonation/Protonation of $1(3)$-methylimidazole
C: Deprotonation/Protonation of 5-methylimidazole
D: Deprotonation/Protonation of 15-dimethylimidazole
E: Deprotonation/Protonation of 35-dimethylimidazole

Experimental pK_a-values

Figure 3.7 shows the experimental values for the different reaction pathways of imidazole and 5-methylimidazole. To simplify the notation, the states are written in a shortened form, with the number representing the nitrogen atom position, an underscore representing an unoccupied binding site and a H representing an occupied binding site. The pK_a-value between the two macrostates of the singly ($3H1\_$, 3_1H) and doubly protonated ($3H1H$) imidazole is $6.95\ldots6.97$ (figure 3.7 A). The experimental pK_a-value for the transition of the doubly protonated macrostate to a microstate of the singly protonated imidazole is 7.21. The equation (3.7) is used to calculate the theoretical pK_a-value for this situation.

$$\begin{aligned} pk_{a,3H1H\rightarrow 3H1\_} = pk_{a,3H1H\rightarrow 3\_1H} &= \underbrace{-log_{10}\left(\frac{[MiS_1][H^+]}{[MiS_1']}\right)}_{\text{exp. } pk_a\text{-value: } 6.95...6.97} \underbrace{-log_{10}\ \left(\frac{\#MiS}{\#MiS'}\right)}_{\frac{1\text{ (double protonated state)}}{2\text{ (single protonated states)}}} \\ &= [6.95\ldots7.00] + 0.30 \\ &= 7.25\ldots7.30 \end{aligned} \tag{3.31}$$

That results in microscopic pK_a-values of $7.25\ldots7.30$ starting from the experimental macroscopic pK_a-values of $6.95\ldots6.97$, so the calculated values are very close to the experimental microscopic pK_a-values of $7.19\ldots7.21$. Using this procedure, the pK_a-value for the transition from the singly

protonated to the fully deprotonated state can be calculated and result in a pK_a-value of 14.22.
For 5-methylimidazole, such a calculation is not as straightforward because the molecule is not symmetric (figure 3.7 B).

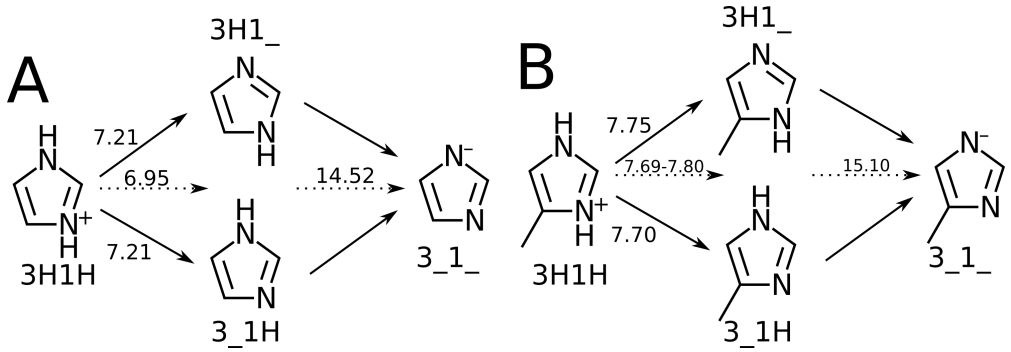

Figure 3.7: Different known experimental pK_a-values for imidazole (A) and 5-methylimidazole (B) (table 3.1).

Table 3.1: Different experimental pK_a-values for imidazole and imidazole analogs in water (*15*). The letters in bold represent the different molecular compounds from the figure 3.6. "H"s in gray represent a singly protonated structure.

	A	**B**	**C**	**D**	**E**
$3H1\_ \leftarrow 3H1H$					7.75[16]
$3\_1H \leftarrow 3H1H$				7.70[17]	
$3H1H \leftarrow 3H1H$	6.95[18]	6.95[19]	7.56[17]		
	7.00[17]	7.13[20]			
$3H1H \leftarrow 3\_1\_$	14.52[21]		15.10[22]		
	14.17[23]				

After reviewing the experimental values and checking equation (3.7), an analysis of the results of the quantum mechanical calculations is needed. The table 3.2 contains the results of these calculations. The values are the absolute determined pK_a-values. On the basis of these values the G_{model}-values can be calculated later. Therefore, it is necessary to pay more attention to the pK_a-difference between the different forms of protonation than to the absolute pK_a-values.

Table 3.2: Different calculated pK_a-values for imidazole and imidazole analogs in DMF/water without/with explicit water (ow/ww).

	A		C		D		E	
	ow	ww	ow	ww	ow	ww	ow	ww
$3H1H \rightarrow 3H1\_$	6.90	9.31	8.16	9.29			8.97	5.57
$3H1H \rightarrow 3\_1H$	6.91	9.77	8.15	9.75	8.71	5.57		
$3H1\_ \rightarrow 3\_1\_$	21.55	18.77	22.61	19.05				
$3\_1H \rightarrow 3\_1\_$	21.54	18.32	22.62	18.58				
$3H1H \rightarrow 3H1\_$	7.42	9.56	8.65	9.54			9.43	8.85
$3H1H \rightarrow 3\_1H$	7.42	9.50	8.63	9.49	9.16	8.84		
$3H1\_ \rightarrow 3\_1\_$	21.02	18.65	22.08	18.65				
$3\_1H \rightarrow 3\_1\_$	21.02	18.71	22.10	18.71				

Calculated pK_a-values without water

Table 3.2 shows the calculated values for imidazole and 5-methylimidazole without water (ow). It is clear based on comparison that the pK_a-values of imidazole to each MiS are the same and even the pK_a-values of 5-methylimidazole do not differ. That is interesting because imidazole is symmetric, while 5-methylimidazole is no longer symmetric because of the methyl group and is therefore asymmetric. The influence of the methyl group and the asymmetry on the pK_a-value is therefore small and can thus also be applied to a histidine, for example.

The calculated absolute pK_a-values are very close to the experimental values for the deprotonation from the doubly to the singly protonated state with a difference of about 0.2 pK_a-units for imidazole and 0.9 pK_a-units for 5-methylimidazole (compare figure 3.7 and table 3.2). When another hydrogen atom is removed, the calculated value is more than 6 pK_a-units higher than the experimental value. This circumstance is true for imidazole and 5-methylimidazole. To solve this problem, other basis sets have been tried in addition to the one given here, but they do not show a better result of the pK_a-values for the transition from the singly protonated to deprotonated states. It seems to be a problem with the energy of the fully deprotonated state, because the first transition agrees very well with the experimental values but the energies for the second transition do not.

According to Thapa *et al.* (*24*), for anionic molecules, explicit waters are better for pK_a-value calculation, since an implicit solvent environment is not sufficient.

Calculated pK_a-values with water

Table 3.2 shows the calculated values for imidazole and 5-methylimidazole with water (ww). It is clear based on comparison that by adding two explicit waters, the pK_a-values of imidazole to each MiS become unequal while the pK_a-values of 5-methylimidazole become equalized. Thus, it appears that the properties of the molecules are reversed with explicit water. That is due to the symmetry breaking caused by the dipole nature of water. When the nitrogen atom is deprotonated, the hydrogen atom of the water is oriented towards the nitrogen atom. If the nitrogen atom is protonated, the oxygen atom of the water is oriented in the direction of the bound hydrogen atom of the nitrogen atom. The pK_a-values for the transition between the singly protonated to the deprotonated state are closer to the experimental values with about 4 pK_a-units for the imidazole but the symmetry properties of the molecule are destroyed by the explicit water. The pK_a-values for the transition between the singly protonated to the deprotonated state are closer to the experimental values with about 3.5 pK_a-units for the 5-methylimidazole, but the symmetry properties of the molecule are also destroyed. However,

for imidazole as well as 5-methylimidazole, the pK_a-value worsened by about 1 to 2 pK_a-units upon deprotonation from the doubly protonated to the singly protonated state.
By determining the Gibbs free energy, various other values such as entropy, enthalpy and zero point energy are also determined figure 3.8. It is clearly seen that the zero point energy has the greatest influence in all calculations. The influence of entropy is about half as large when considering energy. It is remarkable that by adding the explicit water to the calculations the vibronic energy or entropy increases 4 to 10 times, which is due to the ”mobility” of the water molecules. Using the imidazole example, I was able to show that the theory of the MiS and MaS model in combination with the thermodynamic cycle is suitable to determine pK_a-values that can be used to determine our G_{model}-values.

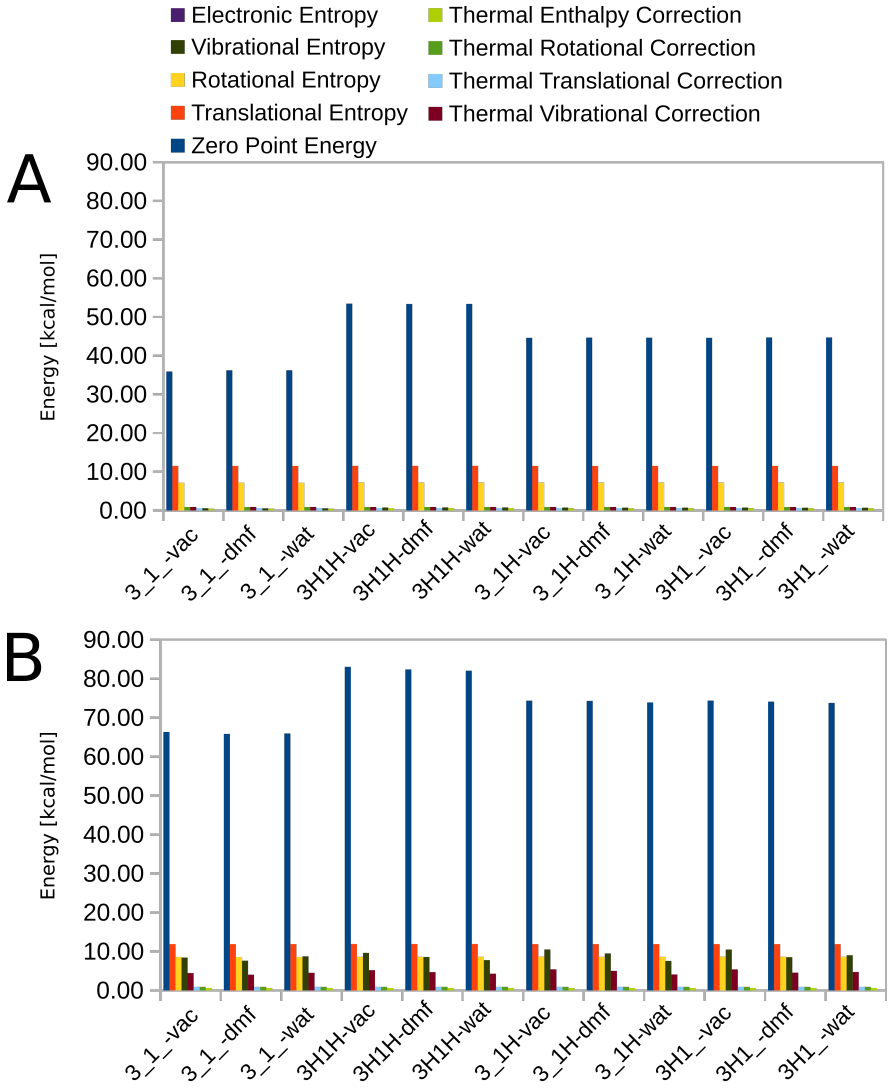

Figure 3.8: Bar chart of the different energies that have an influence on the thermodynamic cycle. The energies were calculated with *orca*.
A: Energy values without explicit water
B: Energy values with explicit water

3.5 Ubiquinol

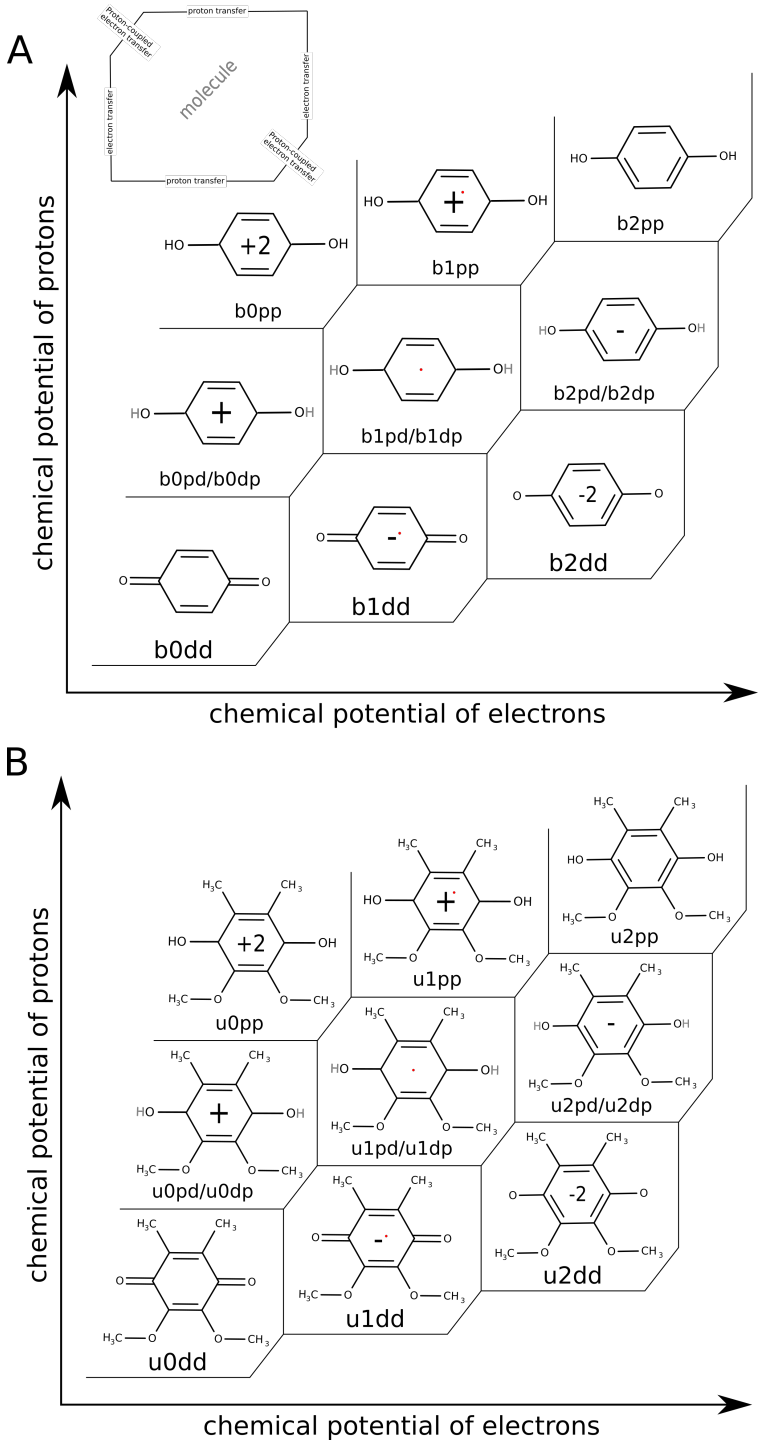

Figure 3.9: Two Pourbaix-like plot as an overview of the individual structures and their names. In structures with gray hydrogen atoms one position is occupied.
A: Structures of benzoquinones, benzosemiquinones and benzoquinols
B: Structures of model compound for ubiquinones, ubisemiquinones and ubiquinols

In the progress of the calculations, it became apparent that the strictly theoretical calculations with `orca` were not sufficient to describe the energetic transitions between the individual states. Geometry optimization showed that at least four conformations are possible for the hydrogen atoms at the oxygen atoms O1 and O4. The position of the hydrogen atoms depends on the protonation state and the electronic state of the ubiquinone. The hydrogen atom positioning affects the pK_a-values and redox potentials as well as the atomic point charges, which were also calculated. To prevent the hydrogen atom positions from being influenced by the manual placement of hydrogen atoms at O1 and O4, I decided to create a basic structure ("all up") for all protonation states, to optimize this geometry, and to use it to perform all further calculations. That eliminated the influence of this factor, but the position of the hydrogen atoms still changed depending on the protonation state and the electronic state. Therefore, the four conformations are not a "product of chance". With these different structures, the corresponding pK_a-values and redox potentials were now determined.

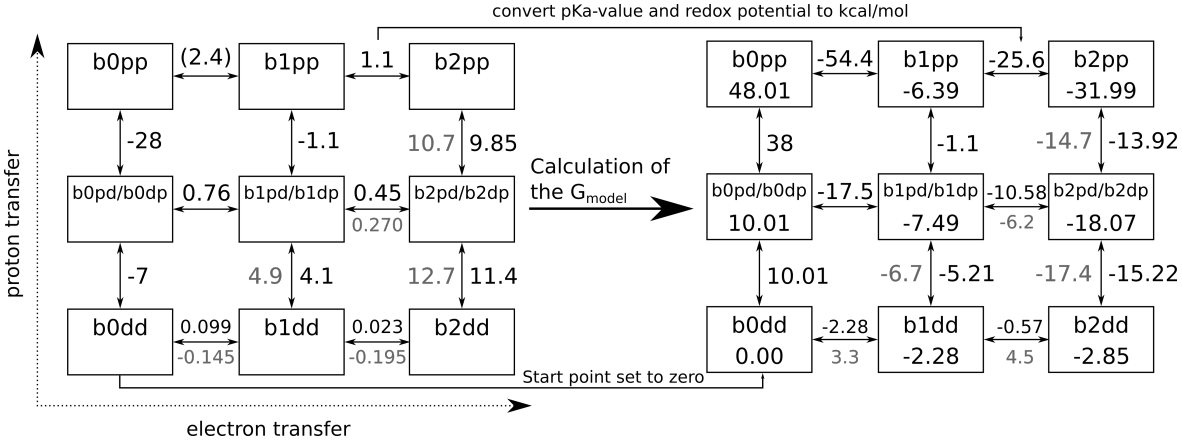

Figure 3.10: Calculation of the G_{model}-values for benzoquinone. The left figure contains the experimental pK_a-values and redox potential $[V]$ (*25*). The right figure contains the determined G_{model}-values (value inside box), the experimental pK_a-values and redox potential in $\left[\frac{kcal}{mol}\right]$. The dark gray values are the few known experimental values for ubiquinone from Zhu *et al.* (*26*).
To get from left to right, a starting point is determined and set to zero. Furthermore, the pK_a-values and redox potential are converted to $\frac{kcal}{mol}$. The conversion is calculated by multiplication with the two conversion factors -1.372 for the pK_a-values and -23.061 for the redox potentials. Starting from the starting point, only the individual transition energies are added to it if it is a forward step and subtracted if it is a backward step.

It turned out that the deviations from the few known experimental values for ubiquinone (*26*) were nevertheless far too large, up to 38.71 $\frac{kcal}{mol}$ for the reaction of u1dd to u2dd (figure 3.10 and table 3.4). So different functionals (B3LYP, M062X and WB97X-D3) were additionally tested, as there was a hint in Huynh *et al.* (*27*) that it might improve the results. However, no improvement was obtained in this case and the standard base set (Def2-TZVPPD) and functional (B3LYP) were used. To briefly summarize, the influence of the used functionals was less than the structural geometry (see figure 3.11).

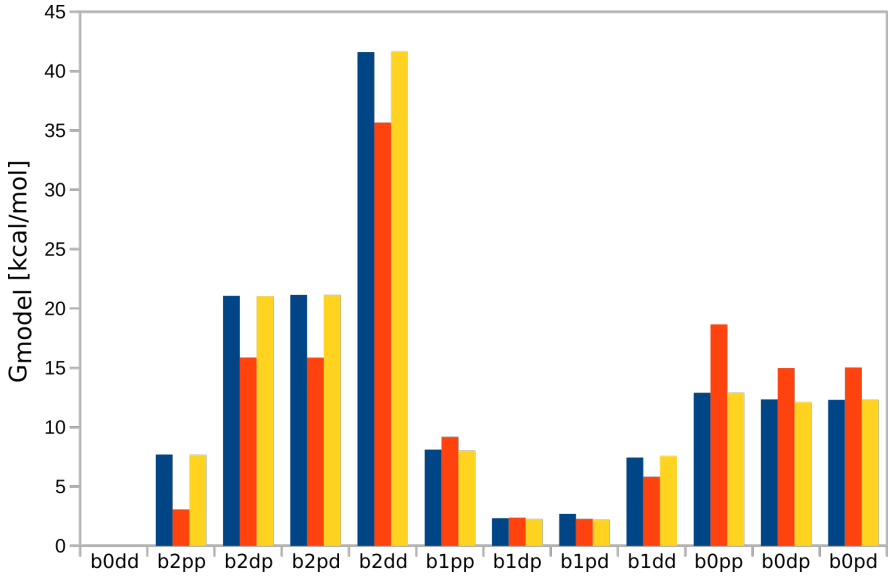

Figure 3.11: Comparison of the different functionals and the resulting G_{model}-values (blue: B3LYP, orange: M062X and yellow: WB97X-D3). The state b0dd is set to zero.

Because of the problem with calculating the pK_a-values and redox potentials for ubiquinone, an intermediate step was developed. First, the G_{model}-values for benzoquinone were calculated based on quantum chemical calculation and experimental data (*25*). The quantum chemical calculation took place in implicit water. But a direct use of the determined values of benzoquinone, of which more and better experimental values are available, as a model structure was not possible. That can be explained by the fact that already the experimental values of benzoquinone and ubiquinone differ in the pH-dependency and pK_a-values (*28*). Thus, benzoquinone and ubiquinone behave differently. Benzoquinone is not simply a simplified structure of ubiquinone despite the similar basic structure. The substituents of ubiquinone lead to the loss of the symmetry axis by the two oxygen atoms O1 and O4. That also explains why the position of the hydrogen atoms at O1 and O4 have an effect on the pK_a-values or redox potentials. Subsequently, equation (3.32) was used to perform further calculations to determine a correction factor.

$$\Delta G_{model} = G_{model}(calc) - G_{model}(exp) \tag{3.32}$$

In table 3.3 are the results of the respective calculations. Clearly seen in the ΔG_{model}-value column is that the b2dp, b2pd, b2dd, b0pp, b0dp, and b0pd states show large deviations from the experimental results. These states are all difficult to determine experimentally and in the case of ubiquinone impossible to determine at all. The combination of protons and electrons makes it difficult to stabilize the respective structures in water. But also theoretically it was difficult to describe the states like b2dd and b0pp energetically, as can be seen from the corresponding energies. The reason for these difficulties could not be conclusively determined, since the structures did not show any abnormalities and the electron and spin densities were also unremarkable. Changing the functionals did not help either, as mentioned above.

Table 3.3: G_{model}-values calculated from theoretical and experimental pK_a-values and redox potentials for benzoquinone. The ΔG_{model}-values is the difference between theoretical and experimental G_{model}-values. The states are explained in figure 3.9 A. All G_{model}-values are in $\frac{kcal}{mol}$.

states	#protons	#electrons	G_{model} theoretical	G_{model} experimental	ΔG_{model}
b0dd	0	0	0.00	0.00	0.00
b2pp	2	2	−24.30	−31.99	7.69
b2dp	1	2	2.99	−18.07	21.06
b2pd	1	2	3.07	−18.07	21.14
b2dd	0	2	38.75	−2.85	41.60
b1pp	2	1	1.71	−6.39	8.10
b1dp	1	1	−5.16	−7.49	2.33
b1pd	1	1	−4.80	−7.49	2.69
b1dd	0	1	5.15	−2.28	7.43
b0pp	2	0	60.91	48.01	12.90
b0dp	1	0	22.35	10.01	12.34
b0pd	1	0	22.31	10.01	12.30

In the next step, the determined correction factors, which should compensate the existing weaknesses in the theoretical determination, are used to correct the pK_a-values and redox potentials for ubiquinone (table 3.4). Here, it is not crucial that benzoquinone cannot serve as a model compound for ubiquinone. It is much more crucial that the same functionals are used and that a similar "computational error" can be assumed in the theoretical consideration. In the case of benzoquinone and ubiquinone, that is possible because both have the same electronic configuration. The determination of the corresponding ΔG_{model}-values as a correction for ubiquinone allowed to improve the G_{model}-values. For example, there is a smaller difference of now 0.05 $\frac{kcal}{mol}$ for reaction of u1dd to u2dd (figure 3.10 and table 3.4). The procedure involving benzoquinone also made it possible to determine corrected values for ubiquinone that could not be measured experimentally and could not have been determined without a theoretical calculation. Afterwards, the G_{model}-values for the (u2dp,u2pd), (u1dp,u1pd) and (u0dp,u0pd) states were symmetrized, because calculations on imidazole and methylimidazole showed that despite an asymmetry in the molecule, the sites should be treated symmetrically, since they have the same or very similar pK_a-values. Figure 3.12 shows the occupancy probabilities of the individual states of ubiquinol/ubiquinone. The occupancy probabilities clearly show that the semiquinone states, with the exception of the u1dd state, are not visibly populated in aqueous ionic solution. The lack of occupancy probabilities for the semiquinone states u1dp or u1pd is chemically counterintuitive and is caused by problems with the experimental values. However, there is no alternative for these experimental values up to now.

Table 3.4: G_{model}-values calculated from theoretical pK_a-values and redox potentials for ubiquinone and the corrected G_{model}-values for benzoquinone. The ΔG_{model}-values are the difference between theoretical G_{model}-values for ubiquinone corrected G_{model}-values for benzoquinone. The states are explained in figure 3.9 B. All G_{model}-values are in $\frac{kcal}{mol}$.

states	#protons	#electrons	G_{model} theoretical	ΔG_{model} benzoquinone	ΔG_{model}	ΔG_{model} symmetrized
u0dd	0	0	0.00	0.00	0.00	0.00
u2pp	2	2	−12.99	7.69	−20.68	−20.68
u2dp	1	2	13.52	21.06	−7.54	−6.74
u2pd	1	2	15.20	21.14	−5.94	−6.74
u2dd	0	2	51.85	41.60	10.25	10.25
u1pp	2	1	4.04	8.10	−4.06	−4.06
u1dp	1	1	−1.05	2.33	−3.38	−2.66
u1pd	1	1	0.75	2.69	−1.94	−2.66
u1dd	0	1	13.14	7.43	5.70	5.70
u0pp	2	0	55.99	12.90	43.09	43.09
u0dp	1	0	14.79	12.34	2.45	3.05
u0pd	1	0	15.94	12.30	3.64	3.05

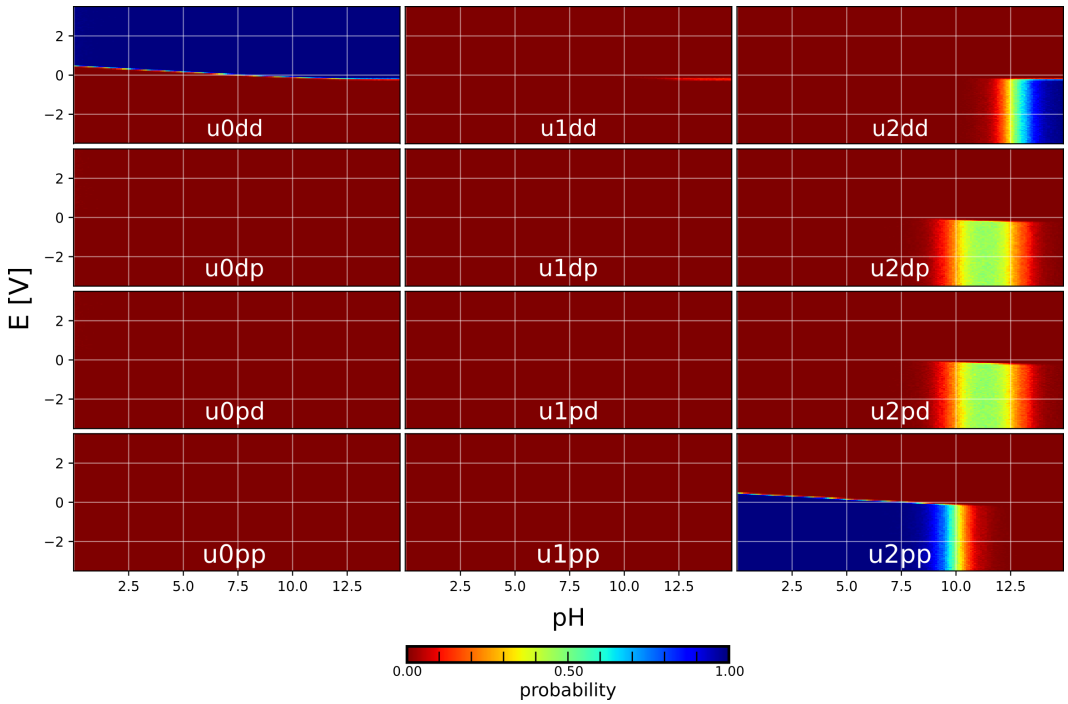

Figure 3.12: Pourbaix-like diagram of probabilities based on the symmetrized ΔG_{model}-values for all twelve states which can be found in table 3.4.

3.6 Conclusion

The G_{model}-values for imidazole and the corresponding analogues could be calculated with sufficient accuracy with the problems discussed. Difficulties are encountered in determining significant energies for certain states because the implicit solvent, especially water, cannot cover all properties. That is evidenced by the fact that explicit water molecules give the corresponding energy or pK_a-values much closer to the experimental pK_a-values. However, the use of explicit water molecules leads to other problem because the dipole properties can lead to computational problems. When determining the pK_a-values for ubiquinol, even more problems become apparent because the molecule is more complex and has semiquinone states. For example, the orientation of the hydrogen atoms at O1 and O4 and the methyl esters were found to affect the pK_a-values and redox potentials. The use of explicit water is not useful because it would affect the position of the hydrogen atoms too much. Further tests regarding basis sets and functionals to improve the determined correction factor would be useful for future investigations, since for the calculations performed here the obtained accuracy was sufficient.

References

(*1*) Radzisewski, B. (1882). Ueber Glyoxalin und seine Homologe. *Ber Dtsch Chem Ges 15*, 2706–2708, DOI: 10.1002/cber.188201502245.

(*2*) Debus, H. (1858). Ueber die Einwirkung des Ammoniaks auf Glyoxal. *Annalen der Chemie und Pharmacie 107*, 199–208, DOI: 10.1002/jlac.18581070209.

(*3*) Carnot, S. (1824). Réflexions sur la puissance motrice du feu et sur les machines propres à développer cette puissance.

(*4*) Casasnovas, R., Frau, J., Ortega-Castro, J., Salvà, A., Donoso, J., and Muñoz, F. (2009). Absolute and relative pKa calculations of mono and diprotic pyridines by quantum methods. *J Mol Struc-Theochem 912*, 5–12, DOI: 10.1016/j.theochem.2008.11.020.

(*5*) Casasnovas, R., Ortega-Castro, J., Frau, J., Donoso, J., and Muñoz, F. (2014). Theoretical pKa calculations with continuum model solvents, alternative protocols to thermodynamic cycles. *Int J Quantum Chem 114*, 1350–1363, DOI: 10.1002/qua.24699.

(*6*) McQuarrie, D. A., *Statistical Mechanics*; Harper's chemistry series; Longman: London, England, 1976.

(*7*) Liptak, M. D., and Shields, G. C. (2001). Accurate pKa Calculations for Carboxylic Acids Using Complete Basis Set and Gaussian-n Models Combined with CPCM Continuum Solvation Methods. *J Am Chem Soc 123*, 7314–7319, DOI: 10.1021/ja010534f.

(*8*) Liptak, M. D., Gross, K. C., Seybold, P. G., Feldgus, S., and Shields, G. C. (2002). Absolute pKa Determinations for Substituted Phenols. *J Am Chem Soc 124*, 6421–6427, DOI: 10.1021/ja012474j.

(*9*) Palascak, M. W., and Shields, G. C. (2004). Accurate Experimental Values for the Free Energies of Hydration of H+, OH-, and H3O+. *J Phys Chem A 108*, 3692–3694, DOI: 10.1021/jp049914o.

(*10*) Pliego, J. R., and Riveros, J. M. (2000). New values for the absolute solvation free energy of univalent ions in aqueous solution. *Chem Phys Lett 332*, 597–602, DOI: 10.1016/s0009-2614(00)01305-1.

(*11*) Marković, Z., Tošović, J., Milenković, D., and Marković, S. (2016). Revisiting the solvation enthalpies and free energies of the proton and electron in various solvents. *Comput Theor Chem 1077*, 11–17, DOI: 10.1016/j.comptc.2015.09.007.

(*12*) Shields, G. C., *Computational Approaches for the Prediction of pKa Values*; CRC Press: 2013, DOI: 10.1201/b16128.

(*13*) BKChem, https://bkchem.zirael.org/, Accessed: 2022-05-28.

(*14*) Neese, F. (2012). The ORCA program system. *Wires Comput Mol Sci 2*, 73–78.

(*15*) University, T., and University, N. iBonD 2.0 http://http://ibond.nankai.edu.cn/pka/ (accessed June 18, 2023).

(*16*) LENARCIK, B., KURDZIEL, K., and CZOPEK, R. (1986). Search Foh Optimum Conditions Of Extraction Of Metal Complexes With Alkylimidazoles. III. Structure - Extractability Relationships For 1,4-DiMethylImidazole Complexes Of Co(II), Ni(II), Cu(II), Zn(II), And Cd(II). *Solvent Extr Ion Exc 4*, 165–182, DOI: 10.1080/07366298608917860.

(*17*) Broughton, H. B., Green, S. M., and Rzepa, H. S. (1995). Studies of imidazole and pyrazole protonation using electrostatically trained neural networks. *J Chem Soc Perk T 2*, 431, DOI: 10.1039/p29950000431.

(*18*) Kirby, A. H., and Neuberger, A. (1938). Glyoxalines: the determination of their pK values and the use of their salts as buffers. *Biochem J 32*, 1146–1151, DOI: 10.1042/bj0321146.

(*19*) Guthrie, J. P., and Pike, D. C. (1987). Hydration of acylimidazoles: tetrahedral intermediates in acylimidazole hydrolysis and nucleophilic attack by imidazole on esters. The question of concerted mechanisms for acyl transfers. *Can J Chem 65*, 1951–1969, DOI: 10.1139/v87-326.

(*20*) Danovich, D. K., and Turchaninov, V. K. (1989). Basicity of azoles. 1. Investigation of total energy of pyrazole and imidazole derivatives by the partitioning method. *B Acad Sci Ussr Ch+ 38*, 1182–1187, DOI: 10.1007/bf00957150.

(*21*) Walba, H., and Isensee, R. W. (1961). Acidity Constants of Some Arylimidazoles and Their Cations. *J Org Chem 26*, 2789–2791, DOI: 10.1021/jo01066a039.

(*22*) Catalan, J., and Elguero, J. In *Adv Heterocycle Chem Volume 41*; Elsevier: 1987, pp 187–274, DOI: 10.1016/s0065-2725(08)60162-2.

(*23*) Yagil, G. (1967). The proton dissociation constant of pyrrole, indole and related compounds. *Tetrahedron 23*, 2855–2861, DOI: 10.1016/0040-4020(67)85151-2.

(*24*) Thapa, B., and Schlegel, H. B. (2016). Density Functional Theory Calculation of pKa's of Thiols in Aqueous Solution Using Explicit Water Molecules and the Polarizable Continuum Model. *J Phys Chem A 120*, 5726–5735, DOI: 10.1021/acs.jpca.6b05040.

(*25*) Che, C., *Electrochemical Reactions of Quinones at Conducting Polymer Electrodes*; Linköping University Electronic Press: 2019, DOI: 10.3384/diss.diva-161645.

(*26*) Zhu, Z., and Gunner, M. R. (2004). Energetics of Quinone-Dependent Electron and Proton Transfers in Rhodobacter sphaeroides Photosynthetic Reaction Centers. *Biochemistry 44*, 82–96, DOI: 10.1021/bi048348k.

(*27*) Huynh, M. T., Anson, C. W., Cavell, A. C., Stahl, S. S., and Hammes-Schiffer, S. (2016). Quinone 1 e- and 2 e- Reduction Potentials: Identification and Analysis of Deviations from Systematic Scaling Relationships. *J Am Chem Soc 138*, 15903–15910, DOI: 10.1021/jacs.6b05797.

(*28*) Mukai, K., Tokunaga, A., Itoh, S., Kanesaki, Y., Ohara, K., Nagaoka, S.-i., and Abe, K. (2007). Structure-Activity Relationship of the Free-Radical-Scavenging Reaction by Vitamin E (alpha-, beta-, gamma-, delta-Tocopherols) and Ubiquinol-10: pH Dependence of the Reaction Rates. *J Phys Chem B 111*, 652–662, DOI: 10.1021/jp0650580.

4

OBTAINING G_{model} DIRECTLY FROM EXPERIMENTAL DATA USING VIRTUAL MODEL COMPOUNDS WITH APPLICATIONS TO HEME GROUPS

In this chapter, the micro/macrostate model is used to determine the redox potential within the programs `preptitra` (*1*) and `gmct` (*2*). In contrast to the chapters 3 and 5, no quantum mechanical calculations were used but only electrostatic calculations and it is an intuitive way to determine the G_{model}-value. The cofactors of the bc_1-complex the b-type and c-type heme groups will be considered. The model redox potential must be determined. No model compounds could be found or created for the two heme groups. Only experimental values for the cytochrome b_5 and c type proteins are available.These proteins cannot be used as model compounds because they do not satisfy the conditions from chapter 2. However, it is still possible to use the proteins as a model for the corresponding heme groups. A model should be correct, complete, general and simple. The conditions are fulfilled by these proteins. They contain only one heme group and are therefore simple. They represent the heme group correctly and completely. Because several proteins are used, the model is also generally valid. So all conditions of a model are fulfilled. But no model compound is directly given and also several proteins are combined to one model(compound). For this reason, it is a so-called virtual model compound.

Cytochromes *per se* were discovered as early as 1884 (*3*), but it took 40 years (*4*) until various classes of cytochromes were defined. Cytochrome c consists of about 100 amino acids - depending on the organism. It is like cytochrome b involved in metabolic processes (*5*). But cytochrome b is much larger, consisting of up to 400 amino acids. Because of the property of iron in the heme group to change its oxidation state, they act as electron transporters and carriers. Thus, they play an important role not only in the respiratory chain but also in photosynthesis, for example, in the bc_1-complex. For their theoretical study, it is crucial to have good model representations for the heme groups heme c and heme b. The available model redox potentials should be critically reviewed (see Moa *et al.* (*6*)). Because of that the model redox potentials are determined by a method developed in your group.

4.2 Theory

Crystal structures and experimental redox potentials are needed to calculate and validate the redox potentials. Using the methods of the programs `preptitra` and `gmct`, the redox potentials of cytochrome b_5 and c were calculated. The cytochrome b_5 represents the model compound for a bis-His heme and the cytochrome c represents a His-Met heme. To determine the model redox potential, the G_{model}-value is set to zero during the calculation and the redox potential is calculated. The redox potentials calculated in this way are plotted against the experimental redox potentials and fit a straight line with a slope of one. The intercept of this straight line with the y-axis is our model redox potential (G_{model}-value). To find the linear regression for N data points with a least squares method the following equation (4.1) has to be solved.

$$\sum_{i=1}^{N} \left(f\left(x_i, \vec{a}\right) - y_i\right)^2 \rightarrow \min_{a_0, a_1} \tag{4.1}$$

with the model function

$$f\left(x, \vec{a}\right) = a_0 + a_1 \cdot x \tag{4.2}$$

The resulting linear equation system can be solved (see appendix D) and the result is the intercept

$$a_0 = \overline{y} - a_1 \cdot \overline{x} \text{ with } \overline{x} \text{ and } \overline{y} \text{ as mean value} \tag{4.3}$$

and the slope

$$a_1 = \frac{\sum_{i=1}^{n}\left(x_i - \overline{x}\right)\left(y_i - \overline{y}\right)}{\sum_{i=1}^{n}\left(x_i - \overline{x}\right)^2} \text{ with } \overline{x} \text{ and } \overline{y} \text{ as mean value} \tag{4.4}$$

The equation (2.7) can be rewritten as an equation in the form of equation (4.2). The two energies are thereby summed up to form ΔE_{shift}.

$$f\left(x, \vec{a}\right) = G_{model} + a_1 \cdot \underbrace{\left(G_{solv,c} + G_{back,c}\right)}_{\Delta E_{shift}} \tag{4.5}$$

In this case the slope is one to fulfill equation (2.7), so the intercept a_0 can be calculated directly. With this approach, the equation (4.3) can be written as

$$\underbrace{G_{model}}_{a_0} = \frac{1}{N}\sum_{i=1}^{N}\left(\underbrace{E_{exp,i}}_{y_i} - \underbrace{\Delta E_{shift,i}}_{x_i}\right) \tag{4.6}$$

The y-values correspond to the found experimental redox potentials ($E_{exp,i}$) and the x-values are the calculated shifts of the redox potential by the protein environment ($E_{shift,i}$). The intercept is then the G_{model}-value.

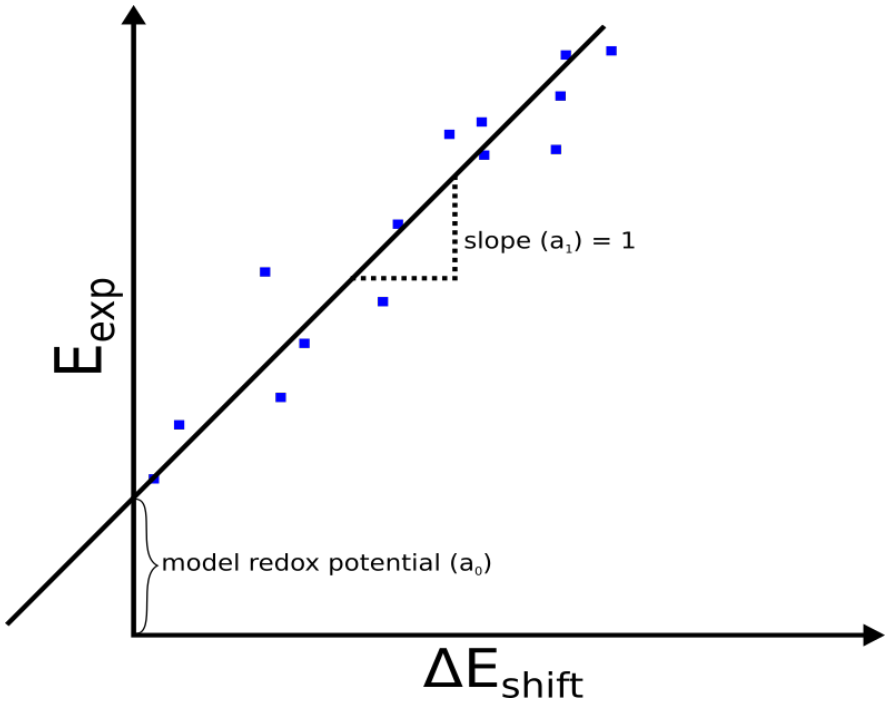

Figure 4.1: Example for the plotting of experimental and calculated values and determination of linear regression.

4.3 Methods

Before starting the calculations, suitable candidates had to be found, for which both a good crystal structure with a resolution of less than 2.5 Å and the experimental redox potential are known. The required crystal structures of the two cytochromes b_5 and c_x are available on the site *Protein Data Bank (PDB)* and the potentials are known. C_x represents the different types of C-type heme with c_6, c_2 or $c_{55.}$. NMR structures were not used because the structures showed too large deviations. For this reason only the crystal structures were used.

The crystal structures for which electron densities are available were re-refined by hand in `phenix-1.17.1-3660` (*7*). The unrefined and re-refined structures were then converted into a pqr file using `CHARMM` and an in-house program. The redox potential for the various protein structures were then calculated using the two programs `preptitra` and `gmct`. Two different calculations were performed in `preptitra`. One calculation was done with an ionic strength of 0.150 M. The other calculation used the ionic strength in the determination of the redox potential. To determine the model redox potential based on these redox potentials, the G_{model}-value was set to zero in the xst-files. The structure of xst-files for b-type and c-type heme is described in listings A.1 and A.2. The required charges for the xst-files were determined for the b-type and c-type hemes using the quantum chemistry program package `orca` and CHELPG. To compare the different structures of the cytochromes, TM alignments (*8*) were performed with default settings and then a hierarchically-clustered heatmap was generated for the determined RMSD. All settings for the different programs and the computational details are listed in appendices A.1, A.3 and A.4. The mean absolute error (MAE) was used as a measure for the evaluation and classification of the results.

$$MAE = \frac{1}{n} \sum_{i=1}^{n} \mid \hat{Y}_i - Y_i \mid \tag{4.7}$$

with

n: Number of values

$\hat{Y}_i$: experimental redox potential

Y_i: calculated redox potential

Another measure for the evaluation and classification of results would be the coefficient of determination (R^2).

$$R^2 = 1 - \frac{\sum_{i=1}^{n} \left(Y_i - \hat{Y}_i\right)^2}{\sum_{i=1}^{n} \left(Y_i - \overline{Y}\right)^2} \tag{4.8}$$

with

n: Number of values

$\hat{Y}_i$: experimental value/redox potential

Y_i: calculated value/redox potential

$\overline{Y}$: mean value/calculated redox potential

The interpretation of the R^2-value is a little bit difficult in the given context, because there is one degree of freedom less due to the determination of the slope of the model. Based on this described fact, the R^2-value can be misleading and is not used as a quality measure in this work. The MAE, on the other hand, is a measure of the accuracy of the calculated values. In contrast to the coefficient of determination, the mean absolute error is more robust with respect to correlation effects (*9*).

4.4 Determination of the G_{model}-values for B-type and C-type Hemes

It is needed to determine the G_{model}-values for b-type and c-type hemes, since, as mentioned in the introduction, they are present in the bc_1-complex. This complex is composed, among others, of cytochromes b and cytochromes c. These proteins also occur in simpler and non-complexed structural units such as cytochrome b_5 and cytochrome c_x. Proteins are suitable for our method because they contain only one heme group as a cofactor. In addition, they are quite small with about 100 amino acids and the calculations can be done quickly. Wilson *et al.* (*10*) already have experimental model redox potentials for these heme types. These data are from 1974 and did not show any redox potentials in our calculations that correspond to experimental values. For this reason the decision was to determine the values again with the here described determination methods. There was no splitting of the data set into a test set and a fit set as described in Roy *et al.* (*11*) because the method was already evaluated sufficiently there and the small data set would have been further reduced.

4.4.1 Cytochrome b_5

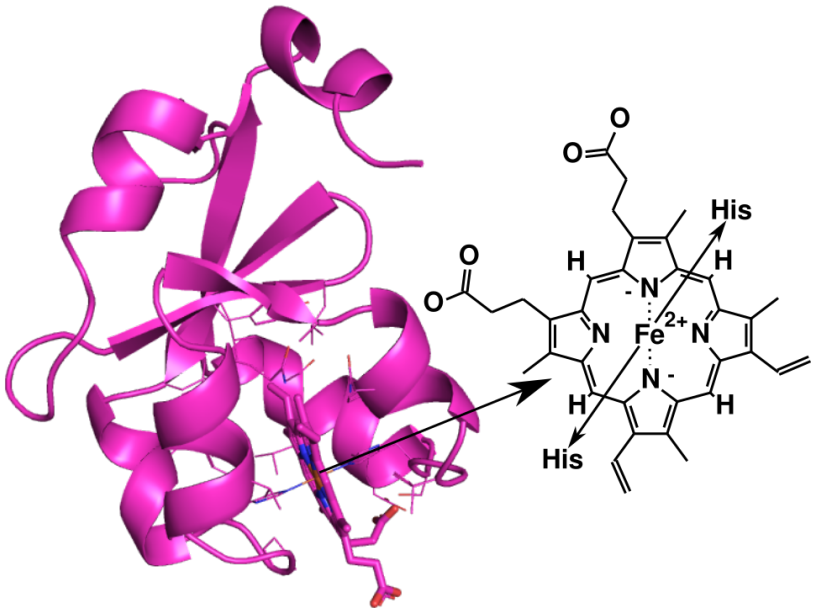

Figure 4.2: Representing example of all cytochrome b_5 structures (pdb-ID: 1CYO) with enlarged heme group.

14 different cytochromes b_5 were found for which experimental redox potentials are known. Of these 14 cytochromes, the structure factors of twelve structures were submitted to the PDB database. These twelve structures were re-refined in Phenix, which improved the clash score of all structures except with the pdb-IDs 4HIL, 1M2I and 2IBJ. The R-value has also improved for all structures except 4HIL. Thus, 4HIL is the only structure where the clash score as well as the R-value worsened due to the refinement.

The hierarchically-clustered heatmap (figure 4.3) generated based on TM alignments clearly shows that cytochromes b_5 occur in a large cluster with the exception of 1X3X. Within this large cluster, the structures of 1LR6, 1ES1, 1LQX, 1EHB, and 1M2I show a large correspondence. That is because the structures are different point mutations of the same b-type cytochrome. The other structures are also not significantly different when looking at the RMSD values.

Table 4.1: G_{model}-values and mean absolute error for the fits of figure 4.5 in $[V]$ for not re-refined (noref) and re-refined (ref) cytochromes b_5. The different experimental ionic strengths are listed in table D.2. The experimental model redox potential for a bis-his-mesoheme is -0.220 V measured by Wilson *et al.* (*10*, *12*).

	value $[V]$ at ionic strength 150 mM	value $[V]$ at different experimental ionic strength
G_{model} (noref)	-0.028	-0.012
G_{model} (ref)	-0.037	-0.021
MAE (noref)	0.036	0.030
MAE (ref)	0.035	0.025

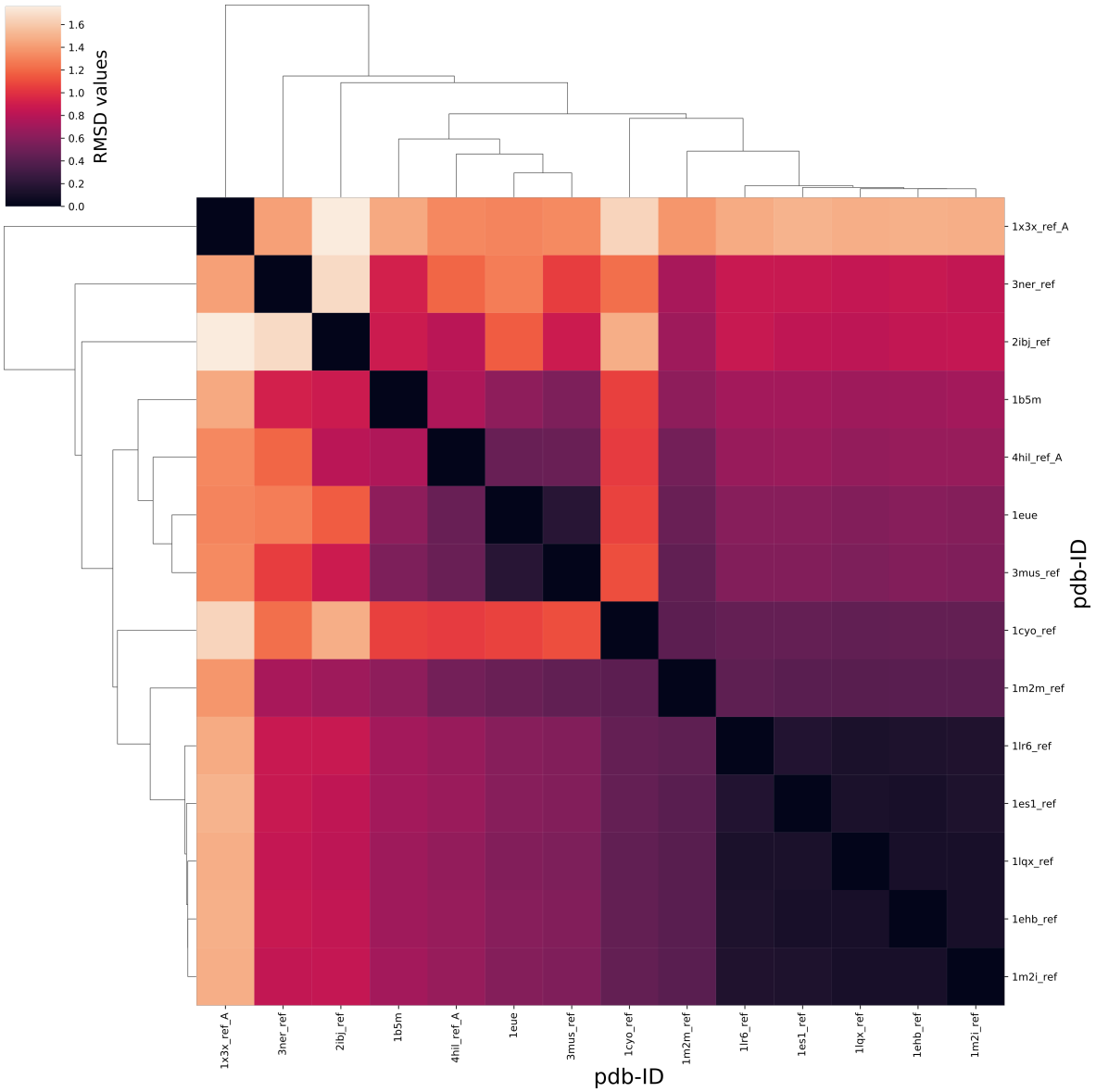

Figure 4.3: Hierarchically-clustered heatmap based on RMSD values from pairwise TM alignments of different cytochromes b_5. The darker the coloration the lower the RMSD value.

The figure 4.5 shows the results of the redox potential calculations plotted against the experimental values. Refinement has shifted the regression line downwards in both cases, making the G_{model}-value more negative. It can also be seen that the refinement has reduced the spread of the values. The MAE has improved from 0.036 V to 0.035 V and from 0.035 V to 0.025 V in the variable ionic strength case. The G_{model}-value has decreased from -0.028 V to -0.037 V and from -0.012 V to -0.021 V in the variable ionic strength case. The MAE becomes smaller from 0.036 to 0.030 when using the re-refined structures, but only minimally. The difference in G_{model}-value between fixed ionic strength and variable ionic strength is greater than for cytochromes c_x because the average ionic strength of 0.068 M is less than half the fixed value of 0.150 M. That leads to a strong shift of the values. However, the G_{model}-values differ up to 0.208 V to the experimental value of -0.220 V for a bis-his-mesoheme measured by Wilson *et al.* (*10*, *12*).

The re-refined structures 4HIL and 1M2I, which show a reduction of the R-value or clash score, are now closer to the experimental redox potential. That is in contrast to structure 2IBJ which redox potential shifts away from the experimental value by 10 mV after refinement. However, no evidence could be found in the protein structure to explain this deterioration. A superposition of the original structure with the re-refined structure shows no major change in the vicinity of the redox center. The structures 1EHB, 1LQX, 1M2M, 1LR6, and 3NER show an improvement in R-values and clash scores after refinement. At the same time, the shift of the calculated redox potential worsens with respect to the experimental values.

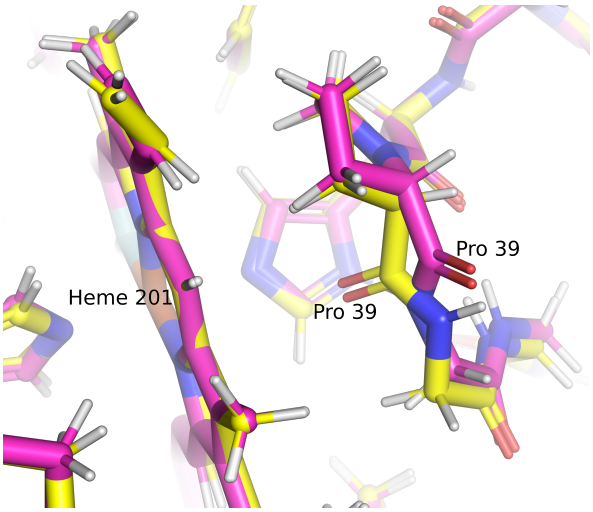

Figure 4.4: Problematic position of oxygen in the peptide bond to Pro39 opposite of the b-type heme group in the yellow structure (pdb-ID: 1X3X), which was eliminated by a refinement (purple structure).

The protein structure 1X3X is a good example to illustrate why a re-refinement may be necessary in general. In figure 4.4 the chain B of the protein can be seen. This chain contains the Pro39. This Pro39 is located near the redox active heme. It can be seen that the oxygen of the peptide bond of the yellow structure (re-refined) points towards the heme, while in the pink structure this oxygen points away from the heme. The electron density makes it clear that the oxygen must have the position of the yellow structure. That is the most obvious change within this structure and results in a shift of the calculated redox potential from 0.020 V to 0.080 V. Thus this "small" change in the structure leads to a shift of 60 mV. This shift also leads to a closer approximation to the experimental redox potential. For this reason, a close examination and possibly a re-refinement of the structure should always be considered. However, as MAE improves, it is a sign that all structures show only a similar shift and in that case the G_{model}-value becomes more generally valid since the G_{model}-value also represents a shift in the calculated theoretical redox potential.
The figure 4.5 shows that the use of different ionic strengths and refinements leads to an improvement in the representation of the experimental redox potential. The regression line is much closer to the theoretical best regression line (figure 4.5 blue straight line). The theoretical best regression line indicates that experimental and theoretical redox potential are identical and perfectly described by the theory.

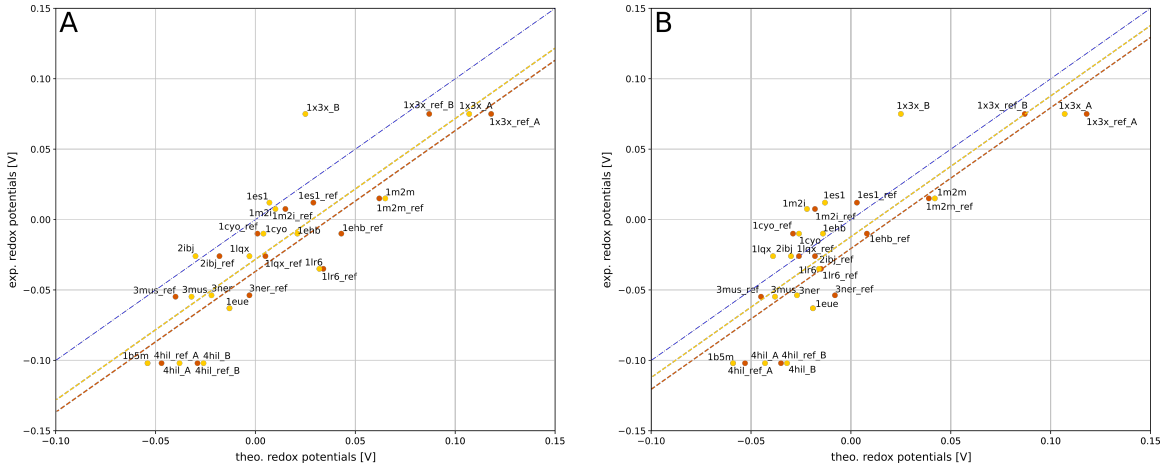

Figure 4.5: Regression line for cytochrome b_5. In orange are the re-refined, in yellow are the not re-refined structures and in blue the perfect fit line if all experimental and theoretical redox potential match each other.
A: All calculations with a ionic strength of 0.150 M NaCl
B: All calculations with the ionic strength from table D.2

4.4.2 Cytochrome c

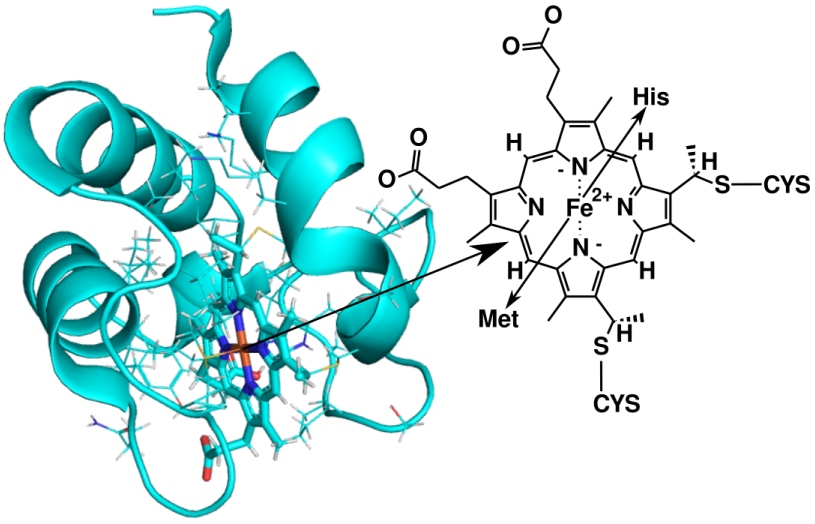

Figure 4.6: Representing example of all cytochrome c structures (pdb-ID: 1C75) with enlarged heme group.

24 different cytochromes c_x could be found for which experimental redox potentials are known. Of these 24 cytochromes, the structure factors of 18 structures were submitted to the PDB database. These 18 structures were re-refined in Phenix, which improved the clash score of all structures except 1CTJ, 1CYI, 2DGE and 351C. For all structures except 1C75, 1CTJ, 1CYI, 1LS9, 2YCC and 6U97 the R-value has also been improved. For the 1CTJ and 1CYI structures, the clash score and R value worsened as a result of the refinement.
The hierarchically-clustered heatmap (figure 4.7) based on the TM alignments clearly shows that the c-type cytochromes are divided into two large clusters and one to three smaller clusters. The diversity

of the structures is also evident from the larger scatter of the RMSD values. The distribution of these clusters does not fully correspond to the later clusters in the shift of redox potentials. But they give a first indication that the structures of the different c-type cytochromes are more distinct and yet have structural similarities. The two major clusters include cytochromes c_2 and cytochromes c_6. In the smaller clusters are the cytochromes c_{552}, c_{553} and c_{551}. The figure 4.8 shows the results of the redox

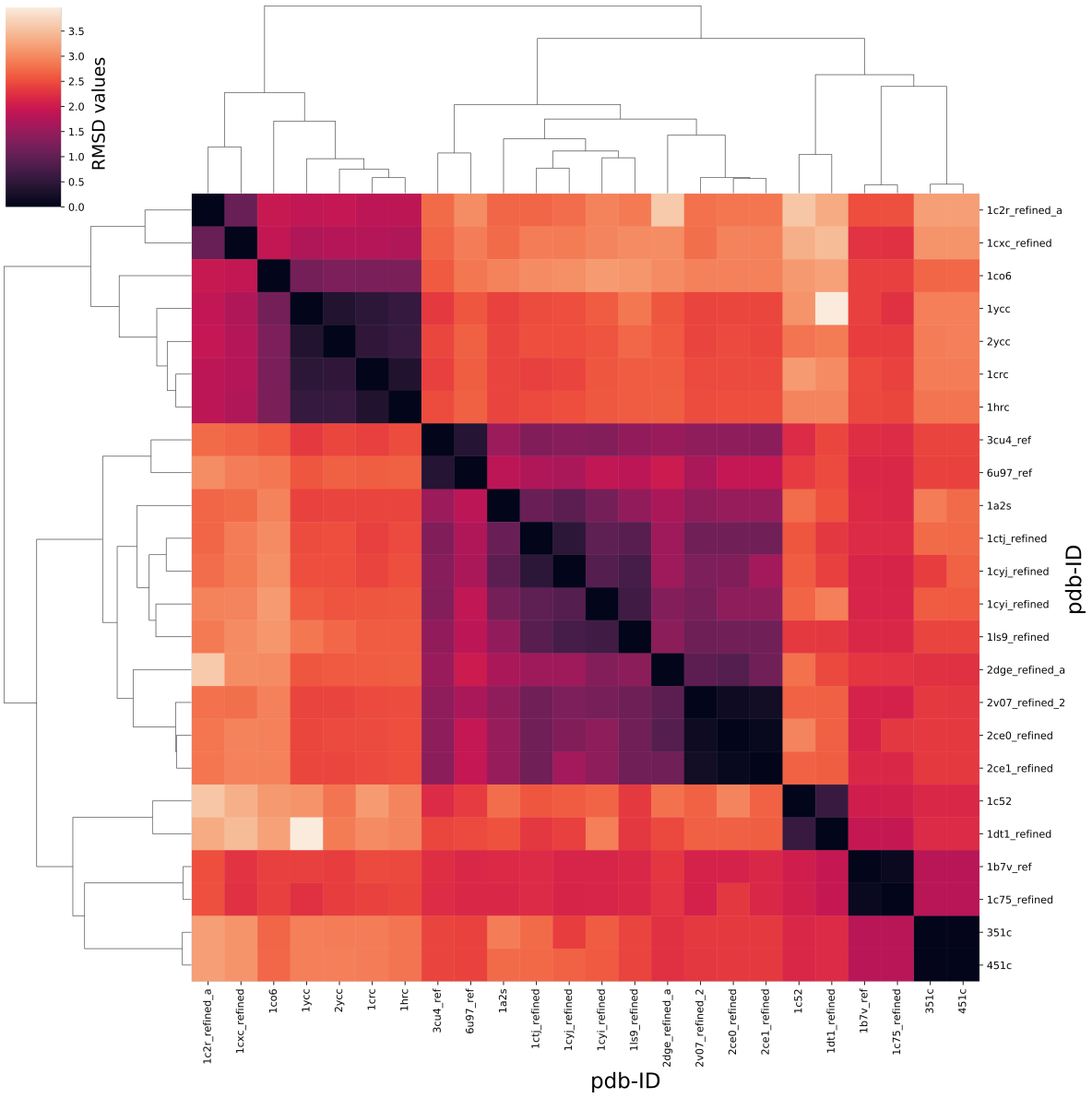

Figure 4.7: Hierarchically-clustered heatmap based on RMSD values from pairwise TM alignments of different cytochromes c_x. The darker the coloration the lower the RMSD value.

potential calculations plotted against the experimental values. The refinement has shifted the balance line downward in both cases, making the G_{model}-value more negative, as it did for the b_5 cytochromes. It can also be seen that the refinement has reduced the dispersion of the values. The mean absolute error (MAE) was also determined here. The MAE difference is very small with 0.001 V. The MAE values have not improved from 0.188 V to 0.187 V and from 0.188 V to 0.187 V in the variable ionic strength case. The G_{model}-value has decreased from 0.188 V to 0.181 V and from 0.188 V to

Table 4.2: G_{model}-values and mean absolute error for the fits of figure 4.5 in $[V]$ for not re-refined (noref) and re-refined (ref) cytochromes c_x. The different experimental ionic strengths are listed in tables D.5 and D.6. The experimental model redox potential for a hismet-mesoheme is -0.074 V measured by Wilson *et al.* (*10*, *12*).

	value $[V]$ at ionic strength 150 mM	value $[V]$ at different experimental ionic strength
G_{model} (noref)	0.188	0.188
G_{model} (ref)	0.181	0.181
MAE (noref)	0.188	0.188
MAE (ref)	0.187	0.187

0.181 V in the case of variable ionic strength. In contrast to the cytochromes b_5, the difference of the G_{model}-value between fixed ionic strength and variable ionic strength is very small. This is because the average ionic strength of 0.125 M is already very close to the fixed value of 0.150 M. However, the G_{model}-values are about 0.255 V higher than the -0.074 V for a hismet-mesoheme and 0.075 V lower than the 0.256 V for a cytochrome c measured by Wilson *et al.* (*10*, *12*). As mentioned in section 4.4.1, less attention should be paid to the absolute shift in redox potential due to the re-refinement, but more to the MAE value, which reflects the dispersion of the values. This value improves when re-refined structures are used. Despite the improvement of the calculated redox potential, the figure 4.8 shows that the regression line deviates from the theoretical best regression line with the magnitude of the MAE. This deviation is considerable and is probably caused by the diversity of the c-type heme. This diversity can also be seen in the figure 4.8, as the experimental redox potential scatter in a range of about 350 mV. In b-type heme this scattering is only in a range of about 200 mV.

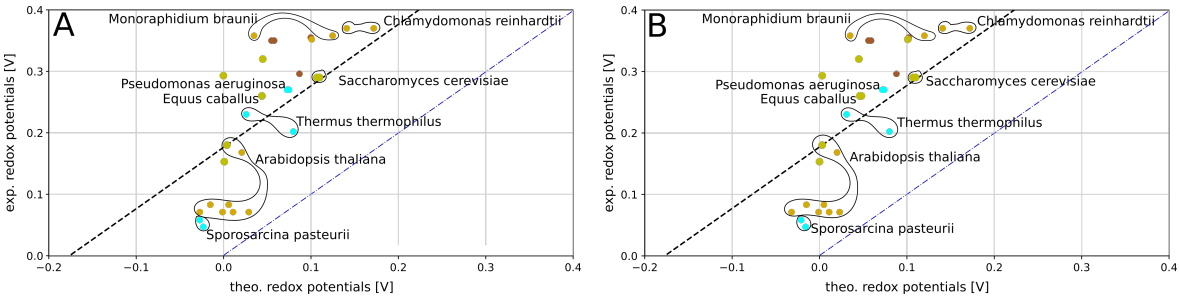

Figure 4.8: Regression line for cytochrome c_x. For subfigures A and B, all cytochromes c_2 are shown in ochre, all cytochromes c_{55x} in turquoise and all cytochromes c_6 in brown. The prefect fit line if all experimental and theoretical redox potential match each other is shown in blue.
A: All calculations run with a ionic strength of 0.150 M NaCl
B: All calculations run with the ionic strength from tables D.5 and D.6

4.5 Conclusion

The determined G_{model}-values for cytochromes b_5 and c_x differ strongly from the experimentally determined values of Wilson *et al.* (*10*) at approximately 0.2 V and 0.255 V, respectively. Weaknesses are also apparent in the model compounds proposed by Wilson *et al.* (*10*) because it was not exactly clear whether the model compounds really looked as expected, as in the protonation state, for example. Another weakness is that the used model compound is synthesized by the covalent binding of the coordinating histidines or methionines to the propionic acid groups through a peptide bond. However,

this procedure causes a negative charge by the acid group of the amino acid used near the iron. This negative charge can have a strong influence on the measured redox potentials and is not present like that in a protein environment. The deviation of the G_{model}-values determined here from the values of Wilson *et al.* (*10*) is therefore not decisive for the evaluation. The redox potentials determined from these G_{model}-values for the respective cytochromes are much closer to the experimental values than with the values of Wilson *et al.* (*10*). In the work of Roy *et al.* (*11*) it became clear that refinements and ion concentration adjustment had an important and large effect on the redox potentials. This influence was also evident in when cytochromes were considered. The refinements improve the values and the reached accuracy of the determined G_{model}-values is sufficient to describe the bc_1-complex in chapter 7.

Furthermore, the comparison of cytochromes b_5 and c_x showed that cytochromes b_5 have less scattering in structures. In contrast, cytochromes c_x showed a strong difference between the individual structures. One reason for this is the large variance in cytochromes c_x which cover a broader redox potential spectrum than cytochromes b_5. For this reason, it was more difficult to find a generally valid G_{model}-value for the cytochromes c_x.

References

(*1*) Ullmann, G. M. (2023). GMCT@UBT Manual - Version 2.0.

(*2*) Ullmann, R. T., and Ullmann, G. M. (2012). GMCT : a Monte Carlo simulation package for macromolecular receptors. *J Comput Chem 33*, 887–900, DOI: 10.1002/jcc.22919.

(*3*) McMunn (1885). Proceeding Of The Physiological Society, 1884. No. IV. December13. *Jpn J Physiol 5*, xix–xxvi, DOI: 10.1113/jphysiol.1885.sp000178.

(*4*) Keilin, D. (1925). On cytochrome, a respiratory pigment, common to animals, yeast, and higher plants. *P R Soc Lond B-Conta 98*, 312–339, DOI: 10.1098/rspb.1925.0039.

(*5*) Fitch, W. M. (1976). The molecular evolution of cytochrome c in eukaryotes. *J Mol Evol 8*, 13–40, DOI: 10.1007/bf01738880.

(*6*) Mao, J., Hauser, K., and Gunner, M. R. (2003). How Cytochromes with Different Folds Control Heme Redox Potentials. *Biochemistry 42*, 9829–9840, DOI: 10.1021/bi027288k.

(*7*) Liebschner, D., Afonine, P. V., Baker, M. L., Bunkóczi, G., Chen, V. B., Croll, T. I., Hintze, B., Hung, L.-W., Jain, S., McCoy, A. J., Moriarty, N. W., Oeffner, R. D., Poon, B. K., Prisant, M. G., Read, R. J., Richardson, J. S., Richardson, D. C., Sammito, M. D., Sobolev, O. V., Stockwell, D. H., Terwilliger, T. C., Urzhumtsev, A. G., Videau, L. L., Williams, C. J., and Adams, P. D. (2019). Macromolecular structure determination using X-rays, neutrons and electrons: recent developments in Phenix. *Acta Crystallogr D 75*, 861–877, DOI: 10.1107/s2059798319011471.

(*8*) Zhang, Y. (2005). TM-align: a protein structure alignment algorithm based on the TM-score. *Nucleic Acids Res 33*, 2302–2309, DOI: 10.1093/nar/gki524.

(*9*) Schwen, L. O., and Rueschenbaum, S. (2018). Ten quick tips for getting the most scientific value out of numerical data. *PLOS Comput Biol 14*, e1006141, DOI: 10.1371/journal.pcbi.1006141.

(*10*) Wilson, G. S. (1974). Electrochemical studies of porphyrin redox reactions as cytochrome models. *Bioelectroch Bioener 1*, 172–179, DOI: 10.1016/0302-4598(74)85018-X.

(*11*) Roy, R. R., and Ullmann, G. M. (2023). Virtual Model Compound Approach for Calculating Redox Potentials of [Fe2S2]-Cys4 Centers in Proteins – Structure Quality Matters. *Journal of Chemical Theory and Computation 19*, 8930–8941, DOI: 10.1021/acs.jctc.3c00779.

(*12*) Warme, P. K., and Hager, L. P. (1970). Heme sulfuric anhydrides. II. Properties of heme models prepared from mesoheme sulfuric anhydrides. *Biochemistry-Us 9*, 1606–1614, DOI: 10.1021/bi00809a020.

5

OBTAINING G_{model} DIRECTLY FROM EXPERIMENTAL DATA USING EXTENDED MICRO AND MACROSTATE MODEL WITH APPLICATIONS TO FMN/RIESKE CENTER

In the previous chapter 3, the micro and macrostate model was introduced. It was shown that based on this model, using quantum mechanical calculations and thermodynamic cycles, the pK_a-values and redox potentials can be determined without the need of experimental values. In this chapter, the focus is now on compounds for which experimental values are available. But the evaluation of them is complicated because there are many states or the states are difficult to evaluate because of their chemical behaviors/properties, e.g. radical states. As also mentioned in chapter 3, micro and macrostate are also known from statistical physics and thermodynamics. It is also known from these fields that all systems in equilibrium have a Boltzmann distribution. So micro and macrostate systems in equilibrium adopt also a Boltzmann distribution:

$$\frac{n_i}{N} = \frac{e^{\frac{G_i}{kT}}}{\sum^N e^{\frac{G_i}{kT}}} \tag{5.1}$$

with

n_i: number of states in a site state i

N: total number of states in the system

G_i: energy of states in a site state i

T: temperature

k: Boltzmann constant.

The fraction $\frac{n_i}{N}$ can also be viewed as the probability of occurrence of state i (p_i). The equation (5.1) can also be written as

$$p_i = \frac{e^{\frac{G_i}{kT}}}{\sum^N e^{\frac{G_i}{kT}}} \tag{5.2}$$

building on the definitions and findings from chapter 3. Section 5.2 defines and extends the micro and macrostate model in more detail. The goal is to be able to determine pK_a-values and redox potentials as mentioned above. For this purpose, a program was written that can calculate the corresponding values. In the beginning of the work of Mayhew (*1*) was used as a basis to describe the behavior of flavin mathematically. In 1999 Mayhew presented a re-evaluation of the results of the pK_a-values and redox potentials for flavin which is not easy to evaluate. Flavins contain an isoalloxazine as a head group which can have very different side chains at the nitrogen N10. The isoalloxazine ring system

can accept two protons and two electrons at N5 and N1, resulting in nine different microstates. These nine different microstates are to be found in the experimental values. However, during the work of Dominik Lemm, an undergraduate student in our group, serious weaknesses in Mayhew's theoretical ideas became apparent and are explained in Lemm's thesis (*2*). As a result, the own existing theoretical framework was extended and a better description of the problem was found. This is now explained in the following and tested on an artificial system and used to determine the redox potentials and pK_a-values of a flavin and iron-sulfur system. The Rieske system has less microstates than a flavin. The iron-sulfur system studied here consists of an iron-sulfur center, two cysteines, and two histidines and is therefore also called a Rieske center. This structure results in one protonation site at each of the histidine and one electron binding site at the iron-sulfur center. Due to the combinatorics, this structure results in twelve different microstates which need to be investigated.

5.2 Theory

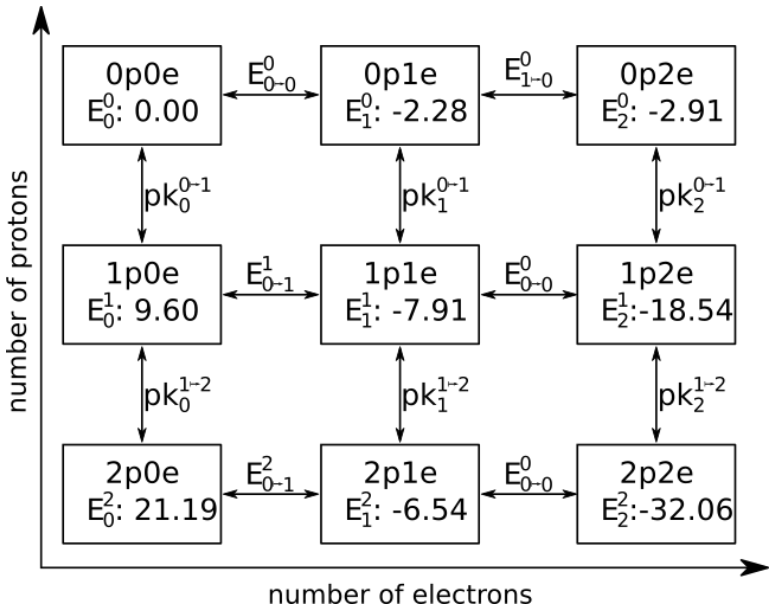

Figure 5.1: Artificial test system with nine different macrostate. Each macrostate is described by an energy. The transitions between the macrostates are described by redox potentials or pK_a-values.

Similar to chapter 3, an example will also be the test system for the algorithms and scripts. For this reason this system (figure 5.1) is introduced right at the beginning.

5.2.1 Micro and Macrostate

This example (figure 5.1) has nine different states: 0p0e, 0p1e, 0p2e, 1p0e, 1p1e, 1p2e, 2p0e, 2p1e and 2p2e. Each of these nine states is a macrostate and each state has a state energy. Each macrostate describes the number of reactive electrons and protons in this molecule. Each arrow describes a possible transfer of electrons or protons. Figure 5.1 shows the nine macrostates. The Boltzmann factor of a macrostate is defined in equation (5.3). In this example, which is based on a quinone, each state with only one proton can be split into two tautomers, because there are two possible hydrogen atom binding sites. So a macrostate can be divided into microstate in which the individual tautomers are taken into account (equations (5.4) and (5.5)).

$$\mathfrak{b}_m^n(\mu_{H^+}, \mu_{e^-}) = e^{-\beta\left(G_m^{\circ,n} - n\mu_{H^+} - m\mu_{e^-}\right)} = e^{-\beta G_m^{\circ,n}} \cdot e^{\beta n \mu_{H^+}} \cdot e^{\beta m \mu_{e^-}} \in \mathbb{R} \tag{5.3}$$

with

$\beta := \frac{1}{RT}$

R is the universal gas constant

T is a temperature

$n \in N$: Number of protons

$m \in M$: Number of electrons

μ_{H^+} is the chemical potential of protons

μ_{e^-} is the chemical potential of electrons

$G_m^{\circ,n}$ is the G_{model}-value

For simplification purposes, the dependence on redox potential and pH is not marked separately e.g. $\mathfrak{b}_m^n(\mu_{H^+}, \mu_{e^-}) := \mathfrak{b}_m^n$ and also the number of protons (n) and the number of electrons (m) is not marked separately e.g. $G_m^n := G$.

$$\mathfrak{b}_m^n = e^{-\beta G} = \underbrace{e^{-\beta G^{t_1}}}_{\text{tautomer 1}} + \underbrace{e^{-\beta G^{t_2}}}_{\text{tautomer 2}} + \underbrace{e^{-\beta G^{t_3}}}_{\text{tautomer 3}} + \ldots \tag{5.4}$$

or as a sum

$$\mathfrak{b}_m^n = \sum_{t_k \in \#tautomers} \mathfrak{b}^{t_k} \in \mathbb{R} \tag{5.5}$$

with

Boltzmann factor of a specific microstate t_k

$$\mathfrak{b}^{t_k} = e^{-\beta G^{t_k}} \tag{5.6}$$

a Gibbs free energy E^{t_k} or the total energy of the system in the respective microstate

$$G^{t_k} = G^{\circ,t_k} - n\mu_{H^+} - m\mu_{e^-} \in \mathbb{R} \tag{5.7}$$

with $\mu_{H^+}, \mu_{e^-} \in \mathbb{R}$

μ_{H^+} is the chemical potential of protons

μ_{e^-} is the chemical potential of electrons

G°,t_k} is the $G_{model}^{t_k}$ of a specific tautomer

5.2.2 Tautomers

The individual tautomers do not have to be energetically equivalent and show an energetic difference with respect to a reference tautomer, which is usually the tautomer with the lowest energy. This difference between the reference tautomer and another tautomer can be determined by quantum mechanical calculations.

$$\Delta G_{qm}^{\circ} = G_{qm}^{\circ,t_k} - G_{qm}^{\circ,t_{ref}} \tag{5.8}$$

The electrostatic part $\left(G_{elec}^{\circ,t_k}\right)$ is just needed if a protein should be fitted instead of a model compound and consists of G_{solv} and G_{back}. So the energy difference $\left(\Delta G^{\circ,t_k-t_{ref}}\right)$ between reference tautomer and another tautomer can be calculated in two ways (equation (5.9)).

$$\Delta G^{\circ,t_k-t_{ref}} = \begin{cases} G_{qm}^{\circ,t_k} - G_{qm}^{\circ,t_{ref}} & \text{, if a model compound is fitted} \\ G_{qm}^{\circ,t_k} - G_{qm}^{\circ,t_{ref}} + G_{elec}^{\circ,t_k} & \text{, if a protein is fitted} \end{cases} \tag{5.9}$$

It follows from equation (5.9) that G°,t_k} from equation (5.7) can be expressed as

$$\begin{aligned} G^{\circ,t_k} &= G^{t_{ref},\circ} + \underbrace{\Delta G_{qm}^{\circ} + G_{elec}^{\circ,t_k}}_{\Delta G^{\circ,t_k}} \\ \Rightarrow G^{t_k} &= G^{\circ,t_{ref}} + \Delta G_{qm}^{\circ} + G_{elec}^{\circ,t_k} - n\mu_{H^+} - m\mu_{e^-} \\ \Rightarrow G^{t_k} &= \underbrace{G^{\circ,t_{ref}} - n\mu_{H^+} - m\mu_{e^-}}_{G^{t_{ref}}} + \underbrace{\Delta G_{qm}^{\circ} + G_{elec}^{\circ,t_k}}_{\Delta G^{t_k}} \\ \Rightarrow G^{t_k} &= G^{t_{ref}} + \Delta G^{t_k} \end{aligned} \tag{5.10}$$

If this energy difference approach is transferred into the microstate model, the following modification of the equation (5.4) results

$$\mathfrak{b}_m^n = \underbrace{\underbrace{e^{-\beta(G^{t_{ref}}+\Delta G^{t_1})}}_{\text{tautomer 1}} + \underbrace{e^{-\beta(G^{t_{ref}}+\Delta G^{t_2})}}_{\text{tautomer 2}} + \underbrace{e^{-\beta(G^{t_{ref}}+\Delta G^{t_3})}}_{\text{tautomer 3}} + \ldots}_{=e^{-\beta G}} \tag{5.11}$$

The equation (5.11) can now be written as a sum simplified as

$$\mathfrak{b}_m^n = e^{-\beta G} \Leftrightarrow e^{-\beta G^{t_{ref}}} \sum_{k \in \#tautomer} e^{-\beta \Delta G^{t_k}} \in \mathbb{R} \tag{5.12}$$

The correct G_{model}-value has to be determined. For this the equation (5.12) changes to the equation (5.13).

$$G^{t_{ref}} = -\frac{1}{\beta} ln \left(\frac{e^{-\beta G}}{\sum_{k \in \#tautomer} e^{-\beta \Delta G^{t_k}}} \right) \tag{5.13}$$

The reference tautomer has now the energy $G^{t_{ref}}$. All other tautomers now differ from the reference tautomer by ΔG_{qm}°.

$$G^{t_k} = G^{t_{ref}} + \Delta G_{qm}^{\circ} = G^{t_{ref}} + \left(G_{qm}^{\circ,t_k} - G_{qm}^{\circ,t_{ref}} \right) \tag{5.14}$$

The theory represents the determination of the G_{model}-values after the fit. For the fit itself, only the macrostates are used, not the microstate, and the following points are still necessary.

5.2.3 Partition function and probabilities

The sum of the macrostate is a partition function of this system. The summation of all macrostates leads to the total partition, which is defined by

$$Z_{total} := \sum_{m \in M} \sum_{n \in N} \mathfrak{b}_m^n \in \mathbb{R} \tag{5.15}$$

with

N is set of protons

M is set of electrons

The partition function of a constant number of electrons (q) but a variable number of protons, or vice versa, is defined, called super-macrostate (SMaS), as

$$Z_q = \sum_{n \in N'} \mathfrak{b}_q^n \in \mathbb{R} \tag{5.16}$$

with

q: constant number of electrons

N': all states with a number of electrons q but a variable number of protons

The same can be defined for a constant number of protons

$$Z_q = \sum_{m \in M'} \mathfrak{b}_m^q \in \mathbb{R} \tag{5.17}$$

with

M':all states with a number of protons q but a variable number of electrons

It is not only interesting which macrostate occur but also with which probability they occur. The probability of occupancy for a macrostate (equation (5.3)) is

$$P(Z_m^n) = \frac{\mathfrak{b}_m^n}{Z_{total}} = \frac{\mathfrak{b}_m^n}{\sum_{m \in M, n \in N} \mathfrak{b}_m^n} \in [0, 1] \tag{5.18}$$

with

$\sum_{m \in M, n \in N} P(Z_m^n) = 1$: probability of all macrostates or microstates is 1

The possibility of a partition function (equation (5.16)) is defined as

$$P(Z_q) = \frac{Z_q}{Z_{total}} = \frac{\sum_{n \in N'} \mathfrak{b}_q^n}{\sum_{m \in M, n \in N} \mathfrak{b}_m^n} \in [0, 1] \tag{5.19}$$

with

$\sum_q P(Z_q) = 1$: probability of all super-macrostate is 1

That extends to the equation (5.17) with the necessary changes. Since this example is completely defined, it is possible to determine all G_{model}-values as well as the partition functions and probabilities. When a system is completely determined experimentally, the calculation of the G_{model}-value is very simple (table 5.1). It should be noted that only relative energies to an "arbitrary" zero point are calculated. In general, the macrostate with the lowest energy is used as a reference state. The energy of this reference state is then subtracted from all other macrostate energies. This results in the mentioned relative energies to an "arbitrary" zero point. These energies can now be used to describe the partition functions. A partition function for one macrostate with 0 protons and 0 electrons at pH of 7 $\left(\mu_{H^+} = -9.6 \frac{kcal}{mol}\right)$ and redox potential 100 mV $\left(\mu_{e^-} = -2.3 \frac{kcal}{mol}\right)$ is

$$\mathfrak{b}_0^0 = e^{-\beta(E_0^0)} = e^{-\beta(0+0 \cdot 9.6+0 \cdot 2.3)} = 1 \tag{5.20}$$

and its probability is

$$P(\mathfrak{b}_0^0) = \frac{\mathfrak{b}_0^0}{Z_{total}} = \frac{1}{1.11 \cdot 10^6} = 9.04 \cdot 10^{-7} \tag{5.21}$$

In order to calculate the probability, all partition functions must be first determined so that Z_{total} can be calculated. As mentioned above the transition of electrons is considered. The partition functions and probabilities for that can be easily calculated.

$$Z_0 = \sum_{n \in \{0,1,2\}} \mathfrak{b}_0^n = 1 + 8.15 \cdot 10^{-15} + 2.33 \cdot 10^{-30} = 1 \tag{5.22}$$

$$P(Z_0) = \frac{Z_0}{Z_{total}} = \frac{1}{1.11 \cdot 10^6} = 9.04 \cdot 10^{-7} \tag{5.23}$$

The calculation of the other partition functions and probabilities, which are shown in table 5.1, is not shown in detail here.

5.2.4 super-macrostate energies and energy differences between these super-macrostates

On the basis of the equations in the appendix (equations (E.1) to (E.3)), the energy can be defined for one state with a constant number of electrons (q) but a variable number of protons or vice versa as

$$G_q = -\beta^{-1} ln \left(\frac{Z_q}{Z_{total}} \right) \in \mathbb{R} \tag{5.24}$$

In the same way as described above, one more state is defined with q' electrons or protons, with $q \neq q'$ The energy difference between these two states is

$$\Delta G_{q \mapsto q'} = \left(G_{q'} - G_q \right) \in \mathbb{R} \tag{5.25}$$

After a conversion of this formula (equation (E.4) in the appendix), the result is

$$\Delta G_{q \mapsto q'} = -\beta^{-1} \ln \left(\frac{Z_{q'}}{Z_q} \right) \in \mathbb{R} \tag{5.26}$$

After the simplification of equation (5.26) (for details see appendix equation (E.5)), the result is

$$\Delta G_{q \mapsto q'} = (q - q')\mu_{e^-} - \beta^{-1} \cdot \left(\ln \left[\frac{\sum_{n \in N''} e^{-\beta \left(G_{q'}^{\circ,n} - n\mu_{H^+} \right)}}{\sum_{n \in N'} e^{-\beta \left(G_q^{\circ,n} - n\mu_{H^+} \right)}} \right] \right) \in \mathbb{R} \tag{5.27}$$

with $\begin{cases} q' > q \Rightarrow \mu_{e^-} < 0 \\ q' < q \Rightarrow \mu_{e^-} > 0 \end{cases}$ and N'': all states with a number of electrons q' but a variable number of protons.

This simplification only works if the number of electrons is fix. The same is possible for a fix number of protons. At the transition point between two super-macrostates, both energies $G_{q'}$ and G_q are equal. (By the way, the experimental values are also determined at this transition point.) Based on this fact, it follows that $\Delta G_{q \mapsto q'} = 0$. Based on $\Delta G_{q \mapsto q'} = 0$, the cost function $\mathfrak{F}$ is obtained later. If the equation (5.27) is transformed, a chemical potential $\mu_{e^-, q \mapsto q'}^{eq}$ is obtained for the equilibrium described above.

$$\mu_{e^-, q \mapsto q'}^{eq} = \frac{1}{q - q'} \cdot \beta^{-1} \cdot \left(\ln \left[\frac{\sum_{n \in N''} e^{-\beta \left(G_{q'}^{\circ,n} - n\mu_{H^+} \right)}}{\sum_{n \in N'} e^{-\beta \left(G_q^{\circ,n} - n\mu_{H^+} \right)}} \right] \right) \tag{5.28}$$

Based on this chemical potential, the cost function $\mathfrak{D}$ can be determined later.

Using the results of the partition functions the energy of a super-macrostate can be calculated.

$$G_0 = -\beta^{-1} ln\left(\frac{Z_0}{Z_{total}}\right) = -\beta^{-1} ln\left(\frac{1}{1.11 \cdot 10^6}\right) = 8.24\frac{kcal}{mol} \tag{5.29}$$

Afterwards the energy difference between the super-macrostate Z_0 and Z_1 can be calculated

$$G_{0\mapsto 1} = G_1 - G_0 = 8.26\frac{kcal}{mol} - 8.24\frac{kcal}{mol} = 2.23 \cdot 10^{-2}\frac{kcal}{mol} \tag{5.30}$$

And the calculation of the interaction energy is not shown here.

Table 5.1: Definition of the different states based on the number of protons (n) and electrons (m). Each state is assigned an energy and a probability as well as a transition energy. All energies are in $\frac{kcal}{mol}$. The calculation was performed at a pH of 7 and a redox potential of 100 mV.

		$G_m^{\circ,n}$	$\mathfrak{b}_m^n$	P($\mathfrak{b}_m^n$)	Z_q	P(Z_q)	G_q	$G_{q\mapsto q'}$
	$\mathfrak{b}_0^0$	0.00	1	$9.04 \cdot 10^{-7}$				
Z_0	$\mathfrak{b}_0^1$	9.60	$8.15 \cdot 10^{-15}$	$7.41 \cdot 10^{-21}$	1	$9.04 \cdot 10^{-7}$	8.24	$2.23 \cdot 10^{-2}$
	$\mathfrak{b}_0^2$	21.19	$2.33 \cdot 10^{-30}$	$2.11 \cdot 10^{-36}$				
	$\mathfrak{b}_1^0$	-2.28	0.96	$8.70 \cdot 10^{-7}$				$-2.23 \cdot 10^{-2}$
Z_1	$\mathfrak{b}_1^1$	-7.91	$1.16 \cdot 10^{-3}$	$1.05 \cdot 10^{-9}$	0.96	$8.71 \cdot 10^{-7}$	8.26	
	$\mathfrak{b}_1^2$	-6.54	$1.04 \cdot 10^{-11}$	$9.38 \cdot 10^{-18}$				-8.26
	$\mathfrak{b}_2^0$	-2.91	$5.60 \cdot 10^{-2}$	$5.06 \cdot 10^{-8}$				
Z_2	$\mathfrak{b}_2^1$	-18.54	$1.50 \cdot 10^{3}$	$1.35 \cdot 10^{-3}$	$1.11 \cdot 10^{6}$	1.00	$1.05 \cdot 10^{-6}$	8.26
	$\mathfrak{b}_2^2$	-32.06	$1.10 \cdot 10^{6}$	1.00				

But a full determination like in table 5.1 is not every time possible because e.g. molecular states are not populated or less populated. Such states are contained in the experimental data, but minor populated. Then such states are hidden in the experimental data, to say the least. For this reason it is necessary to extract the required G_{model}-value from the experimental data in a different way.

5.2.5 Difference functions and cost function for difference functions

A cost function can be used in combination with a difference function. There are two ways to define such a difference function. For the first way to define a difference function, it is important to verify how close the calculated values, based on a G_{model}-values, are to the experimental values and to adjust then the G_{model}-values. It is important to mention that using this first way it is needed to reduce the dimensionality of the problem. To reduce the dimensionality one of the chemical potentials is set to zero and used as the experimental value for the fitting. The difference function ($\mathfrak{D}$) which is a measure for the difference between the calculated and the experimental value

$$\mathfrak{D} = \sum_{j=0}^{T} \left(G_{exp}^j - \mu_{e^-,q\mapsto q'}^{eq}\right)^{\circ 2} \in \mathbb{R}^e \tag{5.31}$$

with

T := number of transitions

e := number of experimental values

$G_{exp}^j \in \mathbb{R}^e$: experimental value as vector

$G_{q\mapsto q'} \in \mathbb{R}^e$: calculated value

$\circ$: Hadamard power (element-wise power)

For the second way, the fact is used that $G_{q\mapsto q'}$ has to be zero at the transition point and define the difference function $\mathfrak{F}$

$$\mathfrak{F} = \sum_{j=0}^{T} \left(\mathbf{0} - \Delta G^j_{q\mapsto q'} \right)^{\circ 2} \in \mathbb{R}^e \tag{5.32}$$

with

T := number of transitions

e := number of experimental values

$G_{q\mapsto q'} \in \mathbb{R}^e$: calculated value for each experimental value as vector

$\circ$: Hadamard power (element-wise power)

The cost function is for both difference functions the same. The basic structure of the cost function is the mean value over a L1-norm (sum norm)

$$C(func) = \overline{\|func\|}_1 \in \mathbb{R} \tag{5.33}$$

with

$func \in \mathbb{R}^e$: difference function ($\mathfrak{F}$ or $\mathfrak{D}$)

As a function one of the two difference equation (5.31) or equation (5.32) can be used. With the function C and the two difference functions $\mathfrak{F}$ and $\mathfrak{D}$ it is now possible to determine the G_{model}-values for the individual states on the basis of experimental values.

5.2.6 Coefficient of determination

Of course it is also needed to know how good our fit is at all. For that the coefficient of determination (R^2) is determined. Different quantities are needed for the calculation. These quantities include the **S**um of **S**quares **E**xplained $\left(SSE = \sum \left(G_{q\mapsto q'} - \overline{G_{q\mapsto q'}} \right)^2 \right)$, the **S**um of **S**quares **T**otal $\left(SST = \sum \left(G_{exp} - \overline{G_{q\mapsto q'}} \right)^2 \right)$, and the **S**um of **S**quares **R**esidual $\left(SSR = \sum \left(G_{exp} - G_{q\mapsto q'} \right)^2 \right)$. These quantities can be used to determine R^2 using equation (5.34). It is possible that the value of R^2 will be negative. That is a sign that the fit is worse than a horizontal straight line through the data points.

$$R^2 \equiv \frac{SSE}{SST} = \frac{\sum \left(G_{q\mapsto q'} - \overline{G_{q\mapsto q'}} \right)^2}{\sum \left(G_{exp} - \overline{G_{q\mapsto q'}} \right)^2} = 1 - \frac{SSR}{SST} = 1 - \frac{\sum \left(G_{exp} - G_{q\mapsto q'} \right)^2}{\sum \left(G_{exp} - \overline{G_{q\mapsto q'}} \right)^2} \tag{5.34}$$

5.2.7 Example calculation

Since the experimental data can be fitted and a conclusions about the fit can be made, the theory was tested with this example. Therefore, pseudo-experimental data points are generated based on the known template G_{model}-values (figure 5.1). Furthermore, a python script was implemented, which performs the fit and the calculation of the coefficient of determination. 56 experimental data points were simulated. The script was used and the following $G_m^{\circ,n}$ values (table 5.2) are the result.

If the G_{model}-values $\left(G_m^{\circ,n} \right)$ are checked by comparing the columns $G_m^{\circ,n}$ (template) and $G_m^{\circ,n}$ (fit) in table 5.2, it can be seen that the state 1p0e differs significantly from the template. This state shows

Table 5.2: Definition of the different states based on the number of protons (n) and electrons (m). Each state is assigned an energy and a probability (population). The value written in red was not found directly by fitting, but was determined by the described method via the R^2. All energies are in $\frac{kcal}{mol}$

Z_q	$\mathfrak{b}_m^n$	#protons	#electrons	$G_m^{\circ,n}$		max. Population
				template	fit	template
Z_0	$\mathfrak{b}_0^0$	0	0	0.00	0.00	$1.00 \cdot 10^{0}$
	$\mathfrak{b}_0^1$	1	0	9.60	20457.47	$0.00 \cdot 10^{-0}$
	$\mathfrak{b}_0^2$	2	0	21.19	21.15	$3.09 \cdot 10^{-6}$
Z_1	$\mathfrak{b}_1^0$	0	1	−2.28	−2.27	$6.66 \cdot 10^{-1}$
	$\mathfrak{b}_1^1$	1	1	−7.91	−7.89	$5.56 \cdot 10^{-7}$
	$\mathfrak{b}_1^2$	2	1	−6.54	−6.47	$1.02 \cdot 10^{-2}$
Z_2	$\mathfrak{b}_2^0$	0	2	−2.91	−2.89	$9.97 \cdot 10^{-1}$
	$\mathfrak{b}_2^1$	1	2	−18.54	−18.54	$7.59 \cdot 10^{-1}$
	$\mathfrak{b}_2^2$	2	2	−32.06	−32.01	$1.00 \cdot 10^{-0}$

very low population in the template (column max. Population (template) in table 5.2). States with a low population are difficult to fit because they are not highly populated and therefore overlaid by high(er) populated states in the experimental or here pseudo-experimental data. In this case the state 1p0e could not be fitted. The other states show no or only very slight differences to the template G_{model}-values ($G_m^{\circ,n}$). The very slight differences of the other states also show that the state 1p0e does not influence the fit (figure 5.2 A) and therefore does not influence the G_{model}-values of the other states. The red fitted lines are very close to the blue pseudo-experimental data points. The pseudo-experimental values and the fit show two intersections (figure 5.2 A). That means that both electrons have the same energy.

However, there is still the problem that state 1p0e is not correct. As mentioned before, the state 1p0e does not affect the fit, which also means that the coefficient of determination is not affected. Based on this fact, it was decided to use the the coefficient of determination as a criterion for reaching the lowest possible energy for the state 1p0e. That means that as soon as the the coefficient of determination decreases, the lowest possible energy for the state 1p0e is reached. It means that as soon as the the coefficient of determination decreases, the lowest possible energy for the state 1p0e is reached, because now the state 1p0e would negatively influence the quality of the fit and that is not wanted. To determine this lowest possible energy, the remaining eight $G_m^{\circ,n}$-values are fixed to the fitted values. The energy of the state 1p0e is also fixed to one value, and then this energy is reduced step by step until the the coefficient of determination is negatively affected. At this point, the lower limit of the possible G_{model}-value of state 1p0e is reached. The lowest value is with 8.30 $\frac{kcal}{mol}$ very close to the actual value of 9.60 $\frac{kcal}{mol}$

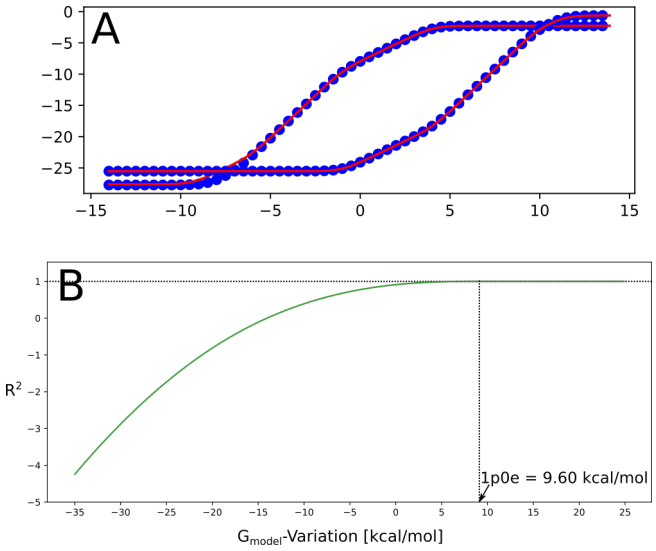

Figure 5.2: A: Fitting (red) of 56 pseudo-experimental data points (blue) with brute force method which calculation the cost function's values at each 2D-grid point of a redox potential-range = [-1000, 1000, 10.0] and pH-range = [-14, 14, 0.1] and Powell minimization method.
B: Coefficient of determination as a function of the G_{model}-value of state 1p0e in an interval of $\left[-35\frac{kcal}{mol}, 25\frac{kcal}{mol}\right)$ with an increment of 0.1 $\frac{kcal}{mol}$.

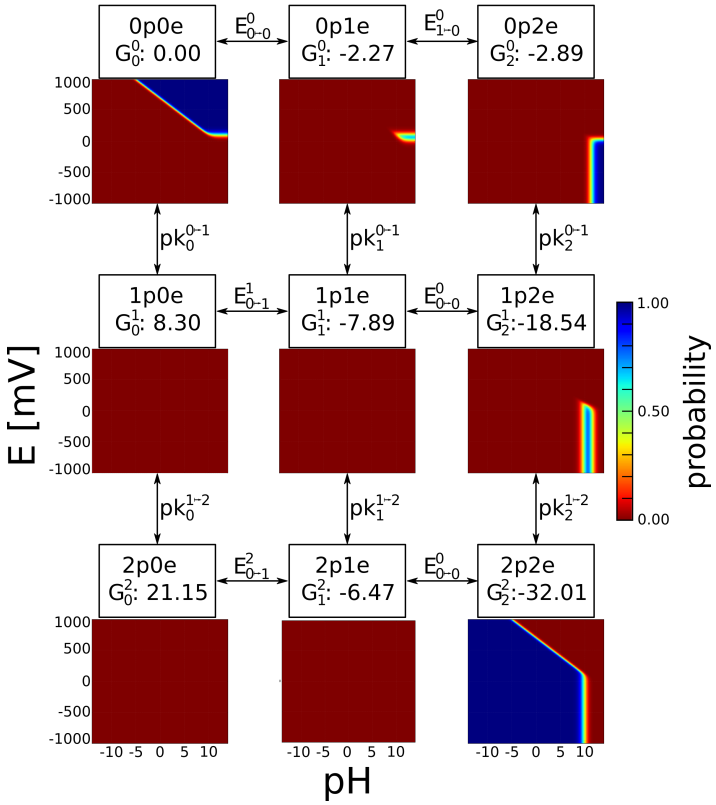

Figure 5.3: Artificial system with nine different macrostates. Each macrostate is described by an fitted energy. The transitions between the macrostates are described by redox potential or pK_a-values. Also shown are the probability plots of the respective states over a redox potential range of -1 to 1 V and a pH range of -15 to 15.

5.3 Methods

Performing the calculations and analyses of the determination of the G_{model}-values, the program-flow of a python script by Dominik Lemm was used as an example and, as mentioned in the theory, a separate `python` script was developed. Due to the complexity of the subject, the `python` script was divided into several modules:

myminimizer: In this module the different minimizers of the python module "optimize"[1] are defined for fitting the G_{model}-values.

mictmo: This module describes the micro and macrostate model as described in chapter 3.

fitting4Gmodel: The largest of the three modules uses the two previously listed modules to determine the G_{model}-values and includes the analysis of the results and the graphical representation of the fitting. Fitting always starts with a brute force method. This method calculates the cost function's values at each grid point of a given pH and redox potential-range.

During the fit, especially at the beginning, it is possible that the R^2 value becomes negative. This is a sign that the fit is worse than a horizontal straight line through the data points. As the number of iterations increases, this effect should disappear, otherwise the fit is very bad.

In addition to these modules, the following two modules have also been written.

mylogging: Write the log files

utilities: Includes all useful methods such as the class MyFitting which includes different regression functions.

An application script only needs to import the fitting4Gmodel module, because this module inherits all other modules. This approach keeps the application script relatively simple and straightforward. It is only necessary to create an appropriate object and then import the experimental data to be fitted. The experimental data can be extracted from graphics with the program `g3data`. After all this is done, the optimization can be started. The `python` program can be found on the zenodo website (*3*).

5.4 Determination of the G_{model} for Flavin mononucleotide/FMN and Rieske center

The theory described above can be applied to two current problems: flavin mononucleotide (FMN) and the Rieske center. Although flavin does not occur in the bc_1-complex, it is an important component of various bioenergetic processes. For this reason, the corresponding G_{model}-values for flavin/FMN were determined in a master thesis of Kilian Zuchan (*4*) in which the respective isomers were determined quantum mechanically. The Rieske complex is relevant for the bc_1-complex. With twelve states it is also less complex than the flavin with 96 states. The Rieske complex has also been studied by Klingen *et al.* (*5*) and Ullmann *et al.* (*6*).

FMN and the Rieske center differ conceptually and represent two different types. The first type includes the determination of the G_{model}-values of the FMN because in this case it is a model compound and only a quantum mechanical differentiation is necessary. The second type includes the determination of the G_{model}-values of the Rieske center because a protein complex was examined and an electrostatic and a quantum mechanical part must be considered.

1 `https://docs.scipy.org/doc/scipy/reference/tutorial/optimize.html`

5.4.1 Flavin/FMN

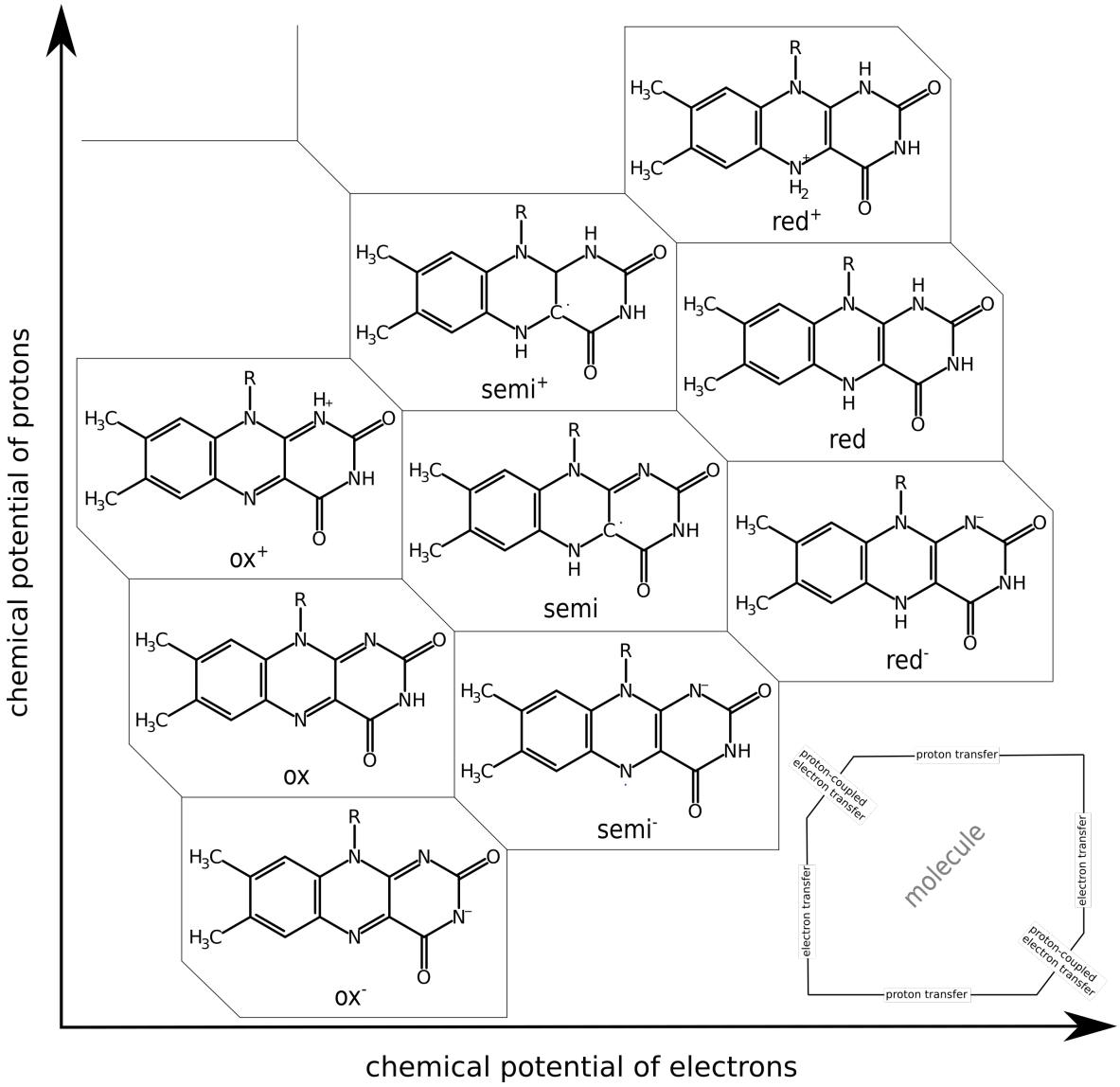

Figure 5.4: Pourbaix-like diagram of Flavin/FMN. The pK_a-values are horizontal and redox potentials are vertical.

The description of the redox behavior of FMN is experimentally difficult because not all states in solution are populated although they can be populated in proteins. For all fits the data from Anderson (*7*), Ehrenberg (*8*) and Draper & Ingraham (*9*) from a Mayhew paper (*1*) were used. These data represent a pH-dependent redox potential of FMN (table 5.3).

Table 5.3: The experimental data were read out from the Fig. 2."Observed and calculated effects of pH on E_m" of Mayhew's publication (*1*) with the program `g3data`. This figure contains the observed and calculated effects of pH on E_m, E_1 and E_2 for FMN at 20 °C by Mayhew (*1*), Anderson (*7*), Ehrenberg (*8*), and Draper & Ingraham (*9*)

pH	redox potential [V]	pH	redox potential [V]	pH	redox potential [V]
4.78	−0.019	4.79	−0.167	4.49	−0.075
5.31	−0.017	5.29	−0.224	5.00	−0.109
5.60	−0.049	5.59	−0.224	5.50	−0.133
5.99	−0.069	5.97	−0.251	6.01	−0.161
6.30	−0.076	6.31	−0.275	6.50	−0.190
6.90	−0.099	6.88	−0.305	6.95	−0.199
7.01	−0.104	6.99	−0.310	7.44	−0.216
7.10	−0.127	7.10	−0.298	8.00	−0.233
7.89	−0.105	7.86	−0.374	9.52	−0.286
9.12	−0.173	9.11	−0.377	10.00	−0.301
9.36	−0.167	9.34	−0.400	10.50	−0.326
11.20	−0.283	11.17	−0.441	10.95	−0.350
12.00	−0.299	11.97	−0.516	11.55	−0.382
12.36	−0.347	12.35	−0.509	11.96	−0.410

Two different state scenarios with six and nine states were fitted to the experimental values. Under physiological conditions, five states (ox, $semi$, $semi^-$, red^- and red) are known (*10*). These five states are extended by another possible state ox^-. This state should also be able to be stabile within a protein. In addition, these six states were extended by three other states (ox^+, $semi^+$ and red^+). These states are very improbable, but it should be checked if they can still be found in the measurement data. The structure of the different states can be found in figure 5.4, and the number of electrons and protons are in table 5.4. The two models with six and nine states are fitted with our algorithm to the experimental data of table 5.3. These two fits result to the $G_m^{\circ,n}$ values in table 5.4.
The values for the model with six states appear to be reasonable and in the correct range. Looking at the fit itself (figure 5.5), the R^2 has a high accuracy of 0.99. If the fitted G_{model}-values are used to determine the distribution probabilities of the individual states, figure 5.5 shows very clearly the high population of the states ox, ox^-, red^- and red and the low population of the semi-states, because the semi-states are hardly occupied and have an occupancy probability of less than 0.4. From these occupancy probabilities, the redox potentials and pK_a-values can also be determined (figure 5.4).
The fit of the 9-states also shows a high coefficient of determination with an R^2 of 0.99 but there is still one outlier, the state $\mathfrak{b}_2^4$. As a result of this very high G_{model}-value for the state red^+ which is similar to our example there are no meaningful pK_a-values and redox potentials. The coefficient of determination is used to find a lower limit for this value at 9-states. With a value of 0.9907 for R^2 the lower limit for this state is -28.2 $\frac{kcal}{mol}$. With this redefined G_{model}-value, pK_a-values and redox potentials are better obtained for the model compound. Also the probability distribution is now comparable with the distribution of the 6-states. It shows the expected splitting and distribution of the newly added states over the evaluated pH range.

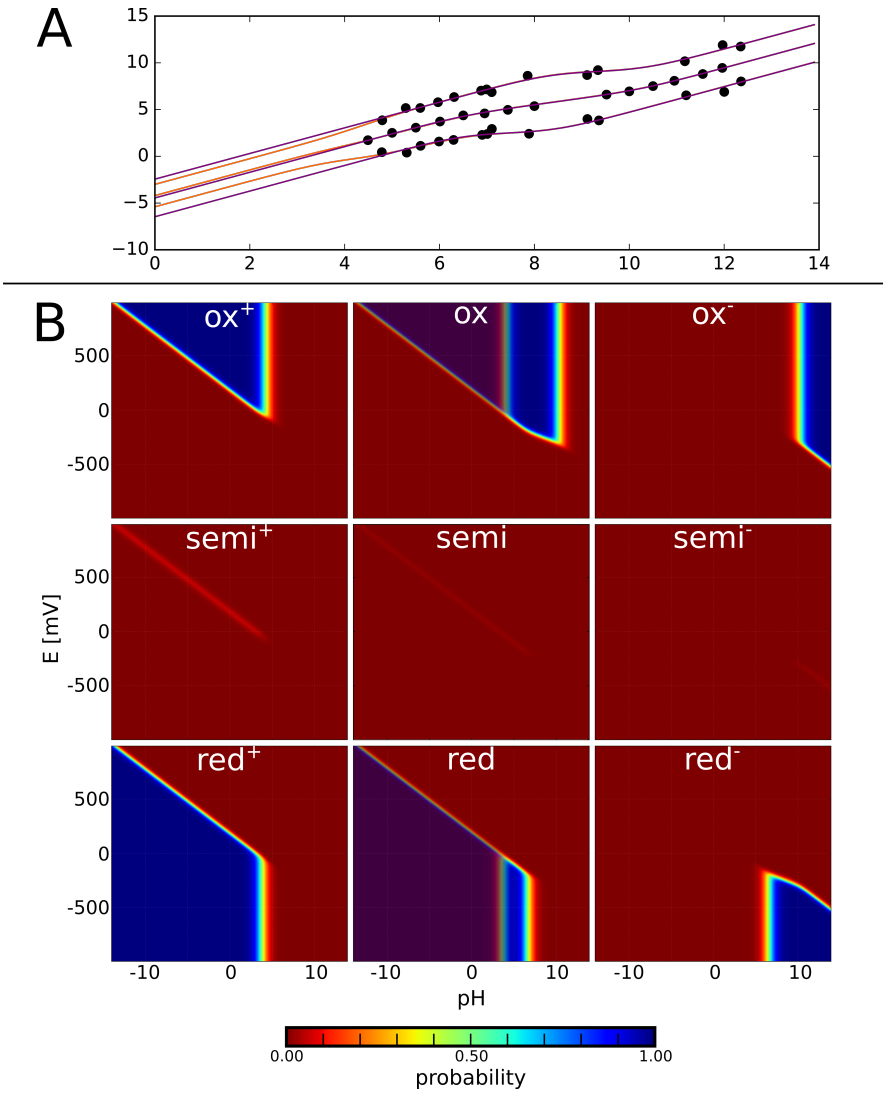

Figure 5.5: The result of fitting process of the Anderson data. Subfigure (A) shows the fit of 42 data points (black) with six (purple) and nine (orange) states. Subfigure (B) is the occupancy probabilities for six (shaded) and nine states (for the state configurations see table 5.4). The probability plots of the respective states are over a redox potential range of -1 to 1 V and a pH range of -15 to 15.

Using these values to predict FMN states within a protein would lead to a misrepresentation because tautomers are not considered in the fit. As also indicated in theory (section 5.2), proton tautomers exist for FMN having different energies. In order to take this into account, the energy difference of the 80 different tautomers was calculated quantum mechanically by Vincent Emann during his bachelor thesis (*11*). That results in a much more detailed picture and a total number of 80 different G_{model}-values which were calculated with equations (5.13) and (5.14) and were named real G_{model}-value in the appendix tables E.1 and E.2. The majority of the 80 tautomers are very unlikely because of their low chemical stability in relation to their energies . This is also shown by the energies resulting from quantum mechanical calculations. These tautomers are also not stabilized by a protein environment. For this reason, only 17 tautomers were selected. These can be stabilized and have low energies.
These tautomers and their energies were used in the master thesis of Kilian Zuchan to calculate occupancy probabilities and kinetics.

Table 5.4: Definition of the different states of Flavin based on the number of protons (n) and electrons (m). Each state is assigned an energy. The value written in red was not found directly by fitting, but was determined by the described method via the R^2.

Z_k	$\mathfrak{b}_m^n$	trivial name	#protons	#electrons	$G_m^{\circ,n}\left[\frac{kcal}{mol}\right]$ 6-states	9-states
Z_0	$\mathfrak{b}_0^0$	ox^-	0	0	0.00	0.00
	$\mathfrak{b}_0^1$	ox	1	0	-14.06	-14.10
	$\mathfrak{b}_0^2$	ox^+	2	0		-19.80
Z_1	$\mathfrak{b}_1^1$	$semi^-$	1	1	-4.99	-5.00
	$\mathfrak{b}_1^2$	$semi$	2	1	-16.50	-16.51
	$\mathfrak{b}_1^3$	$semi^+$	3	1		-22.83
Z_2	$\mathfrak{b}_2^2$	red^-	2	2	-14.00	-14.00
	$\mathfrak{b}_2^3$	red	3	2	-22.96	-23.09
	$\mathfrak{b}_2^4$	red^+	4	2		28.20

5.4.2 Iron-sulfur complex

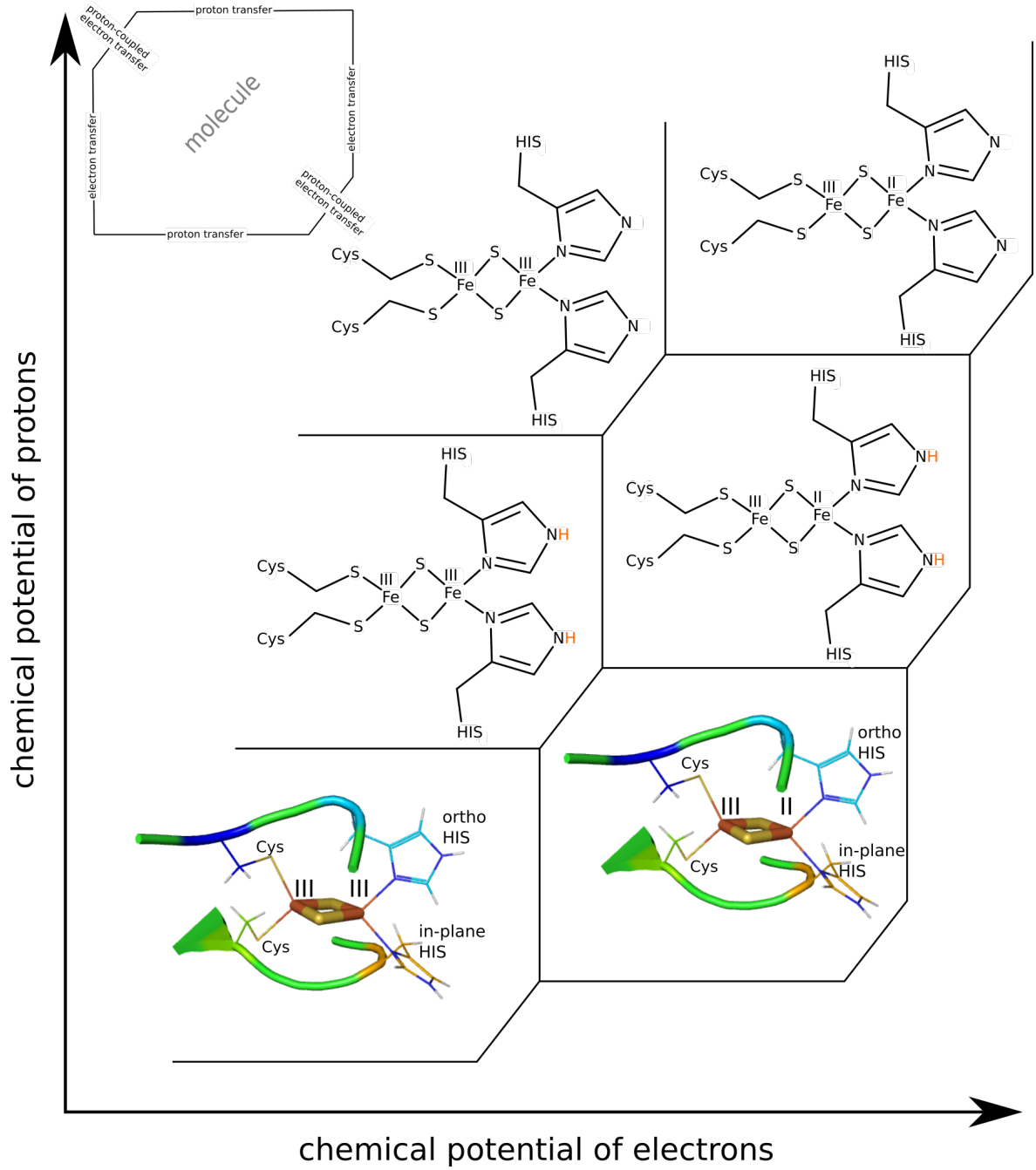

Figure 5.6: Pourbaix-like diagram to compare different states for a Rieske center. The pK_a-values are horizontal and redox potentials are vertical. The hydrogen atoms marked in orange are not both bound, because only one histidine is protonated in any case. In structures with black hydrogen atoms both positions are occupied. Two states are shown in a 3D representation as they occur in protein RsRp (pdb-ID: 2NUK). In this representation, the ortho (orthogonal) and in-plane positions of the histidines with respect to the iron-sulfur complex can be clearly seen. The multicolored tubes are a part of the protein backbone.

In addition to the examination of FMN, a Rieske center was also examined. As mentioned before, this is not a model compound like FMN, because no data are available for a model compound. For this reason, the titration of proteins was used, since data from Zu *et al.* (*12*) exist for this purpose (table 5.6). The titration curve of the protein RsRp (Rieske proteins from *Rhodobacter sphaeroides*) was evaluated to determine the G_{model}-values. The evaluation was performed using `g3data` and the extracted data points (table 5.6) were afterwards used as experimental data points in the fit. The fit of the experimental data was performed with six states (figure 5.7 A). The coefficient of determination is very high at 0.99 and there were no outliers.

The probability distribution of the individual states after the fit is realistic (figure 5.7 B) and is based on the energy values $G_m^{\circ,n}$ (table 5.8, also named G_{macro} (Fit) in table 5.7) determined by the fit. All six states are occupied in the physiological range of pH-values and redox potentials. The experimentally measured redox potentials and pK_a-values are in the probability distribution in the transition regions between the individual states. As explained in the theory, the model obtained up to here is not yet completely correct. The influence of the protein as well as the different proton and electron tautomers are not taken into account. The problem of the influence of the protein does not appear in the probability plot of the fit, because the fit and the determination of the probabilities with electrostatic methods are performed in the same protein. The influence of the protein thus cancels out in this concrete case, but would lead to errors in the determination of probability distributions, pK_a-values and redox potentials for other protein structures.

As shown in the figure 5.6, two states have hydrogen atoms marked in orange, i.e., these two states actually result in four defined states as well. That would result in an extension of the Pourbaix-like diagram to eight different states. But the iron-sulfur complex contains two iron atoms, each of which can be oxidized or reduced. This fact leads to four more possible states for the Pourbaix-like diagram. For this reason, six states (table 5.8) now become in sum twelve states (table 5.7) to have all tautomers.

The influence of the protein on the G_{model}-value by using electrostatics (column $\Delta G_{m,elec}^{\circ,n}$ in table 5.7) will be checked now. It turns out that each state is influenced differently by the protein because of the different state charges. The highest energy difference of 0.95 $\frac{kcal}{mol}$ is between the states $FeS_{red(Cys)}$ and $FeS_{red(His)}$. It can be seen that the influence of the protein on a state can differ and should not be neglected. The energy difference between the different tautomers is much bigger than the influence of the protein environment on them. The quantum mechanical calculation shows a difference of 4.69 $\frac{kcal}{mol}$ for the states $FeS_{red(Cys)}$ and $FeS_{red(His)}$ (column $\Delta G_{m,qm}^{\circ,n}$ in table 5.7). Thus, the energetic difference between the tautomers is larger than the difference between the tautomers caused by the protein environment. Another point that can be seen from the individual energy values ($\Delta G_{m,qm}^{\circ,n}$, $\Delta G_{m,elec}^{\circ,n}$) is that a reduced histidine-coordinated iron is energetically preferred to a reduced cysteine-coordinated iron.

Using $\Delta G_{m,sq}^{\circ,n}$, $\Delta G_{m,elec}^{\circ,n}$ and $G_{macro}(Fit)$ and the equation (5.10), the real G_{model}-values can be determined (table 5.7). The determined real G_{model}-values are now used to determine the pK_a-values and redox potentials and compared with the experimental values for RsRp from the publication of Zu *et al.* (table 5.5). First, the real G_{model}-values are used to determine the population probabilities of each state, and then these probabilities are used to determine the pK_a values and redox potential. Compared to the population probabilities with six states, in the population probabilities with twelve states the states $FeS_{ox}H^+$, $FeS_{ox}2H^+$, $FeS_{red}H^+$ and $FeS_{red}2H^+$ are each split into two states. For example, the state $FeS_{ox}H^+$ is split into the states $FeS_{ox}H_{His_o}^+$ where the proton is at the ortho-histidine and $FeS_{ox}H_{His_p}^+$ where the proton is at the in-plane-histidine. Looking at the plot of the population probabilities for these states, it can be seen that the high probability (dark blue) in figure 5.7 for the state $FeS_{ox}H^+$ turns to medium probability (green) and low probability (yellow) in figure 5.8 for the two states $FeS_{ox}H_{His_p}^+$ and $FeS_{ox}H_{His_o}^+$. That is because the high probability is split from the $FeS_{ox}H^+$ state to the two $FeS_{ox}H_{His_o}^+$ and $FeS_{ox}H_{His_p}^+$ states, if the sum over the probability of the

two states $FeS_{ox}H^+_{His_o}$ and $FeS_{ox}H^+_{His_p}$ were taken, the probability of the state $FeS_{ox}H^+$ would be obtained. This population probability can be used to determine the different pK_a-values and the redox potentials, here the intersection points or intersection lines of the single probability population are looked at. Based on this consideration, the values of table 5.5 are obtained. The largest deviations from the experimental data are 24 mV and 0.6 pK_a-units. The figure 5.8 was chosen from the pK_a-value and redox potential ranges to be comparable to the Pourbaix diagram of Zu *et al.* It can be seen that both representations are similar and thus show similar transitions between states.

Table 5.5: Experimental pK_a-values and redox potentials [mV] from Zu *et al.* (*12*) for RsRp. and own calculated pK_a-values and redox potentials [mV].

	own	Zu *et al.*	Δ
pK_{ox1}	7.3	7.6	0.3
pK_{ox2}	10.2	9.6	0.6
pK_{red1}	12.4	12.4	0.0
pK_{red2}	12.5	12.5	0.1
E_{acid}	284	308	24.0
E_{alk}	−136	−134	2.0

Table 5.6: Experimental data from Zu. for RsRp

pH	redox potential [V]	pH	redox potential [V]
3.06	0.317	9.28	0.202
3.50	0.315	9.75	0.164
3.94	0.313	10.34	0.102
4.38	0.312	10.69	0.064
4.91	0.313	11.00	0.031
5.59	0.310	11.09	0.016
6.22	0.310	11.63	−0.038
6.66	0.305	11.91	−0.066
7.00	0.300	11.97	−0.071
7.59	0.288	12.31	−0.097
8.00	0.273	13.00	−0.126
8.47	0.253	13.47	−0.136
8.88	0.225	14.03	−0.131

Table 5.7: Different states based on the number of protons (n) and electrons (m) from table 5.8. Each state is assigned an energy from electrostatic and quantum mechanical calculation, and a fitted and real G_{model}s. All energies are in $\frac{kcal}{mol}$

	$\Delta G^{\circ,n}_{m,qm}$	$\Delta G^{\circ,n}_{m,elec}$	G_{macro} (Fit)	real G_{model}
$FeS_{ox}2H^+$	0.00	3.81	−23.67	−19.86
$FeS_{red(Cys)}2H^+$	9.76	5.17	−30.86	−15.62
$FeS_{red(His)}2H^+$	0.00	5.48		−25.38
$FeS_{ox}H^+_{His_o}$	0.00	5.25	−13.37	−8.12
$FeS_{red(Cys)}H^+_{His_o}$	8.08	3.10	−14.15	−2.07
$FeS_{red(His)}H^+_{His_o}$	0.00	3.99		−10.15
$FeS_{ox}H^+_{His_p}$	0.00	5.39	−13.37	−7.98
$FeS_{red(Cys)}H^+_{His_p}$	7.86	3.66	−14.15	−1.82
$FeS_{red(His)}H^+_{His_p}$	0.00	4.46		−9.68
FeS_{ox}	0.00	5.36	0.0	5.36
$FeS_{red(Cys)}$	4.69	1.31	3.11	8.33
$FeS_{red(His)}$	0.00	0.36		3.64

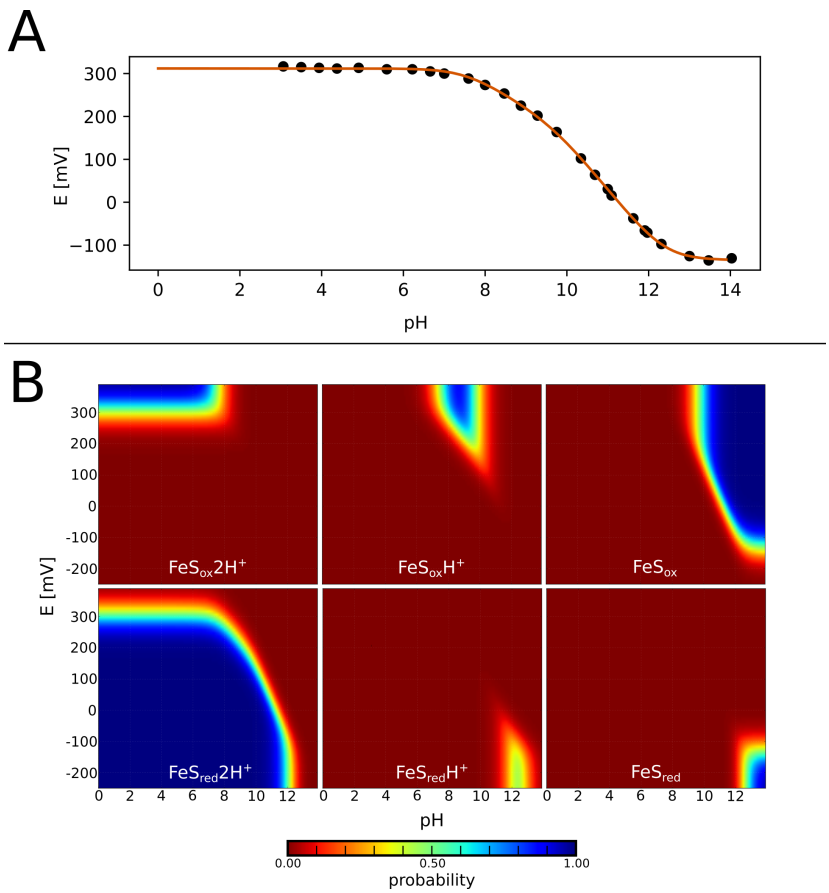

Figure 5.7: The result of fitting process of the Zu *et al.* data. Subfigure (A) shows the fit (orange line) of 26 data points (black) with six states. Subfigure (B) is the occupancy probabilities based on the fitted $G_m^{\circ,n}$ for six states (see table 5.8). The probability plots of the respective states are over a redox potential range of -300 to 400 mV and a pH range of 0 to 14.

Table 5.8: Different states based on the number of protons (n) and electrons (m). Each state is assigned an state energy.

Z_k	$\mathfrak{b}_m^n$	trivial name	#protons	#electrons	$G_m^{\circ,n}$
Z_0	$\mathfrak{b}_0^0$	FeS_{ox}	0	0	0.0
	$\mathfrak{b}_0^1$	$FeS_{ox}H^+$	1	0	-13.37
	$\mathfrak{b}_0^2$	$FeS_{ox}2H^+$	2	0	-23.67
Z_1	$\mathfrak{b}_1^0$	FeS_{red}	0	1	3.11
	$\mathfrak{b}_1^1$	$FeS_{red}H^+$	1	1	-14.15
	$\mathfrak{b}_1^2$	$FeS_{red}2H^+$	2	1	-30.86

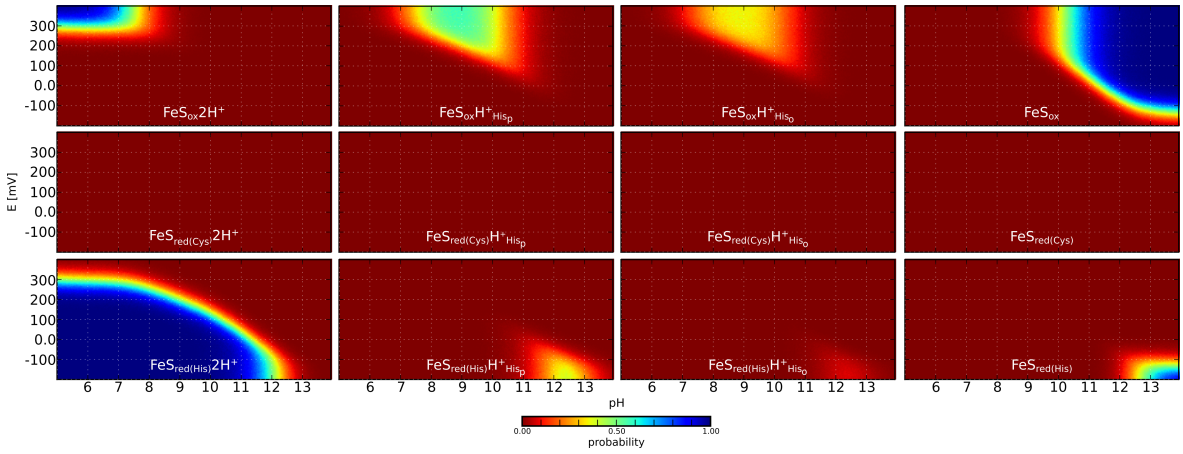

Figure 5.8: Pourbaix-like diagram of probabilities based on the G_{model}-values for all twelve states which can be found in table 5.9. The probability plots of the respective states are over a redox potential range of -200 to 400 mV and a pH range of 5 to 14.

Table 5.9: G_{model}-values for the Rieske center.

	$G_{model}\ \left[\frac{kcal}{mol}\right]$
$FeS_{ox}2H^+$	5.52
$FeS_{red(Cys)}2H^+$	9.60
$FeS_{red(His)}2H^+$	0.00
$FeS_{ox}H^+_{His_p}$	17.26
$FeS_{red(Cys)}H^+_{His_p}$	23.31
$FeS_{red(His)}H^+_{His_p}$	15.23
$FeS_{ox}H^+_{His_o}$	17.40
$FeS_{red(Cys)}H^+_{His_o}$	23.56
$FeS_{red(His)}H^+_{His_o}$	15.70
FeS_{ox}	30.74
$FeS_{red(Cys)}$	33.71
$FeS_{red(His)}$	29.02

5.5 Conclusion

The theoretical example at the beginning of this chapter has shown the functionality of the program and the algorithm. The determination of FMN has shown that it is possible to determine G_{model}-values based on a model compound with existing experimental values. It has also been shown that this method can be used to find states that are lowly populated in the experimental data. The determined G_{model}-values could be successfully used to describe kinetic bifurcation processes in NfnI within the master thesis of K. Zuchan.

The values determined here also represent an improvement and confirmation of the values of Klingen *et al.* (*5*) and Ullmann *et al.* (*6*). With the determination of the G_{model}-values for the Rieske center it could be shown that also a protein with corresponding cofactor can be used as a model compound.

However, when using a whole protein as a model compound, the electrostatic protein effects must be subtracted from the G_{model}-value for the cofactor. This additional step is only necessary when using a cofactor embedded in a protein as a model compound. With this approach, it was possible to determine G_{model}-values that were only lowly present in the measured data.

With this fitting program it is possible to determine G_{model}-values with high accuracy using model structures or "model proteins". It has also been shown that very weakly populated occupancy states can be found.

References

(*1*) Mayhew, S. G. (1999). The effects of pH and semiquinone formation on the oxidation-reduction potentials of flavin mononucleotide. A reappraisal. *Eur J Biochem 265*, 698–702.

(*2*) Lemm, D. Simulation of the Hydride Transfer in Xanthine Dehydrogenase, Bachelor thesis, University of Bayreuth, 2016.

(*3*) Zoller, J. (2024). Obtaining Gmodels by Fitting Experimental Data. DOI: 10.5281/zenodo.10549144.

(*4*) Zuchan, K. Energetics of the bifurcating electron transfer in NfnI, Master thesis, University of Bayreuth, 2019.

(*5*) Klingen, A. R., and Ullmann, G. M. (2004). Negatively Charged Residues and Hydrogen Bonds Tune the Ligand Histidine pKa Values of Rieske Iron-Sulfur Proteins. *Biochemistry 43*, 12383–12389, DOI: 10.1021/bi0488606.

(*6*) Ullmann, M. G., Noodleman, L., and Case, D. A. (2002). Density functional calculation of pK a values and redox potentials in the bovine Rieske iron-sulfur protein. *JBIC 7*, 632–639, DOI: 10.1007/s00775-002-0342-6.

(*7*) Anderson, R. F. (1983). Energetics of the one-electron reduction steps of riboflavin, FMN and FAD to their fully reduced forms. *Biochim Biophys Acta 722*, 158–162.

(*8*) Ehrenberg, A., Muller, F., and Hemmerich, P. (1967). Basicity, Visible Spectra, and Electron Spin Resonance of Flavosemiquinone Anions. *Eur J Biochem 2*, 286–293, DOI: 10.1111/j.1432-1033.1967.tb00137.x.

(*9*) Draper, R. D., and Ingraham, L. L. (1968). A potentiometric study of the flavin semiquinone equilibrium. *Arch Biochem Biophys 125*, 802–808.

(*10*) Kao, Y.-T., Saxena, C., He, T.-F., Guo, L., Wang, L., Sancar, A., and Zhong, D. (2008). Ultrafast dynamics of flavins in five redox states. *J Am Chem Soc 130*, 13132–13139, DOI: 10.1021/ja8045469.

(*11*) Emann, V. R. Quantum chemical Analysis of the Energetics of Flavin-Tautomers, Bachelor thesis, University of Bayreuth, 2017.

(*12*) Zu, Y., Couture, M. M.-J., Kolling, D. R. J., Crofts, A. R., Eltis, L. D., Fee, J. A., and Hirst, J. (2003). Reduction Potentials of Rieske Clusters: Importance of the Coupling between Oxidation State and Histidine Protonation State. *Biochemistry 42*, 12400–12408, DOI: 10.1021/bi0350957.

6

RATE MODEL

In the previous chapters 3 to 5, the G_{model}-values for various cofactors of the bc_1-complex were determined. Specifically in the chapters 2 and 3, the theoretical foundations have been created to now calculate rates using continuum electrostatics. Before examining the bc_1-complex, first a short excursus into the world of chemical potentials and kinetics. These two topics of physical chemistry are important to understand the concept of "steady-state" calculations. This chapter establishes the theoretical basis for the later study of the Q-cycle in the bc_1-complex. An enzymatic cycle serves as an analogy to the Q-cycle as an application example.

6.1 Chemical potential

The chemical potential is a central quantity in physical chemistry and holds a key position. Through the chemical potential, different areas of physical chemistry can be linked. As in chapter 5, the chemical potential can be used to describe redox reactions and acid-base reactions. In this chapter, in addition to the insights from chapter 5, the connection of the chemical potential with reaction kinetics is used. At the beginning, some more connections or definitions of the chemical potential that are useful for describing reaction kinetics are recapitulated. The chemical potential theory presented here in this section is mostly taken from the textbook by Job and Ruffler (*1*).
It is possible to assign a chemical potential (μ) to each substance. With this knowledge, a general equilibrium reaction (equation (6.1)) is defined.

$$\nu_1 S_1 + \cdots + \nu_i S_i \rightleftharpoons \nu_1 P_1 + \cdots + \nu_j P_j \tag{6.1}$$

with

- S: Substrate
- P: Product
- ν: stoichiometric coefficients
- $i, j \in \mathbb{N}^+$

The free energy change of the reaction (ΔG_R) can be determined by equation (6.2) and was formerly named affinity or drive of a reaction ($\mathcal{A}$). Here, if ΔG_R is greater than 0, the reaction is spontaneous, and if ΔG_R is less than 0, the reaction is in the opposite direction. An equilibrium is characterized by ΔG_R equal to 0.

$$\Delta G_R = \underbrace{\sum_j \nu_j \mu_j(P_j)}_{end} - \underbrace{\sum_i \nu_i \mu_i(S_i)}_{begin} \tag{6.2}$$

$$\Delta G_R \begin{cases} < 0, \text{ forward reaction} \\ = 0, \text{ equilibrium reaction} \\ > 0, \text{ backward reaction} \end{cases} \tag{6.3}$$

Especially for biochemical/enzymatic reactions, the possibility of concatenating different ΔG_Rs is interesting; in this case, the other properties are kept.

$$\Delta G_{R,all} = \sum_i \Delta G_{R,i} \tag{6.4}$$

Now, the following linear relationship can be established for the chemical potential with respect to a substance concentration. The change of the chemical potential for a substance S is proportional to the change of concentration.

$$\mu(S) - \mu_0(S) = \gamma \left(c(S) - c_0(S) \right) \tag{6.5}$$

with

- S: Substrat
- μ: chemical potential
- μ_0: start chemical potential
- c: concentration
- c_0: start concentration
- γ: activity coefficient

At constant temperature and concentration, γ can be written as $\frac{RT}{c(S)}$ and thus the following is valid

$$\mu(S) - \mu_0(S) = \frac{RT}{c(S)} \left(c(S) - c_0(S) \right) \tag{6.6}$$

$$\begin{aligned}
\Rightarrow \Delta\mu(S) &= \frac{RT}{c(S)} \Delta c(S) \\
\Rightarrow d\mu(S) &= \frac{RT}{c(S)} dc(S) \\
\Rightarrow \mu(S) &= \mu_0(S) + RTln \left(\frac{c(S)}{c_0(S)} \right) \\
\Rightarrow \mu(S) &= \mu_0(S) + RTln \left(c_r \right) \Leftrightarrow c_r = e^{\frac{1}{RT}(\mu - \mu_0)}
\end{aligned} \tag{6.7}$$

with

- R: ideal gas constant
- T: temperature
- c_r: relativ concentration

Now the most important properties of the chemical potential needed to be calculated the flux are summarized and recapitulated.

6.2 Kinetic calculations

The discussion of kinetics is simpler if the equation (6.1) is transformed into a concentration-dependent equation and written as a mathematical equation.

$$\nu_1 S_1 + \cdots + \nu_i S_i = \nu_1 P_1 + \cdots + \nu_j P_j \tag{6.8}$$

with

- S: Substrat
- P: Product
- ν: stoichiometric coefficients
- $i, j \in \mathbb{N}^+$

Using this equation (6.8), a basic stoichiometric equation ξ can now be derived. Here, the change in substance is related to the stoichiometric coefficients.

$$\xi(t) = \frac{n_{i,t} - n_{i,0}}{\nu_i} = \frac{\Delta n_i}{\nu_i} \tag{6.9}$$

From this equation (6.9), the change in concentration (Δc_i) per time unit (Δt) can be derived.

$$\begin{aligned} &\xi(t) || : V \\ &\Rightarrow \frac{\Delta n_i}{\nu_i * V} \Leftrightarrow \qquad\qquad \frac{\Delta c_i}{\nu_i} || : \Delta t \\ &\Rightarrow \frac{\Delta c_i}{\nu_i * \Delta t} \end{aligned} \tag{6.10}$$

with

- V: volume
- Δn_i: change of the amount of substance i

Reaction order

Furthermore, two reactions can be determined from equation (6.8), which can be used to explain the kinetics of the substance concentration. Higher order reactions are unlikely, since three or more substrates would have to interact at the same time for a reaction to occur. For this purpose, the stoichiometric coefficients (ν_i) are also set to 1.

(I) $S_1 \longrightarrow P_1 + \cdots + P_j$

(II) $S_1 + S_2 \longrightarrow P_1 + \cdots + P_j$

Reaction I is a 1st order reaction and reaction II is a 2nd order reaction.

Rate

With the knowledge of equation (6.10) this results in two differential equations. If $S_1 << S_2$ or $c_2(S_2)$ is constant is true for the 2nd order reaction, then the differential equation can be reduced with $k_1' = k_1 * c_2(S_2)$ to a 1st order reaction. A pseudo-1st order reaction III is the result. These equations are not solved here because the rates (r) are to be determined. For this, however, the rate constants are needed, which will be discussed in the next section.

(I) $\frac{dc_1(S_1)}{dt} = r = k_1 * c_1(S_1)$

(II) $\frac{dc_1(S_1)}{dt} = r = k_1 * c_1(S_1) * c_2(S_2)$

II' $\frac{dc_1(S_1)}{dt} = r = k_1' * c_1(S_1)$

Rate constant

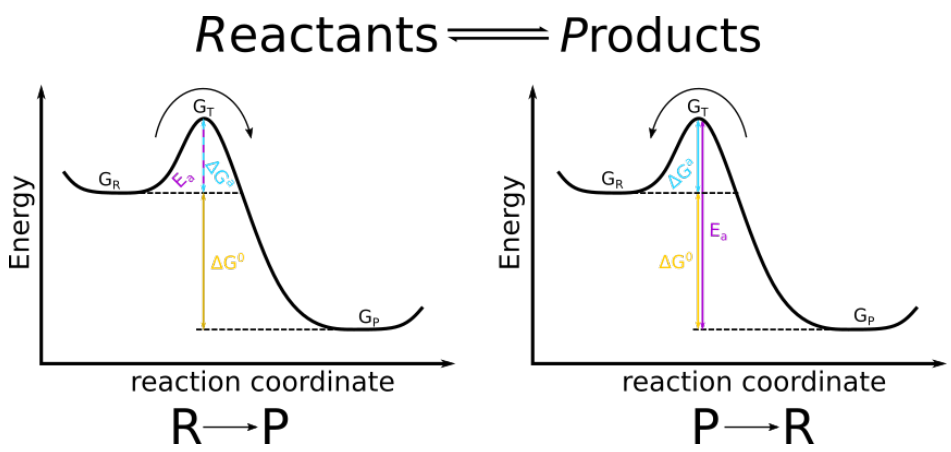

Figure 6.1: Energy diagrams for an equilibrium reaction. The left diagram represents the forward reaction and the right diagram represents the backward reaction.
G_R: State energy of the reactants
G_P: State energy of the products
G_T: State energy of the transition state
E_a: Activation energy
ΔG^a: Difference of reactants state energy and transition state energy
ΔG^0: Difference of reactants state energy and products state energy

The rate constant is a proportionality factor that creates the connection between a substance concentration and the reaction rate, as seen in the previous section. The rate constant can be described by the Arrhenius equation (*2*, *3*).

$$k = A \cdot e^{-\frac{E_a}{R \cdot T}} \tag{6.11}$$

with

A: pre-exponential factor

E_a: activation energy

R: ideal gas constant

T: temperature

Besides the pre-exponential factor A, the activation energy E_a is a crucial quantity of the Arrhenius equation. The activation energy can be divided into different energy components. Figure 6.1 shows this relationship of the energies graphically. Based on this figure, two equations for the activation energy can be derived. To determine which energy diagram occurs for the reaction direction, the sign of ΔG^0 is determined. For this the equation (6.12) is solved, as can be concluded from equation (6.2).

$$\Delta G^0 = G_P - G_R = \mu_0(P) - \mu_0(R) \tag{6.12}$$

If ΔG^0 is greater than zero then equation (6.13) is valid

$$E_a = \Delta G^a \tag{6.13}$$

and if ΔG^0 is less than zero then equation (6.14) is valid

$$\Delta G^0 < 0: \; E_a = \Delta G^a + \Delta G^0 \tag{6.14}$$

For the example from figure 6.1, $\Delta G^0 < 0$ would be for the reaction direction $R \rightarrow P$ and $\Delta G^0 > 0$ would be for the reaction direction $P \rightarrow R$. As described in the reaction order section, in a 2nd order or pseudo 1st order reaction, the concentration of one of the reactants is involved. This concentration has an influence on the energy described here by the chemical potential (equation (6.6)). For this reason, ΔG^0 cannot simply be used, because ΔG^0 describes the energy at pH 0 and a redox potential of 0. Instead, ΔG is used, which is based on the chemical potentials at the corresponding reaction conditions.

$$\Delta G = G_P - G_R = \mu(P) - \mu(R) \tag{6.15}$$

If ΔG is greater than zero then equation (6.16) is valid

$$\Delta G > 0 : \; E_a = \Delta G^a \tag{6.16}$$

and if ΔG is less than zero then equation (6.17) is valid.

$$\Delta G < 0 : \; E_a = \Delta G^a + \Delta G \tag{6.17}$$

Reaction paths and kinetic matrix

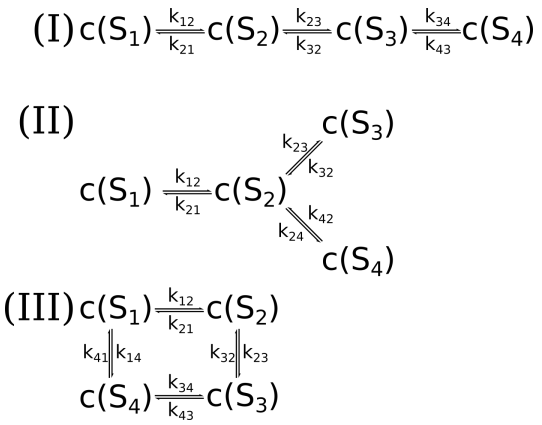

Figure 6.2: Three types of possible reaction paths:
(I): linear reaction path
(II): branched reaction path
(III): circular reaction path

Reaction path matrices:

$$(I) \quad \begin{array}{c|cccc} r \setminus p & c(S_1) & c(S_2) & c(S_3) & c(S_4) \\ \hline c(S_1) & 0 & k_{12} & 0 & 0 \\ c(S_2) & k_{21} & 0 & k_{23} & 0 \\ c(S_3) & 0 & k_{32} & 0 & k_{34} \\ c(S_4) & 0 & 0 & k_{43} & 0 \end{array}$$

$$(II) \quad \begin{array}{c|cccc} r \setminus p & c(S_1) & c(S_2) & c(S_3) & c(S_4) \\ \hline c(S_1) & 0 & k_{12} & 0 & 0 \\ c(S_2) & k_{21} & 0 & k_{23} & k_{24} \\ c(S_3) & 0 & k_{32} & 0 & 0 \\ c(S_4) & 0 & k_{42} & 0 & 0 \end{array}$$

$$(III) \quad \begin{array}{c|cccc} r \setminus p & c(S_1) & c(S_2) & c(S_3) & c(S_4) \\ \hline c(S_1) & 0 & k_{12} & 0 & k_{14} \\ c(S_2) & k_{21} & 0 & k_{23} & 0 \\ c(S_3) & 0 & k_{32} & 0 & k_{34} \\ c(S_4) & k_{41} & 0 & k_{43} & 0 \end{array}$$

In this section, three different base reaction path types (figure 6.2) are discussed, from which all possible paths can be created. The length of the paths can of course be longer than shown here in the examples. Based on these paths, the reaction path matrices are created in the first step, which have the rate constants as elements, and then the differential equation matrices. For the reaction path matrix, the diagonal is zero and all rate constants are zero if no reaction takes place. In the second step, the differential equations for the different reaction path types are now generated. Summarizing the different equations, it can be seen that they almost result in the transposed reaction path matrix with only one difference, that on the diagonal is the negative sum of the respective column of the transposed reaction matrix. Thus, the differential equations can be created or read off very easily from the reaction path matrix.

(I)

$$\begin{pmatrix} \frac{dc(S_1)}{dt} \\ \frac{dc(S_2)}{dt} \\ \frac{dc(S_3)}{dt} \\ \frac{dc(S_4)}{dt} \end{pmatrix} = \begin{bmatrix} -k_{12} & k_{21} & 0 & 0 \\ k_{12} & -k_{21} - k_{23} & k_{32} & 0 \\ 0 & k_{23} & -k_{32} - k_{34} & k_{43} \\ 0 & 0 & k_{34} & -k_{43} \end{bmatrix} \begin{pmatrix} c(S_1) \\ c(S_2) \\ c(S_3) \\ c(S_4) \end{pmatrix} \tag{6.18}$$

(II)

$$\begin{pmatrix} \frac{dc(S_1)}{dt} \\ \frac{dc(S_2)}{dt} \\ \frac{dc(S_3)}{dt} \\ \frac{dc(S_4)}{dt} \end{pmatrix} = \begin{bmatrix} -k_{12} & k_{21} & 0 & 0 \\ k_{12} & -k_{21} - k_{23} - k_{24} & k_{32} & k_{42} \\ 0 & k_{23} & -k_{32} - k_{34} & 0 \\ 0 & k_{24} & k_{34} & -k_{42} \end{bmatrix} \begin{pmatrix} c(S_1) \\ c(S_2) \\ c(S_3) \\ c(S_4) \end{pmatrix} \tag{6.19}$$

(III)

$$\begin{pmatrix} \frac{dc(S_1)}{dt} \\ \frac{dc(S_2)}{dt} \\ \frac{dc(S_3)}{dt} \\ \frac{dc(S_4)}{dt} \end{pmatrix} = \begin{bmatrix} -k_{12} - k_{14} & k_{21} & 0 & k_{41} \\ k_{12} & -k_{21} - k_{23} & k_{32} & 0 \\ 0 & k_{23} & -k_{32} - k_{34} & k_{43} \\ k_{14} & 0 & k_{34} & -k_{41} - k_{43} \end{bmatrix} \begin{pmatrix} c(S_1) \\ c(S_2) \\ c(S_3) \\ c(S_4) \end{pmatrix} \tag{6.20}$$

In this special case the differential equation matrix is a matrix without full rank, that means there is at least one zero row (see appendix F.1). Due to a complexity of up to $O(n^3)$ an elimination of the zero row is omitted and simply a constraint is inserted. The constraint in this case is simply the summation of all concentrations to a constant value $C \in \mathbb{R}_{>0}$, because of the conservation law.

$$c(Total) = c(S_1) + c(S_2) + c(S_3) + c(S_4) = C \tag{6.21}$$

To preserve the quadratic nature of the matrix, another variable ϵ has been inserted, which is zero by definition, but should still remain small for numerical solutions greater than zero. Thus, the variable is an indicator of the quality of the numerical solution. If the variable becomes large, it is an indication of a problem with the system setup. In the end, there are three systems of equations that must be solved to obtain the respective concentration. For the differential equations, the solution of the system of equations is zero, because the steady state is to be described and thus no change of the concentration takes place. For the sum of the concentrations, the solution is C.

(I)

$$\begin{pmatrix} \frac{dc(S_1)}{dt} \\ \frac{dc(S_2)}{dt} \\ \frac{dc(S_3)}{dt} \\ \frac{dc(S_4)}{dt} \\ c_{total} \end{pmatrix} = \begin{bmatrix} -k_{12} & k_{21} & 0 & 0 & 1 \\ k_{12} & -k_{21} - k_{23} & k_{32} & 0 & 1 \\ 0 & k_{23} & -k_{32} - k_{34} & k_{43} & 1 \\ 0 & 0 & k_{34} & -k_{43} & 1 \\ 1 & 1 & 1 & 1 & 0 \end{bmatrix} \begin{pmatrix} c(S_1) \\ c(S_2) \\ c(S_3) \\ c(S_4) \\ \epsilon \end{pmatrix} = \begin{pmatrix} 0 \\ 0 \\ 0 \\ 0 \\ C \end{pmatrix} \tag{6.22}$$

(II)

$$\begin{pmatrix} \frac{dc(S_1)}{dt} \\ \frac{dc(S_2)}{dt} \\ \frac{dc(S_3)}{dt} \\ \frac{dc(S_4)}{dt} \\ c_{total} \end{pmatrix} = \begin{bmatrix} -k_{12} & k_{21} & 0 & 0 & 1 \\ k_{12} & -k_{21}-k_{23}-k_{24} & k_{32} & k_{42} & 1 \\ 0 & k_{23} & -k_{32}-k_{34} & 0 & 1 \\ 0 & k_{24} & k_{34} & -k_{42} & 1 \\ 1 & 1 & 1 & 1 & 0 \end{bmatrix} \begin{pmatrix} c(S_1) \\ c(S_2) \\ c(S_3) \\ c(S_4) \\ \epsilon \end{pmatrix} = \begin{pmatrix} 0 \\ 0 \\ 0 \\ 0 \\ C \end{pmatrix} \tag{6.23}$$

(III)

$$\begin{pmatrix} \frac{dc(S_1)}{dt} \\ \frac{dc(S_2)}{dt} \\ \frac{dc(S_3)}{dt} \\ \frac{dc(S_4)}{dt} \\ c_{total} \end{pmatrix} = \begin{bmatrix} -k_{12}-k_{14} & k_{21} & 0 & k_{41} & 1 \\ k_{12} & -k_{21}-k_{23} & k_{32} & 0 & 1 \\ 0 & k_{23} & -k_{32}-k_{34} & k_{43} & 1 \\ k_{14} & & k_{34} & -k_{41}-k_{43} & 1 \\ 1 & 1 & 1 & 1 & 0 \end{bmatrix} \begin{pmatrix} c(S_1) \\ c(S_2) \\ c(S_3) \\ c(S_4) \\ \epsilon \end{pmatrix} = \begin{pmatrix} 0 \\ 0 \\ 0 \\ 0 \\ C \end{pmatrix} \tag{6.24}$$

As explained at the beginning, the reactions described represent possible basic types, and in an application, combinations of these basic types are more likely to occur. A general form for the reaction path matrix (RPM) and the differential equation matrix (DEM) can be written down. With the DEM, the variable ϵ and the sum over the concentration of the states $c_{total} = \sum_i^N c(x_i) = C$, the system of linear equations to be solved is then in the general form for N reaction states x_i.

$$RPM = \begin{bmatrix} 0 & k_{12} & \dots & k_{1j} \\ \vdots & \ddots & & \vdots \\ \vdots & & \ddots & \vdots \\ k_{i1} & k_{i2} & \dots & 0 \end{bmatrix} \tag{6.25}$$

with

$k_{ij} = 0$, if no reaction exists

$$\begin{aligned} DEM = RPM^T + & \begin{bmatrix} (-1)\cdot \parallel RPM_1^T \parallel_1 & 0 & \dots & 0 \\ \vdots & \ddots & & \vdots \\ \vdots & & \ddots & \vdots \\ 0 & 0 & \dots & (-1)\cdot \parallel RPM_j^T \parallel_1 \end{bmatrix} \\ = & \begin{bmatrix} (-1)\cdot \parallel RPM_1^T \parallel_1 & k_{21} & \dots & k_{i1} \\ \vdots & \ddots & & \vdots \\ \vdots & & \ddots & \vdots \\ k_{1j} & k_{2j} & \dots & (-1)\cdot \parallel RPM_j^T \parallel_1 \end{bmatrix} \end{aligned} \tag{6.26}$$

with

$k_{ji} = 0$, if no reaction exists else $(-1)\cdot \parallel RPM_j^T \parallel_1 = (-1)\cdot \sum_i^N |k_{ij}|$ is the taxicab norm or Manhattan norm

RPM_j^T is the jth column vector of the transposed RPM.

N number of the reaction states

$$\begin{pmatrix} \frac{dc(x_1)}{dt} \\ \vdots \\ \vdots \\ \frac{dc(x_N)}{dt} \\ c_{total} \end{pmatrix} = \begin{bmatrix} (-1)\cdot \parallel RPM_j^T \parallel_1 & k_{21} & \dots & k_{i1} & 1 \\ \vdots & \ddots & & \vdots & 1 \\ \vdots & & \ddots & \vdots & 1 \\ k_{1j} & k_{2j} & \dots & (-1)\cdot \parallel RPM_j^T \parallel_1 & 1 \\ 1 & 1 & & 1 & 0 \end{bmatrix} \begin{pmatrix} c(x_1) \\ \vdots \\ \vdots \\ c(x_N) \\ \epsilon \end{pmatrix} = \begin{pmatrix} 0 \\ \vdots \\ \vdots \\ 0 \\ C \end{pmatrix} \tag{6.27}$$

with

C constant concentration

6.3 Enzyme Reaction

Now all equations and theoretical background are known to calculate the rates or flux of a reaction or reaction network in an equilibrium environment. Using the example model of an isomerase and its enzymatic cycle which was developed by G. Matthias Ullmann. Parts of the calculations shown here are taken from the manuscript (*4*) and the publication of Becker *et al.* (*5*) and Bombarda *et al.* (*6*). The theory is now applied to calculate the flux or rate of this cycle.

Reaction path matrices of the cycle:

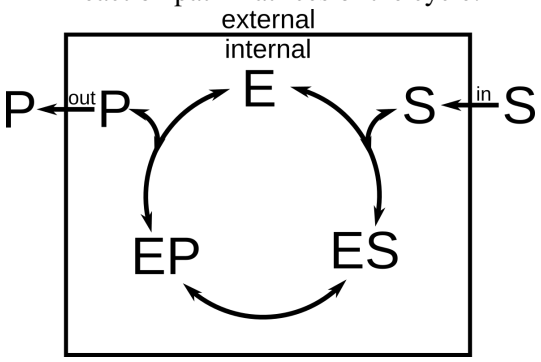

Reaction path matrices of the cycle:

$r \setminus p$	$c(E)$	$c(ES)$	$c(EP)$
$c(E)$	0	k_{12}	k_{13}
$c(ES)$	k_{21}	0	k_{23}
$c(EP)$	k_{31}	k_{32}	0

Figure 6.3: Enzymatic cycle of an isomerase. E is the enzyme, P is the product and S is the substrate. ES is the enzyme substrate complex and EP is the enzyme product complex.

Three equilibrium reactions can be derived from this cycle.

$$\begin{aligned} &(I) && E + S \rightleftharpoons ES \\ &(II) && ES \rightleftharpoons EP \\ &(III) && EP \rightleftharpoons E + P \end{aligned} \tag{6.28}$$

These three equilibrium reactions result in three forward ((I'), (II') and (III')) and three backward ((I''), (II'') and (III'')) reactions. This then results in the following 14 differential equations.

$$
\begin{array}{lll}
(I') \quad E + S \xrightarrow{k_{12}} ES & (II') \quad ES \xrightarrow{k_{23}} EP & (III') \quad EP \xrightarrow{k_{31}} E + P \\
\frac{dc(E)}{dt} = -k_{12}c(E)c(S) & \frac{dc(ES)}{dt} = -k_{23}c(ES) & \frac{dc(EP)}{dt} = -k_{31}c(EP) \\
\frac{dc(S)}{dt} = -k_{12}c(S)c(E) & \frac{dc(EP)}{dt} = k_{23}c(ES) & \frac{dc(E)}{dt} = k_{31}c(EP) \\
\frac{dc(ES)}{dt} = k_{12}c(E)c(S) & & \frac{dc(P)}{dt} = k_{31}c(EP)
\end{array}
$$

$$
\begin{array}{lll}
(I'') \quad E + S \xleftarrow{k_{21}} ES & (II'') \quad ES \xleftarrow{k_{32}} EP & (III'') \quad EP \xleftarrow{k_{13}} E + P \\
\frac{dc(E)}{dt} = k_{21}c(ES) & \frac{dc(ES)}{dt} = k_{32}c(EP) & \frac{dc(EP)}{dt} = k_{13}c(E)c(P) \\
\frac{dc(S)}{dt} = k_{21}c(ES) & \frac{dc(EP)}{dt} = -k_{32}c(EP) & \frac{dc(E)}{dt} = -k_{13}c(E)c(P) \\
\frac{dc(ES)}{dt} = -k_{21}c(ES) & & \frac{dc(P)}{dt} = -k_{13}c(P)c(E)
\end{array}
$$

The various differential equations are now combined.

$$
\begin{array}{lllll}
internal & & & & \\
\frac{dc(E)}{dt} & = -k_{12}c(E)c(S) - k_{13}c(E)c(P) & +k_{21}c(ES) & & +k_{31}c(EP) \\
\frac{dc(ES)}{dt} & = k_{12}c(E)c(S) & -k_{23}c(ES) - k_{21}c(ES) & & +k_{32}c(EP) \\
\frac{dc(EP)}{dt} & = k_{13}c(E)c(P) & +k_{23}c(ES) & & -k_{31}c(EP) - k_{32}c(EP)
\end{array}
$$

$$
\begin{array}{lllll}
external & & & & \\
\frac{dc(S)}{dt} & = -k_{12}c(S)c(E) & +k_{21}c(ES) & & \\
 & + \left(\frac{dc(S)}{dt}\right)_{in} & & & \\
\frac{dc(P)}{dt} & = -k_{13}c(P)c(E) & & & +k_{31}c(EP) \\
 & - \left(\frac{dc(P)}{dt}\right)_{out} & & &
\end{array}
$$

All of these differential equations can also be written as a system of linear equations. To solve this system of equations, some constraints are defined.

1. The concentration of the enzyme does not change, because an enzyme is not consumed in the reaction.
2. In a steady state, the inflow and outflow of substrate and product are proportionally equal.
3. Due to point two and a steady state, the substrate and product concentration can be considered constant.
4. Because of point two and three, an "internal" and an "external" flux can be separated.
5. The substrate and product concentrations are constant and therefore all 2nd order reactions can be converted into a pseudo-1st order reaction (e.g. $-k_{12}c(E)c(S) = -k'_{12}c(E)$).

All these conditions result in the following system of linear equations, in which each linear equation is zero due to the steady state. This system of linear equations describes the internal flux.

$$
\begin{pmatrix} \frac{dc(E)}{dt} \\ \frac{dc(ES)}{dt} \\ \frac{dc(EP)}{dt} \end{pmatrix} = \begin{bmatrix} -k'_{12} - k'_{13} & k_{21} & k_{31} \\ k'_{12} & -k_{21} - k_{23} & k_{32} \\ k'_{13} & k_{23} & -k_{32} - k_{31} \end{bmatrix} \begin{pmatrix} c(E) \\ c(ES) \\ c(EP) \end{pmatrix} = \begin{pmatrix} 0 \\ 0 \\ 0 \end{pmatrix} \tag{6.29}
$$

However, the system of equations 6.29 cannot be solved in this way, because the determinate of the matrix is zero and the matrix rank is two. Only a trivial solution can be guessed by setting all concentrations to zero. With a concentration of zero, however, the system would not make sense in the biochemical meaning. In addition, the conservation law of the enzyme (*7*) can be derived from the matrix or the differential equations and the following applies

$$\frac{dc(E)}{dt} + \frac{dc(ES)}{dt} + \frac{dc(EP)}{dt} = 0 \Rightarrow c(E)(t) + c(E)(t) + c(E)(t) = c(E_{total}) \tag{6.30}$$

$$\begin{pmatrix} \frac{dc(E)}{dt} \\ \frac{dc(ES)}{dt} \\ \frac{dc(EP)}{dt} \\ c_{total} \end{pmatrix} = \begin{bmatrix} -k'_{12} - k'_{13} & k_{21} & k_{31} & 1 \\ k'_{12} & -k_{21} - k_{23} & k_{32} & 1 \\ k'_{13} & k_{23} & -k_{32} - k_{31} & 1 \\ 1 & 1 & 1 & 0 \end{bmatrix} \begin{pmatrix} c(E) \\ c(ES) \\ c(EP) \\ \epsilon \end{pmatrix} = \begin{pmatrix} 0 \\ 0 \\ 0 \\ c(E_{total}) \end{pmatrix} \tag{6.31}$$

Now it is necessary to fill the matrix. The required rate constants are determined on the basis of equations (6.2), (6.6) and (6.11) to (6.14). The determination of the rate constant is exemplified here for the linear reaction scheme I (equation (6.28)) using a differential equation. At the beginning of the calculations, ΔG is considered again in more detail for the situation of an enzymatic reaction or a pseudo 1st order reaction. Based on the concept of the law of the ideal solution (equation (6.32)) is still needed and also the definition of ΔG^0 is needed (equation (6.15)), both are adapted here for this reaction.

$$\Delta G = \Delta G^0 + RTln\left(\gamma \frac{c(S)}{c_0(S)}\right) = \Delta G^0 + RTln\left(a(S)\right) \tag{6.32}$$

Also the relation between activity and chemical potential is needed (equation (6.6)). Now everything is put together and it results in its ΔG, which takes the influence of the activity into account.

(I') $E + S \xrightarrow{k_{12}} ES$

$\Delta G^0 = \mu_0(ES) - (\mu_0(E) + \mu_0(S))$

$\Delta G = \Delta G^0 + RTln\left(a(S)\right)$

$\curvearrowright$ with $a(S) < 1$

$\Delta G = \mu_0(ES) - (\mu_0(E) + \mu_0(S))$

$+ (\mu(S) - \mu_0(S))$

$\Delta G = \mu_0(ES) - (\mu_0(E) + \mu(S))$

(I'') $E + S \xleftarrow{k_{21}} ES$

$\Delta G^0 = (\mu_0(E) + \mu_0(S)) - \mu_0(ES)$

$\Delta G = \Delta G^0 + RTln\left(a(S)\right)$

$\curvearrowright$ with $a(S) > 1$

$\Delta G = (\mu_0(E) + \mu_0(S)) - \mu_0(ES)$

$+ (\mu(S) - \mu_0(S))$

$\Delta G = (\mu_0(E) + \mu(S)) - \mu_0(ES)$

Having defined the forward (I') and backward (I'') reactions, both the forward and backward reactions are now considered separately for the cases $\Delta G > 0$ and $\Delta G < 0$.

$$
\begin{array}{ll}
(I') & E + S \xrightarrow{k_{12}} ES \\
& \Delta G = \mu_0(ES) - (\mu_0(E) + \mu(S)) \\
& \frac{dc(E)}{dt} = -k'_{12} c(E) \\
& \curvearrowright \\
& k'_{12} = k_{12} \cdot c(S) \\
& k_{12} = A \cdot e^{-\frac{E_a}{R \cdot T}} \\
& \Delta G > 0 \Rightarrow E_a = \Delta G^a + \Delta G \\
& \curvearrowright \\
& k'_{12} = A \cdot e^{-\frac{1}{R \cdot T}(\Delta G^a + \mu_0(ES) - (\mu_0(E) + \mu(S)))} \\
& \curvearrowright \\
& \frac{dc(E)}{dt} = \left(-A \cdot e^{-\frac{1}{R \cdot T}(\Delta G^a + \mu_0(ES)}\right) \\
& \qquad \left(e^{-\frac{1}{R \cdot T}(-(\mu_0(E) + \mu(S)))}\right) c(E)
\end{array}
\qquad
\begin{array}{l}
E + S \xrightarrow{k_{12}} ES \\
\Delta G = \mu_0(ES) - (\mu_0(E) + \mu(S)) \\
\frac{dc(E)}{dt} = -k'_{12} c(E) \\
\curvearrowright \\
k'_{12} = k_{12} \cdot c(S) \\
k_{12} = A \cdot e^{-\frac{E_a}{R \cdot T}} \\
\Delta G < 0 \Rightarrow E_a = \Delta G^a \\
\curvearrowright \\
k'_{12} = A \cdot e^{-\frac{1}{R \cdot T}(\Delta G^a)} \\
\curvearrowright \\
\frac{dc(E)}{dt} = \left(-A \cdot e^{-\frac{1}{R \cdot T}(\Delta G^a)}\right) c(E)
\end{array}
$$

$$
\begin{array}{ll}
(I'') & E + S \xleftarrow{k_{21}} ES \\
& \Delta G = (\mu_0(E) + \mu(S)) - \mu_0(ES) \\
& \frac{dc(ES)}{dt} = -k_{21} c(ES) \\
& \curvearrowright \\
& k_{21} = A \cdot e^{-\frac{E_a}{R \cdot T}} \\
& \Delta G < 0 \Rightarrow E_a = \Delta G^a \\
& k_{21} = A \cdot e^{-\frac{1}{R \cdot T} \Delta G^a} \\
& \curvearrowright \\
& \frac{dc(ES)}{dt} = \left(A \cdot e^{-\frac{1}{R \cdot T} \Delta G^a}\right) c(ES)
\end{array}
\qquad
\begin{array}{l}
E + S \xleftarrow{k_{21}} ES \\
\Delta G = (\mu_0(E) + \mu(S)) - \mu_0(ES) \\
\frac{dc(ES)}{dt} = -k_{21} c(ES) \\
\curvearrowright \\
k_{21} = A \cdot e^{-\frac{E_a}{R \cdot T}} \\
\Delta G > 0 \Rightarrow E_a = \Delta G^a + \Delta G \\
k_{21} = A \cdot e^{-\frac{1}{R \cdot T} \Delta G^a + \Delta G} \\
\curvearrowright \\
\frac{dc(ES)}{dt} = \left(A \cdot e^{-\frac{1}{R \cdot T}(\Delta G^a + (\mu_0(E) + \mu(S)) - \mu_0(ES)}\right) c(ES)
\end{array}
$$

In order to solve the equations shown, the parameters A, ΔG^a, $\mu_0(E)$, $\mu_0(ES)$, $\mu_0(EP)$, $\mu_0(S)$, $\mu(S)$, $\mu_0(P)$ and $\mu(P)$ must be defined and R is the ideal gas constant and T is the standard temperature. In this case arbitrary values are used, which are easy to calculate.

A: 10^{13}	$\mu_0(ES)$: $0.000 \cdot 10^0$	$\mu(S)$: $1.000 \cdot 10^0$
ΔG^a: $1.000 \cdot 10^1$	$\mu_0(EP)$: $0.000 \cdot 10^0$	$\mu_0(P)$: $0.000 \cdot 10^0$
$\mu_0(E)$: $0.000 \cdot 10^0$	$\mu_0(S)$: $0.000 \cdot 10^0$	$\mu(P)$: $0.500 \cdot 10^{-1}$

The selected values are now inserted into the equations. First, ΔG is determined for $E + S \xrightarrow{k_{12}} ES$.

$$\Delta G = \mu_0(ES) - (\mu_0(E) + \mu(S)) = 0 - (0 + 1.000 \cdot 10^0) = -1.000 \cdot 10^0 = sgn(\Delta G) < 0$$

From the equation ΔG is less than zero and therefore the equation

$$k'_{12} = A \cdot e^{-\frac{1}{R \cdot T}(E_a)} = 10^{13} \cdot e^{-\frac{1}{1.987204258 * 10^{-3} \cdot 300}(10.0)} = 5.130 \cdot 10^5$$

is used to determine the rate constant. As a small note, the rate constant calculated here, is the maximum possible rate constant, because E_a can not be smaller than ΔG. If all equations are now solved, the result is a reaction path matrix.

$$\begin{bmatrix} 0.000 \cdot 10^0 & 9.575 \cdot 10^4 & 2.216 \cdot 10^5 \\ 5.130 \cdot 10^5 & 0.000 \cdot 10^0 & 5.130 \cdot 10^5 \\ 5.130 \cdot 10^5 & 5.130 \cdot 10^5 & 0.000 \cdot 10^0 \end{bmatrix}$$

and a rate constant matrix

$$\begin{bmatrix} -5.130 \cdot 10^5 - 5.130 \cdot 10^5 & 9.575 \cdot 10^4 & 2.216 \cdot 10^5 \\ 5.130 \cdot 10^5 & -9.575 \cdot 10^4 - 5.130 \cdot 10^5 & 5.130 \cdot 10^5 \\ 5.130 \cdot 10^5 & 5.130 \cdot 10^5 & -5.130 \cdot 10^5 - 2.216 \cdot 10^5 \end{bmatrix}$$

If this matrix is now inserted into the linear system of equations, the following system results.

$$\begin{pmatrix} \frac{dc(E)}{dt} \\ \frac{dc(ES)}{dt} \\ \frac{dc(EP)}{dt} \\ c_{total} \end{pmatrix} = \begin{bmatrix} -1.026 \cdot 10^6 & 9.575 \cdot 10^4 & 2.216 \cdot 10^5 & 1 \\ 5.130 \cdot 10^5 & -6.088 \cdot 10^5 & 5.130 \cdot 10^5 & 1 \\ 5.130 \cdot 10^5 & 5.130 \cdot 10^5 & -7.347 \cdot 10^5 & 1 \\ 1 & 1 & 1 & 0 \end{bmatrix} \begin{pmatrix} c(E) \\ c(ES) \\ c(EP) \\ \epsilon \end{pmatrix} = \begin{pmatrix} 0 \\ 0 \\ 0 \\ 1 \end{pmatrix}$$

The solution to this system of equations is

$$\begin{aligned} c(E) &= 1.315 \cdot 10^{-1} \\ c(ES) &= 4.573 \cdot 10^{-1} \\ c(EP) &= 4.112 \cdot 10^{-1} \\ \epsilon &= 0 \end{aligned}$$

Now the differential equations set up at the beginning are solved with the calculated rate constants and concentrations.

(I') $E + S \xrightarrow{k_{12}} ES$

$$\begin{aligned} \frac{dc(E)}{dt} &= -k'_{12}c(E) \\ &= -6.746 \cdot 10^4 \\ \frac{dc(S)}{dt} &= -k'_{12}c(E) \\ &= -6.746 \cdot 10^4 \\ \frac{dc(ES)}{dt} &= k'_{12}c(E) \\ &= 6.746 \cdot 10^4 \end{aligned}$$

(II') $ES \xrightarrow{k_{23}} EP$

$$\begin{aligned} \frac{dc(ES)}{dt} &= -k_{23}c(ES) \\ &= -2.346 \cdot 10^5 \\ \frac{dc(EP)}{dt} &= k_{23}c(ES) \\ &= 2.346 \cdot 10^5 \end{aligned}$$

(III') $EP \xrightarrow{k_{31}} E + P$

$$\begin{aligned} \frac{dc(EP)}{dt} &= -k_{31}c(EP) \\ &= -9.113 \cdot 10^4 \\ \frac{dc(E)}{dt} &= k_{31}c(EP) \\ &= 9.113 \cdot 10^4 \\ \frac{dc(P)}{dt} &= k_{31}c(EP) \\ &= 9.113 \cdot 10^4 \end{aligned}$$

(I'') $E + S \xleftarrow{k_{21}} ES$

$$\begin{aligned} \frac{dc(E)}{dt} &= k_{21}c(ES) \\ &= 4.379 \cdot 10^4 \\ \frac{dc(S)}{dt} &= k_{21}c(ES) \\ &= 4.379 \cdot 10^4 \\ \frac{dc(ES)}{dt} &= -k_{21}c(ES) \\ &= -4.379 \cdot 10^4 \end{aligned}$$

(II'') $ES \xleftarrow{k_{32}} EP$

$$\begin{aligned} \frac{dc(ES)}{dt} &= k_{32}c(EP) \\ &= 2.109 \cdot 10^5 \\ \frac{dc(EP)}{dt} &= -k_{32}c(EP) \\ &= -2.109 \cdot 10^5 \end{aligned}$$

(III'') $EP \xleftarrow{k_{13}} E + P$

$$\begin{aligned} \frac{dc(EP)}{dt} &= k'_{13}c(E) \\ &= 6.746 \cdot 10^4 \\ \frac{dc(E)}{dt} &= -k'_{13}c(E) \\ &= -6.746 \cdot 10^4 \\ \frac{dc(P)}{dt} &= -k'_{13}c(E) \\ &= -6.746 \cdot 10^4 \end{aligned}$$

Based on the forward and backward fluxes, the corresponding net fluxes can be determined.

$$\begin{array}{c} r \setminus p \\ c(E) \\ c(ES) \\ c(EP) \end{array} \begin{array}{c} \begin{array}{ccc} c(E) & c(ES) & c(EP) \end{array} \\ \begin{bmatrix} 0 & -2.367 \cdot 10^4 & 2.367 \cdot 10^4 \\ 2.367 \cdot 10^4 & 0 & -2.367 \cdot 10^4 \\ -2.367 \cdot 10^4 & 2.367 \cdot 10^4 & 0 \end{bmatrix} \end{array}$$

The substance flux can be determined from these net fluxes and thus all required quantities could be determined.

Table 6.1: Substance Net Flux for the enzymatic reaction.

Substance	S; E; ES	$2.367 \cdot 10^4$
Substance	P; E; EP	$-2.367 \cdot 10^4$

In the substance net flux, a negative sign is equivalent to an outflow of the substance and a positive sign is equivalent to an inflow of a substance. So in this example the product flows out of the cycle and the substrate flows in of the cycle. In summary, the enzyme converts substrate to product and because the stoichiometries are equal, the flux should also be equal, which it is. In the appendix can be found the script to start the program and the output file of the calculations (listings F.1 to F.8).

References

(*1*) Job, G., and Ruffler, R., *Physikalische Chemie*, 2nd ed.; Studienbucher Chemie; Springer Spektrum: Wiesbaden, Germany, 2021.

(*2*) Arrhenius, S. (1889). Über die Dissociationswärme und den Einfluss der Temperatur auf den Dissociationsgrad der Elektrolyte. *Z Phys Chem 4U*, 96–116, DOI: 10.1515/zpch-1889-0408.

(*3*) Arrhenius, S. (1889). Über die Reaktionsgeschwindigkeit bei der Inversion von Rohrzucker durch Säuren. *Z Phys Chem 4U*, 226–248, DOI: 10.1515/zpch-1889-0416.

(*4*) Ullmann, G. M. (2023). GMCT@UBT Manual - Version 2.0.

(*5*) Becker, T., Ullmann, R. T., and Ullmann, G. M. (2007). Simulation of the Electron Transfer between the Tetraheme Subunit and the Special Pair of the Photosynthetic Reaction Center Using a Microstate Description. *J Phys Chem B 111*, 2957–2968, DOI: 10.1021/jp066264a.

(*6*) Bombarda, E., and Ullmann, G. M. (2011). Continuum electrostatic investigations of charge transfer processes in biological molecules using a microstate description. *Faraday Discuss. 148*, 173–193, DOI: 10.1039/c003905e.

(*7*) Murray, J. D., *Mathematical biology*, 2nd ed.; Biomathematics; Springer: Berlin, Germany, 1993.

7

APPLICATION TO bc_1-COMPLEX

As already mentioned in chapter 1, the bc_1-complex and the Q-cycle have been investigated experimentally and theoretically. In these investigations, the main focus was on the Q_o-binding site, since bifurcation takes place there and a semiquinone can probably be stabilised. The bifurcation was, as mentioned in the introduction, described by Mitchell (*1*). The sequence of events leading to this bifurcation has not yet been finally determined. There are two possible scenarios.

The first scenario is that the first step of this bifurcation is the proton-coupled electron transfer (PCET) on the Rieske center, which is followed by an electron transfer to the heme b_L with the second proton passing to the Glu295. A second possible scenario is to swap the sequence, i.e. electron transfer to the heme b_L occurs first, with the proton passing to Glu295, followed by PCET to the Rieske center. Along with the discussion on the sequence, the rate-determining step is discussed. It should be noted that to transfer the electron from the Rieske center to the cytochrome c_1 a larger domain movement of the Rieske protein is required. Whether this movement is rate-determining, was also investigated. It was shown that the domain motion is not rate-determining, but appears to be precisely synchronized with the oxidation of the quinol in the Q_o-binding site so that no unwanted side reaction occurs like generation of superoxides (*2–4*). At the Q_i-binding site, studies show that a stabilized semiquinone occurs there (*5*), but it is not in the radical state but in the anionic state. The electrons for this reduction originate from the Q_o-binding site and are transferred to the Q_i-binding site via the heme b_L and heme b_H. The necessary protons for protonation are believed to (*6*, *7*) come from His217 and Asp252 and originally from the cytosol.

The Q-cycle described and used in section 7.3.2 represents a separate consideration generated by incorporating the previous findings (see above and section 1.1.3) and is only one possible variant of the Q-cycle. This Q-cycle is not used for the kinetic calculations. Moreover, the kinetic investigation is not to be performed on a specific Q-cycle, but all possible variants are to be investigated. By this type of investigation a graph over all possible variants can be formed and thus all possible Q-cycles can be described. By a simple path search within the graph, the best possible Q-cycle can be found.

The findings from chapters 3 to 5 make it now possible to investigate the bc_1-complex and the Q-cycle. In the chapter 3, the basic theory of the macro and microstate model was described and used to determine the G_{model}-value for ubiquinone in the form of benzoquinone using quantum mechanics. The chapter 4, establishes a virtual model compound and allows the determination of the G_{model}-value of compounds for which no model compounds but proteins, containing only the compound as a cofactor and no pH range was measured, exist. The chapter 5 extends this theory to another level, allowing the determination of G_{model}-value using a fit of experimental values of model compounds or proteins describing the redox potential or pK_a-value over a pH range. Using this method, the G_{model}-values for b and c-type heme could be determined.

7.1.1 Ubiquinol

In chapter 3, it was possible to determine the G_{model}-values for ubiquinol (table 3.4). It has been shown that the determination of especially the semiquinone states is difficult, because of their low population. However, it turns out that the bc_1-complex is able to stabilize such states. This stabilization property is important for the Q-cycle, but is difficult to represent in a solvent and is not possible at all

in water. For this reason, the G_{model}-values had to be calculated theoretically. However, semiquinone states also turned out to be challenging to compute.

7.1.2 Heme type B and C

In chapter 4 the G_{model}-values were determined. In this method, the calculations were also based on protein structures. It is shown that the refinement of the protein structures is of crucial importance for the redox potentials. Even simple refinements can significantly improve the theoretical redox potentials. A consistent G_{model}-value could be determined for cytochromes with b-type heme with these refinements. For c-type heme, the refinements also improved the theoretical redox potentials, but, because of the many different subtypes, it was more difficult to determine a generally valid G_{model}-value.

Table 7.1: G_{model}s for heme type B and C.

	$G_{model}\left[\frac{kcal}{mol}\right]$
Heme C (red)	-4.17
Heme C (ox)	0.00
Heme B (red)	0.28
Heme B (ox)	0.00

7.1.3 Rieske center

In chapter 5, the G_{model}-values for the Rieske center were determined (table 5.9). Similar to ubiquinol, there are states of Rieske center that are easier to stabilize in the protein environment. For this reason, the G_{model}-values could only be determined within a protein after the influence of the protein environment could be removed.

With this last step all preparations for the calculation of the kinetics within the Q-cycle are completed (*8–18*). In addition, the bc_1-complex and the Q-cycle will described in general terms with respect to pK_a-values, redox potentials and protonation probabilities and only after that the kinetics of the cycle will be discussed in more detail.

7.2 Methods

7.2.1 pK_a-values and redox potentials

The different pK_a-values and redox potentials were determined with the programs `CHARMM` (*19*, *20*), `preptitra` and `gmct` (*21–23*) as mentioned in the chapters 4 and 5. The method and settings have also been taken from chapters 4 and 5. The necessary quantum mechanical calculations for the determination of the charges were also carried out as described in chapter 5. However, since the Rieske center and ubiquinol are molecules that have an unpaired electron state, further options were added to the input-file of `orca`. Therefore the option UKS was added for both and a spin flip was performed especially for the Rieske center, since the iron-sulfur cluster has a spin-up and a spin-down iron.

The pK_a-values and redox potentials for the figure 7.3 were calculated in several steps. The figure 7.3 shows twelve different states of the bc_1-complex. For each of these possible states, each site was considered separately for the determination of the pK_a-values and redox potentials. For this purpose, all sites except the site of interest were fixed to the site-state required for this specific state. The site of

interest was then titrated to this environmental configuration. Thus, the influence of the environment on this one cofactor becomes clear. This procedure was repeated for all sites Q_i, Q_o, heme b_L, heme b_H, heme c_1, and the Rieske center.

7.2.2 Preparation of Kinetic/Steady-state calculations

The kinetic calculations were performed in several steps. First, it must be determined which cofactors and amino acid residues are important for a kinetics model (see section 7.4.1). In the second step, the relevant states for the selected cofactors and amino acid residues are determined (③). Protein conformations, binding site occupancies, protonation states, and electronic states are then determined for the entire kinetics model. Thus, the kinetics model as a whole includes several system states that differ in the above properties. Then, for all created system states, the energy for the respective states was calculated using the program `state-energy` (*24*). The system state energies acted as a basis for the correct energetic observation of the states as well as for the calculation of the state distribution probability. The calculated energies for the respective system states were written to a file. All possible reactions/transitions between the system states were also attached to this file. As described in the theory section, the program `kinetics` (*24*) uses the Arrhenius equation to determine the flux. For this reason, values for A and ΔG^a were assigned to the reactions. For simplification, all reactions, including uptake and release of protons, electrons and ligands, as well as conformational changes and the transfer of electrons or protons, were assigned the same values for A with $1.000 \cdot 10^{13}$ and for ΔG^a with 10 $\frac{kcal}{mol}$ (④). The difference of all these reaction types is described by the previously determined state energies or the energetic difference of the reactants. The required μ-values were derived from a combination of experimental considerations and theoretical considerations described in the previous chapters. The table 7.5 contains all set μ-values describing the chemical environment/properties of the kinetic model (②). Finally, an input-file created in this way has the following structure and all values are in $\frac{kcal}{mol}$. The stoichiometric coefficients are from the reaction equation of the Q-cycle (①).

Listing 7.1: Structure of an input-file for the program "kinetics"

```
#       SubstanceName StochiometryCoeff      )
EDUCT      U2PP_MEMB             1            |
.                                             |  ①
.                                             |
.                                             |
PRODUCT     proton_EC            4           )

#     SubstanceName    mu_0      mu'                                           )
CHEMPOT    U2PP_MEMB    0.00     0.00  E_0:proton_2:electron_2:quinone_1        |
.                                                                               |  ②
.                                                                               |
.                                                                               |
CHEMPOT     proton_EC    0.00    -9.60  E_0:proton_1:electron_0:quinone_0      )

#LABEL   ID              CONCENTRATION ENERGY0   Enzyme:LIG1:...:LIGN            ENERGY@mu      )
STATE    C00:1:1:1:1:1:0:0  1.3823e-08    1.6974e+01 E_1:proton_3:electron_0:quinone_0 9.3040e+00  |
.                                                                                               |  ③
.                                                                                               |
.                                                                                               |
STATE    Q11:2:2:2:2:7:9:9  1.5503e-34    3.0771e+01 E_1:proton_4:electron_8:quinone_2 4.4902e+01 )

#       Reactant-state          -- Product-state        : A          dGa        REAKTIONTYP DESCRIPTION        )
REACTION  C11:1:1:1:1:1:1:1 [0]      -- Q11:1:1:1:1:1:1:1 [0]  :  1.000000e+13  1.000000e+01 # ConfChange ...   |
.                                                                                                              |  ④
.                                                                                                              |
.                                                                                                              |
REACTION  Q11:2:2:2:2:7:9:4 proton_CP --  Q11:2:2:2:2:7:9:5 [0]  :  1.000000e+13  1.000000e+01 # Uptake ...   )
```

7.2.3 Kinetic/Steady-state calculations

The created input-file (listing 7.1) from the previous subsection for the program `kinetics` was partly created manually, because not everything was automated. Based on this created input-file, the program was able to determine all the fluxes, as well as other information such as the steady-state concentration of the states. The program created an output file as well as a `graphviz`-file (*25*), which had the same content, but could later be read in more easily for the evaluation of `graph-tool` (*26*). The listing 7.2 shows the output file of the `kinetics` program and its structure.

Listing 7.2: Structure of an output file of the program `kinetics`

```
   ============================================================
   # Kinetics, Version 0.1
   ...
 4 ============================================================
   ============================================================
   Info on the Reactions
   ...
   ============================================================
 9 # Input
   STATE C00:1:1:1:1:1:0:0     8.271e-03      7.224e+00
   ...
   ============================================================
   Rate Constant Parameter:
14 ...
   ============================================================
   Rate Matrix:
   ============================================================
   Analyzing the (potential) thermodynamics of the reaction
19 Reaction:
   ...
   ============================================================
   Equilibrium Constant Matrix
   ...
24 ============================================================
   Analyze the State Network
   ...
   ============================================================
   Steady State Concentrations and State Energy :
29 ...
   ============================================================
   Total Used CPU Time: .... sec
```

7.2.4 Analysis of Kinetic/Steady-state calculation results

The output file of the program `kinetics` was evaluated by using a python script which is available on zenodo (*27*). The python script is able to read in a `graphviz` file by means of the module `graph-tool` and to create a graph. This graph was pre-filtered and all fluxes those had a too low flux were discarded. Filtering sped up the subsequent search. A custom method was written to search and evaluate a cycle which was created with `graph-tool`. The search-method searches for the highest flux and then continues to follow the highest flux until a maximum number of nodes have been followed or a cycle has formed. When a cycle is found, that represents the zeroth layer. The next layer is formed by the program jumping back to the beginning of the cycle and now no longer following the highest flux, but following the second highest flux, if available, and only then following the highest flux again. This is done for all nodes in the cycle and thus results in the first layer. After the first layer follows the second layer and so on. The search for further layers ends as soon as no more new branches could be found in the zeroth layer or the graph is complete or the predefined coverage of the flux has been reached or the maximum number of layers has been reached (see also figure B.2). The coverage of the flux is the ratio between the total flux in the entire graph and the flux described by the cycle with its layers.

7.3 Q-Cycle and the binding sites Q_i and Q_o

Before discussing the Q-cycle, the two binding sites Q_i and Q_o are looked at in more detail, as they are a key element in the Q-cycle. Afterwards, possible criteria for a possible Q-cycle are presented and various pK_a-values and redox potentials are calculated.

7.3.1 Binding sites Q_i and Q_o

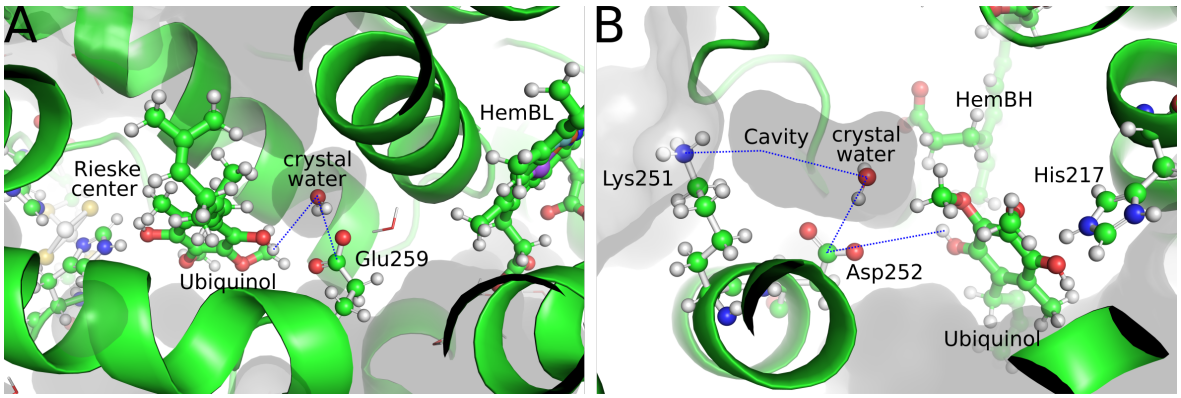

Figure 7.1: Q_i and Q_o-binding site from bc_1-complex:
A: Q_i with bound ubiquinol and marked Rieske center, heme b_L, Glu295, and a crystal water.
B: Q_o with bound ubiquinol and marked Rieske center, heme b_H, Lys251, Asp252, His217, and crystal water.

At the Q_o-binding site, oxidation and deprotonation of the bound ubiquinol occurs (figure 7.1 A). The Q_o-binding site includes the heme b_L, the Rieske center, and Glu295. The study from Victoria *et al.* (*28*) showed that Glu295 may also play a role in the ubiquinol environment. In this study from Victoria *et al.* is a hint that the second proton of the semiquinone formed by the PCET to the Rieske center can be delivered to this Glu295. During the movement of the Rieske protein, on the one hand, the ubiquinone can be exchanged to ubiquinol and, on the other hand, the Glu295 can be deprotonated as the binding site is opened towards the cytosol. The heme b_L, which is also a part of the binding site Q_o, acts as an electron acceptor. The second electron is transferred to the heme b_L.

At the Q_i-binding site, reduction and protonation of the bound ubiquinone takes place (figure 7.1 B). The electrons come from the heme b_H and originally from the Rieske center. The titrations show that the protons for the protonation of ubiquinone come from His217 and Asp252. The His217 receives its proton from the solvent when the binding site is not occupied. The Asp252 receives its proton via a water and Lys251, as can also be seen in figure 7.1 B. In addition to the amino acid residues shown here, Phe216 and Phe244 are also present in the binding pocket, and their ring systems stabilize the semiquinone.

In the following, the two binding sites Q_o and Q_i are investigated electrostatically. Two situations in the two binding sites are considered. One is the binding of a ubiquinol and the other is the binding of a ubiquinone. The electrostatic influence of the binding site on the bound ubiquinol or ubiquinone is considered. The electrostatic potential of the ubiquinol or ubiquinone in the protein environment is also considered. The Q_i-binding site has a stronger positive electrostatic potential, which becomes slightly negative on the heme-facing side, where the Asp252 and heme prosthetic groups are located (figure 7.2 B). The Q_o-binding site is less strongly positive around the Rieske center and has negative regions around the Glu295 (figure 7.2 D). Ubiquinol or ubiquinone exhibits an opposite electrostatic potential to the Q_o-binding site (figure 7.2 A and C). Thus, the ubiquinone or ubiquinol can bind well in the Q_o-binding pocket. Examining the electrostatic potential of ubiquinol under the influence

of the Q_o-binding pocket, it is found that a stronger negative electrostatic potential is formed in the direction of the Rieske center than in the direction of the Glu295. This fact could be an indication that the first transfer of electron and proton to the Rieske center could take place (figure 7.2 A). Examining the electrostatic potential of ubiquinone under the influence of the Q_o-binding pocket, here it is found that the electrostatic potential shifts to the more positive one. This is probably due to the fact that ubiquinone, unlike ubiquinol, has a double-bonded oxygen and no polarized OH bonds. A similar shift is also observed in the Q_i-binding pocket. If the electrostatic potential of ubiquinol or ubiquinone is examined under the influence of the Q_i-binding pocket, a more negative electrostatic potential is generally observed in contrast to the Q_o-binding pocket. This more negative electrostatic potential is stabilized by the positive electrostatic potential of the binding pocket and can still stabilize a semiquinone state.

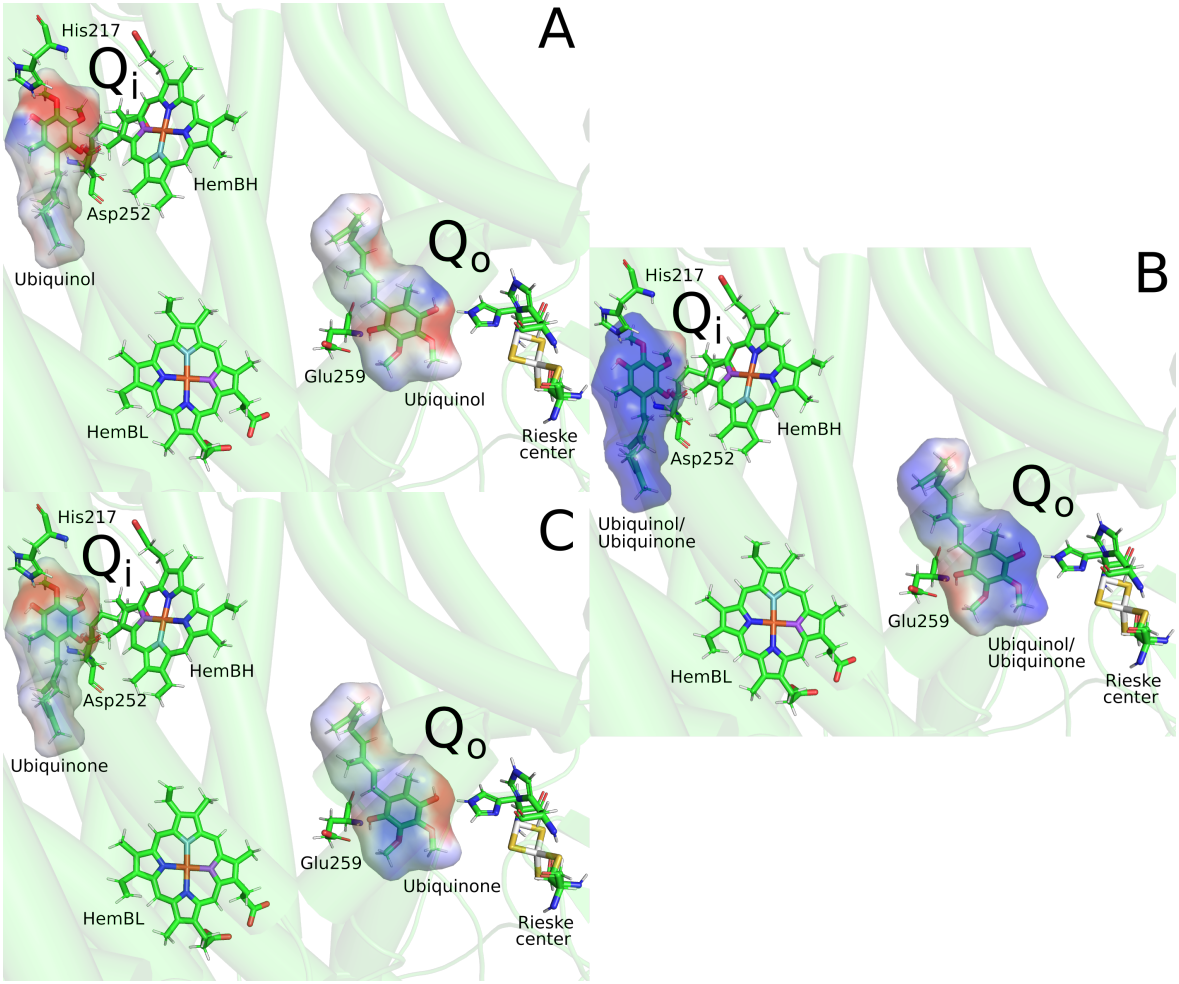

Figure 7.2: Electrostatic potential in a range of $-10\frac{RT}{e}$ to $10\frac{RT}{e}$ (negative potential in red and positive potential in blue) at the Q_i and Q_o-binding site in the bc_1-complex:
A/C: Electrostatic potential of ubiquinol/ubiquinones in the Q_i or Q_o-binding site.
B: Electrostatic potential of the binding site Q_i or Q_o The charges of the labeled groups was:
Rieske center: -2
heme b_L, heme b_H, Glu295, Asp252: -1
His217: 0

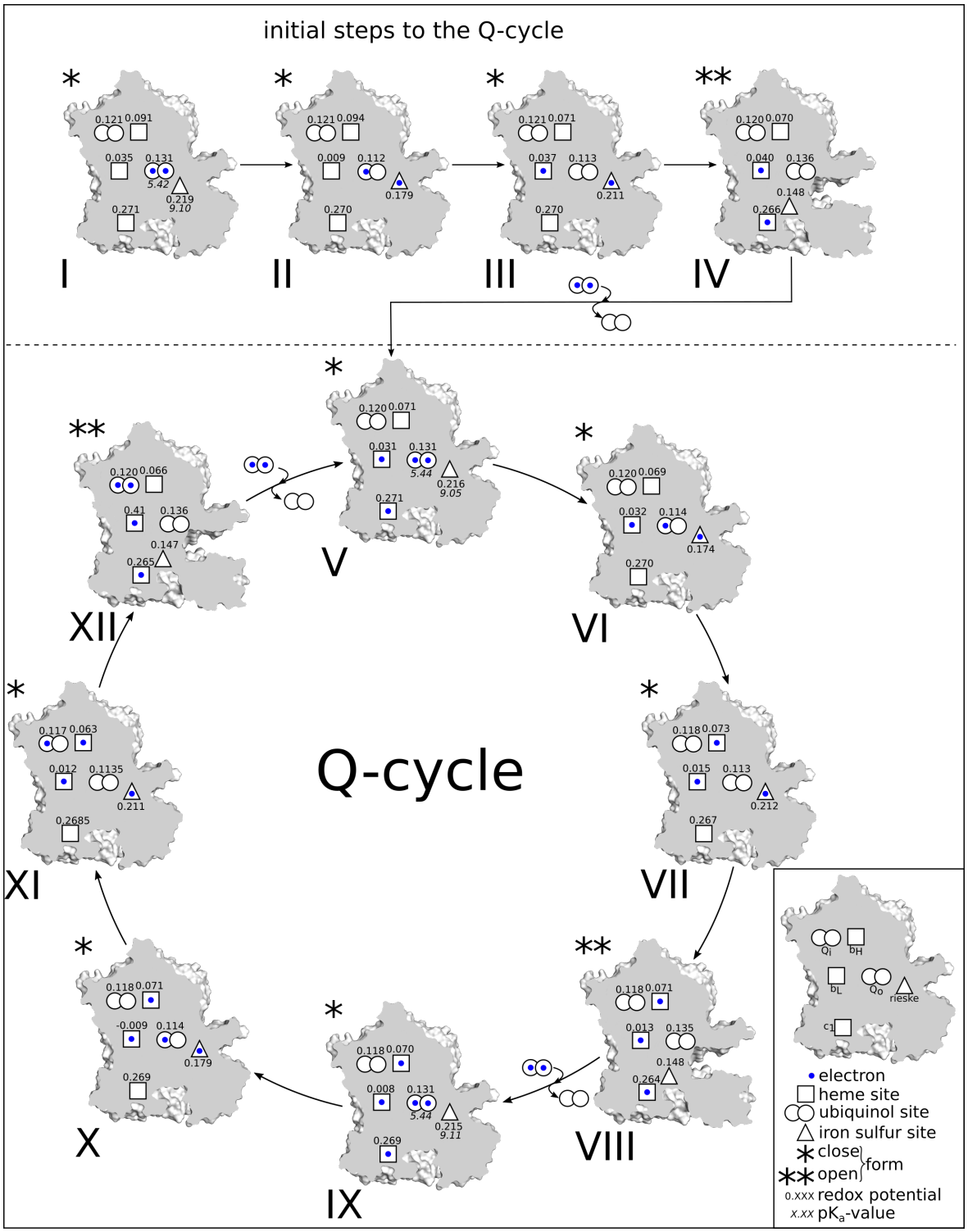

Figure 7.3: Postulated Q-cycle. The first four steps are the initial steps to enter the actual Q-cycle. The numerical values given are the calculated pK_a-values (below the ubiquinone/ubiquinol binding site) and redox potentials [mV].

7.3.2 Requirements for a Q-cycle

The Q-cycle shown in figure 7.3 (I-XII) is a custom consideration based on the scientific evidence presented in the introduction. The consideration assumes that at the beginning of a Q-cycle is a protein that has oxidized heme groups and Rieske centers. The Q_o-binding site is occupied by a ubiquinol and the Q_i-binding site is occupied by a ubiquinone. In the first four steps, the ubiquinol is oxidized and deprotonated at the Q_o-binding site (I-IV). These four steps are considered initializing steps, as it will be shown that a cycle can form between the steps V-XII.

In the first step of the Q-cycle, in our case the heme c_1 and the heme b_L are therefore already reduced. In this step V an ubiquinol is taken up. In the next step the Rieske center is reduced and protonated by the ubiquinol. A semiquinone remains in the Q_o-binding site (VI). In the following step the semiquinone transfers an electron to the heme b_L. That causes the "old" electron to be transferred to the heme b_H. The proton is transferred to the Glu295 which later transfers the proton to the solvent when the ubiquinone is exchanged (VII). Since the Rieske center is reduced and protonated, the structure can open and the electron can be transferred through the Rieske center to the heme c_1. During the opening of the structure the created ubiquinone is exchanged by a new ubiquinol (VIII). Since the Rieske center is now deprotonated and oxidized again, it can be reduced and protonated again by the ubiquinol. The renewed semiquinone gives its electron to the heme b_L (X) again. As a result, an electron can now be transferred to the ubiquinone at the Q_i-binding site and thus becomes a semiquinone. The necessary proton is released by the Asp252 (X). The semiquinone can now very easily take up another electron and proton from Lys251 and be reduced to a ubiquinol and protonated (XI). By exchanging the ubiquinol at the Q_i-binding site with a ubiquinone and oxidizing and deprotonating the Rieske center and reabsorbing a ubiquinol at the Q_o-binding site, the cycle can begin again (XII).

7.3.3 Redox potential and pK_a-value at the binding sites Q_i and Q_o

After a possible Q-cycle has been presented, it is now analyzed with respect to the calculated pK_a-values and redox potentials (figure 7.3) and these are compared with the experimentally determined values (table 7.2). The values shown in figure 7.3 are only for the cofactors heme b_L, b_H, c_1, Rieske center and for bound substrates in the binding sites Q_i and Q_o. This selection was made because there are experimental values for the mentioned ones. The previously mentioned Glu295, Asp252, and His217 were also analyzed, but the corresponding pK_a-values were not included in the figure 7.3 to avoid crowding the plot. Glu295 alternates between being protonated in the closed form of the bc_1-complex and deprotonated in the open form of the bc_1-complex. This change related to the conformation could be an indication that an H^+-atom is transferred from the ubiquinol or semiquinone to the Glu295 and can then be released to the cytosol. An opposite behavior is shown by the Asp252 and His217 at the Q_i-binding site. Both amino acid residues are able to protonate a ubiquinone, or semiquinone, so that a ubiquinol can ultimately be formed.

When considering the Q-cycle step by step with respect to the cofactors mentioned, it becomes clear that the redox potential changes in each step. The calculated redox potentials differ from the experimental values with the exception of cytochrome c_1. However, it should be noted for example in the reaction of ubiquinone to ubiquinol, that the overall reaction was measured and not the individual reactions. If the total reaction is considered theoretically, then values of 92 mV to 104 mV result, depending on the protein environment, and is thus very close to the experimentally measured value. This redox potential also makes it possible to reduce the nearby Rieske center with a redox potential between 149 mV to 219 mV. The pK_a-values were also determined with 5.44 for ubiquinol and 9.11 for the Rieske center. That clearly shows that the Rieske center can be protonated by the ubiquinol. The theoretical pK_a-value for Glu295 is above 6 depending on the protein environment and thus can also be protonated by the ubiquinol. Thus, both proton transfer and electron transfer are possible. The

second electron transfer to the heme b_L is not possible according to the redox potentials. This fact is true for the experimentally as well as for the calculated redox potentials. The redox potential does not yet shift strongly enough in the calculation to allow electron transfer and show the bifurcation. That is probably related to the problem with the semiquinone states. In summary, a redox potential chain can be formed from all redox potential (mV) of the Q-cycle in figure 7.3, which shows that all further electron transfers from the heme b_L to the Q_i-binding site and from the Rieske center to the cytochrome c_1 are possible:

$$\underbrace{[264\dots271]}_{c_1} > \underbrace{[148\dots219]}_{\text{Rieske center}} > \underbrace{[112\dots136]}_{Q_o} < \underbrace{[-9\dots41]}_{b_L} < \underbrace{[69\dots94]}_{b_H} < \underbrace{[117\dots121]}_{Q_i}$$

Table 7.2: Experimental redox potential and pK_a-values for FeS, Q/QH_2, cyt c_1, b_H and b_L

	FeS	Q/QH_2	cyt c_1	b_H	b_L
$E_{m,7}$ (mV)	$280-310^{(18,\,29)}$	$90^{(18,\,29)}$	$270^{(29)}$	$50^{(29,\,30,\,31)}$	$-90^{(18,\,30,\,31)}$
$E_{m,x}$ (mV)	-	$477^{(32)}$	$230^{(33)}$	$160^{(34)}$	$39^{(34)}$
pK_a-value	$7.6, 9.2^{(35)}$	-		$5.7, 7.7^{(34)}$	$5.9, 7.9^{(34)}$

7.4 Kinetic at the binding sites Q_i and Q_o

7.4.1 Model definition

Two structural models were created to calculate energetics and distances between the different sites were calculated. Model I is the smaller model and includes the sites Rieske center, heme c_1, heme b_L, heme b_H, Q_o, Q_i and Glu295 (model V-I). With this configuration it is possible to map all transfers necessary for a Q-cycle and that is the smallest possible configuration. The larger model II includes the model I plus the sites Asp252 and His217 (model V-II). By adding the sites Asp252 and His217, the Q_i is no longer directly connected to the cytoplasm as in model I. The Q_i is now only accessible from the cytoplasm via these two sites.

Crucial in both models is that the Q_i is directly or indirectly connected to the cytoplasm and the Q_o is directly or indirectly connected to the periplasm. However, there is no external connection between the cytoplasm and the periplasm (see figure 1.3). For this reason, as seen in table 7.5, two pools of protons were defined, one located in the cytoplasm (CPp) and one located in the periplasm (ECp). These pools can accept and release protons. A pool is a chemical potential that describes an (im)balance between states or a driving force. In the case of a pool of protons, it is simply the pH-value expressed as a chemical potential, or in the case of an pool of electrons, it is the redox potential expressed as a chemical potential. In the periplasm there is an additional electron carrier, cytochrome c_1, which also needs a pool to accept or donate its electrons. For this reason, an electron pool was defined in the periplasm, which can also accept and release electrons. In addition to a direct or indirect connection to the cytoplasm or periplasm, the two binding sites Q_o/Q_i also require a connection to a pool of ubiquinones or ubiquinols. In general, one pool is sufficient for both sites because the ubiquinones or ubiquinols are present in the membrane and are therefore directly accessible to both sites. However, as was later found, two separate pools are better for evaluating the fluxes. If the same parameters are used for both pools, they are identical to using only one pool.

Both models are embedded within the bc_1-complex and are influenced by this environment. For this reason the proton and electron configurations of the surrounding amino acid residues and cofactors,

respectively, were determined. This environment also includes the different conformations of the whole complex, such as the occupancy of the Q_i and Q_o-binding sites and the position of the Rieske subunit. The environment of the whole bc_1-complex is also relevant, so a dummy membrane was fitted around the membrane-bound region, consisting only of uncharged dummy atoms and shielding the complex.

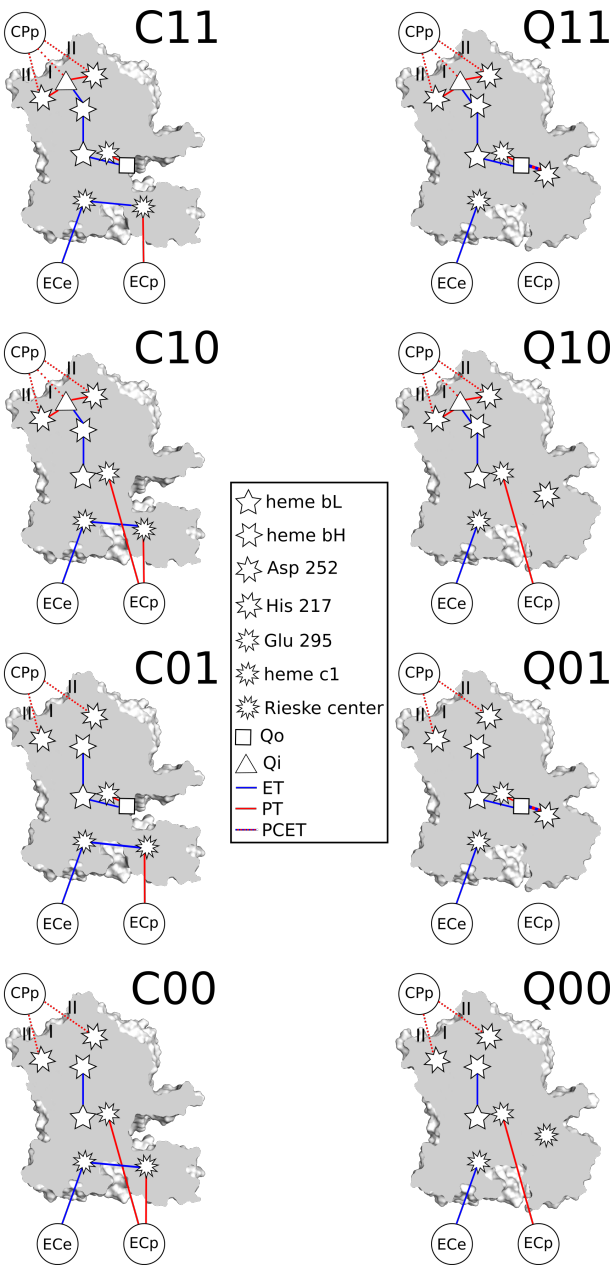

Figure 7.4: All eight different conformations based on table 7.3 with the possible transfer path of protons (red) and electrons (blue) in each conformation. The dashed lines labeled I and II represent the different pathways in model I and model II. Conformation C is the open conformation where the Rieske center is closer to cytochrome c_1, and Q is the closed conformation where the Rieske center is closer to the binding site Q_o. Whether the Q_i or Q_o-binding site is filled or empty can be read from the corresponding numerical code:

00 - both sites are empty
01 - Q_i site is filled
10 - Q_o site is filled
11 - both sites are filled

CPp - Pool for protons in the cytoplasm
ECp - Pool for protons in the periplasm
ECe - Pool for electrons in the periplasm

7.4.2 Model properties

The models have different properties, but also similarities. The table 7.3 sums up the models and distances between the different sites.

Table 7.3: All connection pairs with connection type and occurrence in the two conformations for the two models.
1xPE/PU: Uptake of a proton from periplasm or cytoplasm
1xEE/EU: Uptake of a electron from periplasm or cytoplasm
1xET: Electron transfer
1xPT: Proton transfer
00 - both binding sites are empty
01 - Q_i-binding site is filled
10 - Q_o-binding site is filled
11 - both binding sites are filled
CPp - Pool for protons in the cytoplasm
ECp - Pool for protons in the periplasm
ECe - Pool for electrons in the periplasm

model		Site A	Site B	TT	Conformation				Distances [Å]
					11	10	01	00	-
		Rieske center	ECp	1xPE/PU	-/C	-/C	-/C	-/C	-
		heme c_1	ECe	1xEE/EU	Q/-	Q/-	Q/-	Q/-	-
		Q_o	heme b_L	1xET	Q/C	Q/C	-/-	-/-	9.0
		heme b_L	heme b_H	1xET	Q/C	Q/C	Q/C	Q/C	6.5
	I	heme b_H	Q_i	1xET	Q/C	-/-	Q/C	-/-	2.5
		Rieske center	Q_o	1xPT/ET	Q/-	Q/-	-/-	Q/-	1.7/19.2
II		Rieske center	heme c_1	1xET	-/C	-/C	-/C	-/C	24.7/8.2
		Q_o	Glu295	1xPT	Q/C	-/-	Q/C	-/-	2.9
		Glu295	ECp	1xPT	-/-	Q/C	-/-	Q/C	-
		Q_i	Asp252	1xPT	Q/C	Q/C	-/-	-/-	4.8
		Q_i	His217	1xPT	Q/C	Q/C	-/-	-/-	2.3
		CPp	Asp252	1xPT	Q/C	Q/C	Q/C	Q/C	-
		CPp	His217	1xPT	Q/C	Q/C	Q/C	Q/C	-

Both models have in common that for a decrease in the possible states of the kinetic model, a decrease in the states of the individual sites was done. The decrease was done by removing improbable states from the sites. In the case of the Rieske center, five states (rrcp, rrc1, rrc2, rrct and riot) were excluded and number of states were decreased from twelve to seven states. In the case of the ubiquinol, three states (u0dp, u0pd and u0pp) were excluded and number of states were decreased from twelve to nine states. The number of possible states is $NoS = \sum^{\#CC} \left(\prod^{\#sites} \text{states per site} \right)$ with CC as Conformation Configurations and NoS as number of states. It was possible to decrease the number of states from 64,896 to 22,400 for model V-I and from 519,168 to 179,200 for model V-II (complete calculation see appendix G.1). Thus, the number of states was decreased by about 71 % for both models. The addition of the two sites Asp252 and His217 increased the number of possible states by a factor of 4. The increase in the number of states also increases the computational time by a factor of about 106. For this reason, model V-I also functioned as a test system for the more complex model V-II. The distances between the individual sites in the models. In both models, the distances remain constant and change only when the Rieske subunit undergoes a conformational change. An important

distance of 2.9 Å is the distance between Q_o-binding site and Glu295. Proton transfer between the Q_o-binding site and Glu295 shows that the quinol in the Q_o-binding site moves away from the Rieske center towards Glu295 to reduce the distance and allow proton transfer. Also of interest is the distance of 2.3 Å between His217 and the Q_i-binding site and the distance of 4.8 Å between Asp252 and the Q_i-binding site. Based on the results of the electrostatic study, proton transfer in the Q_i-binding site is possible. These three distances are between sites that complete a pure proton transfer and are short enough to make it possible. The longer distances between the Q_o-binding site and the heme b_L, between Q_i-binding site and heme b_H, between the two hemes b_L and b_H and between Rieske center and heme c_1 are not a problem, because these are pure electron transfers. The smallest distance is 1.7 Å between the Rieske center and the Q_o-binding site. Between these two sites a proton-coupled electron transfer takes place, so the distance has to be shorter than for pure electron transfer. Based on the distances, it can be assumed that the first proton transfer between His217 and a quinone occurs in the Q_i-binding site. Subsequently, similar to the case of Glu295, movement could occur to allow the second proton transfer from Asp252.

Table 7.5 contains the parameter values set for the different chemical potentials used as pools for electrons, protons, ubiquinone and ubiquinol. The two proton pools are set by the chemical potentials so that they correspond to a pH of 7 and thus no proton gradient is present. This setting makes the pool neutral and does not favor the uptake or release of protons. The electron pool has been adjusted to allow the electron transporter cytochrome c_1 to donate its electrons rather than accept them. The redox potential of the pool is 300 mV and the redox potential of cytochrome c_1 is about 270 mV.

The pool for ubiquinones and ubiquinols was set differently to calculate the flux. In one variation, the two pools were set equal so that they behaved as one pool. This setting was chosen so that there was an abundance of ubiquinol (variant 1). This setting was chosen because it takes two ubiquinols at the Q_o-binding site to form one ubiquinone at the Q_i-binding site into one ubiquinol within the Q-cycle, and thus a slight abundance of ubiquinol is beneficial. In the other variant, the pools were defined in such a way that ubiquinone was present in abundance at the Q_i-binding site, because here the ubiquinol is formed from ubiquinone. At the Q_o-binding site, on the other hand, ubiquinol was present in abundance, because this is degraded to ubiquinone (variant 2). This variant 2 has no biological or biochemical basis and is an attempt to enable or facilitate a Q-cycle. The μ_0-values also chosen represent the energetic difference between ubiquinone and ubiquinol and are calculated from the G_{model}-values.

The model properties, as already noted in the model definition, include the environment of the model. The tables G.2 and G.3 in the appendix summarize all protonation states of the entire bc_1-complex. The redox and protonation states were determined by electrostatic calculations and their evaluation, as also described in chapter 5. The energetic transition between each conformation was adjusted so that the conformations were equally likely to be occupied. The conformation energies were calculated in the first analysis from the binding energies for ubiquinone and ubiquinol. For this purpose, electrostatic methods were used to calculate the binding energy for each binding site for ubiquinone and ubiquinol. The binding energies for inhibitors stigmatellin and antimycin A were also calculated and compared with the experimentally known binding energies for the inhibitors. In order to calibrate the values for ubiquinone and ubiquinol, the differences between theoretical and experimental binding energies for the inhibitors were offset against the binding energies for ubiquinone and ubiquinol. In order to fulfill the condition that the conformations are equally occupied, the energies were manually adjusted afterwards. After this adjustment, the values result from the table 7.4.

Table 7.4: conformation energies in $\frac{kcal}{mol}$ for a equal occupancy of the conformations.

conformations							
both binding sites are filled		Q_o-binding sites is filled		Q_i-binding sites is filled		both binding sites are empty	
Q11	C11	Q10	C10	Q01	C01	Q00	C00
-0.47	-0.30	-0.59	-0.43	0.15	-0.05	-0.15	0.00

Table 7.5: All used chemical potentials (μ) to perform all kinetic calculation.

Substance	μ_0 $\left[\frac{kcal}{mol}\right]$	μ' $\left[\frac{kcal}{mol}\right]$		Description
		variant 1	variant 2	
U2PP_MEMB_CP	-20.68	5.14	0.14	ubiquinol for the Q_i-site
U0DD_MEMB_CP	0.00	3.14	3.14	ubiquinone for the Q_i-site
U2PP_MEMB_EC	-20.68	5.14	6.14	ubiquinol for the Q_o-site
U0DD_MEMB_EC	0.00	3.14	3.14	ubiquinone for the Q_o-site
proton_CP	0.00	-9.60	-9.60	Proton in the cytoplasm
electron_EC	0.00	-7.00	-7.00	Electron in the periplasm
proton_EC	0.00	-9.60	-9.60	Proton in the periplasm

7.4.3 Flux Calculation

As a reminder, the important reaction equations for the Q-cycle will be reviewed here, since stoichiometry is important in the analysis of flux.

$$Q\text{-cycle: } QH_2 + 2c_1^{3+} + 2H_{CP}^{+} \xrightarrow{bc_1} Q + 2c_1^{2+} + 4H_{EC}^{+} \tag{7.1}$$

with

Q: quinone
Q_2: quinol
H_{CP}^{+}: Proton from the cytoplasm
H_{EC}^{+}: Proton from the periplasm

After defining and analyzing the model for the flux calculations, the results of these four calculations are now considered. Figure 7.5 shows an example of the whole network that results from the various reactions. In the figure the model V-I (model I) is shown representatively. This is the smallest model studied here and has 22,400 states. The figure should make clear that even the smallest model forms a very complex and large graph. The model II, which is about eight times larger with 179,200 states, would not be representable in the way shown in figure 7.5. Even the representation of the 22,400 states shown here was not very simple, but figure 7.5 shows very well how complex even a model with only seven sites can become. All fluxes, rate constants, and steady-state concentrations were calculated for the entire networks of all four models: model I in variant 1, model I in variant 2, model II in variant 1, and model II in variant 2 (V-I.1, V-I.2, V-II.1, and V-II.2). From the signs of the fluxes for the whole network it can be seen that for the three models V-I.1, V-I.2 and V-II.1 ubiquinol flows into the cycle at both binding sites and ubiquinone flows out of the cycle (table 7.6). Thus, at both binding sites, ubiquinol is degraded to ubiquinone, which does not correspond to the intrenched sequence of

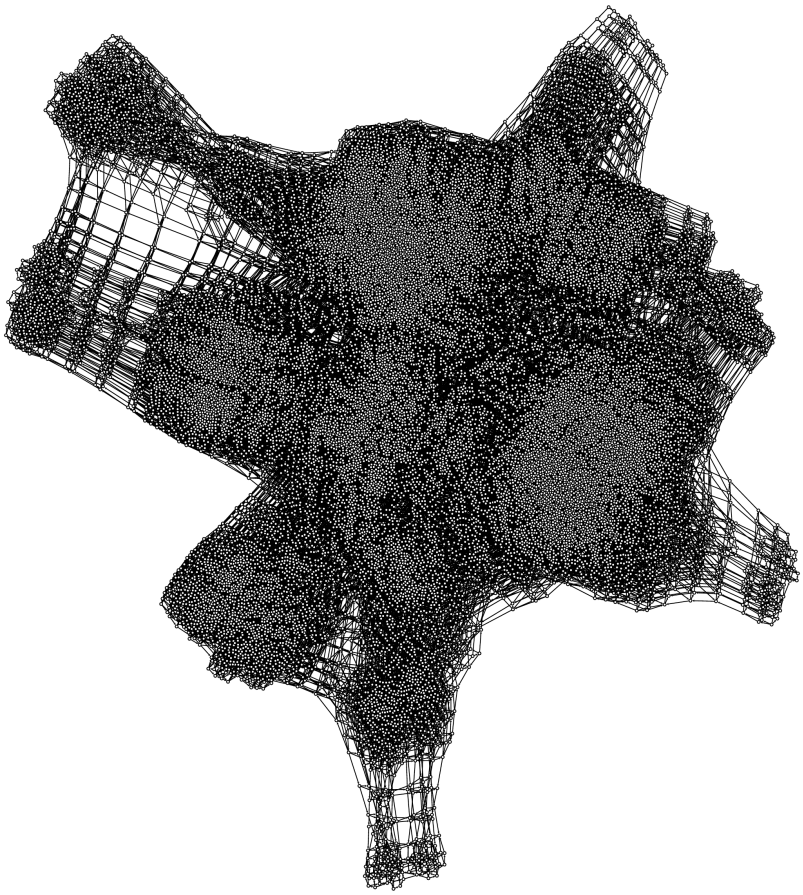

Figure 7.5: Complete flux network of the model 1 (model V-I). All white dots represent a state of model V-I and all black lines are a possible transition between two states. 22,400 states are represented and represent the smallest model studied here.

Table 7.6: Calculated netto substance fluxes $\left[\frac{M}{s}\right]$ for the different models with the parameters set from table 7.5.

Substance Name	V-I.1	V-I.2	V-II.1	V-II.2
U2PP_MEMB_CP	$4.700 \cdot 10^{0}$	$2.699 \cdot 10^{-2}$	$6.052 \cdot 10^{-1}$	$-1.700 \cdot 10^{-3}$
U0DD_MEMB_CP	$-4.700 \cdot 10^{0}$	$-2.699 \cdot 10^{-2}$	$-6.052 \cdot 10^{-1}$	$1.700 \cdot 10^{-3}$
U2PP_MEMB_EC	$5.437 \cdot 10^{0}$	$1.008 \cdot 10^{1}$	$1.142 \cdot 10^{1}$	$1.263 \cdot 10^{1}$
U0DD_MEMB_EC	$-5.437 \cdot 10^{0}$	$-1.008 \cdot 10^{1}$	$-1.142 \cdot 10^{1}$	$-1.263 \cdot 10^{1}$
proton_CP	$-9.401 \cdot 10^{0}$	$-5.397 \cdot 10^{-2}$	$-1.210 \cdot 10^{0}$	$3.399 \cdot 10^{-3}$
electron_EC	$-2.027 \cdot 10^{1}$	$-2.021 \cdot 10^{1}$	$-2.404 \cdot 10^{1}$	$-2.526 \cdot 10^{1}$
proton_EC	$-1.087 \cdot 10^{1}$	$-2.015 \cdot 10^{1}$	$-2.283 \cdot 10^{1}$	$-2.526 \cdot 10^{1}$

the Q-cycle (*1*, *36*), as can be seen from the reaction equation. However, the proton fluxes indicate that more protons are released into the periplasm than into the cytoplasm. Thus, a proton gradient is formed in this case as well. However, this is only based on the degradation of ubiquinol. The electrons released during the degradation are transferred from cytochrome c_1 to the cytochrome c. This fact

can be seen from the flux for the electrons, since this flux is the sum of the fluxes of U2PP_CP·2 and U2PP_EC·2. The factor two has to be used, because each U2PP has two electrons. If a bifurcation takes place, it cannot be directly read from flux. It is also shown that the net flux of electrons is the maximum predominant flux in the whole system. This is due to the fact that electrons can only flow into this electron pool from both binding sites. Model V-II.2 represents a special case because in this model, with the chemical potential settings applied, a network was created which is able to build up ubiquinone to ubiquinol at the Q_i-binding site and breaking ubiquinol down to ubiquinone at the Q_o-binding site. However, it remains the case that a much higher degradation of ubiquinol occurs at the Q_o-binding site and therefore the actually expected stoichiometric ratio of ubiquinol to ubiquinone is not maintained. Thus, bifurcation appears to occur due to electron flux and the build up of ubiquinol at the Q_i-binding site, but there appears to be problems. In order to make a more accurate prediction of the whole network, the elementary reactions in the respective networks will now be considered. The elementary reactions include the uni- and bimolecular reactions occurring in the network, such as the proton transfer from ubiquinol to Glu295 or the proton transfer from Glu295 to the solvent. There are 128 elementary reactions for model V-I and 166 elementary reactions for model V-II. All these elementary reactions have a flux unequal to zero. Figure 7.4 shows in a simplified way the possible elementary reactions in model V-II. The higher number of elementary reactions results from the fact that the respective sites still have different states which also have links. However, showing all possible representations in the figure would not have added to the clarity of the figure and have been dropped. For these elementary reactions, fluxes can also be determined, as well as the rate constants for the respective elementary reactions.

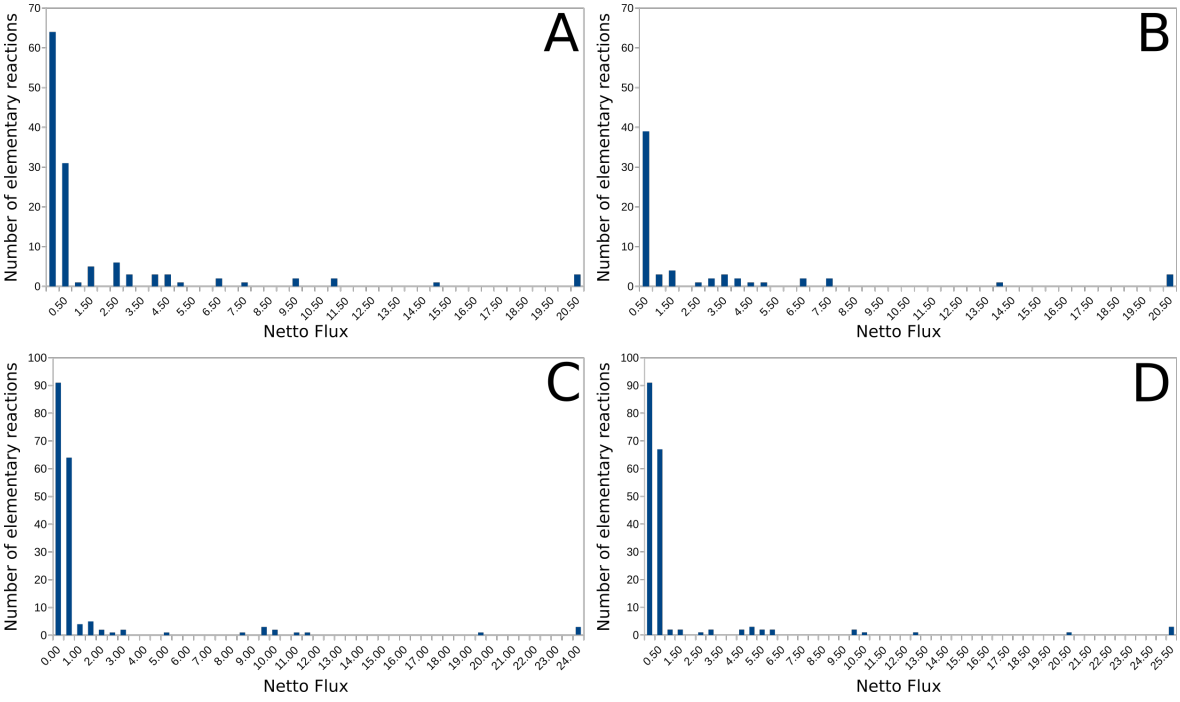

Figure 7.6: These histograms show the positive netto fluxes of elementary reactions for the four different models.
A: model VI.1 and the fluxes can be found in (tables G.5 to G.7)
B: model VII.1 and the fluxes can be found in (tables G.11 to G.13 and G.14)
C: model VI.2 and the fluxes can be found in (tables G.8 to G.10)
D: model VII.2 and the fluxes can be found in (tables G.15 to G.18)

Table 7.7: The three maximal and minimal values for calculated fluxes $\left[\frac{M}{s}\right]$, steady-state concentrations $[M]$ and rate constants $\left[\frac{1}{s}\right]$ for all four models.
"->": Transition between two states
"=": separation between two sites, if two sites are involved and no pool.

#LABEL	Netto	Forward	Backward	SSconcA	SSconcB	Forward	Backward
		Flux				Rates	
model V-I.1							
4::HemOx:0:0:0->HemRed:0:1:0=5::RRHP:2:1:0->RIOP:2:0:0	2.02E+01	6.57E+02	6.36E+02	1.28E-03	1.74E-01	5.13E+05	3.520E+03
5::RIOP:2:0:0->RIO2:1:0:0	2.02E+01	9.78E+04	9.77E+04	7.18E-01	1.91E-01	5.13E+05	1.203E+05
4::HemRed:0:1:0->HemOx:0:0:0	2.03E+01	1.17E+05	1.17E+05	2.27E-01	7.73E-01	1.90E+05	5.130E+05
1::GLUP:1:0:0->GLUD:0:0:0=6::U2DD:0:2:1->U2DP:1:2:1	9.71E-13	1.59E-08	1.59E-08	3.10E-14	8.15E-08	9.08E-02	5.130E+05
2::HemOx:0:0:0->HemRed:0:1:0=7::U2PP:2:2:1->U1PP:2:1:1	1.75E-12	1.87E-11	1.69E-11	5.13E-02	3.29E-17	5.13E+05	5.119E-10
2::HemOx:0:0:0->HemRed:0:1:0=7::U2DD:0:2:1->U1DD:0:1:1	2.26E-12	2.59E-12	3.21E-13	5.04E-18	3.80E-05	6.50E-09	5.130E+05
model V-I.2							
4::HemOx:0:0:0->HemRed:0:1:0=5::RRHP:2:1:0->RIOP:2:0:0	2.02E+01	6.65E+02	6.45E+02	1.30E-03	1.78E-01	5.13E+05	3.52E+03
5::RIOP:2:0:0->RIO2:1:0:0	2.02E+01	9.93E+04	9.93E+04	7.27E-01	1.94E-01	5.13E+05	1.20E+05
4::HemRed:0:1:0->HemOx:0:0:0	2.02E+01	1.18E+05	1.18E+05	2.29E-01	7.71E-01	1.90E+05	5.13E+05
1::GLUP:1:0:0->GLUD:0:0:0=6::U2DD:0:2:1->U2DP:1:2:1	7.93E-13	6.10E-09	6.10E-09	1.19E-14	3.17E-08	9.08E-02	5.13E+05
2::HemOx:0:0:0->HemRed:0:1:0=7::U2DD:0:2:1->U1DD:0:1:1	1.95E-12	1.95E-12	1.88E-15	3.80E-18	2.23E-07	6.50E-09	5.13E+05
2::HemRed:0:1:0->HemOx:0:0:0=7::U1PP:2:1:1->U2PP:2:2:1	2.03E-12	2.14E-12	1.08E-13	4.17E-18	2.76E-04	5.13E+05	4.91E-10
model V-II.1							
6::HemOx:0:0:0->HemRed:0:1:0=7::RRHP:2:1:0->RIOP:2:0:0	2.42E+01	6.64E+02	6.40E+02	1.29E-03	1.73E-01	5.13E+05	3.77E+03
7::RIOP:2:0:0->RIO2:1:0:0	2.42E+01	9.77E+04	9.77E+04	7.21E-01	1.90E-01	5.13E+05	1.22E+05
6::HemRed:0:1:0->HemOx:0:0:0	2.43E+01	1.16E+05	1.16E+05	2.25E-01	7.75E-01	1.92E+05	5.13E+05
3::HSP:2:0:0->HSD:1:0:0=9::U2DD:0:2:1->U2PD:1:2:1	8.73E-12	1.00E-10	9.13E-11	1.95E-16	6.36E-13	5.13E+05	3.87E+02
3::HSP:2:0:0->HSD:1:0:0=9::U2DD:0:2:1->U2DP:1:2:1	9.06E-12	1.00E-10	9.10E-11	1.95E-16	3.21E-11	5.13E+05	4.52E+00
3::HSP:2:0:0->HSE:1:0:0=9::U2DD:0:2:1->U2PD:1:2:1	9.37E-12	1.00E-10	9.07E-11	1.95E-16	3.14E-06	5.13E+05	1.49E-04
model V-II.2							
6::HemOx:0:0:0->HemRed:0:1:0=7::RRHP:2:1:0->RIOP:2:0:0	2.54E+01	6.74E+02	6.48E+02	1.31E-03	1.76E-01	5.13E+05	3.77E+03
7::RIOP:2:0:0->RIO2:1:0:0	2.55E+01	9.90E+04	9.90E+04	7.30E-01	1.93E-01	5.13E+05	1.22E+05
6::HemRed:0:1:0->HemOx:0:0:0	2.55E+01	1.16E+05	1.16E+05	2.26E-01	7.75E-01	1.92E+05	5.13E+05
3::HSD:1:0:0->HSP:2:0:0=9::U1PP:2:1:1->U1DP:1:1:1	6.90E-12	5.14E-11	4.45E-11	1.00E-16	2.48E-09	1.31E-06	5.13E+05
3::HSD:1:0:0->HSP:2:0:0=9::U1PP:2:1:1->U1PD:1:1:1	7.26E-12	5.14E-11	4.42E-11	1.00E-16	2.18E-08	1.39E-06	5.13E+05
3::HSP:2:0:0->HSE:1:0:0=9::U2DD:0:2:1->U2DP:1:2:1	9.92E-12	1.01E-11	1.71E-13	1.97E-17	1.97E-09	5.13E+05	1.44E-04

The figure 7.6 shows a histogram of all positive netto fluxes. A netto flux is the difference between forward and backward fluxes and thus indicates the direction of the reaction. It is sufficient to look at the positive netto fluxes because the negative netto fluxes are the same as the positive netto fluxes except for the sign. For all models in all variants, the majority of the netto fluxes are close to zero. The table 7.7 shows the elementary responses with the highest positive netto fluxes. The fastest reactions are oxidation of Rieske center by cytochrome c_1, deprotonation of Rieske center, and oxidation of cytochrome c_1. At the Q_i-binding site, the re-protonation of ubiquinone by Glu295 is very slow. At the Q_o-binding site, depending on the state of the ubiquinone, reduction or oxidation by the heme b_H is very slow. The same is true for the protonation or deprotonation by the His217 at the Q_o-binding site. Looking at the elementary reactions, it is noticeable that the proton uptake at the Q_o-binding site is very slow with $10^{-11} \ldots 10^{-12}$. The reactions at the Q_i-binding site tend to be faster. Also, the conformational change as well as the uptake/delivery of ubiquinone/ubiquinol are not rate-determining. To search for a Q-cycle, the elementary reactions were now linked together, resulting in a graph as in figure 7.5. A special search algorithm was used to search for cycles in the resulting graphs. The search algorithm is described in appendix B. Figure 7.7 shows exemplarily the result of the search for a cycle starting from the highest flux in model I in variant 2 (V-I.2).

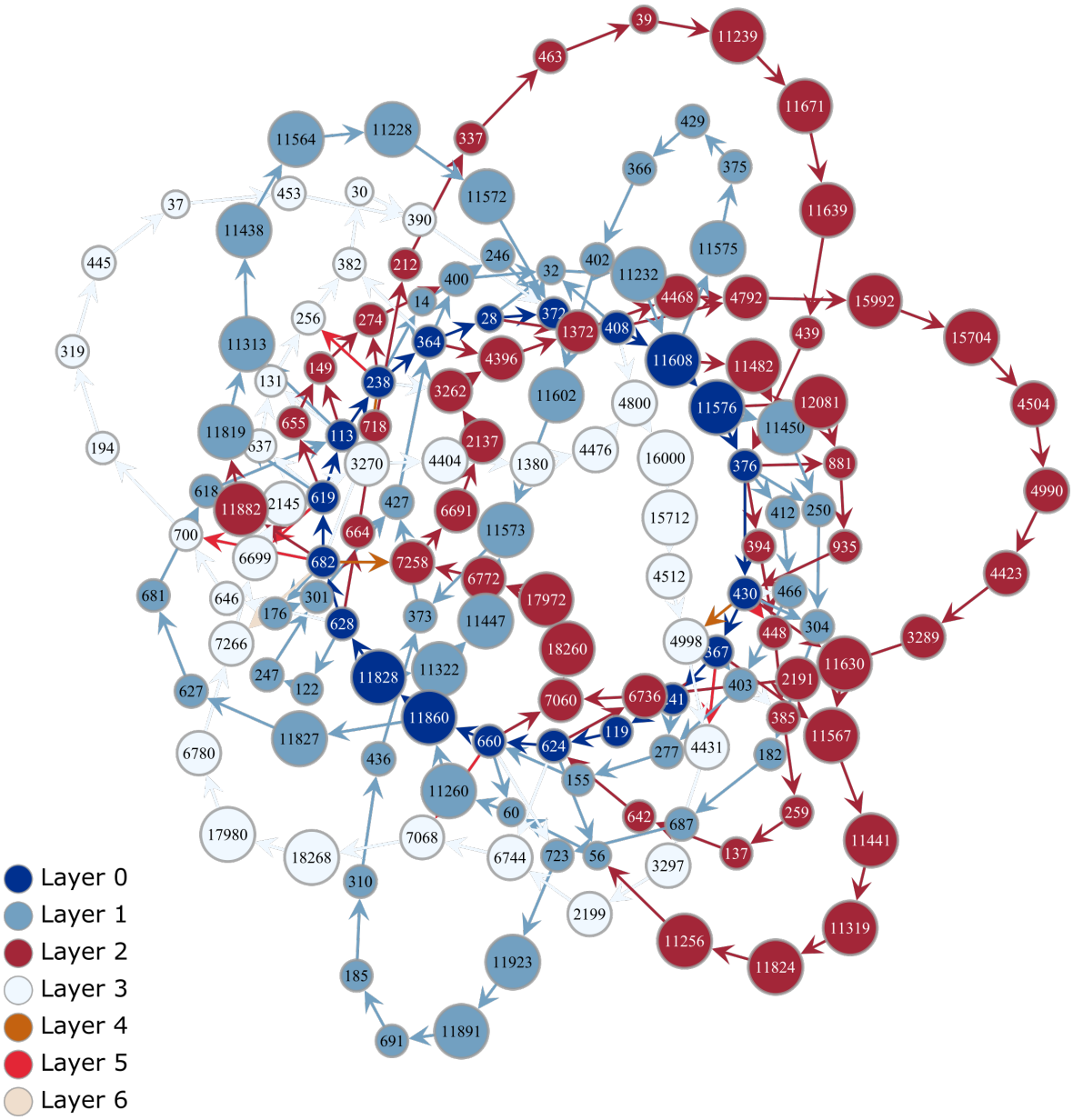

Figure 7.7: Result of the search for a cycle starting from the highest flux in a network of the model V-I.2. Layer 0 is the main cycle and the other layers are second, third and fourth largest outgoing flux of a node.

The main cycle found (dark blue in the figure 7.7) with the largest fluxes does not represent a Q-cycle as expected, but only a "Q_o-cycle" that can proceed at the Q_o-binding site. The "Q_o-cycle" oxidizes and deprotonates ubiquinol to ubiquinone at the Q_o-binding site, as it should be in a functioning Q-cycle. A high-energy compound is converted and the energy is used to reduce and protonate ubiquinone at the Q_i-binding site. However, at the Q_i-binding site, this process of reduction and protonation of ubiquinone does not occur. The energy coming from the "Q_o-cycle" is not used and is thus wasted. The "Q_i-cycle" at the Q_i-binding site should, as mentioned, reduce and protonate ubiquinone to ubiquinol, but this cycle also converts ubiquinol to ubiquinone, so it works in reverse. So energy is also wasted in the "Q_i-cycle". None of the layers form a Q-cycle, they are mostly variants of the Q_o-cycle or Q_i-cycles, which also oxidize and deprotonate ubiquinol to ubiquinone. This picture is also seen in

all other models, even in model V-II.2. Model V-II.2 does not show a build up of ubiquinol at the Q_i-binding site, but starting from the highest flux, no complete cycle is found. However, it cannot be excluded that there is a cycle corresponding to a Q-cycle in this network. In the other model networks it is rather unlikely to find a Q-cycle because of the total fluxes. In general, however, it is not possible to evaluate all possible cycles within an acceptable period of time, since there may be some 10,000 to 100,000 cycles. Furthermore, when searching for cycles in general, it was noticed that there are no initial steps to a Q-cycle as previously considered (see figure 7.3), but that it is more likely to be a complete cycle. However, that does not change the previously determined redox potentials or pK_a-values, since the respective state does not change.

The findings about a "Q_o-cycle" or "Q_i-cycles" have led to the consideration that the reaction equation shown in the introduction should perhaps rather be written as follows:

$$\begin{aligned} &Q_o\text{-cycle: } 2QH_2 + 2c_1^{3+} \rightarrow 2Q + 2c_1^{2+} + 2e^- + 4H^+_{EC} \\ &Q_i\text{-cycle: } Q + 2H^+_{CP} + 2e^- \rightarrow QH_2 \\ \hline &Q\text{-cycle: } QH_2 + 2c_1^{3+} + 2H^+_{CP} \xrightarrow{bc_1} Q + 2c_1^{2+} + 4H^+_{EC} \end{aligned} \tag{7.2}$$

Also changed the way the Q-cycle is represented, away from one cycle to two cycles connected via the b_H and b_L hems (figure 7.8). Viewed from the outside, however, it remains one large Q-cycle.

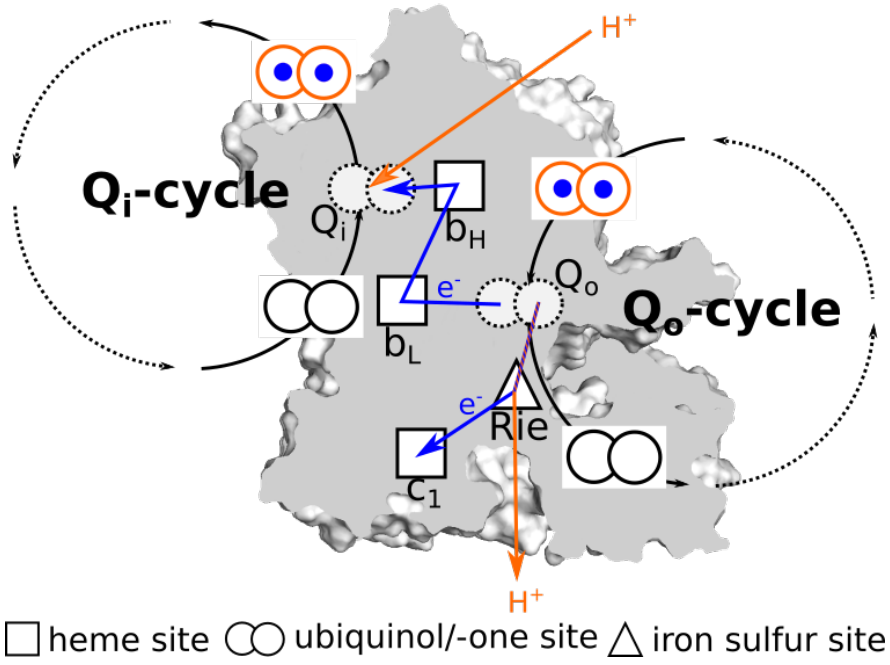

Figure 7.8: A detailed view on the Q-cycle for one monomer of the bc_1-complex. The blue circles represent the electrons and the orange frames are protonated sites.

Based on these results, a new possible cycle was created using model I as a basis. A handcrafted creation based on model II would simply have too many possibilities. The result of this handcrafted cycle can be found in table 7.8. It is clear that the flux in the handcrafted network is lower than in the full network. This fact is not very surprising, since the cycle only covers a part of a larger network and was not designed with high flux intention. This cycle also shows the expected ratio between Q_o and Q_i-binding site.

Table 7.8: Calculated netto substance fluxes $\left[\frac{M}{s}\right]$ for the different handcrafted models with the parameters set from table 7.5.

Substance Name	V-I.1 (hand craft)	V-I.2 (hand craft)
U2PP_MEMB_CP	$-2.272 \cdot 10^{-6}$	$-1.595 \cdot 10^{-6}$
U0DD_MEMB_CP	$2.272 \cdot 10^{-6}$	$1.595 \cdot 10^{-6}$
U2PP_MEMB_EC	$4.545 \cdot 10^{-6}$	$3.190 \cdot 10^{-6}$
U0DD_MEMB_EC	$-4.545 \cdot 10^{-6}$	$-3.190 \cdot 10^{-6}$
proton_CP	$4.545 \cdot 10^{-6}$	$3.190 \cdot 10^{-6}$
electron_EC	$-4.545 \cdot 10^{-6}$	$-3.190 \cdot 10^{-6}$
proton_EC	$-9.089 \cdot 10^{-6}$	$-6.380 \cdot 10^{-6}$

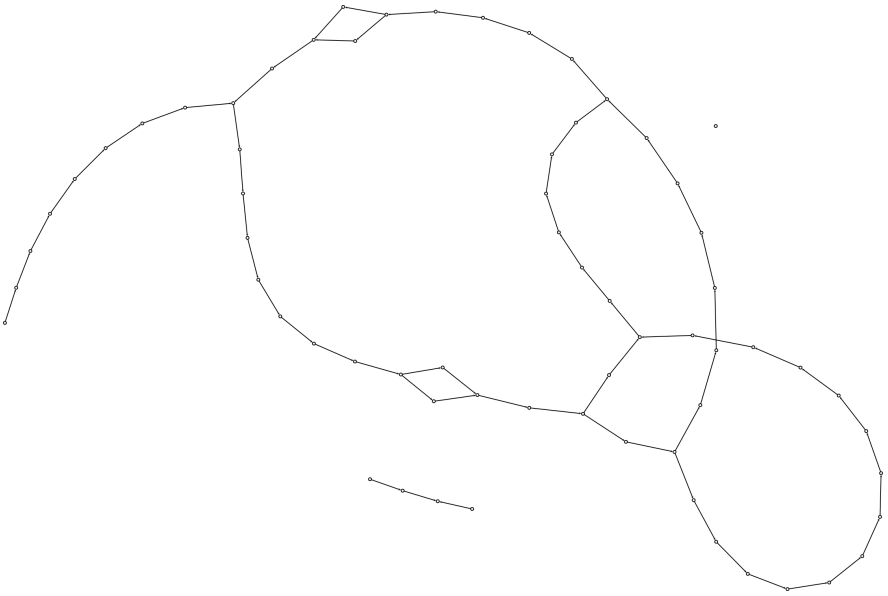

Figure 7.9: Complete flux network of the handcrafted model 1 in variant 1 (model V-I.1).

It is interesting about this manually created flux that it is actually constructed contiguously and represents a cycle with multiple layers. However, the figure 7.9 does not show a continuous graph where all nodes have at least two connections. The reason for this absence is that for these connections the flux is zero and therefore these connections are dropped. Even if the network loses some connections, it still results in a cycle, that describes a complete working Q-cycle (figure 7.10). This Q-cycle is not split to the outside into a "Q_o-cycle" or a "Q_i-cycle", but these two cycles are also hidden here. This Q-cycle also has three alternative reaction paths, which have a lower flux than the main cycle. Tables 7.9 and 7.10 show all calculated values for the two handcrafted cycles. The netto flux in the elementary reactions is larger in V-I.1-handcraft than in V-I.2-handcraft, which is consistent with the substance fluxes. As can be seen from the handcrafted network, only three reactions are affected by the changed chemical potential of the ubiquinone/ubiquinol pool (table 7.5). These three reactions do not slow down like the other reactions but speed up. These reactions include a conformational change from C11 to Q11, proton release from the Rieske center to the proton pool, and the release of an electron by the Rieske center to cytochrome c_1. However, the last two reactions have an alternative pathway that is preferred. Thus, the conformational change appears to be rate-determining. However, looking at the forward rate constants as $5.915 \cdot 10^3 \ \frac{1}{s}$, this is not the slowest rate constant in the network. However, the

C11 state has a low state concentration of $1.142 \cdot 10^{-2}$ $\frac{mol}{l}$. The same is true for the back reaction from Q11 to C11, which is why the netto flux is low. If the state concentration of C11 could be increased, a higher flux would also result. Looking at all the elementary reactions, it is striking that the reduction of a ubiquinone by heme b_H has a high state concentration but a low rate constant. This reaction seems to "pile up" and that is the actual rate-determining step. This effect is seen in the V-I.1-handcraft model (0.9871 $\frac{mol}{l}$) and in the V-I.2-handcraft model (0.5406 $\frac{mol}{l}$), but especially in the V-I.1-handcraft model. In the V-I.2-handcraft model there is another "jam step" with a state concentration of 0.2407 $\frac{mol}{l}$. This step is the incorporation of a ubiquinone at the Q_i-binding site. Thus, model V-I.1-handcraft has one strongly rate-determining step and model V-I.2-handcraft has two rate-determining steps. Such a precise investigation is difficult for the larger models presented previously. In these smaller handcraft systems, however, it was possible and two or one rate-determining step was found.

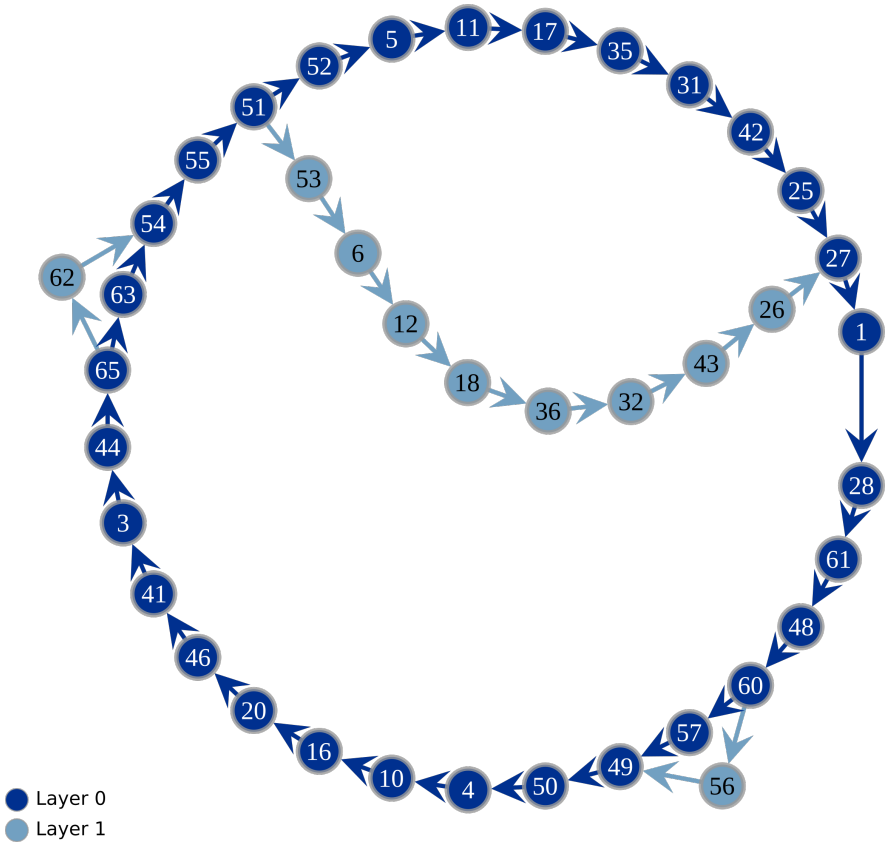

Figure 7.10: Result of the search for a cycle starting from the highest flux in a network of the handcrafted models. Layer 0 is the main cycle and the other layer is second largest outgoing flux of a node.

Table 7.9: All calculated fluxes $\left[\frac{M}{s}\right]$, steady-state concentrations $[M]$ and rate constants $\left[\frac{1}{s}\right]$ for a hand craft cycle based on model V-I.1.

#LABEL	Netto	Forward	Backward	SSconcA	SSconcB	Forward	Backward
		Flux				Rates	
C11->Q11	1.38E-14	6.57E+01	6.57E+01	1.14E-02	1.28E-04	5.92E+03	5.13E+05
5::RRHP:2:1:0->RRH1:1:1:0	1.63E-14	7.26E-06	7.26E-06	8.42E-09	1.41E-11	8.62E+02	5.13E+05
4::HemOx:0:0:0->HemRed:0:1:0=5::RRH1:1:1:0->RIO1:1:0:0	1.76E-14	7.26E-06	7.26E-06	1.41E-11	6.52E-08	5.13E+05	1.11E+02
1::GLUD:0:0:0->GLUP:1:0:0=6::U1DP:1:1:1->U1DD:0:1:1	3.95E-08	2.07E-04	2.07E-04	4.03E-10	5.11E-08	5.13E+05	4.87E+03
5::RIO2:1:0:0->RRHP:2:1:0=6::U2PP:2:2:1->U1DP:1:1:1	3.95E-08	2.07E-04	2.07E-04	9.38E-08	4.03E-10	2.20E+03	5.13E+05
2::HemRed:0:1:0->HemOx:0:0:0=7::U1PD:1:1:1->U2PD:1:2:1	1.35E-06	5.45E-02	5.45E-02	1.11E-06	1.06E-07	4.93E+04	5.13E+05
7::U1DD:0:1:1->U1PD:1:1:1	1.35E-06	8.85E-04	8.84E-04	2.32E-08	1.72E-09	3.81E+04	5.13E+05
7::U2PD:1:2:1->U2PP:2:2:1	1.35E-06	5.45E-02	5.45E-02	1.06E-07	1.95E-04	5.13E+05	2.80E+02
2::HemRed:0:1:0->HemOx:0:0:0=7::U1DP:1:1:1->U2DP:1:2:1	1.81E-06	5.20E-02	5.20E-02	7.72E-07	1.01E-07	6.74E+04	5.13E+05
7::U1DD:0:1:1->U1DP:1:1:1	1.81E-06	1.17E-03	1.17E-03	2.32E-08	2.28E-09	5.04E+04	5.13E+05
7::U2DP:1:2:1->U2PP:2:2:1	1.81E-06	5.20E-02	5.20E-02	1.01E-07	1.95E-04	5.13E+05	2.67E+02
2::HemRed:0:1:0->HemOx:0:0:0=7::U0DD:0:0:1->U1DD:0:1:1	3.16E-06	1.19E-02	1.19E-02	9.87E-01	2.32E-08	1.21E-02	5.13E+05
Q11->Q01=7::U2PP:2:2:1->EMPTY	3.16E-06	9.53E+00	9.53E+00	1.26E-04	1.86E-05	7.55E+04	5.13E+05
Q01->Q11=7::EMPTY->U0DD:0:0:1	3.16E-06	7.32E+00	7.32E+00	1.86E-05	1.43E-05	3.98E+05	5.13E+05
1::GLUD:0:0:0->GLUP:1:0:0=6::U1PD:1:1:1->U1DD:0:1:1	6.28E-06	2.62E-02	2.62E-02	5.20E-07	5.11E-08	4.16E+04	5.13E+05
5::RIO2:1:0:0->RRHP:2:1:0=6::U2PP:2:2:1->U1PD:1:1:1	6.28E-06	4.81E-02	4.81E-02	9.38E-08	5.20E-07	5.13E+05	9.26E+04
C11->C10=6::U0DD:0:0:1->EMPTY	6.32E-06	1.05E+02	1.05E+02	2.04E-04	1.15E-03	5.13E+05	9.01E+04
1::GLUP:1:0:0->GLUD:0:0:0	6.32E-06	9.45E-01	9.45E-01	9.26E-06	1.84E-06	1.03E+05	5.13E+05
4::HemOx:0:0:0->HemRed:0:1:0=5::RRH2:1:1:0->RIO2:1:0:0	6.32E-06	9.25E-06	2.94E-06	1.80E-11	4.33E-08	5.13E+05	6.78E+01
5::RRHP:2:1:0->RRH2:1:1:0	6.32E-06	1.56E-05	9.25E-06	8.42E-09	1.80E-11	1.85E+03	5.13E+05
3::HemOx:0:0:0->HemRed:0:1:0=6::U1DD:0:1:1->U0DD:0:0:1	6.32E-06	2.62E-02	2.62E-02	5.11E-08	9.87E-01	5.13E+05	7.39E-03
2::HemOx:0:0:0->HemRed:0:1:0=3::HemRed:0:1:0->HemOx:0:0:0	6.32E-06	4.28E-02	4.28E-02	8.34E-08	1.11E-05	5.13E+05	4.56E+03
4::HemRed:0:1:0->HemOx:0:0:0	6.32E-06	9.45E-01	9.45E-01	1.84E-06	8.94E-06	5.13E+05	1.07E+05
C10->C11=6::EMPTY->U2PP:2:2:1	6.32E-06	5.92E+02	5.92E+02	1.15E-03	1.14E-02	5.13E+05	5.19E+04

Table 7.10: All calculated fluxes $\left[\frac{M}{s}\right]$, steady-state concentrations $[M]$ and rate constants $\left[\frac{1}{s}\right]$ for a hand craft cycle based on model V-I.2.

#LABEL	Netto	Forward	Backward	SSconcA	SSconcB	Forward	Backward
		Flux				Rates	
5::RRH1:1:1:0->RRHP:2:1:0	3.72E-12	3.38E-06	3.38E-06	6.58E-12	3.92E-09	8.62E+02	5.13E+05
4::HemRed:0:1:0->HemOx:0:0:0=5::RIO1:1:0:0->RRH1:1:1:0	4.00E-12	3.38E-06	3.38E-06	3.03E-08	6.58E-12	5.13E+05	1.11E+02
Q11->C11	4.77E-12	1.92E+02	1.92E+02	3.74E-04	3.27E-02	4.37E+05	5.13E+05
1::GLUD:0:0:0->GLUP:1:0:0=6::U1DP:1:1:1->U1DD:0:1:1	2.16E-08	1.13E-04	1.13E-04	2.21E-10	2.80E-08	5.13E+05	4.87E+03
5::RIO2:1:0:0->RRHP:2:1:0=6::U2PP:2:2:1->U1DP:1:1:1	2.16E-08	1.13E-04	1.13E-04	5.14E-08	2.21E-10	2.20E+03	5.13E+05
2::HemRed:0:1:0->HemOx:0:0:0=7::U1PD:1:1:1->U2PD:1:2:1	7.40E-07	2.98E-02	2.98E-02	6.05E-07	5.81E-08	4.93E+04	5.13E+05
7::U1DD:0:1:1->U1PD:1:1:1	7.40E-07	4.85E-04	4.84E-04	1.27E-08	9.44E-10	3.81E+04	5.13E+05
7::U2PD:1:2:1->U2PP:2:2:1	7.40E-07	2.98E-02	2.98E-02	5.81E-08	1.07E-04	5.13E+05	2.80E+02
2::HemRed:0:1:0->HemOx:0:0:0=7::U1DP:1:1:1->U2DP:1:2:1	9.90E-07	2.85E-02	2.85E-02	4.23E-07	5.56E-08	6.74E+04	5.13E+05
7::U1DD:0:1:1->U1DP:1:1:1	9.90E-07	6.42E-04	6.41E-04	1.27E-08	1.25E-09	5.04E+04	5.13E+05
7::U2DP:1:2:1->U2PP:2:2:1	9.90E-07	2.85E-02	2.85E-02	5.56E-08	1.07E-04	5.13E+05	2.67E+02
2::HemRed:0:1:0->HemOx:0:0:0=7::U0DD:0:0:1->U1DD:0:1:1	1.73E-06	6.53E-03	6.53E-03	5.41E-01	1.27E-08	1.21E-02	5.13E+05
Q11->Q01=7::U2PP:2:2:1->EMPTY	1.73E-06	1.90E+02	1.90E+02	3.71E-04	2.41E-01	5.13E+05	7.90E+02
Q01->Q11=7::EMPTY->U0DD:0:0:1	1.73E-06	9.49E+04	9.49E+04	2.41E-01	1.85E-01	3.98E+05	5.13E+05
1::GLUD:0:0:0->GLUP:1:0:0=6::U1PD:1:1:1->U1DD:0:1:1	3.44E-06	1.44E-02	1.44E-02	2.85E-07	2.80E-08	4.16E+04	5.13E+05
5::RIO2:1:0:0->RRHP:2:1:0=6::U2PP:2:2:1->U1PD:1:1:1	3.44E-06	2.64E-02	2.64E-02	5.14E-08	2.85E-07	5.13E+05	9.26E+04
C11->C10=6::U0DD:0:0:1->EMPTY	3.46E-06	5.58E+01	5.58E+01	1.09E-04	6.18E-04	5.13E+05	9.01E+04
1::GLUP:1:0:0->GLUD:0:0:0	3.46E-06	2.34E-01	2.34E-01	2.29E-06	4.55E-07	1.03E+05	5.13E+05
4::HemOx:0:0:0->HemRed:0:1:0=5::RRH2:1:1:0->RIO2:1:0:0	3.46E-06	3.78E-06	3.23E-07	7.37E-12	4.76E-09	5.13E+05	6.78E+01
5::RRHP:2:1:0->RRH2:1:1:0	3.46E-06	7.24E-06	3.78E-06	3.92E-09	7.37E-12	1.85E+03	5.13E+05
3::HemOx:0:0:0->HemRed:0:1:0=6::U1DD:0:1:1->U0DD:0:0:1	3.46E-06	1.44E-02	1.44E-02	2.80E-08	5.41E-01	5.13E+05	7.39E-03
2::HemOx:0:0:0->HemRed:0:1:0=3::HemRed:0:1:0->HemOx:0:0:0	3.46E-06	1.10E-02	1.10E-02	2.14E-08	3.30E-06	5.13E+05	4.56E+03
4::HemRed:0:1:0->HemOx:0:0:0	3.46E-06	2.34E-01	2.34E-01	4.55E-07	2.06E-06	5.13E+05	1.07E+05
C10->C11=6::EMPTY->U2PP:2:2:1	3.46E-06	3.17E+02	3.17E+02	6.18E-04	3.27E-02	5.13E+05	9.69E+03

7.5 Conclusion

Inspection of the bc_1-complex from different angles revealed several things. First, the proton-coupled electron transfer is not rate-determining, this was shown by flux analysis and analysis of redox potentials and pK_a-values. Second, the binding of ubiquinone or ubiquinol is supported by the electrostatics of the surrounding amino acid residues and by possible hydrogen bridge donors or acceptors. Third, the hydrogen bridge donors and acceptors at the binding sites are also involved in proton transfer. Fourth, the determined G_{model}-values are suitable for calculating redox potentials and pK_a-values and are in agreement with experimental results.

Based on the previous findings during research, various flux calculations and analyses were performed on the bc_1-complex. It was shown that different networks and fluxes could be created and studied. A clear identification of a complete Q-cycle could not yet be achieved with the previous means. Smaller Q_o or Q_i-cycles could be found, but no complete Q-cycle. Looking at a handcrafted cycle allowed a more detailed analysis of individual reactions, which was not possible in the large network due to tens of thousands of reactions. It was clearly shown in this handcrafted cycle that parameter settings that were supposed to accelerate the cycle can have a negative effect and there are only a few key reactions that had a large impact on the whole cycle. The identification of such reactions needs further investigation.

References

(*1*) Mitchell, P. (1976). Possible molecular mechanisms of the protonmotive function of cytochrome systems. *Journal of Theoretical Biology 62*, 327–367, DOI: 10.1016/0022-5193(76)90124-7.

(*2*) Crofts, A. R., Shinkarev, V. P., Kolling, D. R. J., and Hong, S. (2003). The modified Q-cycle explains the apparent mismatch between the kinetics of reduction of cytochromes c1 and bH in the bc1 complex. *J Biol Chem 278*, 36191–36201, DOI: 10.1074/jbc.M305461200.

(*3*) Darrouzet, E., Valkova-Valchanova, M., Moser, C. C., Dutton, P. L., and Daldal, F. (2000). Uncovering the [2Fe2S] domain movement in cytochrome bc1 and its implications for energy conversion. *Proceedings of the National Academy of Sciences 97*, 4567–4572, DOI: 10.1073/pnas.97.9.4567.

(*4*) Mulkidjanian, A. Y. (2005). Ubiquinol oxidation in the cytochrome bc1 complex: reaction mechanism and prevention of short-circuiting. *Biochim Biophys Acta 1709*, 5–34, DOI: 10.1016/j.bbabio.2005.03.009.

(*5*) Hong, S., de Almeida, W. B., Taguchi, A. T., Samoilova, R. I., Gennis, R. B., O'Malley, P. J., Dikanov, S. A., and Crofts, A. R. (2014). The Semiquinone at the Qi Site of the bc1 Complex Explored Using HYSCORE Spectroscopy and Specific Isotopic Labeling of Ubiquinone in Rhodobacter sphaeroides via 13C Methionine and Construction of a Methionine Auxotroph. *Biochemistry 53*, 6022–6031, DOI: 10.1021/bi500654y.

(*6*) Gray, K. A., Dutton, P. L., and Daldal, F. (1994). Requirement of histidine 217 for ubiquinone reductase activity (Qi site) in the cytochrome bc1 complex. *Biochemistry 33*, 723–733, DOI: 10.1021/bi00169a014.

(*7*) Barragan, A. M., Crofts, A. R., Schulten, K., and Solov'yov, I. A. (2014). Identification of Ubiquinol Binding Motifs at the Qo-Site of the Cytochrome bc1 Complex. *J Phys Chem B 119*, 433–447, DOI: 10.1021/jp510022w.

(*8*) Osyczka, A., Zhang, H., Mathé, C., Rich, P. R., Moser, C. C., and Dutton, P. L. (2006). Role of the PEWY glutamate in hydroquinone-quinone oxidation-reduction catalysis in the Qo Site of cytochrome bc1. *Biochemistry-Us 45*, 10492–10503, DOI: 10.1021/bi060013a.

(*9*) Pietras, R., Sarewicz, M., and Osyczka, A. (2016). Distinct properties of semiquinone species detected at the ubiquinol oxidation Qo site of cytochrome bc1 and their mechanistic implications. *J R Soc Interface 13*, 20160133.

(*10*) Postila, P. A., Kaszuba, K., Sarewicz, M., Osyczka, A., Vattulainen, I., and Rog, T. (2013). Key role of water in proton transfer at the Qo-site of the cytochrome bc1 complex predicted by atomistic molecular dynamics simulations. *Biochim Biophys Acta 1827*, 761–768, DOI: 10.1016/j.bbabio.2013.02.005.

(*11*) Postila, P. A., Kaszuba, K., Kuleta, P., Vattulainen, I., Sarewicz, M., Osyczka, A., and Róg, T. (2016). Atomistic determinants of co-enzyme Q reduction at the Qi-site of the cytochrome bc1 complex. *Sci Rep-Uk 6*, 33607.

(*12*) Salo, A. B., Husen, P., and Solov'yov, I. A. (2017). Charge Transfer at the Qo-Site of the Cytochrome bc1 Complex Leads to Superoxide Production. *J Phys Chem B 121*, 1771–1782.

(*13*) Sarewicz, M., Dutka, M., Pintscher, S., and Osyczka, A. (2013). Triplet state of the semiquinone-Rieske cluster as an intermediate of electronic bifurcation catalyzed by cytochrome bc1. *Biochemistry-Us 52*, 6388–6395, DOI: 10.1021/bi400624m.

(*14*) Yu, C.-A., Wen, X., Xiao, K., Di Xia, and Yu, L. (2002). Inter- and intra-molecular electron transfer in the cytochrome bc1 complex. *Bba-Bioenergetics 1555*, 65–70, DOI: 10.1016/S0005-2728(02)00256-6.

(*15*) Zhang, Z., Huang, L., Shulmeister, V. M., Chi, Y. I., Kim, K. K., Hung, L. W., Crofts, A. R., Berry, E. A., and Kim, S. H. (1998). Electron transfer by domain movement in cytochrome bc1. *Nature 392*, 677–684, DOI: 10.1038/33612.

(*16*) Hong, S., de Almeida, W. B., Taguchi, A. T., Samoilova, R. I., Gennis, R. B., O'Malley, P. J., Dikanov, S. A., and Crofts, A. R. (2014). The Semiquinone at the Qi Site of the bc1 Complex Explored Using HYSCORE Spectroscopy and Specific Isotopic Labeling of Ubiquinone in Rhodobacter sphaeroides via 13C Methionine and Construction of a Methionine Auxotroph. *Biochemistry 53*, 6022–6031, DOI: 10.1021/bi500654y.

(*17*) Hong, S., de Almeida, W. B., Taguchi, A. T., Samoilova, R. I., Gennis, R. B., O'Malley, P. J., Dikanov, S. A., and Crofts, A. R. (2015). Correction to The Semiquinone at the Qi Site of the bc1 Complex Explored Using HYSCORE Spectroscopy and Specific Isotopic Labeling of Ubiquinone in Rhodobacter sphaeroides via 13C Methionine and Construction of a Methionine Auxotroph. *Biochemistry 54*, 7307–7307, DOI: 10.1021/acs.biochem.5b01251.

(*18*) Crofts, A. R. (2004). The Cytochrome bc1 Complex: Function in the Context of Structure. *Annu Rev Physiol 66*, 689–733, DOI: 10.1146/annurev.physiol.66.032102.150251.

(*19*) Brooks, B. R., Bruccoleri, R. E., Olafson, B. D., States, D. J., Swaminathan, S., and Karplus, M. (1983). CHARMM: A program for macromolecular energy, minimization, and dynamics calculations. *J Comput Chem 4*, 187–217.

(*20*) Brooks, B. R., Brooks, C. L., Mackerell, A. D., Nilsson, L., Petrella, R. J., Roux, B., Won, Y., Archontis, G., Bartels, C., Boresch, S., Caflisch, A., Caves, L., Cui, Q., Dinner, A. R., Feig, M., Fischer, S., Gao, J., Hodoscek, M., Im, W., Kuczera, K., Lazaridis, T., Ma, J., Ovchinnikov, V., Paci, E., Pastor, R. W., Post, C. B., Pu, J. Z., Schaefer, M., Tidor, B., Venable, R. M., Woodcock, H. L., Wu, X., Yang, W., York, D. M., and Karplus, M. (2009). CHARMM: the biomolecular simulation program. *J Comput Chem 30*, 1545–1614.

(*21*) Ullmann, R. T., and Ullmann, G. M. (2011). A generalized free energy perturbation theory accounting for end states with differing configuration space volume. *J Phys Chem B 115*, 507–521, DOI: 10.1021/jp1093838.

(*22*) Ullmann, R. T., and Ullmann, G. M. (2012). GMCT : a Monte Carlo simulation package for macromolecular receptors. *J Comput Chem 33*, 887–900, DOI: 10.1002/jcc.22919.

(*23*) Matthias Ullmann, Thomas Ullmann GMCT Manual: A Monte Carlo simulation package for complex ligand binding phenomena: Version 1.2.3, ed. by Bioinformatics/Structural Biology Group, University of Bayreuth, 2007-2014.

(*24*) Ullmann, G. M. (2023). GMCT@UBT Manual - Version 2.0.

(*25*) Ellson, J., Gansner, E., Hu, Y., North, S., Jacobsson, M., Fernandez, M., Hansen, M., Alexiev, V., Bilgin, A., Caldwell, D., Daniel, R. G., Dobkin, D., Dwyer, T., Janssen, E., Kelman, T., Koren, Y., Koutsofios, E., Lilly, B., Low, G., and Woodhull, G. Graphviz https://www.graphviz.org/ (accessed June 25, 2023).

(*26*) Peixoto, T. P. (2014). The graph-tool python library. *figshare*, DOI: 10.6084/m9.figshare.1164194.

(*27*) Zoller, J. (2024). Analyze Flux Graphs. DOI: 10.5281/zenodo.10549170.

(*28*) Victoria, D., Burton, R., and Crofts, A. R. (2013). Role of the -PEWY-glutamate in catalysis at the Qo-site of the Cyt bc1 complex. *Biochimica et Biophysica Acta (BBA) - Bioenergetics 1827*, 365–386, DOI: 10.1016/j.bbabio.2012.10.012.

(*29*) Crofts, A. R., and Wraight, C. A. (1983). The electrochemical domain of photosynthesis. *Biochim Biophys Acta 726*, 149–185, DOI: 10.1016/0304-4173(83)90004-6.

(*30*) Dutton, P. L., and Jackson, J. B. (1972). Thermodynamic and Kinetic Characterization of Electron-Transfer Components in situ in Rhodopseudomonas spheroides and Rhodospirillum rubrum. *Eur J Biochem 30*, 495–510, DOI: 10.1111/j.1432-1033.1972.tb02121.x.

(*31*) Gabellini, N., and Hauska, G. (1983). Characterization of cytochrome b in the isolated ubiquinol-cytochrome c2 oxidoreductase from Rhodopseudomonas sphaeroides GA. *FEBS Letters 153*, 146–150, DOI: 10.1016/0014-5793(83)80136-7.

(*32*) Ohnishi, T., and Trumpower, B. (1980). Differential effects of antimycin on ubi-semiquinone bound in different environments in isolated succinate . cytochrome c reductase complex. *J Biol Chem 255*, 3278–3284, DOI: 10.1016/s0021-9258(19)85696-x.

(*33*) Chance, B., Wilson, D. F., Dutton, P. L., and Erecinska, M. (1970). Energy-Coupling Mechanisms In Mitochondria: Kinetic, Spectroscopic, And Thermodynamic Properties Of An Energy-Transducing Form Of Cytochrome B. *P Natl A Sci 66*, 1175–1182, DOI: 10.1073/pnas.66.4.1175.

(*34*) Rich, P. R., Jeal, A. E., Madgwick, S. A., and Moody, A. (1990). Inhibitor effects on redox-linked protonations of the b haems of the mitochondrial bc1 complex. *Biochim Biophys Acta 1018*, 29–40, DOI: 10.1016/0005-2728(90)90106-e.

(*35*) LINK, T. A., HAGEN, W. R., PIERIK, A. J., ASSMANN, C., and JAGOW, G. (1992). Determination of the redox properties of the Rieske [2Fe-2S] cluster of bovine heart bc1 complex by direct electrochemistry of a water-soluble fragment. *Eur J Biochem 208*, 685–691, DOI: 10.1111/j.1432-1033.1992.tb17235.x.

(*36*) Mitchell, P. (1975). The protonmotive Q cycle: A general formulation. *FEBS Letters 59*, 137–139, DOI: 10.1016/0014-5793(75)80359-0.

8

OVERALL CONCLUSION AND OUTLOOK

After more than seven years of development and research, major problems in determining the necessary G_{model}-values have now been solved. Three methods for determining the G_{model}-values in chapters 3 to 5 were presented and used. Using these methods, G_{model}-values could be determined for all cofactors present in the bc_1-complex. The important point about these G_{model}-values is that they are independent of the structure and protein environment of the bc_1-complex. The G_{model}-values were not determined in the bc_1-complex itself but in other structures and also, as mentioned for example in chapter 5, the structural influence was factored out. For this reason, it is possible to use the G_{model}-values in a generally valid way.

quinone/quinol The determination of the G_{model}-value, using quantum mechanics and thermodynamic cycles, revealed difficulties in the uptake/release of protons in the form of H^+-atoms. The representation of water by an implicit model showed certain weaknesses in the determination because the dipolarity of water was not fully represented. The introduction of explicit water molecules in the immediate vicinity of the proton binding sites showed improvement. However, the alignment of the water molecules through the quantum mechanical calculations proved to be problematic in terms of computational time, among other issues. Finally, the weaknesses of the implicit model were accepted for this reason.

b-type and c-type heme The determination of G_{model}-values is often highly dependent on crystal structures; this became particularly striking in the determination of the G_{model}-value for cytochromes. In the case of cytochromes, it has been shown that the re-refinement of the crystal structures can improve the determination of the necessary values; that is also shown in the work of Roy *et al.* (*1*). The work of Roy *et al.* shows how strong the influence of the structure on the redox potential is and how it can be improved by refinement. There is still potential for improving the determined G_{model}-values with respect to the cofactors b_L, b_H and c_1 in the bc_1-complex by refinements.

Rieske center The G_{model}-values for the Rieske center were successfully determined. The self-developed program for "extracting" the G_{model}-values from experimental values was able to find even very weakly populated states and to assign them exactly G_{model}-values. From that, the experimental pK_a-values and redox potentials could be reproduced well (*2*).

Q-Cycle Based on all G_{model}-values, the pK_a-values and redox potentials of the Q-cycle could be calculated for all cofactors and compared with experimental values. Good agreement with the experimental values was shown. It was also shown that the amino acids Glu295 (Q_i-binding site), Lys251 (Q_o-binding site), Asp252 (Q_o-binding site), His217 (Q_o-binding site), and a crystal water (Q_o-binding site) play an important role in the de/protonation of quinols/quinones, as also reported by Barragan et. al (*3*), Crofts et. al (*4*, *5*) and Postila et. al (*6*).

The final determination of a Q-cycle from the various overall networks formed based on the cofactors and their connections to each other could not be fully achieved. However, it could be shown that the bc_1-complex and its function can be described by the theoretical methods developed and used here, but further investigations are needed to identify a Q-cycle from the overall network.

Here in this work it was comprehensively shown that it is possible to determine or calculate the G_{model}-values necessary for the electrostatic calculations based on experimental values especially without experimental values. There is still room for refinement in the determination of the G_{model}-values as mentioned in the paragraphs above, nevertheless the results are already reasonable. For the determination and investigation of the bc_1-complex with respect to the Q-cycle, further critical considerations are needed with respect to the identification of the rate-determining reactions, the setting of energy barriers and state energies, the methodology for calculating the kinetics (Arrhenius, Markov theory), the methodology for searching cycles in the network, and the consideration of the setting of the total concentration in the network. If these problems are solved, with the setting of energy barriers and states energies being considered particularly critical, a complete description of the Q-cycle in the bc_1-complex will be possible and will open the possibility of a complete theoretical description of other metabolic pathways at the atomic level by means of a fast methodology based on electrostatics and chemical potentials.

References

(*1*) Roy, R. R., and Ullmann, G. M. (2023). Virtual Model Compound Approach for Calculating Redox Potentials of [Fe2S2]-Cys4 Centers in Proteins – Structure Quality Matters. *Journal of Chemical Theory and Computation 19*, 8930–8941, DOI: 10.1021/acs.jctc.3c00779.

(*2*) Zu, Y., Couture, M. M.-J., Kolling, D. R. J., Crofts, A. R., Eltis, L. D., Fee, J. A., and Hirst, J. (2003). Reduction potentials of Rieske clusters: importance of the coupling between oxidation state and histidine protonation state. *Biochemistry-Us 42*, 12400–12408, DOI: 10.1021/bi0350957.

(*3*) Barragan, A. M., Crofts, A. R., Schulten, K., and Solov'yov, I. A. (2015). Identification of ubiquinol binding motifs at the Qo-site of the cytochrome bc1 complex. *J Phys Chem B 119*, 433–447, DOI: 10.1021/jp510022w.

(*4*) Crofts, A. R., Hong, S., Ugulava, N., Barquera, B., Gennis, R., Guergova-Kuras, M., and Berry, E. A. (1999). Pathways for proton release during ubihydroquinone oxidation by the bc1 complex. *P Natl Acad Sci Usa 96*, 10021–10026.

(*5*) Crofts, A. R., Barquera, B., Gennis, R. B., Kuras, R., Guergova-Kuras, M., and Berry, E. A. (1999). Mechanism of ubiquinol oxidation by the bc(1) complex: different domains of the quinol binding pocket and their role in the mechanism and binding of inhibitors. *Biochemistry-Us 38*, 15807–15826.

(*6*) Postila, P. A., Kaszuba, K., Sarewicz, M., Osyczka, A., Vattulainen, I., and Rog, T. (2013). Key role of water in proton transfer at the Qo-site of the cytochrome bc1 complex predicted by atomistic molecular dynamics simulations. *Biochim Biophys Acta 1827*, 761–768, DOI: 10.1016/j.bbabio.2013.02.005.

A

COMPUTATIONAL DETAILS

A.1 ORCA

A.1.1 Settings

All settings shown here are, if not mentioned otherwise, the self-set default settings for the calculations performed in this thesis. Settings not mentioned are the default settings of `orca 5.0.3`, which can be found in the corresponding `orca` manual. The settings for the implicit solvent model C-PCM are as followed for all calculations of water, DMF, and acetonitrile, permittivity of 80, 38.3, and 36.6, refractive index 1.33, 1.43, and 1.344, and solvent radius of 1.3, 2.647, and 1.3 respectively. Explanation of other set options:

SlowConv: Damping factor of the SCF convergence

Grid7: DFT integration grid - deprecated in orca 5

FinalGrid7: DFT final integration grid - deprecated in orca 5

TightOpt: The optimization finished when the energy change is smaller than 3e-3 a.u.

TightSCF: The SCF finished when the energy change is smaller than 1.0e-08 a.u.

CHELPG: CHarges from ELectrostatic Potentials using a Grid-based method

Flipspin: This option was only needed when calculating the Rieske center because it is a low spin complex. It is indicated which atom undergoes a flip of the spin.

FinalMs: This option was only needed for the calculation of the Rieske center, because it is a low spin complex. It is indicated which final spin is to be achieved.

A.2 CHARMM

A.2.1 Settings

The force fields from CHARMM36 were used as force fields for the different calculation. Separate patches were created for the Rieske center, the heme groups B and C and for the ubiquinol. The charges were determined using CHELPG of `orca` on the basis of geometry-optimised structures in vacuum. If distances, angles or dihedrals were required, these were used from various publications or measured from the crystal structure.

A.3 Preptitra

A.3.1 Settings

The following list shows the settings for all calculations with `preptitra` in this dissertation. Other settings are mentioned separately in the respective chapter.

- blab 3
- temp 298.15
- solrad 1.4
- stern 2.0
- epssol 80.0
- epsin 4.0
- ionicstr 0.15
- meaddir my_mead_2.3.2/bin/
- nfocus 5
- spacing 4.0 2.0 1.0 0.4 0.1
- gridpoints 151 151 151 151 151
- xstdir /xst

Following are the newly created xst files for heme B, heme C, ubiquinol, Rieske center with all possible states.

Listing A.1: Heme B

```
LABEL                   HemOx     HemRed
GMODEL                      0       0.48
#
LIGAND  electron            0          1
SITE    $1:HEM:FE       0.837      0.470
SITE    $1:HEM:NA      -0.308      0.020
SITE    $1:HEM:NB      -0.097      0.112
SITE    $1:HEM:NC      -0.215     -0.097
SITE    $1:HEM:ND      -0.424     -0.329
SITE    $1:HEM:C1A      0.028     -0.165
SITE    $1:HEM:C2A      0.094      0.130
SITE    $1:HEM:C3A      0.180      0.159
SITE    $1:HEM:C4A     -0.111     -0.284
SITE    $1:HEM:C1B     -0.171     -0.347
SITE    $1:HEM:C2B      0.287      0.360
SITE    $1:HEM:C3B     -0.003     -0.099
SITE    $1:HEM:C4B     -0.054     -0.122
SITE    $1:HEM:C1C     -0.184     -0.311
SITE    $1:HEM:C2C      0.305      0.411
SITE    $1:HEM:C3C     -0.079     -0.189
SITE    $1:HEM:C4C      0.095      0.078
SITE    $1:HEM:C1D      0.012     -0.017
SITE    $1:HEM:C2D      0.184      0.162
SITE    $1:HEM:C3D      0.094      0.140
SITE    $1:HEM:C4D      0.058     -0.089
SITE    $1:HEM:CHA     -0.187     -0.078
SITE    $1:HEM:HA       0.158      0.124
SITE    $1:HEM:CHB     -0.087     -0.027
SITE    $1:HEM:HB       0.141      0.133
SITE    $1:HEM:CHC     -0.155     -0.112
SITE    $1:HEM:HC       0.155      0.135
SITE    $1:HEM:CHD     -0.229     -0.221
SITE    $1:HEM:HD       0.152      0.136
SITE    $1:HEM:CMA     -0.450     -0.386
SITE    $1:HEM:HMA1     0.126      0.102
SITE    $1:HEM:HMA2     0.126      0.099
SITE    $1:HEM:HMA3     0.139      0.100
SITE    $1:HEM:CMB     -0.489     -0.498
SITE    $1:HEM:HMB1     0.145      0.126
SITE    $1:HEM:HMB2     0.131      0.118
SITE    $1:HEM:HMB3     0.144      0.124
SITE    $1:HEM:CAB     -0.087     -0.009
SITE    $1:HEM:HAB      0.116      0.094
SITE    $1:HEM:CBB     -0.391     -0.501
SITE    $1:HEM:HBB1     0.174      0.184
SITE    $1:HEM:HBB2     0.171      0.164
SITE    $1:HEM:CMC     -0.473     -0.503
SITE    $1:HEM:HMC1     0.122      0.117
SITE    $1:HEM:HMC2     0.136      0.127
SITE    $1:HEM:HMC3     0.149      0.131
SITE    $1:HEM:CAC     -0.088     -0.023
SITE    $1:HEM:HAC      0.124      0.108
SITE    $1:HEM:CBC     -0.397     -0.482
SITE    $1:HEM:HBC2     0.171      0.175
SITE    $1:HEM:HBC1     0.171      0.159
SITE    $1:HEM:CMD     -0.420     -0.461
SITE    $1:HEM:HMD1     0.131      0.124
SITE    $1:HEM:HMD2     0.126      0.119
SITE    $1:HEM:HMD3     0.118      0.112
#
SITE    $2:HIS:CB      -0.512     -0.502
SITE    $2:HIS:CD2     -0.464     -0.506
SITE    $2:HIS:CE1     -0.099     -0.063
SITE    $2:HIS:CG       0.399      0.436
SITE    $2:HIS:HB1      0.235      0.205
SITE    $2:HIS:HB2      0.235      0.205
SITE    $2:HIS:HD1      0.362      0.350
SITE    $2:HIS:HD2      0.221      0.223
SITE    $2:HIS:HE1      0.170      0.149
SITE    $2:HIS:ND1     -0.339     -0.397
SITE    $2:HIS:NE2      0.190      0.153
#
SITE    $3:HIS:CB      -0.504     -0.491
SITE    $3:HIS:CD2     -0.493     -0.465
SITE    $3:HIS:CE1     -0.090     -0.096
SITE    $3:HIS:CG       0.408      0.405
SITE    $3:HIS:HB1      0.232      0.203
SITE    $3:HIS:HB2      0.232      0.203
SITE    $3:HIS:HD1      0.363      0.346
SITE    $3:HIS:HD2      0.238      0.217
```

```
SITE    $3:HIS:HE1     0.167   0.151
SITE    $3:HIS:ND1    -0.343  -0.369
SITE    $3:HIS:NE2     0.191   0.140
#
# This defines the rest of the model.
# For avoiding problems, the charge of the atoms linking
# directly to the SITE are set to zero
#
MODEL $1:HEM:CAA        0.00
MODEL $1:HEM:HAA1       0.00
MODEL $1:HEM:HAA2       0.00
MODEL $1:HEM:CAD        0.00
MODEL $1:HEM:HAD1       0.00
MODEL $1:HEM:HAD2       0.00
```

```
MODEL $2:HIS:CA      0.000000
MODEL $2:HIS:HA      0.000000

MODEL $3:HIS:CA      0.000000
MODEL $3:HIS:HA      0.000000


MODIFY $2:HIS:N      -0.400000
MODIFY $2:HIS:H       0.400000
MODIFY $2:HIS:C       0.510000
MODIFY $2:HIS:O      -0.510000

MODIFY $3:HIS:N      -0.400000
MODIFY $3:HIS:H       0.400000
```

Listing A.2: Heme C

```
LABEL                   HemOx      HemRed
GMODEL                      0       -4.17
#
LIGAND  electron              0           1
SITE    $1:HEM:FE         1.579       1.766
SITE    $1:HEM:NA        -0.377      -0.418
SITE    $1:HEM:NB        -0.131      -0.212
SITE    $1:HEM:NC        -0.638      -0.337
SITE    $1:HEM:ND        -0.450      -0.394
SITE    $1:HEM:C1A        0.007      -0.083
SITE    $1:HEM:C2A        0.099       0.120
SITE    $1:HEM:C3A        0.182       0.166
SITE    $1:HEM:C4A       -0.107      -0.063
SITE    $1:HEM:C1B       -0.050       0.014
SITE    $1:HEM:C2B        0.087       0.022
SITE    $1:HEM:C3B        0.223       0.289
SITE    $1:HEM:C4B       -0.252      -0.356
SITE    $1:HEM:C1C       -0.039      -0.210
SITE    $1:HEM:C2C        0.302       0.375
SITE    $1:HEM:C3C       -0.281      -0.344
SITE    $1:HEM:C4C        0.468       0.311
SITE    $1:HEM:C1D        0.081      -0.048
SITE    $1:HEM:C2D        0.150       0.178
SITE    $1:HEM:C3D        0.159       0.128
SITE    $1:HEM:C4D       -0.065      -0.125
SITE    $1:HEM:CHA       -0.130      -0.076
SITE    $1:HEM:HA         0.139       0.124
SITE    $1:HEM:CHB       -0.120      -0.173
SITE    $1:HEM:HB         0.140       0.140
SITE    $1:HEM:CHC       -0.162      -0.135
SITE    $1:HEM:HC         0.156       0.140
SITE    $1:HEM:CHD       -0.360      -0.310
SITE    $1:HEM:HD         0.149       0.162
SITE    $1:HEM:CMA       -0.456      -0.462
SITE    $1:HEM:HMA1       0.131       0.127
SITE    $1:HEM:HMA2       0.128       0.116
SITE    $1:HEM:HMA3       0.135       0.118
SITE    $1:HEM:CMB       -0.334      -0.376
SITE    $1:HEM:HMB1       0.101       0.097
SITE    $1:HEM:HMB2       0.104       0.103
SITE    $1:HEM:HMB3       0.102       0.098
SITE    $1:HEM:CAB        0.133       0.182
SITE    $1:HEM:HAB1       0.080       0.068
SITE    $1:HEM:CBB       -0.520      -0.551
SITE    $1:HEM:HXB1       0.165       0.168
SITE    $1:HEM:HXB2       0.164       0.149
SITE    $1:HEM:HXB3       0.131       0.128
SITE    $1:HEM:CMC       -0.399      -0.426
SITE    $1:HEM:HMC1       0.110       0.106
SITE    $1:HEM:HMC2       0.117       0.099
SITE    $1:HEM:HMC3       0.111       0.105
SITE    $1:HEM:CAC        0.251       0.376
SITE    $1:HEM:HAC1       0.043       0.007
SITE    $1:HEM:CBC       -0.501      -0.537
SITE    $1:HEM:HYC1       0.160       0.148
SITE    $1:HEM:HYC2       0.126       0.122
SITE    $1:HEM:HYC3       0.164       0.160
SITE    $1:HEM:CMD       -0.475      -0.479
SITE    $1:HEM:HMD1       0.138       0.124
SITE    $1:HEM:HMD2       0.138       0.118
SITE    $1:HEM:HMD3       0.146       0.129
#
SITE    $2:CYS:SG        -0.229      -0.301
SITE    $2:CYS:CB        -0.241      -0.198
SITE    $2:CYS:HB1        0.162       0.139
SITE    $2:CYS:HB2        0.162       0.139
#
SITE    $3:CYS:SG        -0.255      -0.337
SITE    $3:CYS:CB        -0.218      -0.195
SITE    $3:CYS:HB2        0.157       0.147
SITE    $3:CYS:HB1        0.157       0.147
#
SITE    $4:HIS:CB        -0.478      -0.481
SITE    $4:HIS:HB1        0.216       0.193
SITE    $4:HIS:HB2        0.216       0.193
SITE    $4:HIS:ND1       -0.323      -0.341
SITE    $4:HIS:HD1        0.354       0.337
SITE    $4:HIS:CG         0.403       0.383
SITE    $4:HIS:NE2       -0.102      -0.329
SITE    $4:HIS:CD2       -0.440      -0.366
SITE    $4:HIS:HD2        0.243       0.215
SITE    $4:HIS:CE1       -0.031       0.018
SITE    $4:HIS:HE1        0.154       0.124
#
SITE    $5:MET:CB        -0.341      -0.308
SITE    $5:MET:HB1        0.143       0.112
SITE    $5:MET:HB2        0.143       0.112
SITE    $5:MET:CG         0.317       0.302
SITE    $5:MET:HG1       -0.042      -0.063
SITE    $5:MET:HG2        0.015      -0.001
SITE    $5:MET:SD        -0.175      -0.351
SITE    $5:MET:CE        -0.404      -0.317
SITE    $5:MET:HE1        0.174       0.132
SITE    $5:MET:HE2        0.177       0.132
SITE    $5:MET:HE3        0.134       0.095
#
# This defines the rest of the model.
# For avoiding problems, the charge of the
     atoms linking
# directly to the SITE are set to zero
#
MODEL $1:HEM:CAA        0.00
MODEL $1:HEM:HAA1       0.00
MODEL $1:HEM:HAA2       0.00
MODEL $1:HEM:CAD        0.00
MODEL $1:HEM:HAD1       0.00
```

```
MODEL $1:HEM:HAD2       0.00

MODEL $2:CYS:CA      0.000000
MODEL $2:CYS:HA      0.000000
MODIFY $2:CYS:N      -0.400000
MODIFY $2:CYS:H       0.400000
MODIFY $2:CYS:C       0.510000
MODIFY $2:CYS:O      -0.510000

MODEL $3:CYS:CA      0.000000
MODEL $3:CYS:HA      0.000000
MODIFY $3:CYS:N      -0.400000
MODIFY $3:CYS:H       0.400000
MODIFY $3:CYS:C       0.510000
MODIFY $3:CYS:O      -0.510000

MODEL $4:HIS:CA      0.000000
MODEL $4:HIS:HA      0.000000
MODIFY $4:HIS:N      -0.400000
MODIFY $4:HIS:H       0.400000
MODIFY $4:HIS:C       0.510000
MODIFY $4:HIS:O      -0.510000

MODEL $5:MET:CA      0.000000
MODEL $5:MET:HA      0.000000
MODIFY $5:MET:N      -0.400000
MODIFY $5:MET:H       0.400000
MODIFY $5:MET:C       0.510000
MODIFY $5:MET:O      -0.510000
```

```
# RIOP -- oxidized,          fully protonated  Rieske Center
# RRCP -- reduced (Cys 1), fully protonated  Rieske Center
# RRHP -- reduced (His 2), fully protonated  Rieske Center
# .
# RIO1 -- oxidized,          deprotonated His1 Rieske Center
# RRC1 -- reduced (Cys 1), deprotonated His1 Rieske Center
# RRH1 -- reduced (His 2), deprotonated His1 Rieske Center
# .
# RIO2 -- oxidized,          deprotonated His2 Rieske Center
# RRC2 -- reduced (Cys 1), deprotonated His2 Rieske Center
# RRH2 -- reduced (His 2), deprotonated His2 Rieske Center
# .
# RIOT -- oxidized, totally deprotonated Rieske Center
# RRCT -- reduced (Cys 1), totally deprotonated Rieske Center
# RRHT -- reduced (His 2), totally deprotonated Rieske Center

```

LABEL		RIOP	RRCP	RRHP	RIO1	RRC1	RRH1	RIO2	RRC2	RRH2	RIOT	RRCT	RRHT
GMODEL		5.52	9.76	0.0	17.26	23.31	15.23	17.40	23.56	15.70	30.74	33.71	29.02
LIGAND	proton	2	2	2	1	1	1	1	1	1	0	0	0
LIGAND	electron	0	1	1	0	1	1	0	1	1	0	1	1
SITE	$1:FES:FE1	0.516	0.752	0.849	0.711	0.866	0.887	0.764	0.926	0.926	0.787	0.922	0.962
SITE	$1:FES:FE2	0.458	0.512	0.448	0.719	0.746	0.630	0.636	0.641	0.516	0.787	0.811	0.705
SITE	$1:FES:S1	−0.387	−0.620	−0.601	−0.467	−0.670	−0.646	−0.483	−0.674	−0.662	−0.521	−0.715	−0.727
SITE	$1:FES:S2	−0.429	−0.679	−0.656	−0.556	−0.802	−0.743	−0.529	−0.768	−0.728	−0.601	−0.852	−0.822
#													
SITE	$2:CYS:CB	0.135	−0.039	−0.020	0.045	−0.175	−0.107	0.043	−0.146	−0.103	−0.018	−0.213	−0.171
SITE	$2:CYS:HB1	0.006	0.032	0.023	0.013	0.060	0.041	0.012	0.056	0.042	0.022	0.060	0.055
SITE	$2:CYS:HB2	0.014	0.051	0.049	0.026	0.082	0.062	0.030	0.073	0.065	0.038	0.087	0.076
SITE	$2:CYS:SG	−0.288	−0.398	−0.522	−0.432	−0.514	−0.524	−0.496	−0.623	−0.577	−0.509	−0.617	−0.582
#													
SITE	$3:CYS:CB	0.250	0.110	0.124	0.160	0.021	0.051	0.159	0.011	0.043	0.120	−0.034	0.002
SITE	$3:CYS:HB1	−0.038	−0.009	−0.672	−0.023	0.000	−0.011	−0.029	−0.001	−0.010	−0.021	0.013	−0.001
SITE	$3:CYS:HB2	−0.041	−0.018	−0.023	−0.027	0.004	−0.004	−0.017	0.005	−0.003	−0.021	0.013	0.001
SITE	$3:CYS:SG	−0.414	−0.613	−0.019	−0.610	−0.759	−0.733	−0.597	−0.763	−0.717	−0.663	−0.822	−0.776
#													
SITE	$4:HIS:NE2	−0.279	−0.296	−0.289	−0.550	−0.606	−0.597	−0.317	−0.343	−0.330	−0.608	−0.654	−0.652

```
SITE    $4:HIS:HE2   0.371   0.349   0.355   0.000   0.000   0.000   0.372   0.353   0.331   0.000   0.000   0.000
SITE    $4:HIS:CD2  -0.232  -0.247  -0.259   0.010  -0.048  -0.046  -0.205  -0.248  -0.258  -0.003  -0.037  -0.045
SITE    $4:HIS:HD2   0.231   0.208   0.217   0.133   0.123   0.119   0.203   0.193   0.188   0.112   0.089   0.085
SITE    $4:HIS:ND1  -0.033  -0.033   0.016  -0.154  -0.187  -0.058  -0.073  -0.063   0.001  -0.156  -0.161  -0.095
SITE    $4:HIS:CG   -0.086  -0.052  -0.065  -0.224  -0.148  -0.189  -0.081  -0.029  -0.055  -0.200  -0.131  -0.153
SITE    $4:HIS:CE1  -0.159  -0.196  -0.217  -0.039  -0.027  -0.117  -0.112  -0.135  -0.162   0.008  -0.029  -0.076
SITE    $4:HIS:HE1   0.216   0.221   0.222   0.171   0.161   0.183   0.218   0.231   0.243   0.171   0.170   0.189
SITE    $4:HIS:CB    0.161   0.065   0.061   0.047  -0.097  -0.085   0.105  -0.019   0.001  -0.039  -0.179  -0.161
SITE    $4:HIS:HB1  -0.064  -0.030  -0.026  -0.015   0.037   0.020  -0.044   0.016  -0.017   0.004   0.091   0.038
SITE    $4:HIS:HB2   0.005   0.023   0.038   0.026   0.054   0.054   0.031   0.049   0.048   0.043   0.054   0.061
#
SITE    $5:HIS:NE2  -0.130  -0.160  -0.147  -0.128  -0.105  -0.184  -0.519  -0.552  -0.565  -0.551  -0.598  -0.631
SITE    $5:HIS:HE2   0.336   0.315   0.319   0.323   0.285   0.297   0.000   0.000   0.000   0.000   0.000   0.000
SITE    $5:HIS:CD2  -0.369  -0.407  -0.402  -0.398  -0.456  -0.415  -0.077  -0.151  -0.141  -0.104  -0.146  -0.129
SITE    $5:HIS:HD2   0.247   0.232   0.235   0.242   0.229   0.218   0.136   0.129   0.124   0.122   0.106   0.099
SITE    $5:HIS:ND1  -0.250  -0.276  -0.205  -0.427  -0.335  -0.382  -0.418  -0.399  -0.349  -0.518  -0.476  -0.483
SITE    $5:HIS:CG    0.102   0.123   0.103   0.214   0.209   0.194  -0.012   0.021  -0.019   0.068   0.071   0.055
SITE    $5:HIS:CE1  -0.180  -0.210  -0.247  -0.095  -0.187  -0.165   0.112   0.081   0.026   0.111   0.083   0.091
SITE    $5:HIS:HE1   0.231   0.220   0.235   0.220   0.222   0.217   0.127   0.115   0.130   0.128   0.119   0.117
SITE    $5:HIS:CB    0.007  -0.009  -0.007  -0.017  -0.085  -0.079   0.019  -0.016  -0.036  -0.061  -0.073  -0.129
SITE    $5:HIS:HB1   0.048   0.016   0.020   0.034   0.027   0.025  -0.011  -0.031  -0.024   0.000  -0.028  -0.011
SITE    $5:HIS:HB2   0.045   0.063   0.063   0.068   0.075   0.087   0.053   0.061   0.072   0.073   0.076   0.108
#
MODEL  $2:CYS:CA  0.0
MODEL  $2:CYS:HA  0.0
#
MODEL  $3:CYS:CA  0.0
MODEL  $3:CYS:HA  0.0
#
MODEL  $4:HIS:CA  0.0
MODEL  $4:HIS:HA  0.0
#
MODEL  $5:HIS:CA  0.0
MODEL  $5:HIS:HA  0.0
#
MODIFY  $2:CYS:C          0.51
```

```
    MODIFY  $2:CYS:O        -0.51
    MODIFY  $2:CYS:N        -0.40
    MODIFY  $2:CYS:H         0.40
76  #
    MODIFY  $3:CYS:C         0.51
    MODIFY  $3:CYS:O        -0.51
    MODIFY  $3:CYS:N        -0.40
    MODIFY  $3:CYS:H         0.40
81  #
    MODIFY  $4:HIS:C         0.51
    MODIFY  $4:HIS:O        -0.51
    MODIFY  $4:HIS:N        -0.40
    MODIFY  $4:HIS:H         0.40
86  #
    MODIFY  $5:HIS:C         0.51
    MODIFY  $5:HIS:O        -0.51
    MODIFY  $5:HIS:N        -0.40
    MODIFY  $5:HIS:H         0.40
```

```
# U2PP -- double reduced, double protonated
# U2PD -- double reduced, single protonated at O1
# U2DP -- double reduced, single protonated at O4
# U2DD -- double reduced, deprotonated
# U1PP -- single reduced, double protonated
# U1PD -- single reduced, single protonated at O1
# U1DP -- single reduced, single protonated at O4
# U1DD -- single reduced, unprotonated
# U0PP -- oxidized, double protonated
# U0PD -- oxidized, single protonated at O1
# U0DP -- oxidized, single protonated at O4
# U0DD -- oxidized, unprotonated
LABEL                    U0DD    U0DP    U0PD    U0PP    U1DD    U1DP    U1PD    U1PP    U2DD    U2DP    U2PD    U2PP
GMODEL                   0.00    23.70   23.13   44.17   -11.25  -7.15   -7.15   4.54    -19.56  -24.05  -23.92  -27.99
#
LIGAND   proton          0       1       1       2       0       1       1       2       0       1       1       2
LIGAND   electron        0       0       0       0       1       1       1       1       2       2       2       2
#
SITE     $1:UQ2:C2       0.160   -0.162  0.236   -0.119  -0.098  -0.160  0.102   0.070   -0.101  -0.069  -0.173  -0.072
SITE     $1:UQ2:O2       -0.210  -0.206  -0.175  -0.227  -0.242  -0.255  -0.213  -0.130  -0.288  -0.265  -0.187  -0.221
SITE     $1:UQ2:CM2      -0.109  -0.167  -0.113  -0.134  -0.083  -0.121  -0.095  -0.270  0.003   -0.085  -0.162  -0.162
SITE     $1:UQ2:H2M1     0.099   0.130   0.131   0.131   0.060   0.092   0.091   0.159   0.014   0.067   0.074   0.106
SITE     $1:UQ2:H2M2     0.099   0.130   0.131   0.131   0.060   0.092   0.091   0.159   0.014   0.067   0.074   0.106
SITE     $1:UQ2:H2M3     0.099   0.130   0.131   0.131   0.060   0.092   0.091   0.159   0.014   0.067   0.074   0.106
SITE     $1:UQ2:C3       -0.096  0.144   0.037   0.230   0.139   0.066   0.080   0.173   0.118   0.001   0.094   0.176
SITE     $1:UQ2:CM3      -0.298  -0.369  -0.314  -0.329  -0.061  -0.368  -0.264  -0.228  0.027   -0.129  -0.093  -0.147
SITE     $1:UQ2:O3       -0.138  -0.001  -0.180  -0.011  -0.270  -0.003  -0.201  -0.202  -0.308  -0.203  -0.275  -0.203
SITE     $1:UQ2:H3M1     0.136   0.188   0.161   0.189   0.054   0.153   0.129   0.136   0.006   0.064   0.069   0.092
SITE     $1:UQ2:H3M2     0.136   0.188   0.161   0.189   0.054   0.153   0.129   0.136   0.006   0.064   0.069   0.092
SITE     $1:UQ2:H3M3     0.136   0.188   0.161   0.189   0.054   0.153   0.129   0.136   0.006   0.064   0.069   0.092
SITE     $1:UQ2:C5       0.217   0.113   0.200   0.018   0.207   0.151   0.253   0.245   0.165   0.103   0.294   0.295
SITE     $1:UQ2:CM5      -0.492  -0.357  -0.424  -0.336  -0.287  -0.355  -0.419  -0.450  -0.245  -0.311  -0.340  -0.424
SITE     $1:UQ2:H5M1     0.152   0.142   0.153   0.138   0.067   0.112   0.124   0.152   0.028   0.070   0.083   0.120
SITE     $1:UQ2:H5M2     0.152   0.142   0.153   0.138   0.067   0.112   0.124   0.152   0.028   0.070   0.083   0.120
SITE     $1:UQ2:H5M3     0.152   0.142   0.153   0.138   0.067   0.112   0.124   0.152   0.028   0.070   0.083   0.120
SITE     $1:UQ2:C6       -0.389  -0.342  -0.312  -0.163  -0.506  -0.421  -0.470  -0.321  -0.511  -0.373  -0.610  -0.520
```

	SITE	$1:UQ2:C7	0.234	0.113	0.119	0.102	0.143	0.166	0.247	0.214	0.218	0.095	0.177	0.303
	SITE	$1:UQ2:HA7	0.044	0.071	0.098	0.108	0.027	0.043	0.049	0.050	−0.024	0.040	0.021	0.025
	SITE	$1:UQ2:HB7	0.019	0.085	0.063	0.084	0.050	0.060	0.027	0.051	0.015	0.062	0.038	0.018
	SITE	$1:UQ2:C8	−0.385	−0.338	−0.398	−0.334	−0.329	−0.318	−0.375	−0.356	−0.358	−0.291	−0.323	−0.340
	SITE	$1:UQ2:H8	0.187	0.147	0.196	0.168	0.169	0.146	0.191	0.166	0.170	0.153	0.167	0.167
	SITE	$1:UQ2:C9	0.121	0.165	0.183	0.327	0.096	0.116	0.080	0.128	0.084	0.081	0.104	0.039
	SITE	$1:UQ2:C10	−0.407	−0.418	−0.392	−0.451	−0.399	−0.444	−0.435	−0.448	−0.362	−0.411	−0.429	−0.439
	SITE	$1:UQ2:HA10	0.114	0.129	0.122	0.157	0.096	0.123	0.120	0.138	0.068	0.101	0.100	0.122
	SITE	$1:UQ2:HB10	0.114	0.129	0.122	0.157	0.096	0.123	0.120	0.138	0.068	0.101	0.100	0.122
	SITE	$1:UQ2:HC10	0.114	0.129	0.122	0.157	0.096	0.123	0.120	0.138	0.068	0.101	0.100	0.122
	SITE	$1:UQ2:C11	−0.168	−0.229	−0.215	−0.302	−0.102	−0.160	−0.101	−0.178	−0.091	−0.109	−0.103	−0.049
	SITE	$1:UQ2:HA11	0.046	0.075	0.075	0.132	0.021	0.044	0.031	0.063	0.011	0.017	0.020	0.019
	SITE	$1:UQ2:HB11	0.065	0.098	0.099	0.151	0.022	0.061	0.057	0.094	−0.009	0.023	0.018	0.044
	SITE	$1:UQ2:C12	0.442	0.373	0.321	0.126	0.504	0.438	0.389	0.318	0.620	0.531	0.526	0.367
	SITE	$1:UQ2:HA12	−0.021	0.005	0.019	0.083	−0.046	−0.025	−0.010	0.017	−0.081	−0.049	−0.055	−0.007
	SITE	$1:UQ2:HB12	−0.064	−0.055	−0.042	0.028	−0.068	−0.060	−0.060	−0.046	−0.084	−0.066	−0.081	−0.048
	SITE	$1:UQ2:C13	−0.754	−0.676	−0.657	−0.354	−0.807	−0.738	−0.735	−0.632	−0.928	−0.829	−0.813	−0.739
	SITE	$1:UQ2:H13	0.209	0.206	0.204	0.186	0.210	0.206	0.204	0.200	0.223	0.213	0.212	0.206
	SITE	$1:UQ2:C14	0.567	0.540	0.533	0.504	0.587	0.550	0.567	0.539	0.623	0.594	0.594	0.561
	SITE	$1:UQ2:C15	−0.587	−0.583	−0.565	−0.551	−0.621	−0.592	−0.596	−0.569	−0.618	−0.619	−0.622	−0.570
	SITE	$1:UQ2:HA15	0.151	0.155	0.151	0.180	0.158	0.153	0.153	0.155	0.150	0.156	0.157	0.147
	SITE	$1:UQ2:HB15	0.151	0.155	0.151	0.180	0.158	0.153	0.153	0.155	0.150	0.156	0.157	0.147
	SITE	$1:UQ2:HC15	0.151	0.155	0.151	0.180	0.158	0.153	0.153	0.155	0.150	0.156	0.157	0.147
	SITE	$1:UQ2:C16	−0.547	−0.571	−0.574	−0.606	−0.515	−0.538	−0.556	−0.584	−0.472	−0.507	−0.520	−0.551
	SITE	$1:UQ2:HA16	0.134	0.152	0.154	0.200	0.116	0.132	0.136	0.158	0.090	0.113	0.116	0.134
	SITE	$1:UQ2:HB16	0.134	0.152	0.154	0.200	0.116	0.132	0.136	0.158	0.090	0.113	0.116	0.134
	SITE	$1:UQ2:HC16	0.134	0.152	0.154	0.200	0.116	0.132	0.136	0.158	0.090	0.113	0.116	0.134
	SITE	$1:UQ2:C1	0.466	0.521	0.471	0.382	0.532	0.471	0.467	0.254	0.456	0.286	0.600	0.356
	SITE	$1:UQ2:O1	−0.427	−0.358	−0.336	−0.389	−0.541	−0.479	−0.458	−0.350	−0.702	−0.606	−0.621	−0.495
	SITE	$1:UQ2:HO1	0.000	0.000	0.403	0.425	0.000	0.000	0.392	0.386	0.000	0.000	0.373	0.384
	SITE	$1:UQ2:C4	0.384	0.443	0.160	0.231	0.156	0.311	0.051	0.066	0.083	0.243	−0.007	−0.025
	SITE	$1:UQ2:O4	−0.427	−0.358	−0.336	−0.389	−0.541	−0.479	−0.458	−0.350	−0.702	−0.606	−0.621	−0.495
	SITE	$1:UQ2:HO4	0.000	0.403	0.000	0.425	0.000	0.392	0.000	0.386	0.000	0.373	0.000	0.384

A.4 GMCT

A.4.1 Settings

The definitions of the different setup options have been described and taken from the manual of gmct in a shortened form. More details can be found in the gmct manual.

- nmu: number of chemical potentials
- mu: definition of chemical potential properties (start, stop, increment, membrane site, charge)
- blab: verbose level - default: 0
- seed: seed for random number generator - default: system time
- clustnsitemax: maximum number of sites within a cluster - default: 10
- temp: temperature - default: None
- slopVmemb: definition of the nernst membrane contribution slope - default: None
- nmcfull: number of full Monte Carlo scans - default: None
- nmcequi: equilibration scan amount - default: None
- vmemb: membrane potential - default: None
- ierror: switch for calculation of statistical error, autocorrelation function and the corresponding correlation time - default: 0/no
- itraj: switch for writing “trajectory files” - default: 0/no
- icorr: flag for calculation of unnormalized correlations - default: 0/no

The following list shows the settings for all calculations with gmct in this dissertation. For other settings this is mentioned separately in the respective chapter.

- nmu 2
- mu -19.09944818 -16.7120171575 1.3642487 0 1
- mu -80.71 23.0 0.27284974 0 -1
- blab 3
- seed 240381
- clustnsitemax 5
- temp 298.15
- slopVmemb 0.0
- nmcfull 10^3
- nmcequi 500
- vmemb 0.0
- ierror 1
- itraj 1
- icorr 2

B

ARCHITECTURE OF SELF-WRITTEN PYTHON3-SCRIPTS

A larger framework was written in python which includes the four major modules gcem_new, gmct, kinetics, and protnet, as well as a basic module that writes the log file ("mylogging") and contains useful functions ("utilities"). As the figure B.1 shows, the framework is extensive and includes all the methods that were used here in the PhD thesis in electrostatics.

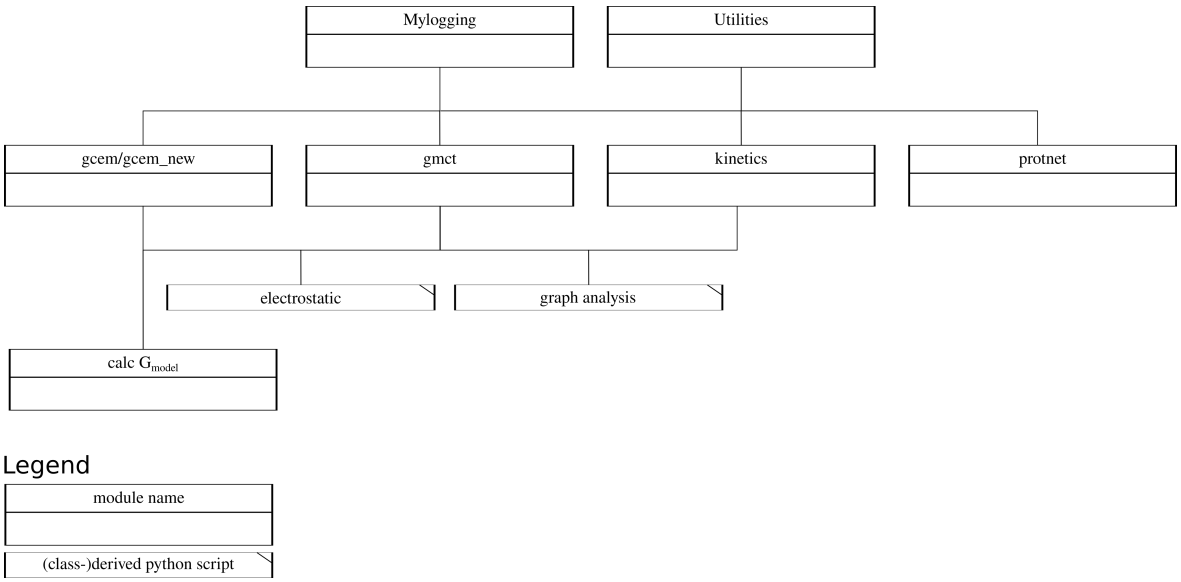

Figure B.1: General overview for the framework structure to calculate with electrostatics.

The module gcem_new is able to use the inhouse program `preptitra` and its subroutines. The module gcem_new also provides functionalities for the two modules kinetics and protnet, such as the calculation of state energy. Furthermore, in the model gcem_new/gcem two smaller frameworks are sealed, which are used to determine G_{model}. The respective modules were used to determine the G_{model}-values in the chapters 3 to 5. The module gmct is again able to use the inhouse program `gmct` and its subroutines. Furthermore, the module can be used to analyze and graphically display the results of the inhouse program `gmct`. The protnet module was written to simulate a proton transfer or a hydrogen transfer within a protein using an inhouse program. This module was in a simpler form part of a bachelor thesis by Sebastian Krausse. The module kinetics is loosely based on the further developed module protnet and was partly inspired by it. The kinetics module is much more comprehensive and builds a graph based on different sites, states and conformations as well as state energies and the results of gcem. The result of all calculations as well as the finished graph is used to prepare the input for an inhouse program `kinetics`, which then calculates the kinetics for the electron and proton transfer using Marcus theory. These results in the flux of the individual reactions/transfers. The results of the inhouse program `kinetics` are then analyzed using the kinetics module, looking for cycles and

determining whether they are complete. Especially notable is the search algorithm for finding cycles within the graph. The algorithm does not follow a classical graph path finding algorithm, but its own design. At the beginning the edge with highest flux is searched in the graph. The initial node of this edge is the start node for the search. Starting from this start node, the edges with the highest flux are always followed until the start node is reached again or the maximum number of nodes is reached. Hereby the main cycle is found. But there might still be side paths that lead back to the main path. Such side paths are characterized by the fact that during the search for the main path, nodes are found which have several output edges. These nodes are stored separately and after finding them the main cycle is visited again. When such a node is revisited, it is no longer followed by the highest flux but by the second highest flux. If there are still more edges unvisited after this search, another run is started, where the next lower unvisited flux is followed. The algorithm is finished when all edges of the found nodes have been visited or a specified percentage of a substance flux has been reached. By this procedure a main cycle is found, which can be surrounded by several layers. The figure B.2 summarizes the algorithm.

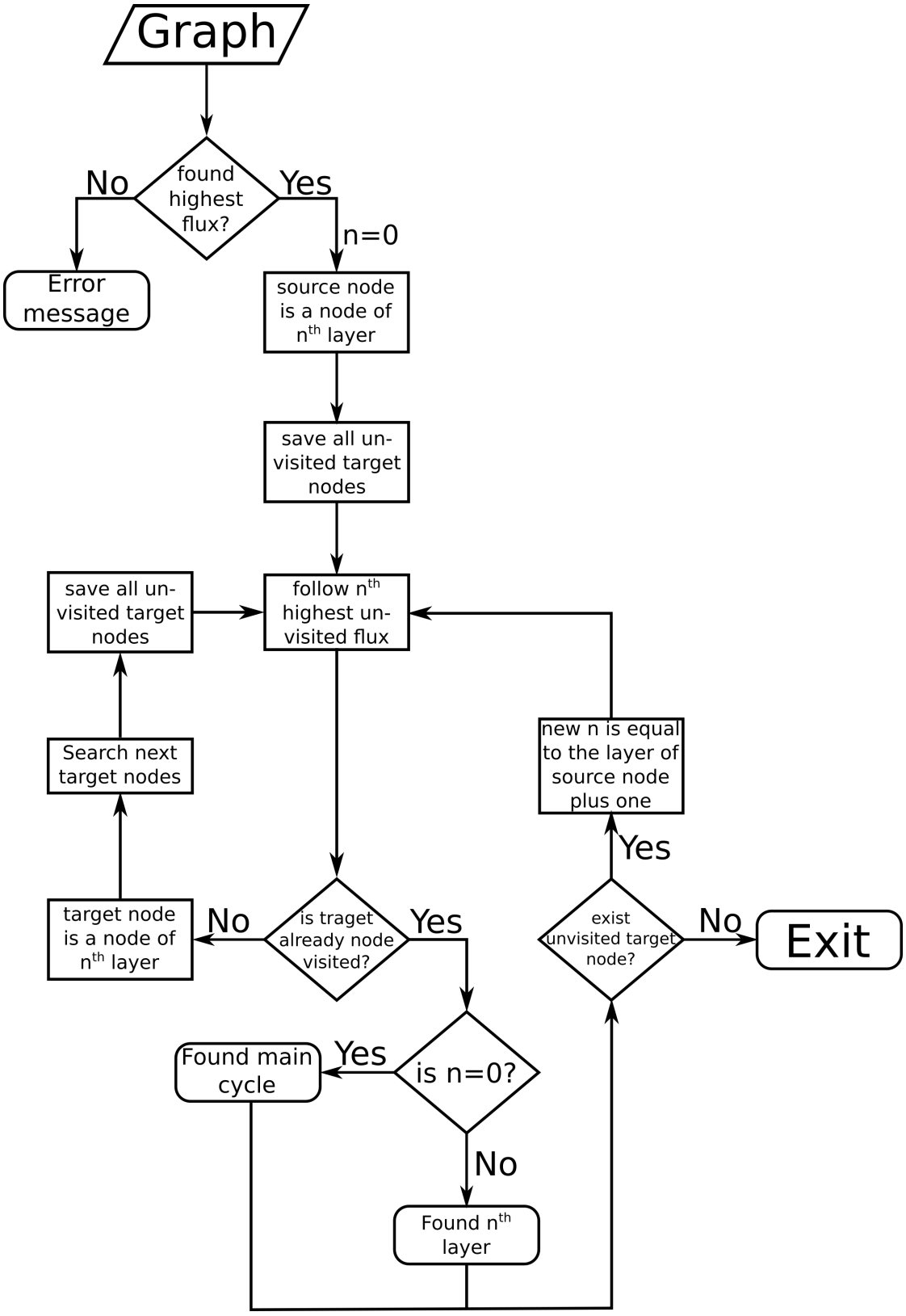

Figure B.2: Search algorithm for finding a main cycle as well as layers around this main cycle.

C

APPENDIX - AB INITIO CALCULATION OF G_{model} WITH APPLICATIONS TO UBIQUINONE/UBIQUINOL

C.1 Theory

C.1.1 Calculation of absolute and relative pK_a-values and redox potentials

Absolute pK_a-values

Equation (C.1) shows the intermediate steps of equation (3.17).

$$
\begin{aligned}
\Delta G_{gas} =& G_{gas}(MH) - G_{gas}(M^-) + (G_{gas}(H^+) + R \cdot T \cdot ln(R_{atm} \cdot T)) \\
=& E^{MH}_{elec} + ZPE^{MH} + U^{MH}_{vib} + \underbrace{U^{MH}_{rot}}_{=\frac{3}{2}\cdot R\cdot T} + \underbrace{U^{MH}_{trans}}_{=\frac{3}{2}\cdot R\cdot T} + k_B T \\
& - T(S^{MH}_{elec} + S^{MH}_{vib} + S^{MH}_{rot} + S^{MH}_{trans}) \\
& - (E^{M^-}_{elec} + ZPE^{M^-} + U^{M^-}_{vib} + \underbrace{U^{M^-}_{rot}}_{=\frac{3}{2}\cdot R\cdot T} + \underbrace{U^{M^-}_{trans}}_{=\frac{3}{2}\cdot R\cdot T} + k_B T \\
& - T(S^{M^-}_{elec} + S^{M^-}_{vib} + S^{M^-}_{rot} + S^{M^-}_{trans})) \\
& + (G_{gas}(H^+) + R \cdot T \cdot ln(R_{atm} \cdot T)) \\
=& E^{MH}_{elec} + ZPE^{MH} + U^{MH}_{vib} - (T(S^{MH}_{elec} + S^{MH}_{vib} + S^{MH}_{rot} + S^{MH}_{trans})) \\
& - (E^{M^-}_{elec} + ZPE^{M^-} + U^{M^-}_{vib} - (T(S^{M^-}_{elec} + S^{M^-}_{vib} + S^{M^-}_{rot} + S^{M^-}_{trans}))) \\
& + (G_{gas}(H^+) + R \cdot T \cdot ln(R_{atm} \cdot T) \\
=& E^{MH}_{elec,gas} - E^{M^-}_{elec,gas} + ZPE^{MH}_{gas} - ZPE^{M^-}_{gas} + \\
& U^{MH}_{vib,gas} - U^{M^-}_{vib,gas} \\
& - T(S^{MH}_{elec,gas} - S^{M^-}_{elec,gas} + S^{MH}_{vib,gas} - S^{M^-}_{vib,gas} + \\
& S^{MH}_{rot,gas} - S^{M^-}_{rot,gas} + S^{MH}_{trans,gas} - S^{M^-}_{trans,gas}) \\
& + \underbrace{(G_{gas}(H^+) + R \cdot T \cdot ln(R_{atm} \cdot T))}_{\Delta G_{gas}(H^+)}
\end{aligned}
\tag{C.1}
$$

with

T: temperature

R: gas constant

R_{atm}: gas constant in atm units

$R \cdot T \cdot ln(R_{atm} \cdot T)$: conversion factor from 1atm to 1M

E_{elec} or U_{elec}: electronic energy

ZPE: zero point energy

U_{vib}: vibrational thermal energy U_{trans}: translational thermal energy

U_{rot}: rotational thermal energy

Equation (C.2) shows the intermediate steps of equation (3.20).

$$
\begin{aligned}
\Delta G_{aq} =& \Delta G_{gas} + \Delta\Delta G_{solv} \qquad \text{(C.2)}\\
=& E^{MH}_{elec,gas} - E^{M^-}_{elec,gas} + ZPE^{MH}_{gas} - ZPE^{M^-}_{gas} +\\
& U^{MH}_{vib,gas} - U^{M^-}_{vib,gas}\\
& -T(S^{MH}_{elec,gas} - S^{M^-}_{elec,gas} + S^{MH}_{vib,gas} - S^{M^-}_{vib,gas} +\\
& S^{MH}_{rot,gas} - S^{M^-}_{rot,gas} + S^{MH}_{trans,gas} - S^{M^-}_{trans,gas})\\
& + E^{M^-}_{elec,gas} - E^{M^-}_{elec,aq} + ZPE^{M^-}_{gas} - ZPE^{M^-}_{aq} +\\
& U^{M^-}_{vib,gas} - U^{M^-}_{vib,aq}\\
& -T(S^{M^-}_{elec,gas} - S^{M^-}_{elec,aq} + S^{M^-}_{vib,gas} - S^{M^-}_{vib,aq} +\\
& S^{M^-}_{rot,gas} - S^{M^-}_{rot,aq} + S^{M^-}_{trans,gas} - S^{M^-}_{trans,aq})\\
& - E^{MH}_{elec,gas} + E^{MH}_{elec,aq} - ZPE^{MH}_{gas} + ZPE^{MH}_{aq} -\\
& U^{MH}_{vib,gas} + U^{MH}_{vib,aq}\\
& +T(S^{MH}_{elec,gas} - S^{MH}_{elec,aq} + S^{MH}_{vib,gas} - S^{MH}_{vib,aq} +\\
& S^{MH}_{rot,gas} - S^{MH}_{rot,aq} + S^{MH}_{trans,gas} - S^{MH}_{trans,aq})\\
& + \Delta G_{solv}(H^+) + \Delta G_{gas}(H^+)\\
=& \underbrace{E^{MH}_{elec,gas} - E^{M^-}_{elec,gas} + E^{M^-}_{elec,gas} - E^{M^-}_{elec,aq} - E^{MH}_{elec,gas} + E^{MH}_{elec,aq}}_{\Delta\Delta E_{elec}}\\
& + \underbrace{ZPE^{MH}_{gas} - ZPE^{M^-}_{gas} + ZPE^{M^-}_{gas} - ZPE^{M^-}_{aq} - ZPE^{MH}_{gas} + ZPE^{MH}_{aq}}_{\Delta\Delta ZPE}\\
& + \underbrace{U^{MH}_{vib,gas} - U^{M^-}_{vib,gas} + U^{M^-}_{vib,gas} - U^{M^-}_{vib,aq} - U^{MH}_{vib,gas} + U^{MH}_{vib,aq}}_{\Delta\Delta U_{vib}}\\
& - \underbrace{T(S^{MH}_{elec,gas} - S^{M^-}_{elec,gas} + S^{M^-}_{elec,gas} - S^{M^-}_{elec,aq} - S^{MH}_{elec,gas} + S^{MH}_{elec,aq})}_{\Delta\Delta S_{elec}}\\
& - \underbrace{T(S^{MH}_{vib,gas} - S^{M^-}_{vib,gas} + S^{M^-}_{vib,gas} - S^{M^-}_{vib,aq} - S^{MH}_{vib,gas} + S^{MH}_{vib,aq})}_{\Delta\Delta S_{vib}}\\
& - \underbrace{T(S^{MH}_{rot,gas} - S^{M^-}_{rot,gas} + S^{M^-}_{rot,gas} - S^{M^-}_{rot,aq} - S^{MH}_{rot,gas} + S^{MH}_{rot,aq})}_{\Delta\Delta S_{rot}}\\
& - \underbrace{T(S^{MH}_{trans,gas} - S^{M^-}_{trans,gas} + S^{M^-}_{trans,gas} - S^{M^-}_{trans,aq} - S^{MH}_{trans,gas} + S^{MH}_{trans,aq})}_{\Delta\Delta S_{trans}}
\end{aligned}
$$

$$
\begin{aligned}
&= \underbrace{E^{MH}_{elec,aq} - E^{M^-}_{elec,aq}}_{\Delta\Delta E_{elec}} + \underbrace{ZPE^{MH}_{aq} - ZPE^{M^-}_{aq}}_{\Delta\Delta ZPE} \\
&+ \underbrace{U^{MH}_{vib,aq} - U^{M^-}_{vib,aq}}_{\Delta\Delta U_{vib}} \\
&- \underbrace{T(S^{MH}_{elec,aq} - S^{M^-}_{elec,aq})}_{\Delta\Delta S_{elec}} - \underbrace{T(S^{MH}_{vib,aq} - S^{M^-}_{vib,aq})}_{\Delta\Delta S_{vib}} \\
&- \underbrace{T(S^{MH}_{rot,aq} - S^{M^-}_{rot,aq})}_{\Delta\Delta S_{rot}} - \underbrace{T(S^{MH}_{trans,aq} - S^{M^-}_{trans,aq})}_{\Delta\Delta S_{trans}} \\
&+ \Delta G_{solv}(H^+) + \Delta G_{gas}(H^+)
\end{aligned}
\tag{C.3}
$$

Absolute redox potentials

Equation (C.4) shows the intermediate steps of equation (3.22).

$$
\begin{aligned}
\Delta G_{gas} =& G_{gas}(MH) - G_{gas}(M^-) \\
=& E^{MH}_{elec} + ZPE^{MH} + U^{MH}_{vib} + \underbrace{U^{MH}_{rot}}_{=\frac{3}{2}\cdot R\cdot T} + \underbrace{U^{MH}_{trans}}_{=\frac{3}{2}\cdot R\cdot T} + k_B T \\
& - T(S^{MH}_{elec} + S^{MH}_{vib} + S^{MH}_{rot} + S^{MH}_{trans}) \\
& - (E^{M^-}_{elec} + ZPE^{M^-} + U^{M^-}_{vib} + \underbrace{U^{M^-}_{rot}}_{=\frac{3}{2}\cdot R\cdot T} + \underbrace{U^{M^-}_{trans}}_{=\frac{3}{2}\cdot R\cdot T} + k_B T \\
& - T(S^{M^-}_{elec} + S^{M^-}_{vib} + S^{M^-}_{rot} + S^{M^-}_{trans})) \\
=& E^{MH}_{elec} + ZPE^{MH} + U^{MH}_{vib} - (T(S^{MH}_{elec} + S^{MH}_{vib} + S^{MH}_{rot} + S^{MH}_{trans})) \\
& - (E^{M^-}_{elec} + ZPE^{M^-} + U^{M^-}_{vib} - (T(S^{M^-}_{elec} + S^{M^-}_{vib} + S^{M^-}_{rot} + S^{M^-}_{trans}))) \\
=& E^{MH}_{elec,gas} - E^{M^-}_{elec,gas} + ZPE^{MH}_{gas} - ZPE^{M^-}_{gas} + \\
& U^{MH}_{vib,gas} - U^{M^-}_{vib,gas} \\
& - T(S^{MH}_{elec,gas} - S^{M^-}_{elec,gas} + S^{MH}_{vib,gas} - S^{M^-}_{vib,gas} + \\
& S^{MH}_{rot,gas} - S^{M^-}_{rot,gas} + S^{MH}_{trans,gas} - S^{M^-}_{trans,gas})
\end{aligned}
\tag{C.4}
$$

(C.5)

Equation (C.6) shows the intermediate steps of equation (3.25).

$$
\begin{aligned}
\Delta G_{aq} =& \Delta G_{gas} + \Delta\Delta G_{solv} \\
=& E^{M}_{elec,gas} - E^{M^-}_{elec,gas} + ZPE^{M}_{gas} - ZPE^{M^-}_{gas} + \\
& U^{M}_{vib,gas} - U^{M^-}_{vib,gas} \\
& -T(S^{M}_{elec,gas} - S^{M^-}_{elec,gas} + S^{M}_{vib,gas} - S^{M^-}_{vib,gas} + \\
& S^{M}_{rot,gas} - S^{M^-}_{rot,gas} + S^{M}_{trans,gas} - S^{M^-}_{trans,gas}) \\
& + E^{M^-}_{elec,gas} - E^{M^-}_{elec,aq} + ZPE^{M^-}_{gas} - ZPE^{M^-}_{aq} + \\
& U^{M^-}_{vib,gas} - U^{M^-}_{vib,aq} \\
& -T(S^{M^-}_{elec,gas} - S^{M^-}_{elec,aq} + S^{M^-}_{vib,gas} - S^{M^-}_{vib,aq} + \\
& S^{M^-}_{rot,gas} - S^{M^-}_{rot,aq} + S^{M^-}_{trans,gas} - S^{M^-}_{trans,aq}) \\
& - E^{M}_{elec,gas} + E^{M}_{elec,aq} - ZPE^{M}_{gas} + ZPE^{M}_{aq} - \\
& U^{M}_{vib,gas} + U^{M}_{vib,aq} \\
& + T(S^{M}_{elec,gas} - S^{M}_{elec,aq} + S^{M}_{vib,gas} - S^{M}_{vib,aq} + \\
& S^{M}_{rot,gas} - S^{M}_{rot,aq} + S^{M}_{trans,gas} - S^{M}_{trans,aq}) \\
=& \underbrace{E^{M}_{elec,aq} - E^{M^-}_{elec,aq}}_{\Delta\Delta E_{elec}} \\
& + \underbrace{ZPE^{M}_{aq} - ZPE^{M^-}_{aq}}_{\Delta\Delta ZPE} \\
& + \underbrace{U^{M}_{vib,aq} - U^{M^-}_{vib,aq}}_{\Delta\Delta U_{vib}} \\
& - \underbrace{T(S^{M}_{elec,aq} - S^{M^-}_{elec,aq})}_{\Delta\Delta S_{elec}} \\
& - \underbrace{T(S^{M}_{vib,aq} - S^{M^-}_{vib,aq})}_{\Delta\Delta S_{vib}} \\
& - \underbrace{T(S^{M}_{rot,aq} - S^{M^-}_{rot,aq})}_{\Delta\Delta S_{rot}} \\
& - \underbrace{T(S^{M}_{trans,aq} - S^{M^-}_{trans,aq})}_{\Delta\Delta S_{trans}}
\end{aligned}
\tag{C.6}
$$

C.2 Imidazole and analogues

Calculated pK_a-values without water

The figure C.1 shows all calculated pK_a-values for imidazole and 5-methylimidazole. The table C.1 includes the calculated G_{model}-values based on the pK_a-values. The other tables C.2 and C.3 contain the results of the calculations with `orca` for imidazole and 5-methylimidazole.

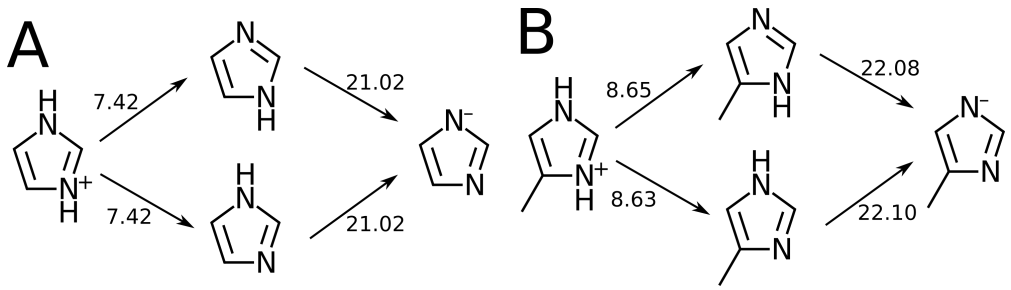

Figure C.1: All theoretically pK_a-values for imidazole (A) and 5-methylimidazole (B). Calculated with orca 5.0.1 without explicit water and the described python-script (more detail see section 3.3).

Table C.1: G_{model}s based on the different calculated pK_a-values for imidazole and imidazole analogs in DMF/water without explicit water.

	imi	4(5)-mimi
$3H1H$	-39.03	-42.21
3_$1H$	-29.56	-31.02
$3H1$_	-29.55	-31.03
3_1_	0.00	0.00
$3H1H$	-39.01	-42.16
3_$1H$	-28.84	-30.29
$3H1$_	-28.83	-30.32
3_1_	0.00	0.00

Table C.2: All energy results from orca for imidazole in DMF/water without explicit water. The energies are in $\frac{kcal}{mol}$.

states	midd-dmf	midd-vac	midd-wat	midp-dmf	midp-vac	midp-wat	mip1-dmf	mip1-vac	mip1-wat	mip2-dmf	mip2-vac	mip2-wat
Final Single Point Energy	-141569.72	-141631.76	-141632.67	-142162.90	-142225.28	-142226.18	-141928.49	-141937.94	-141938.11	-141928.49	-141937.94	-141938.11
Electronic Energy	-141569.72	-141631.76	-141632.67	-142162.90	-142225.28	-142226.18	-141928.49	-141937.94	-141938.11	-141928.49	-141937.94	-141938.11
Zero Point Energy	35.90	36.21	36.22	53.43	53.35	53.36	44.60	44.65	44.64	44.60	44.68	44.68
Thermal Vibrational Correction	0.45	0.43	0.43	0.58	0.60	0.60	0.57	0.55	0.55	0.57	0.55	0.55
Thermal Rotational Correction	0.89	0.89	0.89	0.89	0.89	0.89	0.89	0.89	0.89	0.89	0.89	0.89
Thermal Translational Correction	0.89	0.89	0.89	0.89	0.89	0.89	0.89	0.89	0.89	0.89	0.89	0.89
Total Thermal Correction	2.22	2.21	2.21	2.36	2.37	2.38	2.35	2.33	2.33	2.35	2.32	2.32
Non Thermal Correction	35.90	36.21	36.22	53.43	53.35	53.36	44.60	44.65	44.64	44.60	44.68	44.68
Total Correction	38.12	38.42	38.43	55.79	55.73	55.74	46.94	46.97	46.97	46.94	47.01	47.01
Total Thermal Energy	-141531.60	-141593.34	-141594.24	-142107.10	-142169.56	-142170.44	-141881.54	-141890.97	-141891.14	-141881.54	-141890.93	-141891.10
Total Free Energy	-141531.60	-141593.34	-141594.24	-142107.10	-142169.56	-142170.44	-141881.54	-141890.97	-141891.14	-141881.54	-141890.93	-141891.10
Thermal Enthalpy Correction	0.59	0.59	0.59	0.59	0.59	0.59	0.59	0.59	0.59	0.59	0.59	0.59
Total Enthalpy	-141531.01	-141592.75	-141593.65	-142106.51	-142168.96	-142169.84	-141880.95	-141890.37	-141890.55	-141880.95	-141890.34	-141890.51
Electronic Entropy	0.00	0.00	0.00	0.00	0.00	0.00	0.00	0.00	0.00	0.00	0.00	0.00
Vibrational Entropy	0.56	0.54	0.54	0.74	0.76	0.76	0.73	0.70	0.70	0.73	0.70	0.70
Rotational Entropy	7.15	7.15	7.15	7.22	7.22	7.22	7.18	7.19	7.19	7.18	7.19	7.19
Translational Entropy	11.49	11.49	11.49	11.51	11.51	11.51	11.50	11.50	11.50	11.50	11.50	11.50
Final Entropy Term	19.20	19.18	19.18	19.47	19.49	19.49	19.41	19.38	19.38	19.41	19.38	19.38
Total Entropy Correction	-19.20	-19.18	-19.18	-19.47	-19.49	-19.49	-19.41	-19.38	-19.38	-19.41	-19.38	-19.38
Gibbs Free Enthalpy	-141550.21	-141611.92	-141612.83	-142125.98	-142188.45	-142189.33	-141900.36	-141909.76	-141909.94	-141900.36	-141909.72	-141909.89

Table C.3: All energy results from orca for 5-methyl-imidazole in DMF/water without explicit water. The energies are in $\frac{kcal}{mol}$.

states	midd-dmf	midd-vac	midd-wat	midp-dmf	midp-vac	midp-wat	mip1-dmf	mip1-vac	mip1-wat	mip2-dmf	mip2-vac	mip2-wat
Final Single Point Energy	-166229.87	-166291.92	-166292.85	-166829.36	-166888.59	-166889.66	-166590.87	-166600.04	-166600.21	-166590.33	-166599.96	-166600.26
Electronic Energy	-166229.87	-166291.92	-166292.85	-166829.36	-166888.59	-166889.66	-166590.87	-166600.04	-166600.21	-166590.33	-166599.96	-166600.26
Zero Point Energy	53.47	53.92	53.56	70.95	70.88	70.81	62.33	62.35	62.33	61.83	61.86	61.88
Thermal Vibrational Correction	1.31	1.29	1.42	1.50	1.50	1.51	1.41	1.39	1.40	1.61	1.59	1.58
Thermal Rotational Correction	0.89	0.89	0.89	0.89	0.89	0.89	0.89	0.89	0.89	0.89	0.89	0.89
Thermal Translational Correction	0.89	0.89	0.89	0.89	0.89	0.89	0.89	0.89	0.89	0.89	0.89	0.89
Total Thermal Correction	3.09	3.07	3.20	3.28	3.28	3.29	3.19	3.17	3.17	3.39	3.37	3.35
Non Thermal Correction	53.47	53.92	53.56	70.95	70.88	70.81	62.33	62.35	62.33	61.83	61.86	61.88
Total Correction	56.56	56.99	56.76	74.23	74.16	74.09	65.52	65.52	65.51	65.21	65.23	65.23
Total Thermal Energy	-166173.31	-166234.93	-166236.09	-166755.13	-166814.43	-166815.57	-166525.34	-166534.52	-166534.71	-166525.12	-166534.72	-166535.02
Total Free Energy	-166173.31	-166234.93	-166236.09	-166755.13	-166814.43	-166815.57	-166525.34	-166534.52	-166534.71	-166525.12	-166534.72	-166535.02
Thermal Enthalpy Correction	0.59	0.59	0.59	0.59	0.59	0.59	0.59	0.59	0.59	0.59	0.59	0.59
Total Enthalpy	-166172.72	-166234.34	-166235.50	-166754.54	-166813.84	-166814.98	-166524.75	-166533.93	-166534.11	-166524.52	-166534.13	-166534.43
Electronic Entropy	0.00	0.00	0.00	0.00	0.00	0.00	0.00	0.00	0.00	0.00	0.00	0.00
Vibrational Entropy	1.99	1.96	2.27	2.26	2.24	2.26	2.11	2.08	2.09	2.56	2.55	2.52
Rotational Entropy	7.66	7.66	7.66	7.71	7.71	7.71	7.69	7.69	7.69	7.69	7.69	7.69
Translational Entropy	11.66	11.66	11.66	11.68	11.68	11.68	11.67	11.67	11.67	11.67	11.67	11.67
Final Entropy Term	21.31	21.28	21.59	21.65	21.63	21.65	21.46	21.44	21.44	21.92	21.91	21.88
Total Entropy Correction	-21.31	-21.28	-21.59	-21.65	-21.63	-21.65	-21.46	-21.44	-21.44	-21.92	-21.91	-21.88
Gibbs Free Enthalpy	-166194.03	-166255.62	-166257.09	-166776.20	-166835.46	-166836.63	-166546.21	-166555.37	-166555.56	-166546.44	-166556.04	-166556.30

Calculated pK_a-values with water

The figure C.1 shows all calculated pK_a-values for imidazole and 5-methylimidazole. The table C.1 includes the calculated G_{model}-values based on the pK_a-values. The other tables C.5 and C.6 contain the results of the calculations with `orca` for imidazole and 5-methylimidazole.

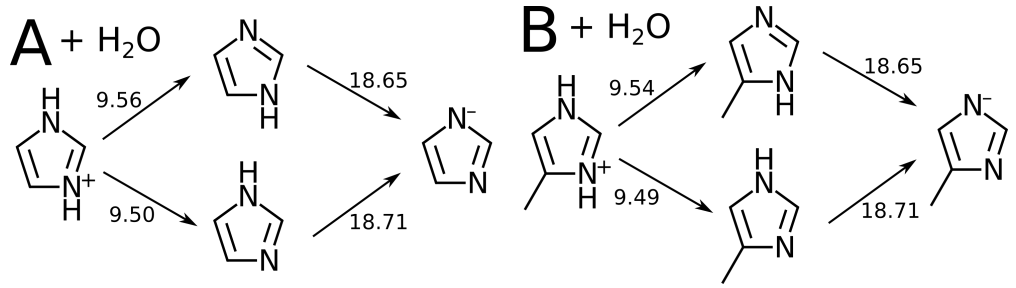

Figure C.2: All theoretically pK_a-values for imidazole (A) and 5-methylimidazole (B). Calculated with orca 5.0.1 with explicit water and the described python-script (more detail see section 3.3).

Table C.4: G_{model}s based on the different calculated pK_a-values for imidazole and imidazole analogues in DMF/water with explicit water.

	imi	4(5)-mimi
$3H1H$	-38.53	-38.67
3_1H	-25.76	-25.59
$3H$1_	-25.13	-25.66
3_1_	0.00	0.00
$3H1H$	-38.70	-38.67
3_1H	-25.59	-25.59
$3H$1_	-25.66	-25.66
3_1_	0.00	0.00

Table C.5: All energy results from orca for imidazole in DMF/water with explicit water. The energies are in $\frac{kcal}{mol}$.

states	midd-dmf	midd-vac	midd-wat	midp-dmf	midp-vac	midp-wat	mip1-dmf	mip1-vac	mip1-wat	mip2-dmf	mip2-vac	mip2-wat
Final Single Point Energy	-262178.48	-262235.67	-262236.84	-262775.89	-262827.29	-262828.63	-262520.69	-262538.07	-262538.58	-262520.17	-262538.09	-262538.59
Electronic Energy	-262178.48	-262235.67	-262236.84	-262775.89	-262827.29	-262828.63	-262520.69	-262538.07	-262538.58	-262520.17	-262538.09	-262538.59
Zero Point Energy	83.64	83.05	83.72	100.16	99.70	99.67	91.61	91.37	91.24	91.89	91.22	91.57
Thermal Vibrational Correction	5.45	5.05	5.18	6.34	4.62	5.83	6.31	5.46	5.55	6.17	5.65	5.91
Thermal Rotational Correction	0.89	0.89	0.89	0.89	0.89	0.89	0.89	0.89	0.89	0.89	0.89	0.89
Thermal Translational Correction	0.89	0.89	0.89	0.89	0.89	0.89	0.89	0.89	0.89	0.89	0.89	0.89
Total Thermal Correction	7.22	6.83	6.96	8.12	6.39	7.61	8.09	7.24	7.32	7.95	7.43	7.68
Non Thermal Correction	83.64	83.05	83.72	100.16	99.70	99.67	91.61	91.37	91.24	91.89	91.22	91.57
Total Correction	90.86	89.88	90.68	108.28	106.09	107.27	99.70	98.61	98.56	99.84	98.65	99.26
Total Thermal Energy	-262087.62	-262145.79	-262146.16	-262667.61	-262721.20	-262721.35	-262420.99	-262439.46	-262440.02	-262420.33	-262439.44	-262439.34
Total Free Energy	-262087.62	-262145.79	-262146.16	-262667.61	-262721.20	-262721.35	-262420.99	-262439.46	-262440.02	-262420.33	-262439.44	-262439.34
Thermal Enthalpy Correction	0.59	0.59	0.59	0.59	0.59	0.59	0.59	0.59	0.59	0.59	0.59	0.59
Total Enthalpy	-262087.03	-262145.20	-262145.57	-262667.02	-262720.61	-262720.76	-262420.40	-262438.87	-262439.43	-262419.74	-262438.84	-262438.74
Electronic Entropy	0.00	0.00	0.00	0.00	0.00	0.00	0.00	0.00	0.00	0.00	0.00	0.00
Vibrational Entropy	10.18	9.47	9.68	12.07	8.09	10.82	12.10	10.03	10.25	11.69	10.56	10.92
Rotational Entropy	8.84	8.83	8.83	8.88	8.87	8.87	8.90	8.88	8.88	8.92	8.88	8.88
Translational Entropy	11.98	11.98	11.98	12.00	12.00	12.00	11.99	11.99	11.99	11.99	11.99	11.99
Final Entropy Term	31.00	30.29	30.50	32.95	28.96	31.69	33.00	30.89	31.12	32.60	31.43	31.79
Total Entropy Correction	-31.00	-30.29	-30.50	-32.95	-28.96	-31.69	-33.00	-30.89	-31.12	-32.60	-31.43	-31.79
Gibbs Free Enthalpy	-262118.02	-262175.48	-262176.06	-262699.96	-262749.56	-262752.45	-262453.39	-262469.76	-262470.55	-262452.33	-262470.27	-262470.53

Table C.6: All energy results from orca for 5-methyl-imidazole in DMF/water with explicit water. The energies are in $\frac{kcal}{mol}$.

states	midd-dmf	midd-vac	midd-wat	midp-dmf	midp-vac	midp-wat	mip1-dmf	mip1-vac	mip1-wat	mip2-dmf	mip2-vac	mip2-wat
Final Single Point Energy	-262178.48	-262235.67	-262236.84	-262775.89	-262827.29	-262828.63	-262520.69	-262538.07	-262538.58	-262520.17	-262538.09	-262538.59
Electronic Energy	-262178.48	-262235.67	-262236.84	-262775.89	-262827.29	-262828.63	-262520.69	-262538.07	-262538.58	-262520.17	-262538.09	-262538.59
Zero Point Energy	83.64	83.05	83.72	100.16	99.70	99.67	91.61	91.37	91.24	91.89	91.22	91.57
Thermal Vibrational Correction	5.45	5.05	5.18	6.34	4.62	5.83	6.31	5.46	5.55	6.17	5.65	5.91
Thermal Rotational Correction	0.89	0.89	0.89	0.89	0.89	0.89	0.89	0.89	0.89	0.89	0.89	0.89
Thermal Translational Correction	0.89	0.89	0.89	0.89	0.89	0.89	0.89	0.89	0.89	0.89	0.89	0.89
Total Thermal Correction	7.22	6.83	6.96	8.12	6.39	7.61	8.09	7.24	7.32	7.95	7.43	7.68
Non Thermal Correction	83.64	83.05	83.72	100.16	99.70	99.67	91.61	91.37	91.24	91.89	91.22	91.57
Total Correction	90.86	89.88	90.68	108.28	106.09	107.27	99.70	98.61	98.56	99.84	98.65	99.26
Total Thermal Energy	-262087.62	-262145.79	-262146.16	-262667.61	-262721.20	-262721.35	-262420.99	-262439.46	-262440.02	-262420.33	-262439.44	-262439.34
Total Free Energy	-262087.62	-262145.79	-262146.16	-262667.61	-262721.20	-262721.35	-262420.99	-262439.46	-262440.02	-262420.33	-262439.44	-262439.34
Thermal Enthalpy Correction	0.59	0.59	0.59	0.59	0.59	0.59	0.59	0.59	0.59	0.59	0.59	0.59
Total Enthalpy	-262087.03	-262145.20	-262145.57	-262667.02	-262720.61	-262720.76	-262420.40	-262438.87	-262439.43	-262419.74	-262438.84	-262438.74
Electronic Entropy	0.00	0.00	0.00	0.00	0.00	0.00	0.00	0.00	0.00	0.00	0.00	0.00
Vibrational Entropy	10.18	9.47	9.68	12.07	8.09	10.82	12.10	10.03	10.25	11.69	10.56	10.92
Rotational Entropy	8.84	8.83	8.83	8.88	8.87	8.87	8.90	8.88	8.88	8.92	8.88	8.88
Translational Entropy	11.98	11.98	11.98	12.00	12.00	12.00	11.99	11.99	11.99	11.99	11.99	11.99
Final Entropy Term	31.00	30.29	30.50	32.95	28.96	31.69	33.00	30.89	31.12	32.60	31.43	31.79
Total Entropy Correction	-31.00	-30.29	-30.50	-32.95	-28.96	-31.69	-33.00	-30.89	-31.12	-32.60	-31.43	-31.79
Gibbs Free Enthalpy	-262118.02	-262175.48	-262176.06	-262699.96	-262749.56	-262752.45	-262453.39	-262469.76	-262470.55	-262452.33	-262470.27	-262470.53

C.3 Ubiquinol

The tables C.7 to C.9 contain the results of the calculations with `orca` for benzoquinone. The other tables C.10 and C.11 contain all calculated pK_a-values and redox potentials for benzoquinone. The tables C.12 to C.14 contain the results of the calculations with `orca` for ubiquinone.

Table C.7: All energy results from orca for benzoquinone in DMF/water without explicit water. The energies are in $\frac{kcal}{mol}$.

states	b0dd-dmf	b0dd-vac	b0dd-wat	b0dp-dmf	b0dp-vac	b0dp-wat	b0pd-dmf	b0pd-vac	b0pd-wat	b0pp-dmf	b0pp-vac	b0pp-wat
Final Single Point Energy	-239352.96	-239345.45	-239353.08	-239608.21	-239546.20	-239609.12	-239608.29	-239546.20	-239609.20	-239845.68	-239640.43	-239848.56
Electronic Energy	-239352.96	-239345.45	-239353.08	-239608.21	-239546.20	-239609.12	-239608.29	-239546.20	-239609.20	-239845.68	-239640.43	-239848.56
Zero Point Energy	53.63	53.70	53.63	62.07	62.35	62.07	62.10	62.50	62.10	70.09	70.81	70.09
Thermal Vibrational Correction	2.01	1.98	2.02	2.03	1.99	2.03	2.03	1.98	2.03	2.04	1.99	2.04
Thermal Rotational Correction	0.89	0.89	0.89	0.89	0.89	0.89	0.89	0.89	0.89	0.89	0.89	0.89
Thermal Translational Correction	0.89	0.89	0.89	0.89	0.89	0.89	0.89	0.89	0.89	0.89	0.89	0.89
Total Thermal Correction	3.79	3.76	3.79	3.81	3.77	3.81	3.81	3.76	3.81	3.82	3.77	3.82
Non Thermal Correction	53.63	53.70	53.63	62.07	62.35	62.07	62.10	62.50	62.10	70.09	70.81	70.09
Total Correction	57.42	57.46	57.42	65.88	66.12	65.88	65.90	66.26	65.90	73.91	74.58	73.91
Total Thermal Energy	-239295.53	-239287.99	-239295.66	-239542.34	-239480.08	-239543.25	-239542.39	-239479.94	-239543.30	-239771.77	-239565.85	-239774.65
Total Free Energy	-239295.53	-239287.99	-239295.66	-239542.34	-239480.08	-239543.25	-239542.39	-239479.94	-239543.30	-239771.77	-239565.85	-239774.65
Thermal Enthalpy Correction	0.59	0.59	0.59	0.59	0.59	0.59	0.59	0.59	0.59	0.59	0.59	0.59
Total Enthalpy	-239294.94	-239287.40	-239295.07	-239541.74	-239479.49	-239542.65	-239541.80	-239479.35	-239542.71	-239771.18	-239565.26	-239774.06
Electronic Entropy	0.00	0.00	0.00	0.00	0.00	0.00	0.00	0.00	0.00	0.00	0.00	0.00
Vibrational Entropy	3.14	3.07	3.14	3.15	3.05	3.15	3.14	3.06	3.14	3.12	3.08	3.11
Rotational Entropy	8.28	8.28	8.28	8.29	8.29	8.29	8.29	8.29	8.29	8.32	8.32	8.32
Translational Entropy	11.91	11.91	11.91	11.92	11.92	11.92	11.92	11.92	11.92	11.93	11.93	11.93
Final Entropy Term	23.33	23.26	23.33	23.36	23.26	23.36	23.35	23.27	23.35	23.36	23.32	23.36
Total Entropy Correction	-23.33	-23.26	-23.33	-23.36	-23.26	-23.36	-23.35	-23.27	-23.35	-23.36	-23.32	-23.36
Gibbs Free Energy	-239318.27	-239310.66	-239318.40	-239565.10	-239502.75	-239566.02	-239565.14	-239502.62	-239566.06	-239794.54	-239588.58	-239797.42

Table C.8: All energy results from orca for benzoquinone in DMF/water without explicit water. The energies are in $\frac{kcal}{mol}$.

states	b1dd-dmf	b1dd-vac	b1dd-wat	b1dp-dmf	b1dp-vac	b1dp-wat	b1pd-dmf	b1pd-vac	b1pd-wat	b1pp-dmf	b1pp-vac	b1pp-wat
Final Single Point Energy	-239446.26	-239392.24	-239447.05	-239735.26	-239724.26	-239735.46	-239735.30	-239724.26	-239735.50	-240006.69	-239948.86	-240007.51
Electronic Energy	-239446.26	-239392.24	-239447.05	-239735.26	-239724.26	-239735.46	-239735.30	-239724.26	-239735.50	-240006.69	-239948.86	-240007.51
Zero Point Energy	52.57	52.52	52.57	60.82	60.93	60.80	61.11	61.16	61.11	69.71	70.50	69.71
Thermal Vibrational Correction	1.95	1.89	1.95	2.12	2.07	2.13	2.02	2.03	2.02	2.06	1.96	2.06
Thermal Rotational Correction	0.89	0.89	0.89	0.89	0.89	0.89	0.89	0.89	0.89	0.89	0.89	0.89
Thermal Translational Correction	0.89	0.89	0.89	0.89	0.89	0.89	0.89	0.89	0.89	0.89	0.89	0.89
Total Thermal Correction	3.72	3.66	3.72	3.90	3.85	3.91	3.80	3.81	3.80	3.84	3.73	3.84
Non Thermal Correction	52.57	52.52	52.57	60.82	60.93	60.80	61.11	61.16	61.11	69.71	70.50	69.71
Total Correction	56.29	56.18	56.30	64.72	64.78	64.71	64.91	64.97	64.91	73.55	74.24	73.55
Total Thermal Energy	-239389.97	-239336.06	-239390.75	-239670.55	-239659.48	-239670.75	-239670.39	-239659.29	-239670.59	-239933.14	-239874.62	-239933.96
Total Free Energy	-239389.97	-239336.06	-239390.75	-239670.55	-239659.48	-239670.75	-239670.39	-239659.29	-239670.59	-239933.14	-239874.62	-239933.96
Thermal Enthalpy Correction	0.59	0.59	0.59	0.59	0.59	0.59	0.59	0.59	0.59	0.59	0.59	0.59
Total Enthalpy	-239389.38	-239335.46	-239390.16	-239669.95	-239658.89	-239670.16	-239669.80	-239658.70	-239670.00	-239932.54	-239874.03	-239933.37
Electronic Entropy	0.41	0.41	0.41	0.41	0.41	0.41	0.41	0.41	0.41	0.41	0.41	0.41
Vibrational Entropy	2.98	2.84	2.98	3.23	3.12	3.24	3.04	3.05	3.04	3.09	2.93	3.09
Rotational Entropy	8.28	8.28	8.28	8.29	8.29	8.29	8.29	8.29	8.29	8.31	8.31	8.31
Translational Entropy	11.91	11.91	11.91	11.92	11.92	11.92	11.92	11.92	11.92	11.93	11.93	11.93
Final Entropy Term	23.58	23.44	23.58	23.86	23.74	23.86	23.66	23.68	23.66	23.74	23.57	23.74
Total Entropy Correction	-23.58	-23.44	-23.58	-23.86	-23.74	-23.86	-23.66	-23.68	-23.66	-23.74	-23.57	-23.74
Gibbs Free Energy	-239412.96	-239358.90	-239413.74	-239693.81	-239682.63	-239694.02	-239693.46	-239682.37	-239693.66	-239956.28	-239897.60	-239957.11

Table C.9: All energy results from orca for benzoquinone in DMF/water without explicit water. The energies are in $\frac{kcal}{mol}$.

states	b2dd-dmf	b2dd-vac	b2dd-wat	b2dp-dmf	b2dp-vac	b2dp-wat	b2pd-dmf	b2pd-vac	b2pd-wat	b2pp-dmf	b2pp-vac	b2pp-wat
Final Single Point Energy	-239510.35	-239314.23	-239513.15	-239825.53	-239764.41	-239826.46	-239825.53	-239764.41	-239826.46	-240132.29	-240123.20	-240132.43
Electronic Energy	-239510.35	-239314.23	-239513.15	-239825.53	-239764.41	-239826.46	-239825.53	-239764.41	-239826.46	-240132.29	-240123.20	-240132.43
Zero Point Energy	51.30	50.63	51.31	59.46	59.25	59.46	59.50	59.45	59.50	68.11	68.63	68.10
Thermal Vibrational Correction	1.92	2.01	1.92	2.44	2.39	2.45	2.41	2.35	2.41	2.54	2.38	2.54
Thermal Rotational Correction	0.89	0.89	0.89	0.89	0.89	0.89	0.89	0.89	0.89	0.89	0.89	0.89
Thermal Translational Correction	0.89	0.89	0.89	0.89	0.89	0.89	0.89	0.89	0.89	0.89	0.89	0.89
Total Thermal Correction	3.70	3.79	3.70	4.22	4.17	4.23	4.18	4.12	4.19	4.32	4.16	4.32
Non Thermal Correction	51.30	50.63	51.31	59.46	59.25	59.46	59.50	59.45	59.50	68.11	68.63	68.10
Total Correction	55.01	54.42	55.01	63.68	63.42	63.68	63.68	63.57	63.68	72.42	72.79	72.42
Total Thermal Energy	-239455.34	-239259.82	-239458.13	-239761.85	-239700.99	-239762.77	-239761.85	-239700.84	-239762.78	-240059.86	-240050.41	-240060.02
Total Free Energy	-239455.34	-239259.82	-239458.13	-239761.85	-239700.99	-239762.77	-239761.85	-239700.84	-239762.78	-240059.86	-240050.41	-240060.02
Thermal Enthalpy Correction	0.59	0.59	0.59	0.59	0.59	0.59	0.59	0.59	0.59	0.59	0.59	0.59
Total Enthalpy	-239454.75	-239259.22	-239457.54	-239761.26	-239700.40	-239762.18	-239761.26	-239700.25	-239762.18	-240059.27	-240049.82	-240059.42
Electronic Entropy	0.00	0.00	0.00	0.00	0.00	0.00	0.00	0.00	0.00	0.00	0.00	0.00
Vibrational Entropy	2.90	3.03	2.90	3.95	3.79	3.97	3.87	3.70	3.88	3.95	3.60	3.95
Rotational Entropy	8.29	8.29	8.29	8.30	8.30	8.30	8.30	8.30	8.30	8.31	8.31	8.31
Translational Entropy	11.91	11.91	11.91	11.92	11.92	11.92	11.92	11.92	11.92	11.93	11.93	11.93
Final Entropy Term	23.10	23.23	23.10	24.17	24.01	24.19	24.09	23.92	24.10	24.19	23.84	24.19
Total Entropy Correction	-23.10	-23.23	-23.10	-24.17	-24.01	-24.19	-24.09	-23.92	-24.10	-24.19	-23.84	-24.19
Gibbs Free Energy	-239477.85	-239282.46	-239480.64	-239785.43	-239724.41	-239786.37	-239785.36	-239724.17	-239786.29	-240083.46	-240073.66	-240083.62

Table C.10: Different calculated pK_a-values (above) and redox potentials (down) for benzoquinone in DMF/water

	b2dp-b2pp	b2pd-b2pp	b2dd-b2dp	b2dd-b2pd	b1dp-b1pp	b1pd-b1pp	b1dd-b1dp	b1dd-b1pd	b0dp-b0pp	b0pd-b0pp	b0dd-b0dp	b0dd-b0pd
DMF	21.45	21.50	28.41	28.36	-4.45	-4.20	8.93	8.68	-28.52	-28.55	-15.84	-15.82
Water	19.86	19.92	26.04	25.98	-5.03	-4.76	7.50	7.24	-28.11	-28.14	-16.29	-16.26
	b1pp-b2pp	b0pp-b1pp	b1dp-b2dp	b0dp-b1dp	b1pd-b2pd	b0pd-b1pd	b1dd-b2dd	b0dd-b1dd				
DMF	1.49	2.99	-0.05	1.56	-0.04	1.54	-1.21	0.09				
Water	1.13	2.57	-0.35	1.19	-0.34	1.18	-1.46	-0.22				

Table C.11: Different calculated pK_a-values (above) and redox potentials (down) for benzoquinone in DMF/water in $\frac{kcal}{mol}$

	b2dp-b2pp	b2pd-b2pp	b2dd-b2dp	b2dd-b2pd	b1dp-b1pp	b1pd-b1pp	b1dd-b1dp	b1dd-b1pd	b0dp-b0pp	b0pd-b0pp	b0dd-b0dp	b0dd-b0pd
DMF	-29.42	-29.49	-38.97	-38.90	6.11	5.76	-12.26	-11.91	39.13	39.17	21.74	21.70
Water	-27.24	-27.33	-35.72	-35.64	6.90	6.54	-10.29	-9.93	38.56	38.60	22.35	22.31
	b1pp-b2pp	b0pp-b1pp	b1dp-b2dp	b0dp-b1dp	b1pd-b2pd	b0pd-b1pd	b1dd-b2dd	b0dd-b1dd				
DMF	-34.47	-69.04	1.08	-36.00	0.81	-35.62	27.81	-1.99				
Water	-26.01	-59.19	8.15	-27.51	7.87	-27.11	33.60	5.15				

Table C.12: All energy results from orca for ubiquinone model compound in DMF/water without explicit water. The energies are in $\frac{kcal}{mol}$.

states	u0dd-dmf	u0dd-vac	u0dd-wat	u0dp-dmf	u0dp-vac	u0dp-wat	u0pd-dmf	u0pd-vac	u0pd-wat	u0pp-dmf	u0pp-vac	u0pp-wat
Final Single Point Energy	-432408.94	-432399.84	-432409.10	-432673.58	-432626.37	-432674.26	-432671.23	-432619.13	-432672.00	-432906.60	-432744.65	-432909.02
Electronic Energy	-432408.94	-432399.84	-432409.10	-432673.58	-432626.37	-432674.26	-432671.23	-432619.13	-432672.00	-432906.60	-432744.65	-432909.02
Zero Point Energy	129.98	130.11	129.99	139.50	139.82	139.49	138.75	138.51	138.74	145.28	147.01	145.49
Thermal Vibrational Correction	6.91	6.91	6.91	6.54	6.53	6.54	6.80	6.88	6.81	7.16	6.59	6.56
Thermal Rotational Correction	0.89	0.89	0.89	0.89	0.89	0.89	0.89	0.89	0.89	0.89	0.89	0.89
Thermal Translational Correction	0.89	0.89	0.89	0.89	0.89	0.89	0.89	0.89	0.89	0.89	0.89	0.89
Total Thermal Correction	8.69	8.68	8.68	8.32	8.31	8.32	8.58	8.66	8.59	8.94	8.37	8.33
Non Thermal Correction	129.98	130.11	129.99	139.50	139.82	139.49	138.75	138.51	138.74	145.28	147.01	145.49
Total Correction	138.66	138.80	138.67	147.82	148.13	147.81	147.33	147.17	147.33	154.22	155.38	153.82
Total Thermal Energy	-432270.28	-432261.04	-432270.42	-432525.76	-432478.24	-432526.45	-432523.90	-432471.96	-432524.67	-432752.38	-432589.26	-432755.20
Total Free Energy	-432270.28	-432261.04	-432270.42	-432525.76	-432478.24	-432526.45	-432523.90	-432471.96	-432524.67	-432752.38	-432589.26	-432755.20
Thermal Enthalpy Correction	0.59	0.59	0.59	0.59	0.59	0.59	0.59	0.59	0.59	0.59	0.59	0.59
Total Enthalpy	-432269.68	-432260.45	-432269.83	-432525.17	-432477.65	-432525.86	-432523.31	-432471.37	-432524.08	-432751.79	-432588.67	-432754.60
Electronic Entropy	0.00	0.00	0.00	0.00	0.00	0.00	0.00	0.00	0.00	0.00	0.00	0.00
Vibrational Entropy	11.80	11.78	11.80	10.93	10.91	10.93	11.53	11.67	11.57	12.49	10.97	10.93
Rotational Entropy	9.42	9.42	9.42	9.43	9.43	9.43	9.43	9.43	9.43	9.45	9.45	9.45
Translational Entropy	12.44	12.44	12.44	12.45	12.45	12.45	12.45	12.45	12.45	12.45	12.45	12.45
Final Entropy Term	33.66	33.64	33.66	32.81	32.79	32.81	33.40	33.55	33.44	34.39	32.86	32.83
Total Entropy Correction	-33.66	-33.64	-33.66	-32.81	-32.79	-32.81	-33.40	-33.55	-33.44	-34.39	-32.86	-32.83
Gibbs Free Energy	-432303.35	-432294.08	-432303.49	-432557.99	-432510.43	-432558.67	-432556.71	-432504.91	-432557.52	-432786.17	-432621.54	-432787.43

Table C.13: All energy results from orca for ubiquinone model compound in DMF/water without explicit water. The energies are in $\frac{kcal}{mol}$.

states	u1dd-dmf	u1dd-vac	u1dd-wat	u1dp-dmf	u1dp-vac	u1dp-wat	u1pd-dmf	u1pd-vac	u1pd-wat	u1pp-dmf	u1pp-vac	u1pp-wat
Final Single Point Energy	-432494.01	-432441.68	-432494.80	-432787.33	-432779.95	-432787.45	-432784.84	-432771.75	-432785.08	-433061.37	-433013.36	-433062.06
Electronic Energy	-432494.01	-432441.68	-432494.80	-432787.33	-432779.95	-432787.45	-432784.84	-432771.76	-432785.08	-433061.37	-433013.36	-433062.06
Zero Point Energy	128.62	128.32	128.63	137.18	138.07	137.18	136.81	137.15	136.80	146.85	147.10	146.85
Thermal Vibrational Correction	6.83	6.95	6.83	6.98	6.79	6.98	7.16	7.00	7.17	6.85	6.82	6.85
Thermal Rotational Correction	0.89	0.89	0.89	0.89	0.89	0.89	0.89	0.89	0.89	0.89	0.89	0.89
Thermal Translational Correction	0.89	0.89	0.89	0.89	0.89	0.89	0.89	0.89	0.89	0.89	0.89	0.89
Total Thermal Correction	8.61	8.73	8.61	8.76	8.57	8.76	8.94	8.78	8.94	8.63	8.60	8.63
Non Thermal Correction	128.62	128.32	128.63	137.18	138.07	137.18	136.81	137.15	136.80	146.85	147.10	146.85
Total Correction	137.24	137.05	137.24	145.94	146.65	145.94	145.75	145.93	145.75	155.48	155.70	155.47
Total Thermal Energy	-432356.77	-432304.63	-432357.56	-432641.39	-432633.31	-432641.51	-432639.09	-432625.83	-432639.33	-432905.89	-432857.66	-432906.59
Total Free Energy	-432356.77	-432304.63	-432357.56	-432641.39	-432633.31	-432641.51	-432639.09	-432625.83	-432639.33	-432905.89	-432857.66	-432906.59
Thermal Enthalpy Correction	0.59	0.59	0.59	0.59	0.59	0.59	0.59	0.59	0.59	0.59	0.59	0.59
Total Enthalpy	-432356.18	-432304.04	-432356.96	-432640.80	-432632.71	-432640.92	-432638.50	-432625.23	-432638.74	-432905.30	-432857.07	-432905.99
Electronic Entropy	0.41	0.41	0.41	0.41	0.41	0.41	0.41	0.41	0.41	0.41	0.41	0.41
Vibrational Entropy	11.62	11.93	11.62	11.82	11.48	11.81	12.18	11.85	12.20	11.59	11.51	11.59
Rotational Entropy	9.42	9.42	9.42	9.43	9.43	9.43	9.42	9.42	9.42	9.43	9.43	9.43
Translational Entropy	12.44	12.44	12.44	12.45	12.45	12.45	12.45	12.45	12.45	12.45	12.45	12.45
Final Entropy Term	33.89	34.20	33.88	34.11	33.77	34.09	34.45	34.12	34.47	33.88	33.81	33.88
Total Entropy Correction	-33.89	-34.20	-33.88	-34.11	-33.77	-34.09	-34.45	-34.12	-34.47	-33.88	-33.81	-33.88
Gibbs Free Energy	-432390.07	-432338.24	-432390.85	-432674.90	-432666.48	-432675.01	-432672.95	-432659.36	-432673.21	-432939.18	-432890.88	-432939.88

Table C.14: All energy results from orca for ubiquinone model compound in DMF/water without explicit water. The energies are in $\frac{kcal}{mol}$.

states	u2dd-dmf	u2dd-vac	u2dd-wat	u2dp-dmf	u2dp-vac	u2dp-wat	u2pd-dmf	u2pd-vac	u2pd-wat	u2pp-dmf	u2pp-vac	u2pp-wat
Final Single Point Energy	-432553.36	-432373.69	-432556.01	-432872.35	-432817.48	-432873.20	-432869.61	-432811.80	-432870.51	-433179.00	-433170.34	-433179.14
Electronic Energy	-432553.36	-432373.69	-432556.01	-432872.35	-432817.48	-432873.20	-432869.61	-432811.80	-432870.51	-433178.99	-433170.34	-433179.14
Zero Point Energy	127.32	126.51	127.34	136.27	136.57	136.30	135.84	134.63	135.85	146.07	146.29	146.07
Thermal Vibrational Correction	6.62	6.71	6.61	6.88	6.91	6.85	7.19	7.60	7.19	6.97	6.89	6.97
Thermal Rotational Correction	0.89	0.89	0.89	0.89	0.89	0.89	0.89	0.89	0.89	0.89	0.89	0.89
Thermal Translational Correction	0.89	0.89	0.89	0.89	0.89	0.89	0.89	0.89	0.89	0.89	0.89	0.89
Total Thermal Correction	8.39	8.48	8.39	8.66	8.69	8.63	8.97	9.38	8.97	8.75	8.66	8.75
Non Thermal Correction	127.32	126.51	127.34	136.27	136.57	136.30	135.84	134.63	135.85	146.07	146.29	146.07
Total Correction	135.72	135.00	135.73	144.92	145.26	144.93	144.81	144.00	144.82	154.82	154.96	154.81
Total Thermal Energy	-432417.65	-432238.70	-432420.28	-432727.43	-432672.23	-432728.26	-432724.80	-432667.79	-432725.70	-433024.18	-433015.38	-433024.33
Total Free Energy	-432417.65	-432238.70	-432420.28	-432727.43	-432672.23	-432728.26	-432724.80	-432667.79	-432725.70	-433024.18	-433015.38	-433024.33
Thermal Enthalpy Correction	0.59	0.59	0.59	0.59	0.59	0.59	0.59	0.59	0.59	0.59	0.59	0.59
Total Enthalpy	-432417.05	-432238.10	-432419.69	-432726.83	-432671.64	-432727.67	-432724.20	-432667.20	-432725.10	-433023.58	-433014.79	-433023.73
Electronic Entropy	0.00	0.00	0.00	0.00	0.00	0.00	0.00	0.00	0.00	0.00	0.00	0.00
Vibrational Entropy	11.09	11.29	11.08	11.48	11.68	11.40	12.30	13.17	12.28	11.79	11.58	11.79
Rotational Entropy	9.42	9.42	9.42	9.42	9.42	9.42	9.42	9.42	9.42	9.43	9.43	9.43
Translational Entropy	12.44	12.44	12.44	12.45	12.45	12.45	12.45	12.45	12.45	12.45	12.45	12.45
Final Entropy Term	32.95	33.15	32.94	33.35	33.54	33.27	34.16	35.03	34.15	33.67	33.46	33.67
Total Entropy Correction	-32.95	-33.15	-32.94	-33.35	-33.54	-33.27	-34.16	-35.03	-34.15	-33.67	-33.46	-33.67
Gibbs Free Energy	-432450.00	-432271.25	-432452.63	-432760.18	-432705.18	-432760.94	-432758.37	-432702.23	-432759.25	-433057.25	-433048.24	-433057.40

D

APPENDIX - OBTAINING G_{model} DIRECTLY FROM EXPERIMENTAL DATA USING VIRTUAL MODEL COMPOUNDS WITH APPLICATIONS TO HEME GROUPS

Equations (D.1), (D.3) and (D.4) show the way equations (4.3) and (4.4) are derived from $f(x_i, \vec{a})$ (equation (4.2)). The equation (D.1) is to be minimized, to achieve this the function g is defined. This function g is then partially derived according to the variables a_0 and a_1.

$$\sum_{i=1}^{N} \left(f(x_i, \vec{a}) - y_i\right)^2 \rightarrow \min_{a_0, a_1} \tag{D.1}$$

$$\xrightarrow{\text{use } f(x_i,\vec{a})} \sum_{i=1}^{N} \left(a_0 + a_1 \cdot x_i - y_i\right)^2 = g(x, \vec{a}) \rightarrow \min_{a_0, a_1} \tag{D.2}$$

The function g should be minimized, that means that the derivative of the function must be zero. Two partial derivatives (equations (D.3) and (D.4)) result from the function g.

$$\begin{aligned} \frac{\delta g(x, \vec{a})}{\delta a_0} &= \sum_{i=1}^{n} \left(2 \cdot a_0 + 2 \cdot a_1 \cdot x_i - 2 \cdot y_i\right) && = 0 \\ &= n \cdot a_0 + a_1 \cdot \sum_{i=1}^{n} x_i - \sum_{i=1}^{n} y_i && = 0 \\ &\Rightarrow a_0 && = \frac{1}{n} \cdot \sum_{i=1}^{n} \cdot y_i - a_1 \cdot \sum_{i=1}^{n} x_i \\ &\Rightarrow a_0 && = \overline{y} - a_1 \cdot \overline{x} \end{aligned} \tag{D.3}$$

with

$\overline{x}$: mean value of x $\overline{y}$: mean value of y

$$\begin{aligned}
\frac{\delta g(x,\vec{a})}{\delta a_1} &= \sum_{i=1}^{n} \left(2 \cdot a_1 \cdot x_i^2 + 2 \cdot a_0 \cdot x_i - 2 \cdot x_i \cdot y_i\right) && = 0 \\
&= a_1 \cdot \sum_{i=1}^{n} x_i^2 + a_0 \cdot \sum_{i=1}^{n} x_i - \sum_{i=1}^{n} x_i \cdot y_i && = 0 \\
\Rightarrow a_1 & && = \frac{\sum_{i=1}^{n} x_i \cdot y_i - a_0 \cdot \sum_{i=1}^{n} x_i}{\sum_{i=1}^{n} x_i^2} \\
\Rightarrow a_1 & && = \frac{\sum_{i=1}^{n} (x_i - \overline{x})(y_i - \overline{y})}{\sum_{i=1}^{n} (x_i - \overline{x})^2}
\end{aligned} \tag{D.4}$$

Table D.1: Ramachandran outliers, clash score, resolution, R-work and R-free values for the original crystal structure and the self-re-refined structures. - Cytochrome b_5

pdb-ID	Ramachandran outliers	Clashscore	Resolution	R-work	R-free
1CYO	0.00%	6.000	1.500	0.160	
1CYO_ref	0.00%	2.050	1.400	0.150	0.183
1EHB	0.00%	9.000	1.900	0.198	
1EHB_ref	0.00%	7.280	1.900	0.186	0.234
1ES1	0.00%	9.000	2.100	0.192	0.244
1ES1_ref	1.25%	3.640	2.100	0.163	0.211
1LQX	0.00%	7.000	1.800	0.189	
1LQX_ref	0.00%	5.830	1.800	0.161	0.183
1LR6	0.00%	7.000	1.900	0.191	0.236
1LR6_ref	0.00%	5.900	1.900	0.177	0.225
1M2I	0.00%	4.000	1.800	0.193	0.232
1M2I_ref	0.00%	5.970	1.800	0.164	0.197
1M2M	0.00%	8.000	1.800	0.194	0.238
1M2M_ref	0.00%	7.370	1.800	0.183	0.209
1X3X	0.00%	8.000	1.800	0.192	
1X3X_ref	0.00%	1.820	1.800	0.167	0.201
2IBJ	0.00%	2.000	1.550	0.163	0.194
2IBJ_ref	0.00%	2.110	1.550	0.137	0.166
3MUS	0.00%	6.000	2.000	0.176	0.223
3MUS_ref	0.60%	2.510	1.990	0.146	0.185
3NER	0.00%	11.000	1.450	0.177	0.215
3NER_ref	0.00%	4.010	1.450	0.162	0.199
4HIL	0.00%	2.000	1.250	0.137	0.152
4HIL_ref	0.00%	2.930	1.250	0.170	0.189

Table D.2: The found experimental redox potentials $[V]$ with the corresponding pH-values and ionic strengths as well as their measuring methods in bracket: CV (cyclic voltammetry)$^{\iota}$, DCV (direct cyclic voltammetry)$^{\varsigma}$ and PFV (protein film voltammetry). The last two columns contain the calculated redox potentials $[V]$ for the different protein structures and also the self-re-refined structures at an ionic strength of 0.150 M NaCl[1] and at the ionic strengths from the publications[2]. - Cytochrome b_5

protein name	exp. redox potential	pH	ionic strength from publication	Ref.	theo. redox potential[1]	theo. redox potential[2]
1CYO	-0.0100	7.0	0.010	(*1*) $^{\iota}$	0.004	-0.02
1CYO_ref	-0.0100	7.0	0.010	(*1*) $^{\iota}$	0.001	-0.02
1EHB	-0.0100	7.0	0.010	(*1*) $^{\iota}$	0.021	-0.01
1EHB_ref	-0.0100	7.0	0.010	(*1*) $^{\iota}$	0.043	0.00
1ES1	0.0120	7.0	0.010	(*1*) $^{\iota}$	0.007	-0.01
1ES1_ref	0.0120	7.0	0.010	(*1*) $^{\iota}$	0.029	0.00
1LQX	-0.0260	7.0	0.001	(*2*) $^{\iota}$	-0.003	-0.03
1LQX_ref	-0.0260	7.0	0.001	(*2*) $^{\iota}$	0.005	-0.02
1B5M	-0.1020	7.0	0.100	(*3*) $^{\iota}$	-0.054	-0.05
4HIL_A	-0.1020	7.0	0.100	(*3*) $^{\iota}$	-0.038	-0.04
4HIL_B	-0.1020	7.0	0.100	(*3*) $^{\iota}$	-0.026	-0.03
4HIL_ref_A	-0.1020	7.0	0.100	(*3*) $^{\iota}$	-0.047	-0.05
4HIL_ref_B	-0.1020	7.0	0.100	(*3*) $^{\iota}$	-0.029	-0.03
1EUE	-0.0630	7.0	0.100	(*3*) $^{\iota}$	-0.013	-0.01
1LR6	-0.0350	7.0	0.001	(*2*) $^{\iota}$	0.032	-0.01
1LR6_ref	0.0350	7.0	0.001	(*2*) $^{\iota}$	0.034	-0.01
2IBJ	-0.0260	7.6	0.150	(*4*) $^{\iota}$	-0.030	-0.03
2IBJ_ref	-0.0260	7.6	0.150	(*4*) $^{\iota}$	-0.018	-0.01
1M2I	0.0075	7.0	0.010	(*5*) $^{\iota}$	0.010	-0.02
1M2I_ref	0.0075	7.0	0.010	(*5*) $^{\iota}$	0.015	-0.01
3MUS	-0.0548	7.4	0.110	(*6*) $^{\iota}$	-0.032	-0.03
3MUS_ref	-0.0548	7.4	0.110	(*6*) $^{\iota}$	-0.040	-0.04
1M2M	0.0150	7.0	0.010	(*5*) $^{\iota}$	0.065	0.04
1M2M_ref	0.0150	7.0	0.010	(*5*) $^{\iota}$	0.062	0.03
1X3X_A	0.0750	7.0	0.150	(*7*) $^{\iota}$	0.107	0.10
1X3X_B	0.0750	7.0	0.150	(*7*) $^{\iota}$	0.025	0.02
1X3X_ref_A	0.0750	7.0	0.150	(*7*) $^{\iota}$	0.118	0.11
1X3X_ref_B	0.0750	7.0	0.150	(*7*) $^{\iota}$	0.087	0.08
3NER	-0.0538	7.4	0.110	(*6*) $^{\iota}$	-0.022	-0.02
3NER_ref	-0.0538	7.4	0.110	(*6*) $^{\iota}$	-0.003	-0.00

Table D.3: Ramachandran outliers, clash score, resolution, R-work and R-free values for the original crystal structure and the self-re-refined structures. - Cytochrome c_x; Part 1

pdb-ID	Ramachandran outliers	Clashscore	Resolution	R-work	R-free
1B7V	0.00%	16.000	1.700	0.174	0.206
1B7V_ref	0.00%	5.690	2.150	0.129	0.186
1C2R	0.00%	17.000	2.500	0.168	
1C2R_ref	0.00%	2.490	2.500	0.157	0.217
1C75	0.00%	7.000	0.970	0.116	
1C75_ref	0.00%	1.810	0.970	0.151	0.161
1CO6	0.00%	12.000	1.600	0.182	
1CO6_ref	0.00%	5.260	1.600	0.172	0.216
1CTJ	1.10%	3.000	1.100	0.138	0.188
1CTJ_ref	0.00%	5.950	1.100	0.176	0.192
1CXC	0.00%	12.000	1.600	0.225	
1CXC_ref	0.00%	2.580	1.540	0.187	0.220
1CYI	1.10%	6.000	1.900	0.197	
1CYI_ref	2.27%	12.640	1.900	0.241	0.296
1CYJ	0.00%	11.000	1.900	0.187	
1CYJ_ref	0.00%	4.920	1.900	0.171	0.209

Table D.4: Ramachandran outliers, clash score, resolution, R-work and R-free values for the original crystal structure and the self-re-refined structures. - Cytochrome c_x; Part 2

pdb-ID	Ramachandran outliers	Clashscore	Resolution	R-work	R-free
1DT1	0.00%	8.000	1.800	0.182	0.262
1DT1_ref	0.00%	0.000	1.710	0.175	0.202
1LS9	0.00%	3.000	1.300	0.143	0.190
1LS9_ref	0.00%	1.380	1.300	0.172	0.189
2CE0	0.00%	8.000	1.240	0.182	0.212
2CE0_ref	0.00%	0.630	1.240	0.178	0.186
2DGE	0.00%	2.000	1.500	0.186	0.215
2DGE_ref	0.00%	3.970	1.500	0.169	0.188
2V07	0.00%	9.000	1.600	1.980	0.236
2V07_ref	0.00%	4.970	1.600	0.204	0.214
2YCC	0.00%	54.000	1.900	0.197	
2YCC_ref	0.00%	5.600	1.900	0.246	0.331
351C	1.20%	6.000	1.600	0.195	
351C_ref	1.25%	6.220	0.960	0.083	0.097
3CU4	0.00%	2.000	1.300	0.169	0.183
3CU4_ref	0.00%	0.000	1.300	0.138	0.155
451C	1.20%	6.000	1.600	0.187	
451C_ref	1.25%	5.440	0.950	0.092	0.096
6U97	0.00%	2.000	1.130	0.126	0.153
6U97_ref	0.00%	0.800	1.130	0.151	0.172
1JDL	0.00%	15.000	1.700	0.190	0.210
1JDL_ref	0.00%	3.260	1.700	0.146	0.159
2C2C	0.00%	14.000	2.000	0.172	
2C2C_ref	0.00%	9.940	1.680	0.151	0.193

Table D.5: The found experimental redox potentials $[V]$ with the corresponding pH-values and ionic strengths as well as their measuring methods in bracket: CV (cyclic voltammetry)$^{\iota}$, DCV (direct cyclic voltammetry)$^{\varsigma}$ and PFV (protein film voltammetry)$^{\zeta}$. The last two columns contain the calculated redox potentials $[V]$ for the different protein structures and also the self-re-refined structures at an ionic strength of 0.150 M NaCl[1] and at the ionic strengths from the publications[2]. - Cytochrome c_x; Part 1

pdb-ID	exp. redox potential	pH	ionic strength from publication	Ref.	theo. redox potential[1]	theo. redox potential[2]	
1C75	-0.065	7.6	0.360	(*8*) $^{\iota}$	-0.025	-0.019	C553
	-0.055						
1C75_ref	-0.065	7.6	0.360	(*8*) $^{\iota}$	-0.023	-0.016	C553ref
	-0.055						
1C75	0.047	7.0	0.360	(*9*, *10*) $^{\varsigma}$	-0.025	-0.019	C553
1C75_ref	0.047	7.0	0.360	(*9*, *10*) $^{\varsigma}$	-0.023	-0.016	C553ref
1B7V	0.058	7.0	0.260	(*10*) $^{\varsigma}$	-0.030	-0.025	C553
1B7V_ref	0.058	7.0	0.260	(*10*) $^{\varsigma}$	-0.027	-0.021	C553ref
2DGE_A	0.071	7.5	0.150	(*11*) $^{\zeta}$	0.030	0.030	C6
2DGE_B	0.071	7.5	0.150	(*11*) $^{\zeta}$	-0.030	-0.033	C6
2DGE_C	0.071	7.5	0.150	(*11*) $^{\zeta}$	0.007	0.002	C6
2DGE_D	0.071	7.5	0.150	(*11*) $^{\zeta}$	-0.003	-0.007	C6
2DGE_ref_A	0.071	7.5	0.150	(*11*) $^{\zeta}$	0.029	0.023	C6ref
2DGE_ref_B	0.071	7.5	0.150	(*11*) $^{\zeta}$	-0.027	-0.032	C6ref
2DGE_ref_C	0.071	7.5	0.150	(*11*) $^{\zeta}$	-0.001	-0.001	C6ref
2DGE_ref_D	0.071	7.5	0.150	(*11*) $^{\zeta}$	0.011	0.011	C6ref
2CE0	0.083	7.0	0.100	(*11*) $^{\zeta}$	-0.020	-0.020	C6
2CE0_ref	0.083	7.0	0.100	(*11*) $^{\zeta}$	0.006	0.005	C6
2CE1	0.083	7.0	0.100	(*11*) $^{\zeta}$	-0.028	-0.029	C6ref
2CE1_ref	0.083	7.0	0.100	(*11*) $^{\zeta}$	-0.015	-0.015	C6ref
6U97	0.153	7.0	0.100	(*12*) $^{\iota}$	0.006	0.005	Cf
6U97_ref	0.153	7.0	0.100	(*12*) $^{\iota}$	0.001	0.000	Cfref
2V07	0.168	7.0	0.040	(*11*) $^{\zeta}$	0.032	0.031	C6
2V07_ref	0.168	7.0	0.040	(*11*) $^{\zeta}$	0.021	0.020	C6ref
3CU4	0.180	7.0	0.100	(*12*) $^{\iota}$	0.011	0.010	Cf
3CU4_ref	0.180	7.0	0.100	(*12*) $^{\iota}$	0.004	0.003	Cfref
1DT1	0.202	7.0	0.150	(*13*) $^{\iota}$	0.087	0.087	C552
1DT1_ref	0.202	7.0	0.100	(*13*) $^{\iota}$	0.080	0.080	C552ref
1C52	0.230	7.0	0.050	(*14*) $^{\iota}$	0.026	0.031	C552
1CRC	0.260	7.0	0.100	(*15*) $^{\iota}$	0.044	0.048	C
1HRC	0.260	7.0	0.100	(*16*) $^{\iota}$	0.044	0.046	C
351C	0.270	6.5	0.100	(*9*) $^{\varsigma}$	0.063	0.062	C551
351C_ref	0.270	6.5	0.100	(*9*) $^{\varsigma}$	0.075	0.074	C551
451C	0.270	6.5	0.100	(*9*) $^{\varsigma}$	0.068	0.068	C551ref
451C_ref	0.270	6.5	0.100	(*9*) $^{\varsigma}$	0.073	0.072	C551ref

Table D.6: The found experimental redox potentials $[V]$ with the corresponding pH-values and ionic strengths as well as their location.The last two columns contain the calculated redox potentials $[V]$ for the different protein structures and also the self-re-refined structures at an ionic strength of 0.150 M NaCl[1] and at the ionic strengths from the publications[2]. - Cytochrome c_x; Part 2

pdb-ID	exp. redox potential	pH	ionic strength from publication	Ref.	theo. redox potential[1]	theo. redox potential[2]	
2YCC	0.290	7.0	0.150	(*9*) [ς]	0.119	0.119	C
2YCC_ref	0.290	7.0	0.150	(*9*) [ς]	0.110	0.110	C
1YCC	0.290	7.0	0.150	(*9*) [ς]	0.107	0.107	Cref
1CO6	0.296	7.0	0.100	(*17*) [ι]	0.111	0.113	C2
1CO6_ref	0.296	7.0	0.100	(*17*) [ι]	0.087	0.088	C2ref
1C2R_A	0.350	7.0	0.100	(*17*) [ι]	0.072	0.073	C2
1C2R_B	0.350	7.0	0.100	(*17*) [ι]	0.089	0.090	C2
1C2R_ref_A	0.350	7.0	0.100	(*17*) [ι]	0.058	0.059	C2ref
1C2R_ref_B	0.350	7.0	0.100	(*17*) [ι]	0.055	0.056	C2ref
1LS9	0.352	7.0	0.100	(*18*) [ι]	0.105	0.104	C6
1LS9_ref	0.352	7.0	0.100	(*18*) [ι]	0.101	0.101	C6ref
1CXC	0.355	7.0	0.010	(*9*) [ς]	0.113	0.116	C2
	$0.369, 0.358$	7.5	0.010	(*19*) [ι]	0.113	0.116	C2
1CXC_ref	0.355	7.0	0.010	(*9*) [ς]	0.113	0.116	C2
	$0.369, 0.358$	7.5	0.010	(*19*) [ι]	0.113	0.116	C2
1CTJ	0.358	7.0	0.050	(*9*) [ς]	0.045	0.039	C6
1CTJ_ref	0.358	7.0	0.050	(*9*) [ς]	0.125	0.120	C6ref
1A2S	0.358	7.0	0.050	(*20*) [ι]	0.035	0.035	C6
1CYJ	0.370	7.0	0.150	(*21*) [ι]	0.021	0.075	C6
1CYJ_ref	0.370	7.0	0.150	(*21*) [ι]	0.172	0.141	C6ref
1CYI	0.370	7.0	0.150	(*21*) [ι]	0.075	0.021	C6
1CYI_ref	0.370	7.0	0.150	(*21*) [ι]	0.141	0.172	C6ref

References Appendix

(*1*) Xue, L.-L., Wang, Y.-H., Xie, Y., Yao, P., Wang, W.-H., Qian, W., Huang, Z.-X., Wu, J., and Xia, Z.-X. (1999). Effect of Mutation at Valine 61 on the Three-Dimensional Structure, Stability, and Redox Potential of Cytochrome b5†,⊥. *Biochemistry-Us 38*, 11961–11972, DOI: 10.1021/bi990893b.

(*2*) Wang, Z.-Q., Wang, Y.-H., Wang, W.-H., Xue, L.-L., Wu, X.-Z., Xie, Y., and Huang, Z.-X. (2000). The effect of mutation at valine-45 on the stability and redox potentials of trypsin-cleaved cytochrome b5. *Biophys Chem 83*, 3–17, DOI: 10.1016/S0301-4622(99)00119-2.

(*3*) Wirtz, M., Oganesyan, V., Zhang, X., Studer, J., and Rivera, M. (2000). Modulation of redox potential in electron transfer proteins: effects of complex formation on the active site microenvironment of cytochrome b5. *Faraday Discuss*, 221–34, discussion 257–68, DOI: 10.1039/B001520M.

(*4*) Guzov, V. M., Houston, H. L., Murataliev, M. B., Walker, F. A., and Feyereisen, R. (1996). Molecular Cloning, Overexpression in Escherichia coli , Structural and Functional Characterization of House Fly Cytochrome b5. *J Biol Chem 271*, 26637–26645, DOI: 10.1074/jbc.271.43.26637.

(*5*) Wu, J., Wang, Y.-H., Gan, J.-H., Wang, W.-H., Sun, B.-Y., Huang, Z.-X., and Xia, Z.-X. (2002). Structures of Cytochrome b5 Mutated at the Charged Surface-Residues and Their Interactions with Cytochrome c†. *Chinese J Chem 20*, 1225–1234, DOI: 10.1002/cjoc.20020201114.

(*6*) Parthasarathy, S., Altuve, A., Terzyan, S., Zhang, X., Kuczera, K., Rivera, M., and Benson, D. R. (2011). Accommodating a nonconservative internal mutation by water-mediated hydrogen bonding between b-sheet strands: a comparison of human and rat type B (mitochondrial) cytochrome b5. *Biochemistry-Us 50*, 5544–5554, DOI: 10.1021/bi2004729.

(*7*) Yokota, T., Nakajima, Y., Yamakura, F., Sugio, S., Hashimoto, M., and Takamiya, S. (2006). Unique structure of Ascaris suum b5-type cytochrome: an additional alpha-helix and positively charged residues on the surface domain interact with redox partners. *Biochem J 394*, 437–447, DOI: 10.1042/BJ20051308.

(*8*) Santos, H., and Turner, D. L. (1988). Characterization and NMR studies of a novel cytochrome c isolated from Methylophilus methylotrophus which shows a redox-linked change of spin state. *Biochim Biophys Acta (Bba) - Protein Structure And Molecular Enzymology 954*, 277–286, DOI: 10.1016/0167-4838(88)90083-0.

(*9*) Benini, S., González, A., Rypniewski, W. R., Wilson, K. S., van Beeumen, J. J., and Ciurli, S. (2000). Crystal structure of oxidized Bacillus pasteurii cytochrome c553 at 0.97-A resolution. *Biochemistry-Us 39*, 13115–13126, DOI: 10.1021/bi000402j.

(*10*) Benini, S., Borsari, M., Ciurli, S., Dikiy, A., and Lamborghini, M. (1998). Modulation of Bacillus pasteurii cytochrome c 553 reduction potential by structural and solution parameters. *J Biol Inorg Chem 3*, 371–382, DOI: 10.1007/s007750050247.

(*11*) Worrall, J. A. R., Schlarb-Ridley, B. G., Reda, T., Marcaida, M. J., Moorlen, R. J., Wastl, J., Hirst, J., Bendall, D. S., Luisi, B. F., and Howe, C. J. (2007). Modulation of heme redox potential in the cytochrome c6 family. *J Am Chem Soc 129*, 9468–9475, DOI: 10.1021/ja072346g.

(*12*) Teixeira, L. R., Cordas, C. M., Fonseca, M. P., Duke, N. E. C., Pokkuluri, P. R., and Salgueiro, C. A. (2020). Modulation of the Redox Potential and Electron/Proton Transfer Mechanisms in the Outer Membrane Cytochrome OmcF From Geobacter sulfurreducens. *Frontiers In Microbiology 10*, 2941, DOI: 10.3389/fmicb.2019.02941.

(*13*) Fee, J. A., Chen, Y., Todaro, T. R., Bren, K. L., Patel, K. M., Hill, M. G., Gomez-Moran, E., Loehr, T. M., Ai, J., Thöny-meyer, L., Williams, P. A., Sturam, E., Sridhar, V., and Mcree, D. E. (2000). Integrity of thermus thermophilus cytochrome c552 Synthesized by escherichia coli cells expressing the host-specific cytochrome c maturation genes, ccmABCDEFGH: Biochemical, spectral, and structural characterization of the recombinant protein. *Protein Science 9*, 2074–2084, DOI: 10.1110/ps.9.11.2074.

(*14*) Bernad, S., Soulimane, T., Mehkalif, Z., and Lecomte, S. (2006). Characterization and redox properties of cytochrome c552 from Thermus thermophilus adsorbed on different self-assembled thiol monolayers, used to model the chemical environment of the redox partner. *Biopolymers 81*, 407–418, DOI: doi.org/10.1002/bip.20432.

(*15*) Myer, Y. P., Saturno, A. F., Verma, B. C., and Pande, A. (1979). Horse heart cytochrome c. The oxidation-reduction potential and protein structures. *J Biol Chem 254*, 11202–11207, DOI: doi.org/10.1016/S0021-9258(19)86470-0.

(*16*) Pande, A., and Myer, Y. P. (1978). The redox potential of horse heart cytochrome c. *Biochemical And Biophysical Research Communications 85*, 7–13, DOI: 10.1016/S0006-291X(78)80003-5.

(*17*) Pettigrew, G. W., Bartsch, R. G., Meyer, T. E., and Kamen, M. D. (1978). Redox potentials of the photosynthetic bacterial cytochromes c2 and the structural bases for variability. *Biochimica et Biophysica Acta (BBA) - Bioenergetics 503*, 509–523, DOI: 10.1016/0005-2728(78)90150-0.

(*18*) Dikiy, A., Carpentier, W., Vandenberghe, I., Borsari, M., Safarov, N., Dikaya, E., van Beeumen, J., and Ciurli, S. (2002). Structural basis for the molecular properties of cytochrome c6. *Biochemistry-Us 41*, 14689–14699, DOI: 10.1021/bi026473v.

(*19*) Drepper, F., Dorlet, P., and Mathis, P. (1997). Cross-linked electron transfer complex between cytochrome c2 and the photosynthetic reaction center of Rhodobacter sphaeroides. *Biochemistry-Us 36*, 1418–1427, DOI: 10.1021/bi961350u.

(*20*) Campos, A. P., Aguiar, A. P., Hervás, M., Regalla, M., Navarro, J. A., Ortega, J. M., Xavier, A. V., de La Rosa, M. A., and Teixeira, M. (1993). Cytochrome c6 from Monoraphidium braunii. A cytochrome with an unusual heme axial coordination. *Eur J Biochem 216*, 329–341, DOI: 10.1111/j.1432-1033.1993.tb18150.x.

(*21*) Gorman, D. S., and Levine, R. P. (1966). Photosynthetic Electron Transport Chain of Chlamydomonas reinhardi. V. Purification and Properties of Cytochrome 553 and Ferredoxin 1. *Plant Physiol 41*, 1643–1647, DOI: 10.1104/pp.41.10.1643.

E

APPENDIX - OBTAINING G_{model} DIRECTLY FROM EXPERIMENTAL DATA USING EXTENDED MICRO AND MACROSTATE MODEL WITH APPLICATIONS TO FMN/RIESKE CENTER

E.1 Derivation of G

First the definition of the expectation value of the energy.

$$\langle E \rangle = -\frac{\partial}{\partial \beta} ln(Z_{total}(\beta)) \tag{E.1}$$

Additional, the statistical entropy has to be defined.

$$S = \frac{1}{T}\langle E \rangle + R \cdot ln(Z_{total}) \tag{E.2}$$

The free energy for a partition function can be define as

$$\begin{aligned} G &= \langle E \rangle - T \cdot S \\ &= \langle E \rangle - \langle E \rangle - RTln(Z_{total}) \\ &= -RTln(Z_{total}) \\ &= -\beta^{-1} ln(Z_{total}) \end{aligned} \tag{E.3}$$

E.2 Useful intermediate steps of transforming equation

How to get equation (5.26) from equation (5.25):

$$
\begin{aligned}
G_{q\mapsto q'} &= \left(G_{q'} - G_q\right) \\
G_{q\mapsto q'} &= \left(G_{q'} - G_q\right) \\
&= G_{q'}(\mu_{H^+}, \mu_{e^-}) - G_q(\mu_{H^+}, \mu_{e^-}) \\
&= -\beta^{-1} ln\left(\frac{Z_{q'}(\mu_{H^+}, \mu_{e^-})}{Z_{total}}\right) - \left[-\beta^{-1} ln\left(\frac{Z_q(\mu_{H^+}, \mu_{e^-})}{Z_{total}}\right)\right] \\
&= -\beta^{-1} ln\left(\frac{Z_{q'}(\mu_{H^+}, \mu_{e^-})}{Z_{total}}\right) - \beta^{-1} ln\left(\frac{Z_{total}}{Z_q(\mu_{H^+}, \mu_{e^-})}\right) \\
&= -\beta^{-1}\left[ln\left(\frac{Z_{q'}(\mu_{H^+}, \mu_{e^-})}{Z_{total}}\right) + ln\left(\frac{Z_{total}}{Z_q(\mu_{H^+}, \mu_{e^-})}\right)\right] \\
&= -\beta^{-1}\left[ln\left(\frac{Z_{q'(\mu_{H^+}, \mu_{e^-})} \cdot Z_{total}}{Z_{total} \cdot Z_q(\mu_{H^+}, \mu_{e^-})}\right)\right] \\
&= -\beta^{-1} ln\left(\frac{Z_{q'}(\mu_{H^+}, \mu_{e^-})}{Z_q(\mu_{H^+}, \mu_{e^-})}\right) \\
G_{q\mapsto q'} &= -\beta^{-1} \ln\left(\frac{Z_{q'}}{Z_q}\right)
\end{aligned}
\tag{E.4}
$$

How to get equation (5.27) from equation (5.26);

$$
\begin{aligned}
G_{q\mapsto q'} &= -\beta^{-1}\ln\left(\frac{Z_{q'}}{Z_q}\right)\\
G_{q\mapsto q'} &= -\beta^{-1}\ln\left(\frac{Z_{q'}}{Z_q}\right)\\
&= -\beta^{-1}\cdot\ln\left[\frac{Z_{q'}(\mu_{H^+},\mu_{e^-})}{Z_q(\mu_{H^+},\mu_{e^-})}\right]\\
&= -\beta^{-1}\cdot\ln\left[\frac{\sum_{n\in N''}e^{-\beta\left(E^{n,0}_{q'}-n\mu_{H^+}-(q')\mu_{e^-}\right)}}{\sum_{n\in N'}e^{-\beta\left(E^{n,0}_{q}-n\mu_{H^+}-q\mu_{e^-}\right)}}\right]\\
&= -\beta^{-1}\cdot\ln\left[\frac{\sum_{n\in N''}e^{-\beta\left(E^{n,0}_{q'}-n\mu_{H^+}\right)}\cdot e^{-(-\beta)(q')\mu_{e^-}}}{\sum_{n\in N'}e^{-\beta\left(E^{n,0}_{q}-n\mu_{H^+}\right)}\cdot e^{-(-\beta)q\mu_{e^-}}}\right]\\
&= -\beta^{-1}\cdot\ln\left[\frac{e^{\beta(q')\mu_{e^-}}\sum_{n\in N''}e^{-\beta\left(E^{n,0}_{q'}-n\mu_{H^+}\right)}}{e^{\beta q\mu_{e^-}}\sum_{n\in N'}e^{-\beta\left(E^{n,0}_{q}-n_j\mu_{H^+}\right)}}\right]\\
&= -\beta^{-1}\cdot\left(\ln\left[\frac{e^{\beta(q')\mu_{e^-}}}{e^{\beta q\mu_{e^-}}}\right]+\ln\left[\frac{\sum_{n\in N''}e^{-\beta\left(E^{n,0}_{q'}-n\mu_{H^+}\right)}}{\sum_{n\in N'}e^{-\beta\left(E^{n,0}_{q}-n\mu_{H^+}\right)}}\right]\right)\\
&= -\beta^{-1}\cdot\left(\ln\left[e^{\beta(q')\mu_{e^-}-\left(\beta q\mu_{e^-}\right)}\right]+\ln\left[\frac{\sum_{n\in N''}e^{-\beta\left(E^{n,0}_{q'}-n\mu_{H^+}\right)}}{\sum_{n\in N'}e^{-\beta\left(E^{n,0}_{q}-n\mu_{H^+}\right)}}\right]\right)\\
&= -\beta^{-1}\cdot\left(\ln\left[e^{\beta(q')\mu_{e^-}-\beta q\mu_{e^-}}\right]+\ln\left[\frac{\sum_{n\in N''}e^{-\beta\left(E^{n,0}_{q'}-n\mu_{H^+}\right)}}{\sum_{n\in N'}e^{-\beta\left(E^{n,0}_{q}-n\mu_{H^+}\right)}}\right]\right)\\
&= -\beta^{-1}\cdot\left(\ln\left[e^{\beta(q-q')\mu_{e^-}}\right]+\ln\left[\frac{\sum_{n\in N''}e^{-\beta\left(E^{n,0}_{q'}-n\mu_{H^+}\right)}}{\sum_{n\in N'}e^{-\beta\left(E^{n,0}_{q}-n\mu_{H^+}\right)}}\right]\right)\\
&= -(q-q')\mu_{e^-}-\beta^{-1}\cdot\left(\ln\left[\frac{\sum_{n\in N''}e^{-\beta\left(E^{n,0}_{q'}-n\mu_{H^+}\right)}}{\sum_{n\in N'}e^{-\beta\left(E^{n,0}_{q}-n\mu_{H^+}\right)}}\right]\right)\\
G_{q\mapsto q'} &= \left((q-q')\mu_{e^-}-\beta^{-1}\cdot\left(\ln\left[\frac{\sum_{n\in N''}e^{-\beta\left(E^{\circ,n}_{q'}-n\mu_{H^+}\right)}}{\sum_{n\in N'}e^{-\beta\left(E^{\circ,n}_{q}-n\mu_{H^+}\right)}}\right]\right)\right) \qquad \text{(E.5)}
\end{aligned}
$$

Table E.1: Calculation of the real G_{model}-values for Flavin (m: Number of electrons, n: Number of protons) for the reference and the next tautomer. The energies are in $\frac{kcal}{mol}$. - Part 1

		prot. Site	elec/proto	ΔQM	$\Delta Elec$	real G_{model}
negative/ox	FOD1	None	0/0	0.00	0	0.00
neutral/ox	FON1	N3	1/0	0.00	0	-14.10
	FON2	O2	1/0	14.10	0	0.00
	FON3	N1	1/0	14.80	0	0.70
	FON4	O4	1/0	16.10	0	2.00
	FON5	N5	1/0	24.40	0	10.30
positive/ox	FOP1	N1 N3	2/0	0.00	0	-19.69
	FOP2	O2 N3	2/0	4.90	0	-14.79
	FOP3	N3 N5	2/0	7.80	0	-11.89
	FOP4	N1 O4	2/0	12.40	0	-7.29
	FOP5	O2 O4	2/0	13.80	0	-5.89
	FOP6	N3 O4	2/0	15.10	0	-4.59
	FOP7	O2 N5	2/0	19.40	0	-0.29
	FOP8	N1 O2	2/0	21.30	0	1.61
	FOP9	N1 N5	2/0	23.20	0	3.51
	FOP10	O4 N5	2/0	25.20	0	5.51
negative/semi	FSD1	N3	1/1	0.00	0	-4.99
	FSD2	N5	1/1	9.60	0	4.61
	FSD3	N1	1/1	11.60	0	6.61
	FSD4	O2	1/1	13.70	0	8.71
	FSD5	O4	1/1	14.40	0	9.41
neutral/semi	FSN1	N3 N5	2/1	0.00	0	-16.47
	FSN2	N1 N3	2/1	6.70	0	-9.77
	FSN3	O2 N5	2/1	11.40	0	-5.07
	FSN4	N1 N5	2/1	11.40	0	-5.07
	FSN5	O2 N3	2/1	13.80	0	-2.67
	FSN6	O4 N5	2/1	16.70	0	0.23
	FSN7	N1 O4	2/1	17.20	0	0.73
	FSN8	N3 O4	2/1	18.30	0	1.83
	FSN9	O2 O4	2/1	18.70	0	2.23
	FSN10	N1 O2	2/1	29.10	0	12.63
positive/semi	FSP1	N1 N3 N5	3/1	0.00	0	-22.71
	FSP2	O2 N3 N5	3/1	4.60	0	-18.11
	FSP3	N3 O4 N5	3/1	9.30	0	-13.41
	FSP4	O2 O4 N5	3/1	12.80	0	-9.91
	FSP5	N1 O4 N5	3/1	13.10	0	-9.61
	FSP6	N1 O2 N5	3/1	19.40	0	-3.31
	FSP7	N1 N3 O4	3/1	20.00	0	-2.71
	FSP8	O2 N3 O4	3/1	25.20	0	2.49
	FSP9	N1 O2 O4	3/1	28.80	0	6.09
	FSP10	N1 O2 N3	3/1	28.90	0	6.19

Table E.2: Calculation of the real G_{model}-values for Flavin (m: Number of electrons, n: Number of protons) for the reference and the next tautomer. The energies are in $\frac{kcal}{mol}$. - Part 2

		prot. Site	elec/proto	ΔQM	$\Delta Elec$	real G_{model}
negative/red	FRD1	N3 N5	2/2	0.00	0	-13.99
	FRD2	N1 N5	2/2	10.00	0	-3.99
	FRD3	O4 N5	2/2	10.60	0	-3.39
	FRD4	O2 N5	2/2	12.00	0	-1.99
	FRD5	N1 N3	2/2	22.80	0	8.81
	FRD6	N1 O4	2/2	25.20	0	11.21
	FRD7	N3 O4	2/2	25.36	0	11.37
	FRD8	O2 N3	2/2	27.20	0	13.21
	FRD9	O2 O4	2/2	27.30	0	13.31
	FRD10	N1 O2	2/2	43.70	0	29.71
neutral/red	FRN1	N1 N3 N5	3/2	0.00	0	-23.01
	FRN2	N3 O4 N5	3/2	7.00	0	-16.01
	FRN3	N1 O4 N5	3/2	7.10	0	-15.91
	FRN4	O2 O4 N5	3/2	7.30	0	-15.71
	FRN5	O2 N3 N5	3/2	8.50	0	-14.51
	FRN6	N1 O2 N5	3/2	20.10	0	-2.91
	FRN7	N1 N3 O4	3/2	28.70	0	5.69
	FRN8	O2 N3 O4	3/2	35.60	0	12.59
	FRN9	N1 O2 O4	3/2	40.30	0	17.29
	FRN10	N1 O2 N3	3/2	49.80	0	26.79
positive/red	FRP1	N1 N3 N5 N5	4/2	0.00	0	-27.68
	FRP2	O2 N3 O4 N5	4/2	2.50	0	-25.18
	FRP3	N1 N3 O4 N5	4/2	3.70	0	-23.98
	FRP4	O2 N3 N5 N5	4/2	6.70	0	-20.98
	FRP5	N1 O2 O4 N5	4/2	11.60	0	-16.08
	FRP6	N1 O2 N3 N5	4/2	12.70	0	-14.98
	FRP7	N1 O4 N5 N5	4/2	13.50	0	-14.18
	FRP8	O2 O4 N5 N5	4/2	14.50	0	-13.18
	FRP9	N3 O4 N5 N5	4/2	16.00	0	-11.68
	FRP10	N1 O2 N5 N5	4/2	19.90	0	-7.78
	FRP11	N1 N3 N3 N5	4/2	29.00	0	1.32
	FRP12	N1 N1 N3 N5	4/2	34.40	0	6.72
	FRP13	O2 N3 N3 N5	4/2	40.60	0	12.92
	FRP14	N1 O2 N3 O4	4/2	44.60	0	16.92
	FRP15	N1 N1 O2 N5	4/2	53.50	0	25.82
	FRP16	N1 N3 N3 O4	4/2	57.80	0	30.12
	FRP17	O2 N3 N3 O4	4/2	68.10	0	40.42
	FRP18	N1 N1 N3 O4	4/2	72.30	0	44.62
	FRP19	N1 O2 N3 N3	4/2	79.40	0	51.72

F

APPENDIX - RATE MODEL

F.1 Theory

All steps to determined the rank of the different matrices in equations (6.18) to (6.20):

$$
\begin{aligned}
&I \\
&\begin{bmatrix} -k_{12} & k_{21} & 0 & 0 \\ k_{12} & -k_{21}-k_{23} & k_{32} & 0 \\ 0 & k_{23} & -k_{32}-k_{34} & k_{43} \\ 0 & 0 & k_{34} & -k_{43} \end{bmatrix} II + I \\
&\begin{bmatrix} -k_{12} & k_{21} & 0 & 0 \\ 0 & -k_{23} & k_{32} & 0 \\ 0 & k_{23} & -k_{32}-k_{34} & k_{43} \\ 0 & 0 & k_{34} & -k_{43} \end{bmatrix} III + II \\
&\begin{bmatrix} -k_{12} & k_{21} & 0 & 0 \\ 0 & -k_{23} & k_{32} & 0 \\ 0 & 0 & -k_{34} & k_{43} \\ 0 & 0 & k_{34} & -k_{43} \end{bmatrix} IV + III \\
&\begin{bmatrix} -k_{12} & k_{21} & 0 & 0 \\ 0 & -k_{23} & k_{32} & 0 \\ 0 & 0 & -k_{34} & k_{43} \\ 0 & 0 & 0 & 0 \end{bmatrix}
\end{aligned}
\tag{F.1}
$$

II

$$\begin{bmatrix} -k_{12} & k_{21} & 0 & 0 \\ k_{12} & -k_{21}-k_{23}-k_{24} & k_{32} & k_{42} \\ 0 & k_{23} & -k_{32}-k_{34} & 0 \\ 0 & k_{24} & k_{34} & -k_{42} \end{bmatrix} II + I$$

$$\begin{bmatrix} -k_{12} & k_{21} & 0 & 0 \\ 0 & -k_{23}-k_{24} & k_{32} & k_{42} \\ 0 & k_{23} & -k_{32}-k_{34} & 0 \\ 0 & k_{24} & k_{34} & -k_{42} \end{bmatrix} III + II$$

$$\begin{bmatrix} -k_{12} & k_{21} & 0 & 0 \\ 0 & -k_{23}-k_{24} & k_{32} & k_{42} \\ 0 & -k_{24} & -k_{34} & k_{42} \\ 0 & k_{24} & k_{34} & -k_{42} \end{bmatrix} IV + III$$

$$\begin{bmatrix} -k_{12} & k_{21} & 0 & 0 \\ 0 & -k_{23}-k_{24} & k_{32} & k_{42} \\ 0 & -k_{24} & -k_{34} & k_{42} \\ 0 & 0 & 0 & 0 \end{bmatrix} \tag{F.2}$$

III

$$\begin{bmatrix} -k_{12}-k_{14} & k_{21} & 0 & k_{41} \\ k_{12} & -k_{21}-k_{23} & k_{32} & 0 \\ 0 & k_{23} & -k_{32}-k_{34} & k_{43} \\ k_{14} & 0 & k_{34} & -k_{41}-k_{43} \end{bmatrix} II + I$$

$$\begin{bmatrix} -k_{12}-k_{14} & k_{21} & 0 & k_{41} \\ -k_{14} & -k_{23} & k_{32} & k_{41} \\ 0 & k_{23} & -k_{32}-k_{34} & k_{43} \\ k_{14} & 0 & k_{34} & -k_{41}-k_{43} \end{bmatrix} III + II$$

$$\begin{bmatrix} -k_{12}-k_{14} & k_{21} & 0 & k_{41} \\ -k_{14} & -k_{23} & k_{32} & k_{41} \\ -k_{14} & 0 & -k_{34} & k_{43}+k_{41} \\ k_{14} & 0 & k_{34} & -k_{41}-k_{43} \end{bmatrix} IV + III$$

$$\begin{bmatrix} -k_{12}-k_{14} & k_{21} & 0 & k_{41} \\ -k_{14} & -k_{23} & k_{32} & k_{41} \\ -k_{14} & 0 & -k_{34} & k_{43}+k_{41} \\ 0 & 0 & 0 & 0 \end{bmatrix} \tag{F.3}$$

Listing F.1: Csh script for calculation an enzym cycle like in section 6.3

```
set bin  = /scratch/ullmann/GIT/gmct/src

cat <<EOF >! reaction.setup
#=========================================================================
#       SubstanceName StochiometryCoeff
EDUCT   S            1
PRODUCT P            1
#=========================================================================
# flow EC --> CP
#     pH H-CP   7.5
#     pH H-EC   6.5
#         SubstanceName     mu_0   mu
# concentration only use for pre-steady state analysis
#       StateName   concentration energy
CHEMPOT   S              0.0     1.0   E_0:L_1
CHEMPOT   P              0.0     0.5   E_0:L_1

STATE E   1.00  0.00  E_1:L_0
STATE ES  0.00  0.00  E_1:L_1
STATE EP  0.00  0.00  E_1:L_1
REACTION  E   S  -- ES [0] : 1.000000e+13  1.000000e+01
REACTION  E   P  -- EP [0] : 1.000000e+13  1.000000e+01
REACTION  ES [0] -- EP [0] : 1.000000e+13  1.000000e+01
EOF

$bin/kinetics  -solve SUPER_LU -v reaction.setup
```

Listing F.2: Output of csh script from listing F.1 - part 1

```
=========================================================================
# Kinetics, Version 0.1
# Authors: G. Matthias Ullmann

# Date: 2023-2-3 12:18:27
#
# This program is free software: you can redistribute it and/or modify
# it under the terms of the GNU General Public License as published by
# the Free Software Foundation, either version 3 of the License, or
# (at your option) any later version.
# This program is distributed in the hope that it will be useful,
# but WITHOUT ANY WARRANTY; without even the implied warranty of
# MERCHANTABILITY or FITNESS FOR A PARTICULAR PURPOSE.  See the
# GNU General Public License for more details.
# You can obtain a copy of the GNU General Public License from
# <http://www.gnu.org/licenses/>.
=========================================================================
=========================================================================
Info on the Reactions
Number of States:                3
Number of Chemical Potential:    2
Number of Reactions:             3
Number of Educts:                1
Number of Products:              1
=========================================================================
Done reading educts.
Done reading products.
Done reading chemical potentials.
Done reading states.
Done reading reactions.
Used Temperature:   300.00
=========================================================================
STATE E          1.000e+00     0.000e+00
STATE ES         0.000e+00     0.000e+00
STATE EP         0.000e+00     0.000e+00
-------------------------------------------------------------------------
Chemical Potential
         ID  Substance            mu            mu0            mu'
ChemPot   1  S             1.000e+00      0.000e+00      1.000e+00
ChemPot   2  P             5.000e-01      0.000e+00      5.000e-01
-------------------------------------------------------------------------
Rates:
                                            Forward     Backward
Reaction             E --         ES :     5.130e+05     9.575e+04
Reaction             E --         EP :     5.130e+05     2.216e+05
Reaction            ES --         EP :     5.130e+05     5.130e+05
=========================================================================
```

Listing F.3: Output of csh script from listing F.1 - part 2

```
Rate Parameter:
-----------------------------------------------------------------------
RATE  Educt           + Substate   --> Product         + Substate   : rate
    --          dGa           dG          dGo          mu'           Ea
    A
-----------------------------------------------------------------------
Rate                E + S          -->              ES + [0]        :    5.130e+05
    --    1.000e+01   -1.000e+00    0.000e+00    1.000e+01    1.000e+01    1.000e
    +13
Rate               ES + [0]        -->               E + S          :    9.575e+04
    --    1.000e+01    1.000e+00   -0.000e+00    0.000e+00    1.100e+01    1.000e
    +13
Rate                E + P          -->              EP + [0]        :    5.130e+05
    --    1.000e+01   -5.000e-01    0.000e+00    5.000e-01    1.000e+01    1.000e
    +13
Rate               EP + [0]        -->               E + P          :    2.216e+05
    --    1.000e+01    5.000e-01   -0.000e+00    0.000e+00    1.050e+01    1.000e
    +13
Rate               ES + [0]        -->              EP + [0]        :    5.130e+05
    --    1.000e+01    0.000e+00    0.000e+00    0.000e+00    1.000e+01    1.000e
    +13
Rate               EP + [0]        -->              ES + [0]        :    5.130e+05
    --    1.000e+01   -0.000e+00   -0.000e+00    0.000e+00    1.000e+01    1.000e
    +13
=======================================================================
Rate Matrix:
    0.000e+00     9.575e+04     2.216e+05
    5.130e+05     0.000e+00     5.130e+05
    5.130e+05     5.130e+05     0.000e+00

=======================================================================
=======================================================================
Analyzing the (potential) thermodynamics of the reaction
Reaction:

 1 S ---> 1 P

Standard Free Energy Change:   0.0000e+00 kcal/mol = (  0.0000e+00 -   0.0000e+00)
     kcal/mol
Free Energy Change:           -5.0000e-01 kcal/mol = (  5.0000e-01 -   1.0000e+00)
     kcal/mol
=======================================================================
Equilibrium Constant Matrix

    0.000e+00     1.866e-01     4.320e-01
    5.358e+00     0.000e+00     1.000e+00
    2.315e+00     1.000e+00     0.000e+00
```

Listing F.4: Output of csh script from listing F.1 - part 3

```
======================================================================
======================================================================
======================================================================

Analyze the State Network

----------------------------------------------------------------------
Graph is fully connected.
----------------------------------------------------------------------
======================================================================
----------------------------------------------------------------------
----------------------------------------------------------------------
Checking the reaction network using the product of
the stoichoimetry matrix and the composition matrix.
Number of Elements: 2
======================================================================
Element Names -- 2 elements:
  E    L
Composition Matrix:
  0    1
  0    1
  1    0
  1    1
  1    1

======================================================================
Check Stoichiometry Vector by Vector
   1     0     1    -1     0
Result Vector:     0    0
   0     1     1     0    -1
Result Vector:     0    0
  -1     0    -1     1     0
Result Vector:     0    0
   0     0     0     1    -1
Result Vector:     0    0
   0    -1    -1     0     1
Result Vector:     0    0
   0     0     0    -1     1
Result Vector:     0    0
Stoichiometry of all reactions ok.
======================================================================
Analyze Matrix Sparcity
Non-zero Elements:                  15
Total number of Elements:           16
Sparsity:                       9.4e-01
```

Listing F.5: Output of csh script from listing F.1 - part 4

```
==========================================================================

Solve the equation to get the steady state concentrations.


Rate Matrix
    0.000e+00     9.575e+04     2.216e+05
    5.130e+05     0.000e+00     5.130e+05
    5.130e+05     5.130e+05     0.000e+00



Matrix A -- to be solved
   -1.026e+06     9.575e+04     2.216e+05     1.000e+00
    5.130e+05    -6.088e+05     5.130e+05     1.000e+00
    5.130e+05     5.130e+05    -7.347e+05     1.000e+00
    1.000e+00     1.000e+00     1.000e+00     0.000e+00



 Right Hand Side Vector:
 0.000e+00
 0.000e+00
 0.000e+00
 1.000e+00


Solve the System using SUPER_LU
NRow: 4   NCol: 4  NVal: 15
  1. val[   1][  1] =        -1.026038e+06
  2. val[   2][  1] =         5.130191e+05
  3. val[   3][  1] =         5.130191e+05
  4. val[   4][  1] =         1.000000e+00
  5. val[   1][  2] =         9.575178e+04
  6. val[   2][  2] =        -6.087708e+05
  7. val[   3][  2] =         5.130191e+05
  8. val[   4][  2] =         1.000000e+00
  9. val[   1][  3] =         2.216359e+05
 10. val[   2][  3] =         5.130191e+05
 11. val[   3][  3] =        -7.346550e+05
 12. val[   4][  3] =         1.000000e+00
 13. val[   1][  4] =         1.000000e+00
 14. val[   2][  4] =         1.000000e+00
 15. val[   3][  4] =         1.000000e+00
CCS Matrix

number of non-zero values -- nnz:   15
number of columns  -- ncol:         4
number of rows  -- nrow:            4
```

Listing F.6: Output of csh script from listing F.1 - part 5

```
value = [ -1026038.119279  513019.059639  513019.059639    1.000000  95751.778716
    -608770.838355  513019.059639    1.000000  221635.934532  513019.059639
    -734654.994171    1.000000    1.000000    1.000000    1.000000 ]

rowind = [ 0  1  2  3  0  1  2  3  0  1  2  3  0  1  2 ]

colptr = [ 0  4  8  12  15 ]

CompCol matrix A:
Stype 0, Dtype 1, Mtype 0
nrow 4, ncol 4, nnz 15
nzval: -1026038.119279  513019.059639  513019.059639  1.000000  95751.778716
    -608770.838355  513019.059639  1.000000  221635.934532  513019.059639
    -734654.994171  1.000000  1.000000  1.000000  1.000000
rowind: 0  1  2  3  0  1  2  3  0  1  2  3  0  1  2
colptr: 0  4  8  12  15

Dense matrix B:
Stype 6, Dtype 1, Mtype 0
nrow 4, ncol 1, lda 4

nzval: 0.000000  0.000000  0.000000  1.000000

Solve the System using dgssv with COLAMD order.
Lagrange Multiplier:       0.00000000e+00
 1.315e-01   4.573e-01   4.112e-01   0.000e+00

CompCol matrix A:
Stype 0, Dtype 1, Mtype 0
nrow 4, ncol 4, nnz 15
nzval: -1026038.119279  513019.059639  513019.059639  1.000000  95751.778716
    -608770.838355  513019.059639  1.000000  221635.934532  513019.059639
    -734654.994171  1.000000  1.000000  1.000000  1.000000
rowind: 0  1  2  3  0  1  2  3  0  1  2  3  0  1  2
colptr: 0  4  8  12  15

Dense matrix B:
Stype 6, Dtype 1, Mtype 0
nrow 4, ncol 1, lda 4

nzval: 0.131498  0.457322  0.411180  0.000000

CompCol matrix U:
Stype 0, Dtype 1, Mtype 4
nrow 4, ncol 4, nnz 10
nzval:
rowind:
colptr: 0  0  0  0  0
```

Listing F.7: Output of csh script from listing F.1 - part 6

```
SuperNode matrix L:
Stype 3, Dtype 1, Mtype 1
nrow 4, ncol 4, nnz 10, nsuper 0
nzval:
0       0       -1.026038e+06
1       0       -5.000000e-01
2       0       -9.746227e-07
3       0       -5.000000e-01
0       1       9.575178e+04
1       1       -5.608949e+05
2       1       -1.949245e-06
3       1       -1.000000e+00
0       2       2.216359e+05
1       2       6.238370e+05
2       2       2.432023e+00
3       2       0.000000e+00
0       3       1.000000e+00
1       3       1.500000e+00
2       3       3.898491e-06
3       3       3.000000e+00

nzval_colptr: 0  4  8  12  16
rowind: 0  1  2  3
rowind_colptr: 0  4  4  4  4
col_to_sup: 0  0  0  0
sup_to_col: 0  4

perm_r
0       0
1       1
2       3
3       2
Used CPU Time for solving (+ overhead): 0.000248 sec
Done solving the steady state equation.
========================================================================
Steady State Concentrations and State Energy :
------------------------------------------------------------------------
                               SSConc       Energy
------------------------------------------------------------------------
SteadyStateConc  E           1.315e-01    0.000e+00
SteadyStateConc  ES          4.573e-01    0.000e+00
SteadyStateConc  EP          4.112e-01    0.000e+00
------------------------------------------------------------------------
sum:                         1.000e+00
========================================================================
```

Listing F.8: Output of csh script from listing F.1 - part 7

```
=====================================================================
SteadyStateFlux   State  State      Netto      Forward     Backward        Ratio
---------------------------------------------------------------------
SteadyStateFLUX   ES     E   -2.36715e+04  4.37894e+04  6.74609e+04  6.49108e-01
SteadyStateFLUX   EP     E    2.36715e+04  9.11323e+04  6.74609e+04  1.35089e+00
SteadyStateFLUX   E      ES   2.36715e+04  6.74609e+04  4.37894e+04  1.54058e+00
SteadyStateFLUX   EP     ES  -2.36715e+04  2.10943e+05  2.34615e+05  8.99105e-01
SteadyStateFLUX   E      EP  -2.36715e+04  6.74609e+04  9.11323e+04  7.40252e-01
SteadyStateFLUX   ES     EP   2.36715e+04  2.34615e+05  2.10943e+05  1.11222e+00
=====================================================================


Netflux in the System
    0.000e+00    -2.367e+04     2.367e+04
    2.367e+04     0.000e+00    -2.367e+04
   -2.367e+04     2.367e+04     0.000e+00

=====================================================================
Substance Flux
Substance          S              E               ES        2.36714796e+04
Substance          P              E               EP       -2.36714796e+04
---------------------------------------------------------------------
Substance Nettoflux           S         2.36714796e+04
Substance Nettoflux           P        -2.36714796e+04
=====================================================================
```

G

APPENDIX - APPLICATION TO bc_1-COMPLEX

G.1 Methods

Table G.1: All connection pairs with connection type and occurrence in the two conformations for the two models.

model		Site	Configuration				Number of states per site	
							all	decreased
			11	10	01	00		
		Rieske center	Q/C	Q/C	Q/C	Q/C	12	7
		heme c_1	Q/C	Q/C	Q/C	Q/C	2	2
	I	Q_o	Q/C	-/-	Q/C	-/-	12	7
II		heme b_L	Q/C	Q/C	Q/C	Q/C	2	2
		heme b_H	Q/C	Q/C	Q/C	Q/C	2	2
		Glu295	Q/C	Q/C	Q/C	Q/C	2	2
		Q_i	Q/C	Q/C	-/-	-/-	12	7
		Asp252	Q/C	Q/C	Q/C	Q/C	2	2
		His217	Q/C	Q/C	Q/C	Q/C	4	4
Conformation Configuration			2	4		2		

The number of states for the different models can be calculate like this

$$
\begin{aligned}
&\underbrace{2 \cdot 2 \cdot 2 \cdot 2 \cdot 12 \cdot 12 \cdot 12}_{\text{Number of states per site}} \cdot \underbrace{2}_{\text{Conformation Configuration}} \\
&+ \underbrace{2 \cdot 2 \cdot 2 \cdot 2 \cdot 12 \cdot 12}_{\text{Number of states per site}} \cdot \underbrace{4}_{\text{Conformation Configuration}} \\
&+ \underbrace{2 \cdot 2 \cdot 2 \cdot 2 \cdot 12}_{\text{Number of states per site}} \cdot \underbrace{2}_{\text{Conformation Configuration}} \\
&= 64,896
\end{aligned}
$$

and this

$$\begin{aligned}
&\underbrace{2\cdot 2\cdot 2\cdot 2\cdot 7\cdot 9\cdot 9}_{\text{Number of states per site}}\cdot \underbrace{2}_{\text{Conformation Configuration}}\\
&+\underbrace{2\cdot 2\cdot 2\cdot 2\cdot 7\cdot 9}_{\text{Number of states per site}}\cdot \underbrace{4}_{\text{Conformation Configuration}}\\
&+\underbrace{2\cdot 2\cdot 2\cdot 2\cdot 7}_{\text{Number of states per site}}\cdot \underbrace{2}_{\text{Conformation Configuration}}\\
&=22,400
\end{aligned}$$

for model I and like this

$$\begin{aligned}
&\underbrace{2\cdot 4\cdot 2\cdot 2\cdot 2\cdot 2\cdot 12\cdot 12\cdot 12}_{\text{Number of states per site}}\cdot \underbrace{2}_{\text{Conformation Configuration}}\\
&+\underbrace{2\cdot 4\cdot 2\cdot 2\cdot 2\cdot 2\cdot 12\cdot 12}_{\text{Number of states per site}}\cdot \underbrace{4}_{\text{Conformation Configuration}}\\
&+\underbrace{2\cdot 4\cdot 2\cdot 2\cdot 2\cdot 2\cdot 12}_{\text{Number of states per site}}\cdot \underbrace{2}_{\text{Conformation Configuration}}\\
&=519,168
\end{aligned}$$

and this

$$\begin{aligned}
&\underbrace{2\cdot 4\cdot 2\cdot 2\cdot 2\cdot 2\cdot 7\cdot 9\cdot 9}_{\text{Number of states per site}}\cdot \underbrace{2}_{\text{Conformation Configuration}}\\
&+\underbrace{2\cdot 4\cdot 2\cdot 2\cdot 2\cdot 2\cdot 7\cdot 9}_{\text{Number of states per site}}\cdot \underbrace{4}_{\text{Conformation Configuration}}\\
&+\underbrace{2\cdot 4\cdot 2\cdot 2\cdot 2\cdot 2\cdot 7}_{\text{Number of states per site}}\cdot \underbrace{2}_{\text{Conformation Configuration}}\\
&=179,200
\end{aligned}$$

for model II.

Table G.2: Set protonation states for all titratable sites, except heme b_L, b_H and c, ubiquinone/ubiquinol and Rieske centers in the bc_1complex. - Part 1

Site	Configuration	Site	Configuration	Site	Configuration
B:5:HIS-HIS.xst	HSE	E:52:GLU-GLU.xst	GLUD	B:82:GLU-GLU.xst	GLUD
E:5:HIS-HIS.xst	HSE	B:52:GLU-GLU.xst	GLUD	E:82:GLU-GLU.xst	GLUD
D:6:HIS-HIS.xst	HSD	C:53:ASP-ASP.xst	ASPD	A:82:HIS-HIS.xst	HSE
A:6:HIS-HIS.xst	HSD	F:53:ASP-ASP.xst	ASPD	D:82:HIS-HIS.xst	HSE
A:7:ASP-ASP.xst	ASPD	A:54:CYS-CYS.xst	CYSP	C:83:GLU-GLU.xst	GLUD
E:7:GLU-GLU.xst	GLUD	D:54:CYS-CYS.xst	CYSP	F:83:GLU-GLU.xst	GLUD
B:7:GLU-GLU.xst	GLUD	E:57:GLU-GLU.xst	GLUD	E:84:LYS-LYS.xst	LYSP
D:7:ASP-ASP.xst	ASPD	B:57:GLU-GLU.xst	GLUD	B:84:LYS-LYS.xst	LYSP
B:8:ASP-ASP.xst	ASPP	F:58:GLU-GLU.xst	GLUD	A:85:ARG-ARG.xst	ARGP
A:8:HIS-HIS.xst	HSE	C:58:GLU-GLU.xst	GLUD	D:85:ARG-ARG.xst	ARGP
D:8:HIS-HIS.xst	HSD	E:60:GLU-GLU.xst	GLUD	C:86:ARG-ARG.xst	ARGP
E:8:ASP-ASP.xst	ASPP	B:60:GLU-GLU.xst	GLUD	F:86:ARG-ARG.xst	ARGP
D:10:GLU-GLU.xst	GLUD	E:61:ASP-ASP.xst	ASPD	E:87:ASP-ASP.xst	ASPD
A:10:GLU-GLU.xst	GLUD	B:61:ASP-ASP.xst	ASPD	B:87:ASP-ASP.xst	ASPD
F:11:ARG-ARG.xst	ARGP	B:64:ARG-ARG.xst	ARGP	B:88:HIS-HIS.xst	HSD
C:11:ARG-ARG.xst	ARGP	E:64:ARG-ARG.xst	ARGP	E:88:HIS-HIS.xst	HSD
F:12:ARG-ARG.xst	ARGP	C:66:LYS-LYS.xst	LYSP	B:91:HIS-HIS.xst	HSP
C:12:ARG-ARG.xst	ARGP	F:66:LYS-LYS.xst	LYSP	E:91:HIS-HIS.xst	HSP
A:12:ARG-ARG.xst	ARGP	A:68:HIS-HIS.xst	HSE	A:94:ARG-ARG.xst	ARGP
D:12:ARG-ARG.xst	ARGP	D:68:HIS-HIS.xst	HSE	D:94:ARG-ARG.xst	ARGP
F:13:ASP-ASP.xst	ASPD	F:70:LYS-LYS.xst	LYSP	F:95:ASP-ASP.xst	ASPD
C:13:ASP-ASP.xst	ASPD	C:70:LYS-LYS.xst	LYSP	C:95:ASP-ASP.xst	ASPD
E:14:GLU-GLU.xst	GLUP	A:72:HIS-HIS.xst	HSE	E:95:GLU-GLU.xst	GLUD
B:14:GLU-GLU.xst	GLUP	D:72:HIS-HIS.xst	HSE	B:95:GLU-GLU.xst	GLUD
D:16:GLU-GLU.xst	GLUD	B:74:ASP-ASP.xst	ASPD	C:99:ARG-ARG.xst	ARGP
A:16:GLU-GLU.xst	GLUD	D:74:ASP-ASP.xst	ASPD	B:99:ASP-ASP.xst	ASPD
D:17:LYS-LYS.xst	LYSP	A:74:ASP-ASP.xst	ASPD	E:99:ASP-ASP.xst	ASPD
A:17:LYS-LYS.xst	LYSP	E:74:ASP-ASP.xst	ASPD	F:99:ARG-ARG.xst	ARGP
D:20:HIS-HIS.xst	HSE	B:75:GLU-GLU.xst	GLUD	C:104:ASP-ASP.xst	ASPD
A:20:HIS-HIS.xst	HSE	C:75:ARG-ARG.xst	ARGP	F:104:ASP-ASP.xst	ASPD
B:21:ASP-ASP.xst	ASPD	F:75:ARG-ARG.xst	ARGP	E:105:LYS-LYS.xst	LYSP
E:21:ASP-ASP.xst	ASPD	E:75:GLU-GLU.xst	GLUD	B:105:LYS-LYS.xst	LYSP
A:22:ARG-ARG.xst	ARGP	E:76:GLU-GLU.xst	GLUD	E:107:ARG-ARG.xst	ARGP
D:22:ARG-ARG.xst	ARGP	F:76:ARG-ARG.xst	ARGP	B:107:ARG-ARG.xst	ARGP
B:23:HIS-HIS.xst	HSP	B:76:GLU-GLU.xst	GLUD	F:108:GLU-GLU.xst	GLUD
E:23:HIS-HIS.xst	HSP	C:76:ARG-ARG.xst	ARGP	C:108:GLU-GLU.xst	GLUD
B:27:ARG-ARG.xst	ARGP	C:77:ARG-ARG.xst	ARGP	E:111:HIS-HIS.xst	HSE
E:27:ARG-ARG.xst	ARGP	F:77:ARG-ARG.xst	ARGP	C:111:ASP-ASP.xst	ASPD
D:31:ASP-ASP.xst	ASPD	C:79:GLU-GLU.xst	GLUD	B:111:HIS-HIS.xst	HSE
A:31:ASP-ASP.xst	ASPD	F:79:GLU-GLU.xst	GLUD	F:111:ASP-ASP.xst	ASPD
B:34:GLU-GLU.xst	GLUD	E:79:GLU-GLU.xst	GLUD	C:114:ARG-ARG.xst	ARGP
E:34:GLU-GLU.xst	GLUD	B:79:GLU-GLU.xst	GLUD	D:114:ARG-ARG.xst	ARGP
D:39:ARG-ARG.xst	ARGP	B:80:ASP-ASP.xst	ASPD	A:114:ARG-ARG.xst	ARGP
A:39:ARG-ARG.xst	ARGP	E:80:ASP-ASP.xst	ASPD	F:114:ARG-ARG.xst	ARGP
F:43:ASP-ASP.xst	ASPD	F:81:ASP-ASP.xst	ASPD	F:117:ASP-ASP.xst	ASPD
B:43:LYS-LYS.xst	LYSP	D:81:GLU-GLU.xst	GLUD	C:117:ASP-ASP.xst	ASPD
C:43:ASP-ASP.xst	ASPD	A:81:GLU-GLU.xst	GLUD	F:118:GLU-GLU.xst	GLUD
E:43:LYS-LYS.xst	LYSP	B:81:ARG-ARG.xst	ARGP	C:118:GLU-GLU.xst	GLUD
B:48:ARG-ARG.xst	ARGP	C:81:ASP-ASP.xst	ASPD	F:121:GLU-GLU.xst	GLUD
E:48:ARG-ARG.xst	ARGP	E:81:ARG-ARG.xst	ARGP	C:121:GLU-GLU.xst	GLUD

Table G.3: Set protonation states for all titratable sites, except heme b_L, b_H and c, ubiquinone/ubiquinol and Rieske centers in the bc_1complex. - Part 2

Site	Configuration	Site	Configuration	Site	Configuration
D:122:LYS-LYS.xst	LYSP	C:180:ASP-ASP.xst	ASPD	E:249:LYS-LYS.xst	LYSP
A:122:LYS-LYS.xst	LYSP	F:180:ASP-ASP.xst	ASPD	B:249:LYS-LYS.xst	LYSP
A:125:ARG-ARG.xst	ARGP	F:181:GLU-GLU.xst	GLUD	B:250:ARG-ARG.xst	ARGP
D:125:ARG-ARG.xst	ARGP	C:181:GLU-GLU.xst	GLUD	E:250:ARG-ARG.xst	ARGP
D:126:GLU-GLU.xst	GLUD	D:187:ASP-ASP.xst	ASPD	A:251:LYS-LYS.xst	LYSP
A:126:GLU-GLU.xst	GLUD	A:187:ASP-ASP.xst	ASPD	D:251:LYS-LYS.xst	LYSP
B:129:GLU-GLU.xst	GLUD	B:191:ASP-ASP.xst	ASPD	D:252:ASP-ASP.xst	ASPP
E:129:GLU-GLU.xst	GLUP	E:191:ASP-ASP.xst	ASPD	A:252:ASP-ASP.xst	ASPP
B:140:GLU-GLU.xst	GLUD	E:192:ASP-ASP.xst	ASPD	E:256:LYS-LYS.xst	LYSP
E:140:GLU-GLU.xst	GLUD	B:192:ASP-ASP.xst	ASPD	B:256:LYS-LYS.xst	LYSP
E:141:GLU-GLU.xst	GLUD	D:193:ARG-ARG.xst	ARGP	D:276:HIS-HIS.xst	HSE
B:141:GLU-GLU.xst	GLUD	A:193:ARG-ARG.xst	ARGP	A:276:HIS-HIS.xst	HSE
F:143:ASP-ASP.xst	ASPD	E:195:GLU-GLU.xst	GLUD	D:278:ASP-ASP.xst	ASPD
C:143:ASP-ASP.xst	ASPD	B:195:GLU-GLU.xst	GLUD	A:278:ASP-ASP.xst	ASPD
B:144:LYS-LYS.xst	LYSP	E:198:ASP-ASP.xst	ASPD	D:282:GLU-GLU.xst	GLUD
E:144:LYS-LYS.xst	LYSP	B:198:ASP-ASP.xst	ASPD	A:282:GLU-GLU.xst	GLUD
E:147:GLU-GLU.xst	GLUD	E:200:HIS-HIS.xst	HSP	D:287:ARG-ARG.xst	ARGP
B:147:GLU-GLU.xst	GLUD	B:200:HIS-HIS.xst	HSP	A:287:ARG-ARG.xst	ARGP
B:149:HIS-HIS.xst	HSD	B:201:ASP-ASP.xst	ASPD	D:291:HIS-HIS.xst	HSE
E:149:HIS-HIS.xst	HSD	E:201:ASP-ASP.xst	ASPD	A:291:HIS-HIS.xst	HSE
E:150:GLU-GLU.xst	GLUD	B:205:HIS-HIS.xst	HSP	A:295:GLU-GLU.xst	GLUP
B:150:GLU-GLU.xst	GLUD	E:205:HIS-HIS.xst	HSP	D:295:GLU-GLU.xst	GLUD
E:152:ASP-ASP.xst	ASPD	B:209:GLU-GLU.xst	GLUD	D:306:ARG-ARG.xst	ARGP
B:152:ASP-ASP.xst	ASPD	E:209:GLU-GLU.xst	GLUD	A:306:ARG-ARG.xst	ARGP
C:155:HIS-HIS.xst	HSE	B:210:ASP-ASP.xst	ASPD	D:311:ASP-ASP.xst	ASPD
F:155:HIS-HIS.xst	HSE	E:210:ASP-ASP.xst	ASPD	A:311:ASP-ASP.xst	ASPD
C:157:ASP-ASP.xst	ASPD	A:217:HIS-HIS.xst	HSE	A:327:ASP-ASP.xst	ASPD
F:157:ASP-ASP.xst	ASPD	D:217:HIS-HIS.xst	HSE	D:327:ASP-ASP.xst	ASPD
B:158:ARG-ARG.xst	ARGP	B:220:GLU-GLU.xst	GLUD	D:329:LYS-LYS.xst	LYSP
E:158:ARG-ARG.xst	ARGP	E:220:GLU-GLU.xst	GLUD	A:329:LYS-LYS.xst	LYSP
F:161:ARG-ARG.xst	ARGP	B:222:LYS-LYS.xst	LYSP	A:350:ASP-ASP.xst	ASPD
C:161:ARG-ARG.xst	ARGP	E:222:LYS-LYS.xst	LYSP	D:350:ASP-ASP.xst	ASPD
C:163:ARG-ARG.xst	ARGP	B:226:ARG-ARG.xst	ARGP	A:355:ARG-ARG.xst	ARGP
F:163:ARG-ARG.xst	ARGP	E:226:ARG-ARG.xst	ARGP	D:355:ARG-ARG.xst	ARGP
C:164:LYS-LYS.xst	LYSP	B:227:LYS-LYS.xst	LYSP	D:358:ARG-ARG.xst	ARGP
F:164:LYS-LYS.xst	LYSP	E:227:LYS-LYS.xst	LYSP	A:358:ARG-ARG.xst	ARGP
B:167:ASP-ASP.xst	ASPD	D:228:GLU-GLU.xst	GLUD	D:360:ARG-ARG.xst	ARGP
E:167:ASP-ASP.xst	ASPD	A:228:GLU-GLU.xst	GLUD	A:360:ARG-ARG.xst	ARGP
C:169:GLU-GLU.xst	GLUD	D:230:ARG-ARG.xst	ARGP	D:364:LYS-LYS.xst	LYSP
F:169:GLU-GLU.xst	GLUD	A:230:ARG-ARG.xst	ARGP	A:364:LYS-LYS.xst	LYSP
E:170:LYS-LYS.xst	LYSP	D:231:ARG-ARG.xst	ARGP	D:373:ASP-ASP.xst	ASPP
B:170:LYS-LYS.xst	LYSP	A:231:ARG-ARG.xst	ARGP	A:373:ASP-ASP.xst	ASPP
B:171:ASP-ASP.xst	ASPD	D:234:LYS-LYS.xst	LYSP	D:390:ASP-ASP.xst	ASPD
E:171:ASP-ASP.xst	ASPD	A:234:LYS-LYS.xst	LYSP	A:390:ASP-ASP.xst	ASPD
A:174:HIS-HIS.xst	HSD	D:236:GLU-GLU.xst	GLUD	A:415:GLU-GLU.xst	GLUD
D:174:HIS-HIS.xst	HSD	A:236:GLU-GLU.xst	GLUD	D:415:GLU-GLU.xst	GLUD
E:176:LYS-LYS.xst	LYSP	A:239:LYS-LYS.xst	LYSP	D:416:LYS-LYS.xst	LYSP
B:176:LYS-LYS.xst	LYSP	D:239:LYS-LYS.xst	LYSP	A:416:LYS-LYS.xst	LYSP
C:177:LYS-LYS.xst	LYSP	A:240:ASP-ASP.xst	ASPD	A:425:GLU-GLU.xst	GLUD
F:177:LYS-LYS.xst	LYSP	D:240:ASP-ASP.xst	ASPD	D:425:GLU-GLU.xst	GLUD

Table G.4: Set protonation states for all titratable sites, except heme b_L, b_H and c, ubiquinone/ubiquinol and Rieske centers in the bc_1complex. - Part 3

Site	Configuration	Site	Configuration	Site	Configuration
D:426:GLU-GLU.xst	GLUD				
A:426:GLU-GLU.xst	GLUD				
A:427:ASP-ASP.xst	ASPD				
D:427:ASP-ASP.xst	ASPD				
I:501:HEM-PROPA-Hem.xst	PropAD				
I:501:HEM-PROPD-Hem.xst	PropD				
I:502:HEM-PROPA-Hem.xst	PropAD				
I:502:HEM-PROPD-Hem.xst	PropD				
J:301:HEM-PROPA-Hem.xst	PropAD				
J:301:HEM-PROPD-Hem.xst	PropD				

Table G.5: Calculated fluxes $\left[\frac{M}{s}\right]$, steady-state concentrations $[M]$ and rate constants $\left[\frac{1}{s}\right]$ for model V-I.1 - Part 1
"->": Transition between two states
"=": separation between two sites, if two sites are involved and no pool.

#LABEL	Netto Flux	Forward Flux	Backward Flux	SSconcA	SSconcB	Forward Rates	Backward Rates
4::HemOx:0:0:0->HemRed:0:1:0	-2.03E+01	1.17E+05	1.17E+05	7.73E-01	2.27E-01	1.55E+05	5.130E+05
5::RIO2:1:0:0->RIOP:2:0:0	-2.02E+01	9.77E+04	9.78E+04	1.91E-01	7.18E-01	5.13E+05	1.827E+05
4::HemRed:0:1:0->HemOx:0:0:0=5::RIOP:2:0:0->RRHP:2:1:0	-2.02E+01	6.36E+02	6.57E+02	1.74E-01	1.28E-03	5.13E+05	3.770E+03
5::RRHP:2:1:0->RIO2:1:0:0=6::U1PD:1:1:1->U2PP:2:2:1	-1.46E+01	3.96E+01	5.42E+01	9.19E-05	1.86E-04	1.98E+05	5.130E+05
1::GLUD:0:0:0->GLUP:1:0:0=6::U2PP:2:2:1->U2PD:1:2:1	-1.07E+01	3.51E+01	4.58E+01	2.31E-01	8.92E-05	7.09E+01	5.130E+05
3::HemOx:0:0:0->HemRed:0:1:0=6::U2PD:1:2:1->U1PD:1:1:1	-1.07E+01	3.40E+02	3.51E+02	7.64E-04	1.05E-03	5.13E+05	1.041E+05
2::HemOx:0:0:0->HemRed:0:1:0=3::HemRed:0:1:0->HemOx:0:0:0	-9.40E+00	2.93E+03	2.94E+03	5.71E-03	6.06E-01	5.13E+05	1.016E+02
1::GLUP:1:0:0->GLUD:0:0:0	-9.40E+00	4.03E+03	4.03E+03	1.33E-02	3.23E-02	7.32E+04	5.130E+05
Q11->Q10=6::U2PP:2:2:1->EMPTY	-7.33E+00	4.77E+03	4.77E+03	1.94E-02	1.35E-02	5.13E+05	5.872E+04
Q10->C10	-6.21E+00	6.26E+03	6.27E+03	1.35E-02	2.59E-02	2.90E+04	5.130E+05
C11->Q11	-6.11E+00	1.26E+04	1.26E+04	7.87E-01	2.46E-02	8.03E+04	5.130E+05
2::HemRed:0:1:0->HemOx:0:0:0=7::U0DD:0:0:1->U1DD:0:1:1	-4.70E+00	9.79E-04	4.70E+00	1.31E-01	9.17E-06	3.85E-03	5.130E+05
C11->C01=7::U2PP:2:2:1->EMPTY	-4.47E+00	7.12E+04	7.12E+04	6.60E-01	1.39E-01	5.13E+05	8.908E+04
C01->C11=7::EMPTY->U0DD:0:0:1	-4.36E+00	6.51E+04	6.51E+04	1.39E-01	1.27E-01	3.15E+05	5.130E+05
5::RRHP:2:1:0->RIO2:1:0:0=6::U1DP:1:1:1->U2PP:2:2:1	-4.03E+00	4.57E+00	8.60E+00	8.91E-06	1.86E-04	3.86E+04	5.130E+05
3::HemRed:0:1:0->HemOx:0:0:0=6::U0DD:0:0:1->U1DD:0:1:1	-3.82E+00	5.53E-03	3.82E+00	1.34E-02	7.45E-06	5.13E+05	8.565E-02
1::GLUP:1:0:0->GLUD:0:0:0=6::U1DD:0:1:1->U1PD:1:1:1	-3.80E+00	5.11E+02	5.15E+02	8.46E-03	1.02E-03	5.13E+05	4.493E+05
C10->C11=6::EMPTY->U0DD:0:0:1	-3.54E+00	5.72E+03	5.73E+03	2.59E-02	2.40E-02	5.13E+05	3.446E+05
C10->C11=6::EMPTY->U2PP:2:2:1	-2.68E+00	1.33E+04	1.33E+04	2.59E-02	7.45E-01	5.13E+05	1.107E+04
1::GLUD:0:0:0->GLUP:1:0:0=6::U2PP:2:2:1->U2DP:1:2:1	-2.53E+00	1.16E+00	3.69E+00	2.31E-01	7.20E-06	2.02E+00	5.130E+05
3::HemOx:0:0:0->HemRed:0:1:0=6::U2DP:1:2:1->U1DP:1:1:1	-2.53E+00	2.57E+00	5.10E+00	7.11E-06	2.33E-04	5.13E+05	1.528E+02
7::U2DP:1:2:1->U2PP:2:2:1	-2.37E+00	1.39E+01	1.63E+01	2.72E-05	7.13E-01	5.13E+05	4.024E+02
2::HemRed:0:1:0->HemOx:0:0:0=7::U1DP:1:1:1->U2DP:1:2:1	-2.37E+00	1.10E+01	1.34E+01	2.10E-04	2.60E-05	3.70E+04	5.130E+05
7::U1DD:0:1:1->U1DP:1:1:1	-2.37E+00	1.99E+01	2.23E+01	4.71E-05	2.12E-04	1.71E+04	5.130E+05
7::U2PD:1:2:1->U2PP:2:2:1	-2.33E+00	1.56E+01	1.79E+01	3.04E-05	7.13E-01	5.13E+05	3.904E+02
2::HemRed:0:1:0->HemOx:0:0:0=7::U1PD:1:1:1->U2PD:1:2:1	-2.33E+00	1.12E+01	1.36E+01	2.95E-04	2.64E-05	2.60E+04	5.130E+05
7::U1DD:0:1:1->U1PD:1:1:1	-2.33E+00	1.98E+01	2.22E+01	4.71E-05	2.96E-04	1.22E+04	5.130E+05
5::RRHP:2:1:0->RIO2:1:0:0=6::U0DD:0:0:1->U1DP:1:1:1	-1.48E+00	9.59E-10	1.48E+00	5.65E-05	2.89E-06	5.13E+05	2.732E-05
Q01->Q00=6::U2PP:2:2:1->EMPTY	-1.21E+00	7.61E+02	7.62E+02	3.12E-03	2.16E-03	5.13E+05	4.984E+04
Q10->Q11=6::EMPTY->U0DD:0:0:1	-1.13E+00	6.70E+02	6.71E+02	1.35E-02	3.36E-03	5.13E+05	2.055E+05
C01->Q01	-1.13E+00	2.04E+03	2.04E+03	1.39E-01	3.98E-03	7.47E+04	5.130E+05
Q00->C00	-1.02E+00	1.00E+03	1.00E+03	2.16E-03	4.13E-03	4.92E+04	5.130E+05
C00->C01=6::EMPTY->U0DD:0:0:1	-5.88E-01	9.49E+02	9.50E+02	4.13E-03	4.24E-03	5.13E+05	3.272E+05
C00->C01=6::EMPTY->U2PP:2:2:1	-4.28E-01	2.12E+03	2.12E+03	4.13E-03	1.31E-01	5.13E+05	1.057E+04
Q01->Q11=7::EMPTY->U0DD:0:0:1	-2.09E-01	1.99E+03	1.99E+03	3.98E-03	4.01E-03	3.38E+05	5.130E+05
Q00->Q01=6::EMPTY->U0DD:0:0:1	-1.82E-01	1.09E+02	1.09E+02	2.16E-03	5.44E-04	5.13E+05	2.011E+05
5::RRHP:2:1:0->RIO2:1:0:0=6::U0DD:0:0:1->U1PD:1:1:1	-1.42E-01	1.62E-10	1.42E-01	5.65E-05	2.76E-07	5.13E+05	3.525E-06
Q11->Q01=7::U2PP:2:2:1->EMPTY	-1.13E-01	2.04E+03	2.04E+03	2.06E-02	3.98E-03	5.13E+05	8.380E+04
C00->C10=7::EMPTY->U0DD:0:0:1	-9.13E-02	2.05E+03	2.05E+03	4.13E-03	4.05E-03	3.57E+05	5.130E+05
C10->C00=7::U2PP:2:2:1->EMPTY	-8.38E-02	2.12E+03	2.12E+03	2.18E-02	4.13E-03	5.13E+05	8.004E+04
Q00->Q10=7::EMPTY->U0DD:0:0:1	-4.33E-02	1.07E+03	1.07E+03	2.16E-03	2.11E-03	3.46E+05	5.130E+05
5::RRH2:1:1:0->RRHP:2:1:0	-3.88E-02	2.64E+00	2.68E+00	5.14E-06	1.61E-03	5.13E+05	2.237E+03
4::HemRed:0:1:0->HemOx:0:0:0=5::RIO2:1:0:0->RRH2:1:1:0	-3.88E-02	2.23E+00	2.27E+00	3.34E-02	4.42E-06	5.13E+05	6.329E+01
Q10->Q00=7::U2PP:2:2:1->EMPTY	-3.68E-02	1.11E+03	1.11E+03	1.13E-02	2.16E-03	5.13E+05	8.055E+04
5::RRH1:1:1:0->RRHP:2:1:0	-1.79E-02	1.26E+00	1.28E+00	2.46E-06	1.61E-03	5.13E+05	1.071E+03
5::RIOP:2:0:0->RIO1:1:0:0	-1.79E-02	2.32E+04	2.32E+04	7.18E-01	4.53E-02	5.13E+05	3.503E+04
4::HemRed:0:1:0->HemOx:0:0:0=5::RIO1:1:0:0->RRH1:1:1:0	-1.79E-02	1.03E+00	1.05E+00	9.45E-03	2.04E-06	5.13E+05	1.037E+02
1::GLUP:1:0:0->GLUD:0:0:0=6::U1DD:0:1:1->U1DP:1:1:1	-1.40E-02	3.24E+01	3.25E+01	8.46E-03	6.33E-05	5.13E+05	8.864E+04
5::RRHP:2:1:0->RIO2:1:0:0=6::U1DD:0:1:1->U2DP:1:2:1	-3.99E-06	1.90E-07	4.17E-06	9.20E-07	8.14E-12	5.13E+05	3.042E-01
1::GLUD:0:0:0->GLUP:1:0:0=6::U1PP:2:1:1->U1DP:1:1:1	-2.70E-06	2.01E-05	2.28E-05	3.92E-11	1.10E-02	5.13E+05	2.905E-03
1::GLUP:1:0:0->GLUD:0:0:0=6::U1PD:1:1:1->U1PP:2:1:1	-2.66E-06	1.75E-05	2.01E-05	1.98E-03	3.92E-11	5.13E+05	1.825E-03
3::HemOx:0:0:0->HemRed:0:1:0=6::U2PP:2:2:1->U1PP:2:1:1	-3.95E-08	6.31E-09	4.58E-08	5.93E-01	8.93E-14	1.89E-09	5.130E+05
5::RRHP:2:1:0->RIO2:1:0:0=6::U1DD:0:1:1->U2PD:1:2:1	-6.50E-10	8.63E-11	7.36E-10	9.20E-07	1.44E-15	5.13E+05	1.125E-04
5::RRH2:1:1:0->RRHT:0:1:0	-5.02E-10	2.58E-06	2.58E-06	5.14E-06	5.03E-12	5.13E+05	6.496E-01
5::RRHT:0:1:0->RRH1:1:1:0	-4.85E-10	2.58E-06	2.58E-06	5.03E-12	2.46E-06	5.13E+05	8.728E-01
3::HemRed:0:1:0->HemOx:0:0:0=6::U1DD:0:1:1->U2DD:0:2:1	-6.96E-12	1.57E-08	1.57E-08	8.45E-03	3.07E-14	5.13E+05	4.807E-07

Table G.6: Calculated fluxes $\left[\frac{M}{s}\right]$, steady-state concentrations $[M]$ and rate constants $\left[\frac{1}{s}\right]$ for model V-I.1 - Part 2
"->": Transition between two states
"=": separation between two sites, if two sites are involved and no pool.

#LABEL	Netto Flux	Forward Flux	Backward Flux	SSconcA	SSconcB	Forward Rates	Backward Rates
7::U1PD:1:1:1->U1PP:2:1:1	-6.74E-12	1.26E-11	1.93E-11	2.96E-04	3.76E-17	3.33E-08	5.130E+05
7::U1DP:1:1:1->U1PP:2:1:1	-6.72E-12	1.26E-11	1.93E-11	2.12E-04	3.76E-17	4.58E-08	5.130E+05
7::U2DP:1:2:1->U2DD:0:2:1	-4.72E-12	4.39E-13	5.16E-12	2.72E-05	1.01E-17	5.13E+05	2.045E-08
7::U2PD:1:2:1->U2DD:0:2:1	-4.72E-12	4.38E-13	5.16E-12	3.04E-05	1.01E-17	5.13E+05	2.118E-08
1::GLUD:0:0:0->GLUP:1:0:0=6::U2PD:1:2:1->U2DD:0:2:1	-3.78E-12	1.59E-08	1.59E-08	6.88E-04	3.10E-14	1.73E-05	5.130E+05
2::HemRed:0:1:0->HemOx:0:0:0=7::U1DD:0:1:1->U2DD:0:2:1	-2.26E-12	3.21E-13	2.59E-12	3.80E-05	5.04E-18	6.22E-09	5.130E+05
2::HemRed:0:1:0->HemOx:0:0:0=7::U1PP:2:1:1->U2PP:2:2:1	-1.75E-12	1.69E-11	1.87E-11	3.29E-17	5.13E-02	5.13E+05	4.907E-10
1::GLUD:0:0:0->GLUP:1:0:0=6::U2DP:1:2:1->U2DD:0:2:1	-9.71E-13	1.59E-08	1.59E-08	8.15E-08	3.10E-14	9.93E-02	5.130E+05
1::GLUP:1:0:0->GLUD:0:0:0=6::U2DD:0:2:1->U2DP:1:2:1	9.71E-13	1.59E-08	1.59E-08	3.10E-14	8.15E-08	9.08E-02	5.130E+05
2::HemOx:0:0:0->HemRed:0:1:0=7::U2PP:2:2:1->U1PP:2:1:1	1.75E-12	1.87E-11	1.69E-11	5.13E-02	3.29E-17	5.13E+05	5.119E-10
2::HemOx:0:0:0->HemRed:0:1:0=7::U2DD:0:2:1->U1DD:0:1:1	2.26E-12	2.59E-12	3.21E-13	5.04E-18	3.80E-05	6.50E-09	5.130E+05
1::GLUP:1:0:0->GLUD:0:0:0=6::U2DD:0:2:1->U2PD:1:2:1	3.78E-12	1.59E-08	1.59E-08	3.10E-14	6.88E-04	1.64E-05	5.130E+05
7::U2DD:0:2:1->U2DP:1:2:1	4.72E-12	5.16E-12	4.39E-13	1.01E-17	2.72E-05	5.13E+05	2.045E-08
7::U2DD:0:2:1->U2PD:1:2:1	4.72E-12	5.16E-12	4.38E-13	1.01E-17	3.04E-05	5.13E+05	2.118E-08
7::U1PP:2:1:1->U1DP:1:1:1	6.72E-12	1.93E-11	1.26E-11	3.76E-17	2.12E-04	1.96E-10	5.130E+05
7::U1PP:2:1:1->U1PD:1:1:1	6.74E-12	1.93E-11	1.26E-11	3.76E-17	2.96E-04	2.75E-10	5.130E+05
3::HemOx:0:0:0->HemRed:0:1:0=6::U2DD:0:2:1->U1DD:0:1:1	6.96E-12	1.57E-08	1.57E-08	3.07E-14	8.45E-03	5.13E+05	3.768E-07
5::RRH1:1:1:0->RRHT:0:1:0	4.85E-10	2.58E-06	2.58E-06	2.46E-06	5.03E-12	5.13E+05	1.357E+00
5::RRHT:0:1:0->RRH2:1:1:0	5.02E-10	2.58E-06	2.58E-06	5.03E-12	5.14E-06	5.13E+05	5.144E-01
5::RIO2:1:0:0->RRHP:2:1:0=6::U2PD:1:2:1->U1DD:0:1:1	6.50E-10	7.36E-10	8.63E-11	1.44E-15	9.20E-07	5.13E+05	1.113E-04
3::HemRed:0:1:0->HemOx:0:0:0=6::U1PP:2:1:1->U2PP:2:2:1	3.95E-08	4.58E-08	6.31E-09	8.93E-14	5.93E-01	2.42E-09	5.130E+05
1::GLUD:0:0:0->GLUP:1:0:0=6::U1PP:2:1:1->U1PD:1:1:1	2.66E-06	2.01E-05	1.75E-05	3.92E-11	1.98E-03	5.13E+05	1.715E-02
1::GLUP:1:0:0->GLUD:0:0:0=6::U1DP:1:1:1->U1PP:2:1:1	2.70E-06	2.28E-05	2.01E-05	1.10E-02	3.92E-11	5.13E+05	5.095E-04
5::RIO2:1:0:0->RRHP:2:1:0=6::U2DP:1:2:1->U1DD:0:1:1	3.99E-06	4.17E-06	1.90E-07	8.14E-12	9.20E-07	5.13E+05	2.917E-01
1::GLUD:0:0:0->GLUP:1:0:0=6::U1DP:1:1:1->U1DD:0:1:1	1.40E-02	3.25E+01	3.24E+01	6.33E-05	8.46E-03	5.13E+05	8.164E+04
5::RIO1:1:0:0->RIOP:2:0:0	1.79E-02	2.32E+04	2.32E+04	4.53E-02	7.18E-01	5.13E+05	4.300E+04
4::HemOx:0:0:0->HemRed:0:1:0=5::RRH1:1:1:0->RIO1:1:0:0	1.79E-02	1.05E+00	1.03E+00	2.04E-06	9.45E-03	5.13E+05	1.152E+02
5::RRHP:2:1:0->RRH1:1:1:0	1.79E-02	1.28E+00	1.26E+00	1.61E-03	2.46E-06	5.13E+05	8.212E+02
Q00->Q10=7::EMPTY->U2PP:2:2:1	3.68E-02	1.11E+03	1.11E+03	2.16E-03	1.13E-02	5.13E+05	8.227E+04
4::HemOx:0:0:0->HemRed:0:1:0=5::RRH2:1:1:0->RIO2:1:0:0	3.88E-02	2.27E+00	2.23E+00	4.42E-06	3.34E-02	5.13E+05	7.011E+01
5::RRHP:2:1:0->RRH2:1:1:0	3.88E-02	2.68E+00	2.64E+00	1.61E-03	5.14E-06	5.13E+05	1.393E+03
Q10->Q00=7::U0DD:0:0:1->EMPTY	4.33E-02	1.07E+03	1.07E+03	2.11E-03	2.16E-03	3.57E+05	5.130E+05
C00->C10=7::EMPTY->U2PP:2:2:1	8.38E-02	2.12E+03	2.12E+03	4.13E-03	2.18E-02	5.13E+05	7.974E+04
C10->C00=7::U0DD:0:0:1->EMPTY	9.13E-02	2.05E+03	2.05E+03	4.05E-03	4.13E-03	3.55E+05	5.130E+05
Q01->Q11=7::EMPTY->U2PP:2:2:1	1.13E-01	2.04E+03	2.04E+03	3.98E-03	2.06E-02	5.13E+05	8.380E+04
5::RIO2:1:0:0->RRHP:2:1:0=6::U1PD:1:1:1->U0DD:0:0:1	1.42E-01	1.42E-01	1.62E-10	2.76E-07	5.65E-05	5.13E+05	3.525E-06
Q01->Q00=6::U0DD:0:0:1->EMPTY	1.82E-01	1.09E+02	1.09E+02	5.44E-04	2.16E-03	5.13E+05	3.153E+05
Q11->Q01=7::U0DD:0:0:1->EMPTY	2.09E-01	1.99E+03	1.99E+03	4.01E-03	3.98E-03	3.38E+05	5.130E+05
C01->C00=6::U2PP:2:2:1->EMPTY	4.28E-01	2.12E+03	2.12E+03	1.31E-01	4.13E-03	5.13E+05	9.867E+03
C01->C00=6::U0DD:0:0:1->EMPTY	5.88E-01	9.50E+02	9.49E+02	4.24E-03	4.13E-03	5.13E+05	3.054E+05
C00->Q00	1.02E+00	1.00E+03	1.00E+03	4.13E-03	2.16E-03	2.90E+04	5.130E+05
Q01->C01	1.13E+00	2.04E+03	2.04E+03	3.98E-03	1.39E-01	3.01E+04	5.130E+05
Q11->Q10=6::U0DD:0:0:1->EMPTY	1.13E+00	6.71E+02	6.70E+02	3.36E-03	1.35E-02	5.13E+05	2.055E+05
Q00->Q01=6::EMPTY->U2PP:2:2:1	1.21E+00	7.62E+02	7.61E+02	2.16E-03	3.12E-03	5.13E+05	5.748E+04
5::RIO2:1:0:0->RRHP:2:1:0=6::U1DP:1:1:1->U0DD:0:0:1	1.48E+00	1.48E+00	9.59E-10	2.89E-06	5.65E-05	5.13E+05	2.732E-05
7::U2PP:2:2:1->U2PD:1:2:1	2.33E+00	1.79E+01	1.56E+01	7.13E-01	3.04E-05	5.13E+05	3.992E+02
7::U1PD:1:1:1->U1DD:0:1:1	2.33E+00	2.22E+01	1.98E+01	2.96E-04	4.71E-05	1.19E+04	5.130E+05
2::HemOx:0:0:0->HemRed:0:1:0=7::U2PD:1:2:1->U1PD:1:1:1	2.33E+00	1.36E+01	1.12E+01	2.64E-05	2.95E-04	2.60E+04	5.130E+05
7::U2PP:2:2:1->U2DP:1:2:1	2.37E+00	1.63E+01	1.39E+01	7.13E-01	2.72E-05	5.13E+05	4.135E+02
7::U1DP:1:1:1->U1DD:0:1:1	2.37E+00	2.23E+01	1.99E+01	2.12E-04	4.71E-05	1.67E+04	5.130E+05
2::HemOx:0:0:0->HemRed:0:1:0=7::U2DP:1:2:1->U1DP:1:1:1	2.37E+00	1.34E+01	1.10E+01	2.60E-05	2.10E-04	3.70E+04	5.130E+05
1::GLUP:1:0:0->GLUD:0:0:0=6::U2DP:1:2:1->U2PP:2:2:1	2.53E+00	3.69E+00	1.16E+00	7.20E-06	2.31E-01	2.02E+00	5.130E+05
3::HemRed:0:1:0->HemOx:0:0:0=6::U1DP:1:1:1->U2DP:1:2:1	2.53E+00	5.10E+00	2.57E+00	2.33E-04	7.11E-06	5.13E+05	1.350E+04
C11->C10=6::U2PP:2:2:1->EMPTY	2.68E+00	1.33E+04	1.33E+04	7.45E-01	2.59E-02	5.13E+05	1.187E+04
C11->C10=6::U0DD:0:0:1->EMPTY	3.54E+00	5.73E+03	5.72E+03	2.40E-02	2.59E-02	5.13E+05	3.692E+05
1::GLUD:0:0:0->GLUP:1:0:0=6::U1PD:1:1:1->U1DD:0:1:1	3.80E+00	5.15E+02	5.11E+02	1.02E-03	8.46E-03	5.13E+05	4.173E+05
3::HemOx:0:0:0->HemRed:0:1:0=6::U1DD:0:1:1->U0DD:0:0:1	3.82E+00	3.82E+00	5.53E-03	7.45E-06	1.34E-02	5.13E+05	6.738E-02

Table G.7: Calculated fluxes $\left[\frac{M}{s}\right]$, steady-state concentrations $[M]$ and rate constants $\left[\frac{1}{s}\right]$ for model V-I.1 - Part 3
"->": Transition between two states
"=": separation between two sites, if two sites are involved and no pool.

#LABEL	Netto Flux	Forward Flux	Backward Flux	SSconcA	SSconcB	Forward Rates	Backward Rates
5::RIO2:1:0:0->RRHP:2:1:0=6::U2PP:2:2:1->U1DP:1:1:1	4.03E+00	8.60E+00	4.57E+00	1.86E-04	8.91E-06	1.81E+03	5.130E+05
C11->C01=7::U0DD:0:0:1->EMPTY	4.36E+00	6.51E+04	6.51E+04	1.27E-01	1.39E-01	3.16E+05	5.130E+05
C01->C11=7::EMPTY->U2PP:2:2:1	4.47E+00	7.12E+04	7.12E+04	1.39E-01	6.60E-01	5.13E+05	8.947E+04
2::HemOx:0:0:0->HemRed:0:1:0=7::U1DD:0:1:1->U0DD:0:0:1	4.70E+00	4.70E+00	9.79E-04	9.17E-06	1.31E-01	3.85E-03	5.130E+05
Q11->C11	6.11E+00	1.26E+04	1.26E+04	2.46E-02	7.87E-01	8.03E+04	5.130E+05
C10->Q10	6.21E+00	6.27E+03	6.26E+03	2.59E-02	1.35E-02	4.79E+04	5.130E+05
Q10->Q11=6::EMPTY->U2PP:2:2:1	7.33E+00	4.77E+03	4.77E+03	1.35E-02	1.94E-02	5.13E+05	5.872E+04
1::GLUD:0:0:0->GLUP:1:0:0	9.40E+00	4.03E+03	4.03E+03	3.23E-02	1.33E-02	5.16E+04	5.130E+05
2::HemRed:0:1:0->HemOx:0:0:0=3::HemOx:0:0:0->HemRed:0:1:0	9.40E+00	2.94E+03	2.93E+03	6.06E-01	5.71E-03	5.13E+05	1.273E+04
1::GLUP:1:0:0->GLUD:0:0:0=6::U2PD:1:2:1->U2PP:2:2:1	1.07E+01	4.58E+01	3.51E+01	8.92E-05	2.31E-01	7.09E+01	5.130E+05
3::HemRed:0:1:0->HemOx:0:0:0=6::U1PD:1:1:1->U2PD:1:2:1	1.07E+01	3.51E+02	3.40E+02	1.05E-03	7.64E-04	1.55E+05	5.130E+05
5::RIO2:1:0:0->RRHP:2:1:0=6::U2PP:2:2:1->U1PD:1:1:1	1.46E+01	5.42E+01	3.96E+01	1.86E-04	9.19E-05	5.13E+05	1.116E+05
4::HemOx:0:0:0->HemRed:0:1:0=5::RRHP:2:1:0->RIOP:2:0:0	2.02E+01	6.57E+02	6.36E+02	1.28E-03	1.74E-01	5.13E+05	3.520E+03
5::RIOP:2:0:0->RIO2:1:0:0	2.02E+01	9.78E+04	9.77E+04	7.18E-01	1.91E-01	5.13E+05	1.203E+05
4::HemRed:0:1:0->HemOx:0:0:0	2.03E+01	1.17E+05	1.17E+05	2.27E-01	7.73E-01	1.90E+05	5.130E+05

Table G.8: Calculated fluxes $\left[\frac{M}{s}\right]$, steady-state concentrations $[M]$ and rate constants $\left[\frac{1}{s}\right]$ for model V-I.2 - Part 1
"->": Transition between two states
"=": separation between two sites, if two sites are involved and no pool.

#LABEL	Netto Flux	Forward Flux	Backward Flux	SSconcA	SSconcB	Forward Rates	Backward Rates
4::HemOx:0:0:0->HemRed:0:1:0	-2.02E+01	1.18E+05	1.18E+05	7.71E-01	2.29E-01	1.55E+05	5.13E+05
5::RIO2:1:0:0->RIOP:2:0:0	-2.02E+01	9.93E+04	9.93E+04	1.94E-01	7.27E-01	5.13E+05	1.83E+05
4::HemRed:0:1:0->HemOx:0:0:0=5::RIOP:2:0:0->RRHP:2:1:0	-2.02E+01	6.45E+02	6.65E+02	1.78E-01	1.30E-03	5.13E+05	3.77E+03
5::RRHP:2:1:0->RIO2:1:0:0=6::U1PD:1:1:1->U2PP:2:2:1	-1.40E+01	3.97E+01	5.36E+01	1.07E-04	1.96E-04	1.98E+05	5.13E+05
3::HemRed:0:1:0->HemOx:0:0:0=6::U0DD:0:0:1->U1DD:0:1:1	-7.24E+00	4.10E-04	7.24E+00	1.03E-03	1.41E-05	5.13E+05	8.57E-02
1::GLUP:1:0:0->GLUD:0:0:0=6::U1DD:0:1:1->U1PD:1:1:1	-7.21E+00	2.08E+02	2.15E+02	3.36E-03	4.52E-04	5.13E+05	4.49E+05
1::GLUD:0:0:0->GLUP:1:0:0=6::U2PP:2:2:1->U2PD:1:2:1	-6.19E+00	4.32E+01	4.94E+01	3.95E-01	9.62E-05	7.09E+01	5.13E+05
3::HemOx:0:0:0->HemRed:0:1:0=6::U2PD:1:2:1->U1PD:1:1:1	-6.19E+00	1.43E+02	1.49E+02	3.57E-04	4.34E-04	5.13E+05	1.04E+05
Q01->Q00=6::U2PP:2:2:1->EMPTY	-4.66E+00	9.83E+02	9.87E+02	1.30E-02	2.30E-03	5.13E+05	9.30E+03
Q11->Q10=6::U2PP:2:2:1->EMPTY	-4.28E+00	8.62E+02	8.66E+02	1.17E-02	2.02E-03	5.13E+05	1.10E+04
C00->C01=6::EMPTY->U0DD:0:0:1	-3.73E+00	7.93E+02	7.97E+02	4.38E-03	2.72E-03	5.13E+05	3.27E+05
C10->C11=6::EMPTY->U0DD:0:0:1	-3.53E+00	6.79E+02	6.83E+02	3.83E-03	2.27E-03	5.13E+05	3.45E+05
C01->Q01	-3.42E+00	7.32E+03	7.33E+03	5.26E-01	1.43E-02	7.47E+04	5.13E+05
5::RRHP:2:1:0->RIO2:1:0:0=6::U1DP:1:1:1->U2PP:2:2:1	-3.39E+00	4.63E+00	8.01E+00	9.02E-06	1.96E-04	3.86E+04	5.13E+05
Q00->C00	-3.19E+00	1.07E+03	1.08E+03	2.30E-03	4.38E-03	4.92E+04	5.13E+05
Q10->C10	-2.94E+00	9.42E+02	9.45E+02	2.02E-03	3.83E-03	2.90E+04	5.13E+05
C11->Q11	-2.70E+00	6.60E+03	6.60E+03	4.34E-01	1.29E-02	8.03E+04	5.13E+05
5::RRHP:2:1:0->RIO2:1:0:0=6::U0DD:0:0:1->U1DP:1:1:1	-2.26E+00	4.09E-10	2.26E+00	2.05E-05	4.41E-06	5.13E+05	2.73E-05
Q00->Q01=6::EMPTY->U0DD:0:0:1	-1.48E+00	6.94E+01	7.09E+01	2.30E-03	3.07E-04	5.13E+05	2.01E+05
Q10->Q11=6::EMPTY->U0DD:0:0:1	-1.35E+00	6.39E+01	6.53E+01	2.02E-03	2.87E-04	5.13E+05	2.06E+05
1::GLUD:0:0:0->GLUP:1:0:0=6::U2PP:2:2:1->U2DP:1:2:1	-1.10E+00	1.73E+00	2.83E+00	3.95E-01	5.51E-06	2.02E+00	5.13E+05
3::HemOx:0:0:0->HemRed:0:1:0=6::U2DP:1:2:1->U1DP:1:1:1	-1.10E+00	1.81E+00	2.91E+00	5.47E-06	1.48E-04	5.13E+05	1.53E+02
C11->C10=6::U2PP:2:2:1->EMPTY	-6.34E-01	1.97E+03	1.97E+03	4.20E-01	3.83E-03	5.13E+05	2.22E+03
5::RRHP:2:1:0->RIO2:1:0:0=6::U0DD:0:0:1->U1PD:1:1:1	-5.76E-01	6.58E-11	5.76E-01	2.05E-05	1.12E-06	5.13E+05	3.53E-06
C01->C00=6::U2PP:2:2:1->EMPTY	-5.01E-01	2.25E+03	2.25E+03	5.10E-01	4.38E-03	5.13E+05	1.84E+03
Q01->Q11=7::EMPTY->U0DD:0:0:1	-2.40E-01	6.51E+03	6.51E+03	1.43E-02	1.29E-02	3.38E+05	5.13E+05
C11->C01=7::U0DD:0:0:1->EMPTY	-1.71E-01	2.22E+05	2.22E+05	4.33E-01	5.26E-01	3.16E+05	5.13E+05
2::HemOx:0:0:0->HemRed:0:1:0=3::HemRed:0:1:0->HemOx:0:0:0	-5.40E-02	1.92E+03	1.92E+03	3.74E-03	5.43E-01	5.13E+05	1.02E+02
1::GLUP:1:0:0->GLUD:0:0:0	-5.40E-02	8.96E+02	8.96E+02	2.46E-03	1.01E-02	7.32E+04	5.13E+05
5::RRH2:1:1:0->RRHP:2:1:0	-3.96E-02	2.70E+00	2.74E+00	5.26E-06	1.64E-03	5.13E+05	2.24E+03
4::HemRed:0:1:0->HemOx:0:0:0=5::RIO2:1:0:0->RRH2:1:1:0	-3.96E-02	2.27E+00	2.31E+00	3.43E-02	4.51E-06	5.13E+05	6.33E+01
C10->C00=7::U0DD:0:0:1->EMPTY	-3.94E-02	1.95E+03	1.95E+03	3.83E-03	4.38E-03	3.55E+05	5.13E+05
2::HemRed:0:1:0->HemOx:0:0:0=7::U0DD:0:0:1->U1DD:0:1:1	-2.70E-02	1.94E-03	2.89E-02	3.18E-01	5.64E-08	3.85E-03	5.13E+05
C11->C01=7::U2PP:2:2:1->EMPTY	-2.66E-02	3.17E+02	3.17E+02	6.17E-04	5.26E-01	6.69E+02	5.13E+05
1::GLUP:1:0:0->GLUD:0:0:0=6::U1DD:0:1:1->U1DP:1:1:1	-2.57E-02	1.37E+01	1.37E+01	3.36E-03	2.67E-05	5.13E+05	8.86E+04
5::RRH1:1:1:0->RRHP:2:1:0	-1.83E-02	1.29E+00	1.30E+00	2.51E-06	1.64E-03	5.13E+05	1.07E+03
5::RIOP:2:0:0->RIO1:1:0:0	-1.83E-02	2.36E+04	2.36E+04	7.27E-01	4.59E-02	5.13E+05	3.50E+04
4::HemRed:0:1:0->HemOx:0:0:0=5::RIO1:1:0:0->RRH1:1:1:0	-1.83E-02	1.05E+00	1.07E+00	9.67E-03	2.08E-06	5.13E+05	1.04E+02
7::U2DP:1:2:1->U2PP:2:2:1	-1.37E-02	7.71E-02	9.08E-02	1.50E-07	6.45E-04	5.13E+05	4.02E+02
2::HemRed:0:1:0->HemOx:0:0:0=7::U1DP:1:1:1->U2DP:1:2:1	-1.37E-02	6.30E-02	7.67E-02	1.23E-06	1.50E-07	3.70E+04	5.13E+05
7::U1DD:0:1:1->U1DP:1:1:1	-1.37E-02	1.17E-01	1.31E-01	2.79E-07	1.23E-06	1.71E+04	5.13E+05
7::U2PD:1:2:1->U2PP:2:2:1	-1.33E-02	7.88E-02	9.21E-02	1.54E-07	6.45E-04	5.13E+05	3.90E+02
2::HemRed:0:1:0->HemOx:0:0:0=7::U1PD:1:1:1->U2PD:1:2:1	-1.33E-02	6.42E-02	7.75E-02	1.72E-06	1.51E-07	2.60E+04	5.13E+05
7::U1DD:0:1:1->U1PD:1:1:1	-1.33E-02	1.16E-01	1.30E-01	2.79E-07	1.72E-06	1.22E+04	5.13E+05
Q10->Q00=7::U0DD:0:0:1->EMPTY	-2.25E-03	1.03E+03	1.03E+03	2.01E-03	2.30E-03	3.57E+05	5.13E+05
Q11->Q01=7::U2PP:2:2:1->EMPTY	-3.48E-04	9.43E+00	9.43E+00	1.84E-05	1.43E-02	7.11E+02	5.13E+05
C10->C00=7::U2PP:2:2:1->EMPTY	-2.24E-05	3.05E+00	3.05E+00	5.94E-06	4.38E-03	7.45E+02	5.13E+05
1::GLUD:0:0:0->GLUP:1:0:0=6::U1PP:2:1:1->U1PD:1:1:1	-2.03E-05	5.77E-05	7.80E-05	1.13E-10	6.70E-03	5.13E+05	1.72E-02
1::GLUP:1:0:0->GLUD:0:0:0=6::U1DP:1:1:1->U1PP:2:1:1	-2.03E-05	3.74E-05	5.77E-05	1.64E-02	1.13E-10	5.13E+05	5.10E-04
5::RRHP:2:1:0->RIO2:1:0:0=6::U1DD:0:1:1->U2DP:1:2:1	-3.18E-06	3.58E-07	3.53E-06	1.35E-06	6.89E-12	5.13E+05	3.04E-01
Q10->Q00=7::U2PP:2:2:1->EMPTY	-2.22E-06	1.59E+00	1.59E+00	3.09E-06	2.30E-03	7.40E+02	5.13E+05
3::HemOx:0:0:0->HemRed:0:1:0=6::U2PP:2:2:1->U1PP:2:1:1	-2.30E-08	2.09E-08	4.39E-08	8.33E-01	8.56E-14	1.89E-09	5.13E+05
5::RRHP:2:1:0->RIO2:1:0:0=6::U1DD:0:1:1->U2PD:1:2:1	-8.58E-10	1.41E-10	9.99E-10	1.35E-06	1.95E-15	5.13E+05	1.13E-04
5::RRH2:1:1:0->RRHT:0:1:0	-5.15E-10	2.66E-06	2.66E-06	5.26E-06	5.19E-12	5.13E+05	6.50E-01
5::RRHT:0:1:0->RRH1:1:1:0	-5.00E-10	2.66E-06	2.66E-06	5.19E-12	2.51E-06	5.13E+05	8.73E-01
3::HemRed:0:1:0->HemOx:0:0:0=6::U1DD:0:1:1->U2DD:0:2:1	-6.20E-12	6.09E-09	6.09E-09	3.35E-03	1.19E-14	5.13E+05	4.81E-07

Table G.9: Calculated fluxes $\left[\frac{M}{s}\right]$, steady-state concentrations $[M]$ and rate constants $\left[\frac{1}{s}\right]$ for model V-I.2 - Part 2
"->": Transition between two states
"=": separation between two sites, if two sites are involved and no pool.

#LABEL	Netto Flux	Forward Flux	Backward Flux	SSconcA	SSconcB	Forward Rates	Backward Rates
7::U2DP:1:2:1->U2DD:0:2:1	-4.24E-12	2.58E-15	4.24E-12	1.50E-07	8.26E-18	5.13E+05	2.05E-08
7::U2PD:1:2:1->U2DD:0:2:1	-4.24E-12	2.58E-15	4.24E-12	1.54E-07	8.26E-18	5.13E+05	2.12E-08
7::U1DP:1:1:1->U1PP:2:1:1	-4.19E-12	7.15E-14	4.27E-12	1.23E-06	8.32E-18	4.58E-08	5.13E+05
7::U1PD:1:1:1->U1PP:2:1:1	-4.19E-12	7.14E-14	4.27E-12	1.72E-06	8.32E-18	3.33E-08	5.13E+05
1::GLUD:0:0:0->GLUP:1:0:0=6::U2PD:1:2:1->U2DD:0:2:1	-3.42E-12	6.10E-09	6.10E-09	2.66E-04	1.19E-14	1.73E-05	5.13E+05
2::HemOx:0:0:0->HemRed:0:1:0=7::U2PP:2:2:1->U1PP:2:1:1	-2.03E-12	1.08E-13	2.14E-12	2.76E-04	4.17E-18	5.13E+05	5.12E-10
2::HemRed:0:1:0->HemOx:0:0:0=7::U1DD:0:1:1->U2DD:0:2:1	-1.95E-12	1.88E-15	1.95E-12	2.23E-07	3.80E-18	6.22E-09	5.13E+05
1::GLUD:0:0:0->GLUP:1:0:0=6::U2DP:1:2:1->U2DD:0:2:1	-7.93E-13	6.10E-09	6.10E-09	3.17E-08	1.19E-14	9.93E-02	5.13E+05
1::GLUP:1:0:0->GLUD:0:0:0=6::U2DD:0:2:1->U2DP:1:2:1	7.93E-13	6.10E-09	6.10E-09	1.19E-14	3.17E-08	9.08E-02	5.13E+05
2::HemOx:0:0:0->HemRed:0:1:0=7::U2DD:0:2:1->U1DD:0:1:1	1.95E-12	1.95E-12	1.88E-15	3.80E-18	2.23E-07	6.50E-09	5.13E+05
2::HemRed:0:1:0->HemOx:0:0:0=7::U1PP:2:1:1->U2PP:2:2:1	2.03E-12	2.14E-12	1.08E-13	4.17E-18	2.76E-04	5.13E+05	4.91E-10
1::GLUP:1:0:0->GLUD:0:0:0=6::U2DD:0:2:1->U2PD:1:2:1	3.42E-12	6.10E-09	6.10E-09	1.19E-14	2.66E-04	1.64E-05	5.13E+05
7::U1PP:2:1:1->U1DP:1:1:1	4.19E-12	4.27E-12	7.15E-14	8.32E-18	1.23E-06	1.96E-10	5.13E+05
7::U1PP:2:1:1->U1PD:1:1:1	4.19E-12	4.27E-12	7.14E-14	8.32E-18	1.72E-06	2.75E-10	5.13E+05
7::U2DD:0:2:1->U2DP:1:2:1	4.24E-12	4.24E-12	2.58E-15	8.26E-18	1.50E-07	5.13E+05	2.05E-08
7::U2DD:0:2:1->U2PD:1:2:1	4.24E-12	4.24E-12	2.58E-15	8.26E-18	1.54E-07	5.13E+05	2.12E-08
3::HemOx:0:0:0->HemRed:0:1:0=6::U2DD:0:2:1->U1DD:0:1:1	6.20E-12	6.09E-09	6.09E-09	1.19E-14	3.35E-03	5.13E+05	3.77E-07
5::RRH1:1:1:0->RRHT:0:1:0	5.00E-10	2.66E-06	2.66E-06	2.51E-06	5.19E-12	5.13E+05	1.36E+00
5::RRHT:0:1:0->RRH2:1:1:0	5.15E-10	2.66E-06	2.66E-06	5.19E-12	5.26E-06	5.13E+05	5.14E-01
5::RIO2:1:0:0->RRHP:2:1:0=6::U2PD:1:2:1->U1DD:0:1:1	8.58E-10	9.99E-10	1.41E-10	1.95E-15	1.35E-06	5.13E+05	1.11E-04
3::HemRed:0:1:0->HemOx:0:0:0=6::U1PP:2:1:1->U2PP:2:2:1	2.30E-08	4.39E-08	2.09E-08	8.56E-14	8.33E-01	2.42E-09	5.13E+05
Q00->Q10=7::EMPTY->U2PP:2:2:1	2.22E-06	1.59E+00	1.59E+00	2.30E-03	3.09E-06	7.25E+02	5.13E+05
5::RIO2:1:0:0->RRHP:2:1:0=6::U2DP:1:2:1->U1DD:0:1:1	3.18E-06	3.53E-06	3.58E-07	6.89E-12	1.35E-06	5.13E+05	2.92E-01
1::GLUD:0:0:0->GLUP:1:0:0=6::U1PP:2:1:1->U1DP:1:1:1	2.03E-05	5.77E-05	3.74E-05	1.13E-10	1.64E-02	5.13E+05	2.91E-03
1::GLUP:1:0:0->GLUD:0:0:0=6::U1PD:1:1:1->U1PP:2:1:1	2.03E-05	7.80E-05	5.77E-05	6.70E-03	1.13E-10	5.13E+05	1.83E-03
C00->C10=7::EMPTY->U2PP:2:2:1	2.24E-05	3.05E+00	3.05E+00	4.38E-03	5.94E-06	7.48E+02	5.13E+05
Q01->Q11=7::EMPTY->U2PP:2:2:1	3.48E-04	9.43E+00	9.43E+00	1.43E-02	1.84E-05	7.11E+02	5.13E+05
Q00->Q10=7::EMPTY->U0DD:0:0:1	2.25E-03	1.03E+03	1.03E+03	2.30E-03	2.01E-03	3.46E+05	5.13E+05
7::U2PP:2:2:1->U2PD:1:2:1	1.33E-02	9.21E-02	7.88E-02	6.45E-04	1.54E-07	5.13E+05	3.99E+02
7::U1PD:1:1:1->U1DD:0:1:1	1.33E-02	1.30E-01	1.16E-01	1.72E-06	2.79E-07	1.19E+04	5.13E+05
2::HemOx:0:0:0->HemRed:0:1:0=7::U2PD:1:2:1->U1PD:1:1:1	1.33E-02	7.75E-02	6.42E-02	1.51E-07	1.72E-06	2.60E+04	5.13E+05
7::U2PP:2:2:1->U2DP:1:2:1	1.37E-02	9.08E-02	7.71E-02	6.45E-04	1.50E-07	5.13E+05	4.14E+02
7::U1DP:1:1:1->U1DD:0:1:1	1.37E-02	1.31E-01	1.17E-01	1.23E-06	2.79E-07	1.67E+04	5.13E+05
2::HemOx:0:0:0->HemRed:0:1:0=7::U2DP:1:2:1->U1DP:1:1:1	1.37E-02	7.67E-02	6.30E-02	1.50E-07	1.23E-06	3.70E+04	5.13E+05
5::RIO1:1:0:0->RIOP:2:0:0	1.83E-02	2.36E+04	2.36E+04	4.59E-02	7.27E-01	5.13E+05	4.30E+04
4::HemOx:0:0:0->HemRed:0:1:0=5::RRH1:1:1:0->RIO1:1:0:0	1.83E-02	1.07E+00	1.05E+00	2.08E-06	9.67E-03	5.13E+05	1.15E+02
5::RRHP:2:1:0->RRH1:1:1:0	1.83E-02	1.30E+00	1.29E+00	1.64E-03	2.51E-06	5.13E+05	8.21E+02
1::GLUD:0:0:0->GLUP:1:0:0=6::U1DP:1:1:1->U1DD:0:1:1	2.57E-02	1.37E+01	1.37E+01	2.67E-05	3.36E-03	5.13E+05	8.16E+04
C01->C11=7::EMPTY->U2PP:2:2:1	2.66E-02	3.17E+02	3.17E+02	5.26E-01	6.17E-04	6.66E+02	5.13E+05
2::HemOx:0:0:0->HemRed:0:1:0=7::U1DD:0:1:1->U0DD:0:0:1	2.70E-02	2.89E-02	1.94E-03	5.64E-08	3.18E-01	3.85E-03	5.13E+05
C00->C10=7::EMPTY->U0DD:0:0:1	3.94E-02	1.95E+03	1.95E+03	4.38E-03	3.83E-03	3.57E+05	5.13E+05
4::HemOx:0:0:0->HemRed:0:1:0=5::RRH2:1:1:0->RIO2:1:0:0	3.96E-02	2.31E+00	2.27E+00	4.51E-06	3.43E-02	5.13E+05	7.01E+01
5::RRHP:2:1:0->RRH2:1:1:0	3.96E-02	2.74E+00	2.70E+00	1.64E-03	5.26E-06	5.13E+05	1.39E+03
1::GLUD:0:0:0->GLUP:1:0:0	5.40E-02	8.96E+02	8.96E+02	1.01E-02	2.46E-03	5.16E+04	5.13E+05
2::HemRed:0:1:0->HemOx:0:0:0=3::HemOx:0:0:0->HemRed:0:1:0	5.40E-02	1.92E+03	1.92E+03	5.43E-01	3.74E-03	5.13E+05	1.27E+04
C01->C11=7::EMPTY->U0DD:0:0:1	1.71E-01	2.22E+05	2.22E+05	5.26E-01	4.33E-01	3.15E+05	5.13E+05
Q11->Q01=7::U0DD:0:0:1->EMPTY	2.40E-01	6.51E+03	6.51E+03	1.29E-02	1.43E-02	3.38E+05	5.13E+05
C00->C01=6::EMPTY->U2PP:2:2:1	5.01E-01	2.25E+03	2.25E+03	4.38E-03	5.10E-01	5.13E+05	1.97E+03
5::RIO2:1:0:0->RRHP:2:1:0=6::U1PD:1:1:1->U0DD:0:0:1	5.76E-01	5.76E-01	6.58E-11	1.12E-06	2.05E-05	5.13E+05	3.53E-06
C10->C11=6::EMPTY->U2PP:2:2:1	6.34E-01	1.97E+03	1.97E+03	3.83E-03	4.20E-01	5.13E+05	2.07E+03
1::GLUP:1:0:0->GLUD:0:0:0=6::U2DP:1:2:1->U2PP:2:2:1	1.10E+00	2.83E+00	1.73E+00	5.51E-06	3.95E-01	2.02E+00	5.13E+05
3::HemRed:0:1:0->HemOx:0:0:0=6::U1DP:1:1:1->U2DP:1:2:1	1.10E+00	2.91E+00	1.81E+00	1.48E-04	5.47E-06	5.13E+05	1.35E+04
Q11->Q10=6::U0DD:0:0:1->EMPTY	1.35E+00	6.53E+01	6.39E+01	2.87E-04	2.02E-03	5.13E+05	2.06E+05
Q01->Q00=6::U0DD:0:0:1->EMPTY	1.48E+00	7.09E+01	6.94E+01	3.07E-04	2.30E-03	5.13E+05	3.15E+05
5::RIO2:1:0:0->RRHP:2:1:0=6::U1DP:1:1:1->U0DD:0:0:1	2.26E+00	2.26E+00	4.09E-10	4.41E-06	2.05E-05	5.13E+05	2.73E-05
Q11->C11	2.70E+00	6.60E+03	6.60E+03	1.29E-02	4.34E-01	8.03E+04	5.13E+05
C10->Q10	2.94E+00	9.45E+02	9.42E+02	3.83E-03	2.02E-03	4.79E+04	5.13E+05
C00->Q00	3.19E+00	1.08E+03	1.07E+03	4.38E-03	2.30E-03	2.90E+04	5.13E+05

Table G.10: Calculated fluxes $\left[\frac{M}{s}\right]$, steady-state concentrations $[M]$ and rate constants $\left[\frac{1}{s}\right]$ for model V-I.2 - Part 3
"->": Transition between two states
"=": separation between two sites, if two sites are involved and no pool.

#LABEL	Netto Flux	Forward Flux	Backward Flux	SSconcA	SSconcB	Forward Rates	Backward Rates
5::RIO2:1:0:0->RRHP:2:1:0=6::U2PP:2:2:1->U1DP:1:1:1	3.39E+00	8.01E+00	4.63E+00	1.96E-04	9.02E-06	1.81E+03	5.13E+05
Q01->C01	3.42E+00	7.33E+03	7.32E+03	1.43E-02	5.26E-01	3.01E+04	5.13E+05
C11->C10=6::U0DD:0:0:1->EMPTY	3.53E+00	6.83E+02	6.79E+02	2.27E-03	3.83E-03	5.13E+05	3.69E+05
C01->C00=6::U0DD:0:0:1->EMPTY	3.73E+00	7.97E+02	7.93E+02	2.72E-03	4.38E-03	5.13E+05	3.05E+05
Q10->Q11=6::EMPTY->U2PP:2:2:1	4.28E+00	8.66E+02	8.62E+02	2.02E-03	1.17E-02	5.13E+05	1.10E+04
Q00->Q01=6::EMPTY->U2PP:2:2:1	4.66E+00	9.87E+02	9.83E+02	2.30E-03	1.30E-02	5.13E+05	1.07E+04
1::GLUP:1:0:0->GLUD:0:0:0=6::U2PD:1:2:1->U2PP:2:2:1	6.19E+00	4.94E+01	4.32E+01	9.62E-05	3.95E-01	7.09E+01	5.13E+05
3::HemRed:0:1:0->HemOx:0:0:0=6::U1PD:1:1:1->U2PD:1:2:1	6.19E+00	1.49E+02	1.43E+02	4.34E-04	3.57E-04	1.55E+05	5.13E+05
1::GLUD:0:0:0->GLUP:1:0:0=6::U1PD:1:1:1->U1DD:0:1:1	7.21E+00	2.15E+02	2.08E+02	4.52E-04	3.36E-03	5.13E+05	4.17E+05
3::HemOx:0:0:0->HemRed:0:1:0=6::U1DD:0:1:1->U0DD:0:0:1	7.24E+00	7.24E+00	4.10E-04	1.41E-05	1.03E-03	5.13E+05	6.74E-02
5::RIO2:1:0:0->RRHP:2:1:0=6::U2PP:2:2:1->U1PD:1:1:1	1.40E+01	5.36E+01	3.97E+01	1.96E-04	1.07E-04	5.13E+05	1.12E+05
4::HemOx:0:0:0->HemRed:0:1:0=5::RRHP:2:1:0->RIOP:2:0:0	2.02E+01	6.65E+02	6.45E+02	1.30E-03	1.78E-01	5.13E+05	3.52E+03
5::RIOP:2:0:0->RIO2:1:0:0	2.02E+01	9.93E+04	9.93E+04	7.27E-01	1.94E-01	5.13E+05	1.20E+05
4::HemRed:0:1:0->HemOx:0:0:0	2.02E+01	1.18E+05	1.18E+05	2.29E-01	7.71E-01	1.90E+05	5.13E+05

Table G.11: Calculated fluxes $\left[\frac{M}{s}\right]$, steady-state concentrations $[M]$ and rate constants $\left[\frac{1}{s}\right]$ for model V-II.1 - Part 1
"->": Transition between two states
"=": separation between two sites, if two sites are involved and no pool.

#LABEL	Netto Flux	Forward Flux	Backward Flux	SSconcA	SSconcB	Forward Rates	Backward Rates
6::HemOx:0:0:0->HemRed:0:1:0	-2.43E+01	1.16E+05	1.16E+05	7.75E-01	2.25E-01	1.56E+05	5.13E+05
7::RIO2:1:0:0->RIOP:2:0:0	-2.42E+01	9.77E+04	9.77E+04	1.90E-01	7.21E-01	5.13E+05	1.85E+05
6::HemRed:0:1:0->HemOx:0:0:0=7::RIOP:2:0:0->RRHP:2:1:0	-2.42E+01	6.40E+02	6.64E+02	1.73E-01	1.29E-03	5.13E+05	3.76E+03
7::RRHP:2:1:0->RIO2:1:0:0=8::U1PD:1:1:1->U2PP:2:2:1	-1.93E+01	4.09E+01	6.02E+01	1.01E-04	1.92E-04	1.92E+05	5.13E+05
5::HemRed:0:1:0->HemOx:0:0:0=8::U0DD:0:0:1->U1DD:0:1:1	-1.15E+01	9.82E-03	1.15E+01	2.08E-02	2.24E-05	5.13E+05	5.26E-02
Q11->Q10=8::U2PP:2:2:1->EMPTY	-1.08E+01	3.87E+03	3.88E+03	2.09E-02	1.09E-02	5.13E+05	5.66E+04
1::GLUD:0:0:0->GLUP:1:0:0=8::U2PP:2:2:1->U2PD:1:2:1	-1.00E+01	3.17E+01	4.17E+01	1.59E-01	8.12E-05	6.17E+01	5.13E+05
5::HemOx:0:0:0->HemRed:0:1:0=8::U2PD:1:2:1->U1PD:1:1:1	-1.00E+01	2.88E+00	1.29E+01	6.23E-05	6.44E-05	5.13E+05	6.24E+04
1::GLUP:1:0:0->GLUD:0:0:0=8::U1DD:0:1:1->U1PD:1:1:1	-9.29E+00	7.85E+00	1.71E+01	3.14E-05	5.68E-05	5.13E+05	4.93E+05
C11->Q11	-9.15E+00	1.29E+04	1.29E+04	8.20E-01	2.53E-02	8.29E+04	5.13E+05
Q10->C10	-9.10E+00	5.05E+03	5.06E+03	1.09E-02	2.08E-02	2.98E+04	5.13E+05
C10->C11=8::EMPTY->U0DD:0:0:1	-8.45E+00	5.42E+03	5.43E+03	2.08E-02	2.73E-02	5.13E+05	3.53E+05
7::RRHP:2:1:0->RIO2:1:0:0=8::U1DP:1:1:1->U2PP:2:2:1	-4.95E+00	4.41E+00	9.36E+00	8.59E-06	1.92E-04	3.75E+04	5.13E+05
1::GLUD:0:0:0->GLUP:1:0:0=8::U2PP:2:2:1->U2DP:1:2:1	-2.72E+00	9.28E-01	3.64E+00	1.59E-01	7.10E-06	1.88E+00	5.13E+05
5::HemOx:0:0:0->HemRed:0:1:0=8::U2DP:1:2:1->U1DP:1:1:1	-2.72E+00	2.49E+00	5.20E+00	6.79E-06	6.99E-05	5.13E+05	9.42E+01
1::GLUP:1:0:0->GLUD:0:0:0=8::U1DD:0:1:1->U1DP:1:1:1	-2.20E+00	7.77E-01	2.98E+00	3.14E-05	5.81E-06	5.13E+05	1.01E+05
Q10->Q11=8::EMPTY->U0DD:0:0:1	-1.67E+00	7.68E+02	7.70E+02	1.09E-02	4.29E-03	5.13E+05	1.98E+05
Q01->Q00=8::U2PP:2:2:1->EMPTY	-1.54E+00	5.89E+02	5.90E+02	3.06E-03	1.60E-03	5.13E+05	4.72E+04
Q00->C00	-1.31E+00	7.42E+02	7.43E+02	1.60E-03	3.15E-03	4.63E+04	5.13E+05
C01->Q01	-1.25E+00	1.89E+03	1.89E+03	1.15E-01	3.69E-03	8.79E+04	5.13E+05
4::HemOx:0:0:0->HemRed:0:1:0=5::HemRed:0:1:0->HemOx:0:0:0	-1.24E+00	1.80E+04	1.80E+04	3.51E-02	4.80E-01	5.13E+05	2.43E+01
1::GLUP:1:0:0->GLUD:0:0:0	-1.24E+00	8.48E+04	8.48E+04	8.15E-01	1.85E-01	6.01E+04	5.13E+05
C00->C01=8::EMPTY->U0DD:0:0:1	-1.17E+00	8.03E+02	8.04E+02	3.15E-03	3.80E-03	5.13E+05	3.84E+05
C10->C11=8::EMPTY->U2PP:2:2:1	-6.28E-01	1.07E+04	1.07E+04	2.08E-02	7.92E-01	5.13E+05	1.12E+04
4::HemRed:0:1:0->HemOx:0:0:0=9::U0DD:0:0:1->U1DD:0:1:1	-6.20E-01	8.36E-03	6.28E-01	1.35E-01	1.23E-06	2.94E-01	5.13E+05
C01->C11=9::EMPTY->U0DD:0:0:1	-6.09E-01	1.83E+04	1.83E+04	1.15E-01	1.31E-01	5.13E+05	1.34E+05
C11->C01=9::U2PP:2:2:1->EMPTY	-5.41E-01	3.46E+04	3.46E+04	6.88E-01	1.15E-01	5.13E+05	1.22E+04
4::HemRed:0:1:0->HemOx:0:0:0=9::U1PD:1:1:1->U2PD:1:2:1	-4.40E-01	1.19E+00	1.63E+00	1.23E-05	4.45E-05	5.13E+05	2.51E+04
3::HSE:1:0:0->HSP:2:0:0	-4.24E-01	9.93E+04	9.93E+04	7.00E-01	2.45E-01	1.22E+04	5.13E+05
2::ASPD:0:0:0->ASPP:1:0:0	-4.08E-01	1.03E+05	1.03E+05	3.37E-01	6.64E-01	2.04E+02	5.13E+05
Q00->Q01=8::EMPTY->U0DD:0:0:1	-2.30E-01	1.08E+02	1.08E+02	1.60E-03	6.15E-04	5.13E+05	1.88E+05
2::ASPP:1:0:0->ASPD:0:0:0=9::U1DD:0:1:1->U1PD:1:1:1	-2.07E-01	1.46E+00	1.66E+00	3.00E-05	6.05E-06	1.20E+04	5.13E+05
4::HemRed:0:1:0->HemOx:0:0:0=9::U1DP:1:1:1->U2DP:1:2:1	-1.80E-01	5.30E-01	7.10E-01	4.87E-06	4.68E-06	5.13E+05	1.35E+05
C00->C01=8::EMPTY->U2PP:2:2:1	-1.55E-01	1.62E+03	1.62E+03	3.15E-03	1.11E-01	5.13E+05	1.23E+04
3::HSP:2:0:0->HSE:1:0:0=9::U1DD:0:1:1->U1PD:1:1:1	-1.54E-01	2.87E+00	3.03E+00	2.93E-05	9.46E-06	1.62E+03	5.13E+05
3::HSP:2:0:0->HSE:1:0:0=9::U2PD:1:2:1->U2PP:2:2:1	-1.29E-01	2.85E+02	2.85E+02	5.56E-04	5.71E-01	5.13E+05	1.30E+04
9::U2PD:1:2:1->U2PP:2:2:1	-1.24E-01	2.86E+02	2.86E+02	5.59E-04	7.36E-01	3.79E+05	5.13E+05
2::ASPP:1:0:0->ASPD:0:0:0=9::U2PD:1:2:1->U2PP:2:2:1	-1.21E-01	2.86E+02	2.86E+02	5.57E-04	2.34E-01	5.13E+05	3.20E+03
3::HSP:2:0:0->HSE:1:0:0=9::U1DD:0:1:1->U1DP:1:1:1	-1.14E-01	2.02E+00	2.13E+00	2.93E-05	4.39E-06	2.28E+03	5.13E+05
3::HSD:1:0:0->HSP:2:0:0	-9.53E-02	4.86E+03	4.86E+03	5.56E-02	2.45E-01	4.90E+02	5.13E+05
9::U1DD:0:1:1->U1PD:1:1:1	-7.60E-02	5.84E-01	6.60E-01	3.00E-05	1.27E-05	2.17E+01	5.13E+05
2::ASPP:1:0:0->ASPD:0:0:0=9::U2DP:1:2:1->U2PP:2:2:1	-6.63E-02	9.85E+00	9.92E+00	1.92E-05	2.34E-01	5.13E+05	3.28E+02
3::HSP:2:0:0->HSD:1:0:0=9::U2PD:1:2:1->U2PP:2:2:1	-6.58E-02	2.78E+02	2.78E+02	5.56E-04	1.95E-03	2.32E+05	5.13E+05
9::U2DP:1:2:1->U2PP:2:2:1	-6.26E-02	9.85E+00	9.92E+00	1.92E-05	7.36E-01	5.13E+05	7.06E+04
Q11->Q01=9::U2PP:2:2:1->EMPTY	-5.76E-02	1.10E+03	1.10E+03	2.12E-02	3.69E-03	5.13E+05	1.30E+04
9::U1DD:0:1:1->U1DP:1:1:1	-4.94E-02	4.46E-01	4.95E-01	3.00E-05	4.93E-06	2.29E+01	5.13E+05
7::RRH2:1:1:0->RRHP:2:1:0	-4.48E-02	2.63E+00	2.67E+00	5.12E-06	1.63E-03	5.13E+05	2.27E+03
6::HemRed:0:1:0->HemOx:0:0:0=7::RIO2:1:0:0->RRH2:1:1:0	-4.48E-02	2.22E+00	2.26E+00	3.30E-02	4.41E-06	5.13E+05	7.01E+01
7::RRHP:2:1:0->RIO2:1:0:0=8::U0DD:0:0:1->U1DP:1:1:1	-3.33E-02	9.28E-10	3.33E-02	6.24E-05	6.49E-08	5.13E+05	2.86E-05
3::HSP:2:0:0->HSE:1:0:0=9::U2DP:1:2:1->U2PP:2:2:1	-2.78E-02	9.09E+00	9.12E+00	1.77E-05	5.71E-01	5.13E+05	1.33E+03
3::HSP:2:0:0->HSD:1:0:0=9::U2DP:1:2:1->U2PP:2:2:1	-2.36E-02	9.09E+00	9.12E+00	1.77E-05	1.95E-03	5.13E+05	1.16E+05
7::RRH1:1:1:0->RRHP:2:1:0	-2.07E-02	1.26E+00	1.28E+00	2.46E-06	1.63E-03	5.13E+05	1.09E+03
7::RIOP:2:0:0->RIO1:1:0:0	-2.07E-02	2.33E+04	2.33E+04	7.21E-01	4.54E-02	5.13E+05	3.55E+04
6::HemRed:0:1:0->HemOx:0:0:0=7::RIO1:1:0:0->RRH1:1:1:0	-2.07E-02	1.03E+00	1.05E+00	9.37E-03	2.05E-06	5.13E+05	1.15E+02
C10->C00=9::U2PP:2:2:1->EMPTY	-1.80E-02	9.46E+02	9.46E+02	1.75E-02	3.15E-03	5.13E+05	1.24E+04
2::ASPP:1:0:0->ASPD:0:0:0=9::U1DD:0:1:1->U1DP:1:1:1	-1.42E-02	1.72E-01	1.86E-01	3.00E-05	3.63E-07	1.16E+03	5.13E+05

Table G.12: Calculated fluxes $\left[\frac{M}{s}\right]$, steady-state concentrations $[M]$ and rate constants $\left[\frac{1}{s}\right]$ for model V-II.1 - Part 2
"->": Transition between two states
"=": separation between two sites, if two sites are involved and no pool.

#LABEL	Netto Flux	Forward Flux	Backward Flux	SSconcA	SSconcB	Forward Rates	Backward Rates
Q00->Q10=9::EMPTY->U0DD:0:0:1	-7.76E-03	2.50E+02	2.50E+02	1.60E-03	1.71E-03	5.13E+05	1.35E+05
Q10->Q00=9::U2PP:2:2:1->EMPTY	-3.67E-03	4.75E+02	4.75E+02	9.14E-03	1.60E-03	5.13E+05	1.24E+04
C00->C10=9::EMPTY->U0DD:0:0:1	-3.45E-03	4.84E+02	4.84E+02	3.15E-03	3.28E-03	5.13E+05	1.35E+05
3::HSP:2:0:0->HSD:1:0:0=9::U1DD:0:1:1->U1DP:1:1:1	-3.05E-03	2.16E-02	2.46E-02	2.93E-05	4.80E-08	6.81E+01	5.13E+05
3::HSP:2:0:0->HSD:1:0:0=9::U1DD:0:1:1->U1PD:1:1:1	-2.98E-03	2.19E-02	2.49E-02	2.93E-05	5.20E-08	3.32E+01	5.13E+05
7::RRHP:2:1:0->RIO2:1:0:0=8::U0DD:0:0:1->U1PD:1:1:1	-1.52E-03	1.56E-10	1.52E-03	6.24E-05	2.96E-09	5.13E+05	3.67E-06
Q11->Q01=9::U0DD:0:0:1->EMPTY	-8.01E-04	5.79E+02	5.79E+02	4.06E-03	3.69E-03	5.13E+05	1.42E+05
7::RRHP:2:1:0->RIO2:1:0:0=8::U1DD:0:1:1->U2DP:1:2:1	-2.84E-06	2.41E-07	3.08E-06	1.10E-06	6.00E-12	5.13E+05	3.20E-01
1::GLUD:0:0:0->GLUP:1:0:0=8::U1PP:2:1:1->U1DP:1:1:1	-1.08E-07	3.31E-07	4.39E-07	6.46E-13	2.87E-04	5.13E+05	3.17E-03
1::GLUP:1:0:0->GLUD:0:0:0=8::U1PD:1:1:1->U1PP:2:1:1	-9.38E-08	2.37E-07	3.31E-07	1.24E-04	6.46E-13	5.13E+05	2.07E-03
5::HemOx:0:0:0->HemRed:0:1:0=8::U2PP:2:2:1->U1PP:2:1:1	-1.44E-08	2.59E-09	1.70E-08	4.61E-01	3.31E-14	3.10E-09	5.13E+05
4::HemRed:0:1:0->HemOx:0:0:0=9::U1PP:2:1:1->U2PP:2:2:1	-5.33E-09	9.60E-09	1.49E-08	1.87E-14	4.79E-02	5.13E+05	3.69E-12
9::U1DP:1:1:1->U1PP:2:1:1	-1.21E-09	8.43E-09	9.65E-09	4.93E-06	1.88E-14	1.03E-10	5.13E+05
9::U1PD:1:1:1->U1PP:2:1:1	-1.04E-09	8.60E-09	9.65E-09	1.27E-05	1.88E-14	5.69E-11	5.13E+05
3::HSP:2:0:0->HSD:1:0:0=9::U1DP:1:1:1->U1PP:2:1:1	-7.93E-10	7.26E-09	8.06E-09	4.91E-07	1.57E-14	1.97E-05	5.13E+05
2::ASPP:1:0:0->ASPD:0:0:0=9::U1PD:1:1:1->U1PP:2:1:1	-7.60E-10	8.86E-09	9.62E-09	6.63E-06	1.87E-14	2.96E-06	5.13E+05
2::ASPP:1:0:0->ASPD:0:0:0=9::U1DP:1:1:1->U1PP:2:1:1	-7.34E-10	8.88E-09	9.62E-09	4.57E-06	1.87E-14	5.38E-06	5.13E+05
3::HSP:2:0:0->HSD:1:0:0=9::U1PD:1:1:1->U1PP:2:1:1	-7.20E-10	7.34E-09	8.06E-09	3.16E-06	1.57E-14	1.08E-05	5.13E+05
7::RRH2:1:1:0->RRHT:0:1:0	-6.79E-10	2.55E-06	2.55E-06	5.12E-06	4.96E-12	5.13E+05	6.58E-01
7::RRHT:0:1:0->RRH1:1:1:0	-4.48E-10	2.55E-06	2.55E-06	4.96E-12	2.46E-06	5.13E+05	8.83E-01
7::RRHP:2:1:0->RIO2:1:0:0=8::U1DD:0:1:1->U2PD:1:2:1	-4.12E-10	1.02E-10	5.14E-10	1.10E-06	1.00E-15	5.13E+05	1.16E-04
3::HSP:2:0:0->HSE:1:0:0=9::U1DP:1:1:1->U1PP:2:1:1	-1.22E-10	1.46E-09	1.58E-09	4.91E-07	3.07E-15	7.61E-07	5.13E+05
3::HSP:2:0:0->HSE:1:0:0=9::U1PD:1:1:1->U1PP:2:1:1	-1.08E-10	1.47E-09	1.58E-09	3.16E-06	3.07E-15	4.19E-07	5.13E+05
1::GLUD:0:0:0->GLUP:1:0:0=8::U2PD:1:2:1->U2DD:0:2:1	-6.03E-11	1.00E-11	7.03E-11	4.21E-07	1.37E-16	1.60E-05	5.13E+05
1::GLUD:0:0:0->GLUP:1:0:0=8::U2DP:1:2:1->U2DD:0:2:1	-5.46E-11	1.57E-11	7.03E-11	8.11E-11	1.37E-16	8.62E-02	5.13E+05
5::HemRed:0:1:0->HemOx:0:0:0=8::U1DD:0:1:1->U2DD:0:2:1	-4.65E-11	1.76E-11	6.41E-11	8.97E-06	1.25E-16	5.13E+05	2.93E-07
4::HemRed:0:1:0->HemOx:0:0:0=9::U1DD:0:1:1->U2DD:0:2:1	-4.58E-11	5.57E-11	1.02E-10	2.88E-05	1.98E-16	9.61E-07	5.13E+05
9::U2DP:1:2:1->U2DD:0:2:1	-2.61E-11	9.80E-11	1.24E-10	1.92E-05	2.42E-16	5.13E+05	4.46E-05
9::U2PD:1:2:1->U2DD:0:2:1	-2.46E-11	9.95E-11	1.24E-10	5.59E-04	2.42E-16	5.13E+05	4.57E-06
2::ASPD:0:0:0->ASPP:1:0:0=9::U2DP:1:2:1->U2DD:0:2:1	-1.43E-11	9.26E-11	1.07E-10	2.81E-09	2.08E-16	5.13E+05	3.37E-02
2::ASPD:0:0:0->ASPP:1:0:0=9::U2PD:1:2:1->U2DD:0:2:1	-1.38E-11	9.31E-11	1.07E-10	1.53E-06	2.08E-16	5.13E+05	7.56E-05
3::HSE:1:0:0->HSP:2:0:0=9::U2DP:1:2:1->U2DD:0:2:1	-9.72E-12	9.03E-11	1.00E-10	1.48E-06	1.95E-16	5.13E+05	1.44E-04
3::HSE:1:0:0->HSP:2:0:0=9::U2PD:1:2:1->U2DD:0:2:1	-9.37E-12	9.07E-11	1.00E-10	3.14E-06	1.95E-16	5.13E+05	1.49E-04
3::HSD:1:0:0->HSP:2:0:0=9::U2DP:1:2:1->U2DD:0:2:1	-9.06E-12	9.10E-11	1.00E-10	3.21E-11	1.95E-16	5.13E+05	4.52E+00
3::HSD:1:0:0->HSP:2:0:0=9::U2PD:1:2:1->U2DD:0:2:1	-8.73E-12	9.13E-11	1.00E-10	6.36E-13	1.95E-16	5.13E+05	3.87E+02
3::HSP:2:0:0->HSD:1:0:0=9::U2DD:0:2:1->U2PD:1:2:1	8.73E-12	1.00E-10	9.13E-11	1.95E-16	6.36E-13	5.13E+05	3.87E+02
3::HSP:2:0:0->HSD:1:0:0=9::U2DD:0:2:1->U2DP:1:2:1	9.06E-12	1.00E-10	9.10E-11	1.95E-16	3.21E-11	5.13E+05	4.52E+00
3::HSP:2:0:0->HSE:1:0:0=9::U2DD:0:2:1->U2PD:1:2:1	9.37E-12	1.00E-10	9.07E-11	1.95E-16	3.14E-06	5.13E+05	1.49E-04
3::HSP:2:0:0->HSE:1:0:0=9::U2DD:0:2:1->U2DP:1:2:1	9.72E-12	1.00E-10	9.03E-11	1.95E-16	1.48E-06	5.13E+05	1.44E-04
2::ASPP:1:0:0->ASPD:0:0:0=9::U2DD:0:2:1->U2PD:1:2:1	1.38E-11	1.07E-10	9.31E-11	2.08E-16	1.53E-06	5.13E+05	7.56E-05
2::ASPP:1:0:0->ASPD:0:0:0=9::U2DD:0:2:1->U2DP:1:2:1	1.43E-11	1.07E-10	9.26E-11	2.08E-16	2.81E-09	5.13E+05	3.37E-02
9::U2DD:0:2:1->U2PD:1:2:1	2.46E-11	1.24E-10	9.95E-11	2.42E-16	5.59E-04	5.13E+05	4.57E-06
9::U2DD:0:2:1->U2DP:1:2:1	2.61E-11	1.24E-10	9.80E-11	2.42E-16	1.92E-05	5.13E+05	4.46E-05
4::HemOx:0:0:0->HemRed:0:1:0=9::U2DD:0:2:1->U1DD:0:1:1	4.58E-11	1.02E-10	5.57E-11	1.98E-16	2.88E-05	1.00E-06	5.13E+05
5::HemOx:0:0:0->HemRed:0:1:0=8::U2DD:0:2:1->U1DD:0:1:1	4.65E-11	6.41E-11	1.76E-11	1.25E-16	8.97E-06	5.13E+05	2.30E-07
1::GLUP:1:0:0->GLUD:0:0:0=8::U2DD:0:2:1->U2DP:1:2:1	5.46E-11	7.03E-11	1.57E-11	1.37E-16	8.11E-11	7.89E-02	5.13E+05
1::GLUP:1:0:0->GLUD:0:0:0=8::U2DD:0:2:1->U2PD:1:2:1	6.03E-11	7.03E-11	1.00E-11	1.37E-16	4.21E-07	1.52E-05	5.13E+05
3::HSE:1:0:0->HSP:2:0:0=9::U1PP:2:1:1->U1PD:1:1:1	1.08E-10	1.58E-09	1.47E-09	3.07E-15	3.16E-06	2.12E-08	5.13E+05
3::HSE:1:0:0->HSP:2:0:0=9::U1PP:2:1:1->U1DP:1:1:1	1.22E-10	1.58E-09	1.46E-09	3.07E-15	4.91E-07	2.00E-08	5.13E+05
7::RIO2:1:0:0->RRHP:2:1:0=8::U2PD:1:2:1->U1DD:0:1:1	4.12E-10	5.14E-10	1.02E-10	1.00E-15	1.10E-06	5.13E+05	1.14E-04
7::RRH1:1:1:0->RRHT:0:1:0	4.48E-10	2.55E-06	2.55E-06	2.46E-06	4.96E-12	5.13E+05	1.38E+00
7::RRHT:0:1:0->RRH2:1:1:0	6.79E-10	2.55E-06	2.55E-06	4.96E-12	5.12E-06	5.13E+05	5.21E-01
3::HSD:1:0:0->HSP:2:0:0=9::U1PP:2:1:1->U1PD:1:1:1	7.20E-10	8.06E-09	7.34E-09	1.57E-14	3.16E-06	1.39E-06	5.13E+05
2::ASPD:0:0:0->ASPP:1:0:0=9::U1PP:2:1:1->U1DP:1:1:1	7.34E-10	9.62E-09	8.88E-09	1.87E-14	4.57E-06	1.81E-06	5.13E+05
2::ASPD:0:0:0->ASPP:1:0:0=9::U1PP:2:1:1->U1PD:1:1:1	7.60E-10	9.62E-09	8.86E-09	1.87E-14	6.63E-06	1.92E-06	5.13E+05
3::HSD:1:0:0->HSP:2:0:0=9::U1PP:2:1:1->U1DP:1:1:1	7.93E-10	8.06E-09	7.26E-09	1.57E-14	4.91E-07	1.31E-06	5.13E+05
9::U1PP:2:1:1->U1PD:1:1:1	1.04E-09	9.65E-09	8.60E-09	1.88E-14	1.27E-05	4.70E-13	5.13E+05
9::U1PP:2:1:1->U1DP:1:1:1	1.21E-09	9.65E-09	8.43E-09	1.88E-14	4.93E-06	4.44E-13	5.13E+05

Table G.13: Calculated fluxes $\left[\frac{M}{s}\right]$, steady-state concentrations $[M]$ and rate constants $\left[\frac{1}{s}\right]$ for model V-II.1 - Part 3
"->": Transition between two states
"=": separation between two sites, if two sites are involved and no pool.

#LABEL	Netto Flux	Forward Flux	Backward Flux	SSconcA	SSconcB	Forward Rates	Backward Rates
4::HemOx:0:0:0->HemRed:0:1:0=9::U2PP:2:2:1->U1PP:2:1:1	5.33E-09	1.49E-08	9.60E-09	4.79E-02	1.87E-14	5.13E+05	3.85E-12
5::HemRed:0:1:0->HemOx:0:0:0=8::U1PP:2:1:1->U2PP:2:2:1	1.44E-08	1.70E-08	2.59E-09	3.31E-14	4.61E-01	3.98E-09	5.13E+05
1::GLUD:0:0:0->GLUP:1:0:0=8::U1PP:2:1:1->U1PD:1:1:1	9.38E-08	3.31E-07	2.37E-07	6.46E-13	1.24E-04	5.13E+05	1.94E-02
1::GLUP:1:0:0->GLUD:0:0:0=8::U1DP:1:1:1->U1PP:2:1:1	1.08E-07	4.39E-07	3.31E-07	2.87E-04	6.46E-13	5.13E+05	5.56E-04
7::RIO2:1:0:0->RRHP:2:1:0=8::U2DP:1:2:1->U1DD:0:1:1	2.84E-06	3.08E-06	2.41E-07	6.00E-12	1.10E-06	5.13E+05	3.07E-01
Q01->Q11=9::EMPTY->U0DD:0:0:1	8.01E-04	5.79E+02	5.79E+02	3.69E-03	4.06E-03	5.13E+05	1.42E+05
7::RIO2:1:0:0->RRHP:2:1:0=8::U1PD:1:1:1->U0DD:0:0:1	1.52E-03	1.52E-03	1.56E-10	2.96E-09	6.24E-05	5.13E+05	3.67E-06
3::HSD:1:0:0->HSP:2:0:0=9::U1PD:1:1:1->U1DD:0:1:1	2.98E-03	2.49E-02	2.19E-02	5.20E-08	2.93E-05	3.32E+01	5.13E+05
3::HSD:1:0:0->HSP:2:0:0=9::U1DP:1:1:1->U1DD:0:1:1	3.05E-03	2.46E-02	2.16E-02	4.80E-08	2.93E-05	6.81E+01	5.13E+05
C10->C00=9::U0DD:0:0:1->EMPTY	3.45E-03	4.84E+02	4.84E+02	3.28E-03	3.15E-03	5.13E+05	1.36E+05
Q00->Q10=9::EMPTY->U2PP:2:2:1	3.67E-03	4.75E+02	4.75E+02	1.60E-03	9.14E-03	5.13E+05	1.24E+04
Q10->Q00=9::U0DD:0:0:1->EMPTY	7.76E-03	2.50E+02	2.50E+02	1.71E-03	1.60E-03	5.13E+05	1.33E+05
2::ASPD:0:0:0->ASPP:1:0:0=9::U1DP:1:1:1->U1DD:0:1:1	1.42E-02	1.86E-01	1.72E-01	3.63E-07	3.00E-05	1.16E+03	5.13E+05
C00->C10=9::EMPTY->U2PP:2:2:1	1.80E-02	9.46E+02	9.46E+02	3.15E-03	1.75E-02	5.13E+05	1.25E+04
7::RIO1:1:0:0->RIOP:2:0:0	2.07E-02	2.33E+04	2.33E+04	4.54E-02	7.21E-01	5.13E+05	4.36E+04
6::HemOx:0:0:0->HemRed:0:1:0=7::RRH1:1:1:0->RIO1:1:0:0	2.07E-02	1.05E+00	1.03E+00	2.05E-06	9.37E-03	5.13E+05	1.15E+02
7::RRHP:2:1:0->RRH1:1:1:0	2.07E-02	1.28E+00	1.26E+00	1.63E-03	2.46E-06	5.13E+05	8.32E+02
3::HSD:1:0:0->HSP:2:0:0=9::U2PP:2:2:1->U2DP:1:2:1	2.36E-02	9.12E+00	9.09E+00	1.95E-03	1.77E-05	5.13E+05	1.16E+05
3::HSE:1:0:0->HSP:2:0:0=9::U2PP:2:2:1->U2DP:1:2:1	2.78E-02	9.12E+00	9.09E+00	5.71E-01	1.77E-05	5.13E+05	1.33E+03
7::RIO2:1:0:0->RRHP:2:1:0=8::U1DP:1:1:1->U0DD:0:0:1	3.33E-02	3.33E-02	9.28E-10	6.49E-08	6.24E-05	5.13E+05	2.86E-05
6::HemOx:0:0:0->HemRed:0:1:0=7::RRH2:1:1:0->RIO2:1:0:0	4.48E-02	2.26E+00	2.22E+00	4.41E-06	3.30E-02	5.13E+05	7.01E+01
7::RRHP:2:1:0->RRH2:1:1:0	4.48E-02	2.67E+00	2.63E+00	1.63E-03	5.12E-06	5.13E+05	1.41E+03
9::U1DP:1:1:1->U1DD:0:1:1	4.94E-02	4.95E-01	4.46E-01	4.93E-06	3.00E-05	2.24E+01	5.13E+05
Q01->Q11=9::EMPTY->U2PP:2:2:1	5.76E-02	1.10E+03	1.10E+03	3.69E-03	2.12E-02	5.13E+05	1.30E+04
9::U2PP:2:2:1->U2DP:1:2:1	6.26E-02	9.92E+00	9.85E+00	7.36E-01	1.92E-05	5.13E+05	7.26E+04
3::HSD:1:0:0->HSP:2:0:0=9::U2PP:2:2:1->U2PD:1:2:1	6.58E-02	2.78E+02	2.78E+02	1.95E-03	5.56E-04	2.32E+05	5.13E+05
2::ASPD:0:0:0->ASPP:1:0:0=9::U2PP:2:2:1->U2DP:1:2:1	6.63E-02	9.92E+00	9.85E+00	2.34E-01	1.92E-05	5.13E+05	3.28E+02
9::U1PD:1:1:1->U1DD:0:1:1	7.60E-02	6.60E-01	5.84E-01	1.27E-05	3.00E-05	2.11E+01	5.13E+05
3::HSP:2:0:0->HSD:1:0:0	9.53E-02	4.86E+03	4.86E+03	2.45E-01	5.56E-02	5.01E+02	5.13E+05
3::HSE:1:0:0->HSP:2:0:0=9::U1DP:1:1:1->U1DD:0:1:1	1.14E-01	2.13E+00	2.02E+00	4.39E-06	2.93E-05	2.28E+03	5.13E+05
2::ASPD:0:0:0->ASPP:1:0:0=9::U2PP:2:2:1->U2PD:1:2:1	1.21E-01	2.86E+02	2.86E+02	2.34E-01	5.57E-04	5.13E+05	3.20E+03
9::U2PP:2:2:1->U2PD:1:2:1	1.24E-01	2.86E+02	2.86E+02	7.36E-01	5.59E-04	3.71E+05	5.13E+05
3::HSE:1:0:0->HSP:2:0:0=9::U2PP:2:2:1->U2PD:1:2:1	1.29E-01	2.85E+02	2.85E+02	5.71E-01	5.56E-04	5.13E+05	1.30E+04
3::HSE:1:0:0->HSP:2:0:0=9::U1PD:1:1:1->U1DD:0:1:1	1.54E-01	3.03E+00	2.87E+00	9.46E-06	2.93E-05	1.62E+03	5.13E+05
C01->C00=8::U2PP:2:2:1->EMPTY	1.55E-01	1.62E+03	1.62E+03	1.11E-01	3.15E-03	5.13E+05	1.14E+04
4::HemOx:0:0:0->HemRed:0:1:0=9::U2DP:1:2:1->U1DP:1:1:1	1.80E-01	7.10E-01	5.30E-01	4.68E-06	4.87E-06	5.13E+05	1.35E+05
2::ASPD:0:0:0->ASPP:1:0:0=9::U1PD:1:1:1->U1DD:0:1:1	2.07E-01	1.66E+00	1.46E+00	6.05E-06	3.00E-05	1.20E+04	5.13E+05
Q01->Q00=8::U0DD:0:0:1->EMPTY	2.30E-01	1.08E+02	1.08E+02	6.15E-04	1.60E-03	5.13E+05	2.99E+05
2::ASPP:1:0:0->ASPD:0:0:0	4.08E-01	1.03E+05	1.03E+05	6.64E-01	3.37E-01	2.11E+02	5.13E+05
3::HSP:2:0:0->HSE:1:0:0	4.24E-01	9.93E+04	9.93E+04	2.45E-01	7.00E-01	1.24E+04	5.13E+05
4::HemOx:0:0:0->HemRed:0:1:0=9::U2PD:1:2:1->U1PD:1:1:1	4.40E-01	1.63E+00	1.19E+00	4.45E-05	1.23E-05	5.13E+05	2.51E+04
C01->C11=9::EMPTY->U2PP:2:2:1	5.41E-01	3.46E+04	3.46E+04	1.15E-01	6.88E-01	5.13E+05	1.22E+04
C11->C01=9::U0DD:0:0:1->EMPTY	6.09E-01	1.83E+04	1.83E+04	1.31E-01	1.15E-01	5.13E+05	1.34E+05
4::HemOx:0:0:0->HemRed:0:1:0=9::U1DD:0:1:1->U0DD:0:0:1	6.20E-01	6.28E-01	8.36E-03	1.23E-06	1.35E-01	2.94E-01	5.13E+05
C11->C10=8::U2PP:2:2:1->EMPTY	6.28E-01	1.07E+04	1.07E+04	7.92E-01	2.08E-02	5.13E+05	1.21E+04
C01->C00=8::U0DD:0:0:1->EMPTY	1.17E+00	8.04E+02	8.03E+02	3.80E-03	3.15E-03	5.13E+05	3.58E+05
1::GLUD:0:0:0->GLUP:1:0:0	1.24E+00	8.48E+04	8.48E+04	1.85E-01	8.15E-01	4.23E+04	5.13E+05
4::HemRed:0:1:0->HemOx:0:0:0=5::HemOx:0:0:0->HemRed:0:1:0	1.24E+00	1.80E+04	1.80E+04	4.80E-01	3.51E-02	5.13E+05	2.52E+03
Q01->C01	1.25E+00	1.89E+03	1.89E+03	3.69E-03	1.15E-01	3.77E+04	5.13E+05
C00->Q00	1.31E+00	7.43E+02	7.42E+02	3.15E-03	1.60E-03	2.94E+04	5.13E+05
Q00->Q01=8::EMPTY->U2PP:2:2:1	1.54E+00	5.90E+02	5.89E+02	1.60E-03	3.06E-03	5.13E+05	5.38E+04
Q11->Q10=8::U0DD:0:0:1->EMPTY	1.67E+00	7.70E+02	7.68E+02	4.29E-03	1.09E-02	5.13E+05	1.98E+05
1::GLUD:0:0:0->GLUP:1:0:0=8::U1DP:1:1:1->U1DD:0:1:1	2.20E+00	2.98E+00	7.77E-01	5.81E-06	3.14E-05	5.13E+05	9.31E+04
1::GLUP:1:0:0->GLUD:0:0:0=8::U2DP:1:2:1->U2PP:2:2:1	2.72E+00	3.64E+00	9.28E-01	7.10E-06	1.59E-01	1.88E+00	5.13E+05
5::HemRed:0:1:0->HemOx:0:0:0=8::U1DP:1:1:1->U2DP:1:2:1	2.72E+00	5.20E+00	2.49E+00	6.99E-05	6.79E-06	5.13E+05	8.31E+03
7::RIO2:1:0:0->RRHP:2:1:0=8::U2PP:2:2:1->U1DP:1:1:1	4.95E+00	9.36E+00	4.41E+00	1.92E-04	8.59E-06	1.75E+03	5.13E+05
C11->C10=8::U0DD:0:0:1->EMPTY	8.45E+00	5.43E+03	5.42E+03	2.73E-02	2.08E-02	5.13E+05	3.79E+05

Table G.14: Calculated fluxes $\left[\frac{M}{s}\right]$, steady-state concentrations $[M]$ and rate constants $\left[\frac{1}{s}\right]$ for model V-II.1 - Part 4
"->": Transition between two states
"=": separation between two sites, if two sites are involved and no pool.

#LABEL	Netto Flux	Forward Flux	Backward Flux	SSconcA	SSconcB	Forward Rates	Backward Rates
C10->Q10	9.10E+00	5.06E+03	5.05E+03	2.08E-02	1.09E-02	4.65E+04	5.13E+05
Q11->C11	9.15E+00	1.29E+04	1.29E+04	2.53E-02	8.20E-01	8.29E+04	5.13E+05
1::GLUD:0:0:0->GLUP:1:0:0=8::U1PD:1:1:1->U1DD:0:1:1	9.29E+00	1.71E+01	7.85E+00	5.68E-05	3.14E-05	5.13E+05	4.58E+05
1::GLUP:1:0:0->GLUD:0:0:0=8::U2PD:1:2:1->U2PP:2:2:1	1.00E+01	4.17E+01	3.17E+01	8.12E-05	1.59E-01	6.17E+01	5.13E+05
5::HemRed:0:1:0->HemOx:0:0:0=8::U1PD:1:1:1->U2PD:1:2:1	1.00E+01	1.29E+01	2.88E+00	6.44E-05	6.23E-05	2.59E+05	5.13E+05
Q10->Q11=8::EMPTY->U2PP:2:2:1	1.08E+01	3.88E+03	3.87E+03	1.09E-02	2.09E-02	5.13E+05	5.66E+04
5::HemOx:0:0:0->HemRed:0:1:0=8::U1DD:0:1:1->U0DD:0:0:1	1.15E+01	1.15E+01	9.82E-03	2.24E-05	2.08E-02	5.13E+05	4.14E-02
7::RIO2:1:0:0->RRHP:2:1:0=8::U2PP:2:2:1->U1PD:1:1:1	1.93E+01	6.02E+01	4.09E+01	1.92E-04	1.01E-04	5.13E+05	1.15E+05
6::HemOx:0:0:0->HemRed:0:1:0=7::RRHP:2:1:0->RIOP:2:0:0	2.42E+01	6.64E+02	6.40E+02	1.29E-03	1.73E-01	5.13E+05	3.77E+03
7::RIOP:2:0:0->RIO2:1:0:0	2.42E+01	9.77E+04	9.77E+04	7.21E-01	1.90E-01	5.13E+05	1.22E+05
6::HemRed:0:1:0->HemOx:0:0:0	2.43E+01	1.16E+05	1.16E+05	2.25E-01	7.75E-01	1.92E+05	5.13E+05

Table G.15: Calculated fluxes $\left[\frac{M}{s}\right]$, steady-state concentrations $[M]$ and rate constants $\left[\frac{1}{s}\right]$ for model V-II.2 - Part 1
"->": Transition between two states
"=": separation between two sites, if two sites are involved and no pool.

#LABEL	Netto Flux	Forward Flux	Backward Flux	SSconcA	SSconcB	Forward Rates	Backward Rates
6::HemOx:0:0:0->HemRed:0:1:0	-2.55E+01	1.16E+05	1.16E+05	7.75E-01	2.26E-01	1.56E+05	5.13E+05
7::RIO2:1:0:0->RIOP:2:0:0	-2.55E+01	9.90E+04	9.90E+04	1.93E-01	7.30E-01	5.13E+05	1.85E+05
6::HemRed:0:1:0->HemOx:0:0:0=7::RIOP:2:0:0->RRHP:2:1:0	-2.54E+01	6.48E+02	6.74E+02	1.76E-01	1.31E-03	5.13E+05	3.76E+03
7::RRHP:2:1:0->RIO2:1:0:0=8::U1PD:1:1:1->U2PP:2:2:1	-2.02E+01	4.33E+01	6.36E+01	1.08E-04	2.04E-04	1.92E+05	5.13E+05
5::HemRed:0:1:0->HemOx:0:0:0=8::U0DD:0:0:1->U1DD:0:1:1	-1.27E+01	2.09E-03	1.27E+01	4.08E-03	2.48E-05	5.13E+05	5.26E-02
1::GLUP:1:0:0->GLUD:0:0:0=8::U1DD:0:1:1->U1PD:1:1:1	-1.03E+01	8.54E+00	1.88E+01	3.36E-05	6.24E-05	5.13E+05	4.93E+05
1::GLUD:0:0:0->GLUP:1:0:0=8::U2PP:2:2:1->U2PD:1:2:1	-9.97E+00	3.40E+01	4.40E+01	1.74E-01	8.58E-05	6.17E+01	5.13E+05
5::HemOx:0:0:0->HemRed:0:1:0=8::U2PD:1:2:1->U1PD:1:1:1	-9.97E+00	2.92E+00	1.29E+01	6.69E-05	6.45E-05	5.13E+05	6.24E+04
Q11->Q10=8::U2PP:2:2:1->EMPTY	-5.97E+00	5.43E+02	5.49E+02	1.35E-02	1.29E-03	5.13E+05	1.06E+04
C10->C11=8::EMPTY->U0DD:0:0:1	-5.65E+00	6.49E+02	6.55E+02	2.49E-03	3.33E-03	5.13E+05	3.53E+05
Q01->Q00=8::U2PP:2:2:1->EMPTY	-5.29E+00	5.13E+02	5.18E+02	1.24E-02	1.21E-03	5.13E+05	8.82E+03
7::RRHP:2:1:0->RIO2:1:0:0=8::U1DP:1:1:1->U2PP:2:2:1	-5.22E+00	4.68E+00	9.91E+00	9.13E-06	2.04E-04	3.75E+04	5.13E+05
C11->Q11	-4.88E+00	7.20E+03	7.21E+03	5.13E-01	1.41E-02	8.29E+04	5.13E+05
C00->C01=8::EMPTY->U0DD:0:0:1	-4.83E+00	6.08E+02	6.13E+02	2.41E-03	2.90E-03	5.13E+05	3.84E+05
Q10->C10	-4.74E+00	6.01E+02	6.05E+02	1.29E-03	2.49E-03	2.98E+04	5.13E+05
Q00->C00	-4.25E+00	5.65E+02	5.69E+02	1.21E-03	2.41E-03	4.63E+04	5.13E+05
C01->Q01	-4.11E+00	6.60E+03	6.61E+03	4.53E-01	1.29E-02	8.79E+04	5.13E+05
1::GLUD:0:0:0->GLUP:1:0:0=8::U2PP:2:2:1->U2DP:1:2:1	-2.74E+00	1.02E+00	3.76E+00	1.74E-01	7.32E-06	1.88E+00	5.13E+05
5::HemOx:0:0:0->HemRed:0:1:0=8::U2DP:1:2:1->U1DP:1:1:1	-2.74E+00	2.52E+00	5.26E+00	7.03E-06	6.43E-05	5.13E+05	9.42E+01
1::GLUP:1:0:0->GLUD:0:0:0=8::U1DD:0:1:1->U1DP:1:1:1	-2.45E+00	8.43E-01	3.29E+00	3.36E-05	6.41E-06	5.13E+05	1.01E+05
Q10->Q11=8::EMPTY->U0DD:0:0:1	-1.23E+00	9.34E+01	9.47E+01	1.29E-03	5.30E-04	5.13E+05	1.98E+05
Q00->Q01=8::EMPTY->U0DD:0:0:1	-1.05E+00	8.18E+01	8.29E+01	1.21E-03	4.71E-04	5.13E+05	1.88E+05
C11->C10=8::U2PP:2:2:1->EMPTY	-9.63E-01	1.27E+03	1.28E+03	5.09E-01	2.49E-03	5.13E+05	2.25E+03
C01->C00=8::U2PP:2:2:1->EMPTY	-5.30E-01	1.24E+03	1.24E+03	4.50E-01	2.41E-03	5.13E+05	2.13E+03
C01->C11=9::EMPTY->U0DD:0:0:1	-1.90E-01	7.23E+04	7.23E+04	4.53E-01	5.12E-01	5.13E+05	1.34E+05
Q11->Q01=9::U0DD:0:0:1->EMPTY	-1.35E-01	2.03E+03	2.03E+03	1.41E-02	1.29E-02	5.13E+05	1.42E+05
C10->C00=9::U0DD:0:0:1->EMPTY	-5.31E-02	3.73E+02	3.73E+02	2.48E-03	2.41E-03	5.13E+05	1.36E+05
7::RRH2:1:1:0->RRHP:2:1:0	-4.71E-02	2.67E+00	2.71E+00	5.20E-06	1.65E-03	5.13E+05	2.27E+03
6::HemRed:0:1:0->HemOx:0:0:0=7::RIO2:1:0:0->RRH2:1:1:0	-4.71E-02	2.25E+00	2.29E+00	3.35E-02	4.47E-06	5.13E+05	7.01E+01
7::RRHP:2:1:0->RIO2:1:0:0=8::U0DD:0:0:1->U1DP:1:1:1	-3.70E-02	2.39E-10	3.70E-02	1.70E-05	7.22E-08	5.13E+05	2.86E-05
7::RRH1:1:1:0->RRHP:2:1:0	-2.18E-02	1.28E+00	1.30E+00	2.49E-06	1.65E-03	5.13E+05	1.09E+03
7::RIOP:2:0:0->RIO1:1:0:0	-2.18E-02	2.36E+04	2.36E+04	7.30E-01	4.60E-02	5.13E+05	3.55E+04
6::HemRed:0:1:0->HemOx:0:0:0=7::RIO1:1:0:0->RRH1:1:1:0	-2.18E-02	1.05E+00	1.07E+00	9.49E-03	2.08E-06	5.13E+05	1.15E+02
4::HemRed:0:1:0->HemOx:0:0:0=5::HemOx:0:0:0->HemRed:0:1:0	-6.51E-03	1.26E+04	1.26E+04	4.85E-01	2.47E-02	5.13E+05	2.52E+03
1::GLUD:0:0:0->GLUP:1:0:0	-6.51E-03	8.78E+04	8.78E+04	1.79E-01	8.21E-01	4.23E+04	5.13E+05
Q10->Q00=9::U0DD:0:0:1->EMPTY	-5.68E-03	1.91E+02	1.91E+02	1.28E-03	1.21E-03	5.13E+05	1.33E+05
C01->C11=9::EMPTY->U2PP:2:2:1	-3.33E-03	3.15E+02	3.15E+02	4.53E-01	6.14E-04	4.91E+03	5.13E+05
4::HemOx:0:0:0->HemRed:0:1:0=9::U1DD:0:1:1->U0DD:0:0:1	-3.26E-03	2.84E-02	3.16E-02	5.53E-08	5.04E-01	2.94E-01	5.13E+05
4::HemOx:0:0:0->HemRed:0:1:0=9::U2PD:1:2:1->U1PD:1:1:1	-2.31E-03	2.48E-03	4.79E-03	4.96E-08	8.75E-08	5.13E+05	2.51E+04
3::HSP:2:0:0->HSE:1:0:0	-2.21E-03	7.40E+04	7.40E+04	3.05E-01	4.91E-01	1.24E+04	5.13E+05
2::ASPP:1:0:0->ASPD:0:0:0	-2.13E-03	8.12E+04	8.12E+04	6.04E-01	3.96E-01	2.11E+02	5.13E+05
7::RRHP:2:1:0->RIO2:1:0:0=8::U0DD:0:0:1->U1PD:1:1:1	-1.69E-03	4.04E-11	1.69E-03	1.70E-05	3.29E-09	5.13E+05	3.67E-06
2::ASPD:0:0:0->ASPP:1:0:0=9::U1PD:1:1:1->U1DD:0:1:1	-1.09E-03	1.50E-02	1.61E-02	5.70E-08	3.31E-07	1.20E+04	5.13E+05
4::HemOx:0:0:0->HemRed:0:1:0=9::U2DP:1:2:1->U1DP:1:1:1	-9.46E-04	1.11E-03	2.06E-03	5.92E-09	3.13E-08	5.13E+05	1.35E+05
3::HSE:1:0:0->HSP:2:0:0=9::U1PD:1:1:1->U1DD:0:1:1	-8.04E-04	1.94E-02	2.02E-02	7.54E-08	3.21E-07	1.62E+03	5.13E+05
9::U2PP:2:2:1->U2PD:1:2:1	-6.71E-04	2.46E-01	2.47E-01	6.35E-04	4.84E-07	3.71E+05	5.13E+05
3::HSE:1:0:0->HSP:2:0:0=9::U2PP:2:2:1->U2PD:1:2:1	-6.69E-04	2.46E-01	2.46E-01	4.94E-04	4.80E-07	5.13E+05	1.30E+04
2::ASPD:0:0:0->ASPP:1:0:0=9::U2PP:2:2:1->U2PD:1:2:1	-6.22E-04	2.46E-01	2.47E-01	2.08E-04	4.81E-07	5.13E+05	3.20E+03
3::HSE:1:0:0->HSP:2:0:0=9::U1DP:1:1:1->U1DD:0:1:1	-5.95E-04	1.40E-02	1.46E-02	3.01E-08	3.21E-07	2.28E+03	5.13E+05
3::HSP:2:0:0->HSD:1:0:0	-5.03E-04	1.53E+04	1.53E+04	3.05E-01	2.05E-01	5.01E+02	5.13E+05
9::U1PD:1:1:1->U1DD:0:1:1	-4.00E-04	4.46E-03	4.86E-03	9.76E-08	3.32E-07	2.11E+01	5.13E+05
3::HSD:1:0:0->HSP:2:0:0=9::U2PP:2:2:1->U2PD:1:2:1	-3.46E-04	2.37E-01	2.37E-01	1.68E-06	4.80E-07	2.32E+05	5.13E+05
2::ASPD:0:0:0->ASPP:1:0:0=9::U2PP:2:2:1->U2DP:1:2:1	-3.46E-04	8.97E-03	9.32E-03	2.08E-04	1.82E-08	5.13E+05	3.28E+02
9::U2PP:2:2:1->U2DP:1:2:1	-3.31E-04	8.99E-03	9.32E-03	6.35E-04	1.82E-08	5.13E+05	7.26E+04
9::U1DP:1:1:1->U1DD:0:1:1	-2.60E-04	3.85E-03	4.11E-03	3.29E-08	3.32E-07	2.24E+01	5.13E+05
Q11->Q01=9::U2PP:2:2:1->EMPTY	-1.52E-04	8.61E+00	8.61E+00	1.68E-05	1.29E-02	4.59E+03	5.13E+05

Table G.16: Calculated fluxes $\left[\frac{M}{s}\right]$, steady-state concentrations $[M]$ and rate constants $\left[\frac{1}{s}\right]$ for model V-II.2 - Part 2
"->": Transition between two states
"=": separation between two sites, if two sites are involved and no pool.

#LABEL	Netto Flux	Forward Flux	Backward Flux	SSconcA	SSconcB	Forward Rates	Backward Rates
3::HSE:1:0:0->HSP:2:0:0=9::U2PP:2:2:1->U2DP:1:2:1	-1.45E-04	8.16E-03	8.31E-03	4.94E-04	1.62E-08	5.13E+05	1.33E+03
3::HSD:1:0:0->HSP:2:0:0=9::U2PP:2:2:1->U2DP:1:2:1	-1.24E-04	8.18E-03	8.31E-03	1.68E-06	1.62E-08	5.13E+05	1.16E+05
2::ASPD:0:0:0->ASPP:1:0:0=9::U1DP:1:1:1->U1DD:0:1:1	-7.49E-05	2.09E-03	2.17E-03	4.09E-09	3.31E-07	1.16E+03	5.13E+05
Q00->Q10=9::EMPTY->U2PP:2:2:1	-5.18E-05	8.11E-01	8.11E-01	1.21E-03	1.58E-06	4.81E+03	5.13E+05
C00->C10=9::EMPTY->U2PP:2:2:1	-2.85E-05	1.57E+00	1.57E+00	2.41E-03	3.06E-06	4.79E+03	5.13E+05
3::HSD:1:0:0->HSP:2:0:0=9::U1DP:1:1:1->U1DD:0:1:1	-1.62E-05	1.58E-04	1.74E-04	3.08E-10	3.21E-07	6.81E+01	5.13E+05
3::HSD:1:0:0->HSP:2:0:0=9::U1PD:1:1:1->U1DD:0:1:1	-1.57E-05	1.70E-04	1.86E-04	3.61E-10	3.21E-07	3.32E+01	5.13E+05
7::RRHP:2:1:0->RIO2:1:0:0=8::U1DD:0:1:1->U2DP:1:2:1	-2.88E-06	2.67E-07	3.14E-06	1.21E-06	6.13E-12	5.13E+05	3.20E-01
1::GLUD:0:0:0->GLUP:1:0:0=8::U1PP:2:1:1->U1DP:1:1:1	-1.20E-07	3.66E-07	4.86E-07	7.13E-13	3.09E-04	5.13E+05	3.17E-03
1::GLUP:1:0:0->GLUD:0:0:0=8::U1PD:1:1:1->U1PP:2:1:1	-1.07E-07	2.59E-07	3.66E-07	1.31E-04	7.13E-13	5.13E+05	2.07E-03
5::HemOx:0:0:0->HemRed:0:1:0=8::U2PP:2:2:1->U1PP:2:1:1	-1.31E-08	2.76E-09	1.58E-08	5.09E-01	3.09E-14	3.10E-09	5.13E+05
7::RRH2:1:1:0->RRHT:0:1:0	-7.03E-10	2.59E-06	2.59E-06	5.20E-06	5.05E-12	5.13E+05	6.58E-01
7::RRHT:0:1:0->RRH1:1:1:0	-4.83E-10	2.59E-06	2.59E-06	5.05E-12	2.49E-06	5.13E+05	8.83E-01
7::RRHP:2:1:0->RIO2:1:0:0=8::U1DD:0:1:1->U2PD:1:2:1	-4.43E-10	1.13E-10	5.55E-10	1.21E-06	1.08E-15	5.13E+05	1.16E-04
1::GLUD:0:0:0->GLUP:1:0:0=8::U2PD:1:2:1->U2DD:0:2:1	-5.80E-11	1.03E-11	6.83E-11	4.27E-07	1.33E-16	1.60E-05	5.13E+05
1::GLUD:0:0:0->GLUP:1:0:0=8::U2DP:1:2:1->U2DD:0:2:1	-5.23E-11	1.59E-11	6.83E-11	8.00E-11	1.33E-16	8.62E-02	5.13E+05
4::HemOx:0:0:0->HemRed:0:1:0=9::U2PP:2:2:1->U1PP:2:1:1	-4.40E-11	1.91E-11	6.30E-11	5.20E-05	1.23E-16	5.13E+05	3.85E-12
5::HemRed:0:1:0->HemOx:0:0:0=8::U1DD:0:1:1->U2DD:0:2:1	-4.37E-11	1.87E-11	6.24E-11	8.82E-06	1.22E-16	5.13E+05	2.93E-07
9::U2PD:1:2:1->U2DD:0:2:1	-3.28E-11	1.23E-13	3.30E-11	4.84E-07	6.43E-17	5.13E+05	4.57E-06
9::U2DP:1:2:1->U2DD:0:2:1	-3.28E-11	1.31E-13	3.30E-11	1.82E-08	6.43E-17	5.13E+05	4.46E-05
9::U1PD:1:1:1->U1PP:2:1:1	-2.61E-11	5.34E-11	7.94E-11	9.76E-08	1.55E-16	5.69E-11	5.13E+05
9::U1DP:1:1:1->U1PP:2:1:1	-2.52E-11	5.42E-11	7.94E-11	3.29E-08	1.55E-16	1.03E-10	5.13E+05
2::ASPD:0:0:0->ASPP:1:0:0=9::U2PD:1:2:1->U2DD:0:2:1	-1.64E-11	1.57E-13	1.66E-11	2.33E-09	3.23E-17	5.13E+05	7.56E-05
2::ASPD:0:0:0->ASPP:1:0:0=9::U2DP:1:2:1->U2DD:0:2:1	-1.64E-11	1.59E-13	1.66E-11	4.83E-12	3.23E-17	5.13E+05	3.37E-02
4::HemRed:0:1:0->HemOx:0:0:0=9::U1DD:0:1:1->U2DD:0:2:1	-1.58E-11	3.22E-13	1.62E-11	2.76E-07	3.15E-17	9.61E-07	5.13E+05
2::ASPP:1:0:0->ASPD:0:0:0=9::U1DP:1:1:1->U1PP:2:1:1	-1.19E-11	5.18E-11	6.37E-11	2.88E-08	1.24E-16	5.38E-06	5.13E+05
2::ASPP:1:0:0->ASPD:0:0:0=9::U1PD:1:1:1->U1PP:2:1:1	-1.18E-11	5.19E-11	6.37E-11	4.06E-08	1.24E-16	2.96E-06	5.13E+05
3::HSP:2:0:0->HSE:1:0:0=9::U1PD:1:1:1->U1PP:2:1:1	-1.05E-11	8.12E-12	1.86E-11	2.18E-08	3.63E-17	4.19E-07	5.13E+05
3::HSP:2:0:0->HSE:1:0:0=9::U1DP:1:1:1->U1PP:2:1:1	-1.05E-11	8.18E-12	1.86E-11	2.48E-09	3.63E-17	7.61E-07	5.13E+05
3::HSD:1:0:0->HSP:2:0:0=9::U2DP:1:2:1->U2DD:0:2:1	-9.92E-12	1.67E-13	1.01E-11	4.84E-14	1.97E-17	5.13E+05	4.52E+00
3::HSD:1:0:0->HSP:2:0:0=9::U2PD:1:2:1->U2DD:0:2:1	-9.92E-12	1.69E-13	1.01E-11	8.41E-16	1.97E-17	5.13E+05	3.87E+02
3::HSE:1:0:0->HSP:2:0:0=9::U2PD:1:2:1->U2DD:0:2:1	-9.92E-12	1.69E-13	1.01E-11	3.36E-09	1.97E-17	5.13E+05	1.49E-04
3::HSE:1:0:0->HSP:2:0:0=9::U2DP:1:2:1->U2DD:0:2:1	-9.92E-12	1.71E-13	1.01E-11	1.97E-09	1.97E-17	5.13E+05	1.44E-04
3::HSP:2:0:0->HSD:1:0:0=9::U1PD:1:1:1->U1PP:2:1:1	-7.26E-12	4.42E-11	5.14E-11	2.18E-08	1.00E-16	1.08E-05	5.13E+05
3::HSP:2:0:0->HSD:1:0:0=9::U1DP:1:1:1->U1PP:2:1:1	-6.90E-12	4.45E-11	5.14E-11	2.48E-09	1.00E-16	1.97E-05	5.13E+05
3::HSD:1:0:0->HSP:2:0:0=9::U1PP:2:1:1->U1DP:1:1:1	6.90E-12	5.14E-11	4.45E-11	1.00E-16	2.48E-09	1.31E-06	5.13E+05
3::HSD:1:0:0->HSP:2:0:0=9::U1PP:2:1:1->U1PD:1:1:1	7.26E-12	5.14E-11	4.42E-11	1.00E-16	2.18E-08	1.39E-06	5.13E+05
3::HSP:2:0:0->HSE:1:0:0=9::U2DD:0:2:1->U2DP:1:2:1	9.92E-12	1.01E-11	1.71E-13	1.97E-17	1.97E-09	5.13E+05	1.44E-04
3::HSP:2:0:0->HSD:1:0:0=9::U2DD:0:2:1->U2PD:1:2:1	9.92E-12	1.01E-11	1.69E-13	1.97E-17	8.41E-16	5.13E+05	3.87E+02
3::HSP:2:0:0->HSE:1:0:0=9::U2DD:0:2:1->U2PD:1:2:1	9.92E-12	1.01E-11	1.69E-13	1.97E-17	3.36E-09	5.13E+05	1.49E-04
3::HSP:2:0:0->HSD:1:0:0=9::U2DD:0:2:1->U2DP:1:2:1	9.92E-12	1.01E-11	1.67E-13	1.97E-17	4.84E-14	5.13E+05	4.52E+00
3::HSE:1:0:0->HSP:2:0:0=9::U1PP:2:1:1->U1DP:1:1:1	1.05E-11	1.86E-11	8.18E-12	3.63E-17	2.48E-09	2.00E-08	5.13E+05
3::HSE:1:0:0->HSP:2:0:0=9::U1PP:2:1:1->U1PD:1:1:1	1.05E-11	1.86E-11	8.12E-12	3.63E-17	2.18E-08	2.12E-08	5.13E+05
2::ASPD:0:0:0->ASPP:1:0:0=9::U1PP:2:1:1->U1PD:1:1:1	1.18E-11	6.37E-11	5.19E-11	1.24E-16	4.06E-08	1.92E-06	5.13E+05
2::ASPD:0:0:0->ASPP:1:0:0=9::U1PP:2:1:1->U1DP:1:1:1	1.19E-11	6.37E-11	5.18E-11	1.24E-16	2.88E-08	1.81E-06	5.13E+05
4::HemOx:0:0:0->HemRed:0:1:0=9::U2DD:0:2:1->U1DD:0:1:1	1.58E-11	1.62E-11	3.22E-13	3.15E-17	2.76E-07	1.00E-06	5.13E+05
2::ASPP:1:0:0->ASPD:0:0:0=9::U2DD:0:2:1->U2DP:1:2:1	1.64E-11	1.66E-11	1.59E-13	3.23E-17	4.83E-12	5.13E+05	3.37E-02
2::ASPP:1:0:0->ASPD:0:0:0=9::U2DD:0:2:1->U2PD:1:2:1	1.64E-11	1.66E-11	1.57E-13	3.23E-17	2.33E-09	5.13E+05	7.56E-05
9::U1PP:2:1:1->U1DP:1:1:1	2.52E-11	7.94E-11	5.42E-11	1.55E-16	3.29E-08	4.44E-13	5.13E+05
9::U1PP:2:1:1->U1PD:1:1:1	2.61E-11	7.94E-11	5.34E-11	1.55E-16	9.76E-08	4.70E-13	5.13E+05
9::U2DD:0:2:1->U2DP:1:2:1	3.28E-11	3.30E-11	1.31E-13	6.43E-17	1.82E-08	5.13E+05	4.46E-05
9::U2DD:0:2:1->U2PD:1:2:1	3.28E-11	3.30E-11	1.23E-13	6.43E-17	4.84E-07	5.13E+05	4.57E-06
5::HemOx:0:0:0->HemRed:0:1:0=8::U2DD:0:2:1->U1DD:0:1:1	4.37E-11	6.24E-11	1.87E-11	1.22E-16	8.82E-06	5.13E+05	2.30E-07
4::HemRed:0:1:0->HemOx:0:0:0=9::U1PP:2:1:1->U2PP:2:2:1	4.40E-11	6.30E-11	1.91E-11	1.23E-16	5.20E-05	5.13E+05	3.69E-12
1::GLUP:1:0:0->GLUD:0:0:0=8::U2DD:0:2:1->U2DP:1:2:1	5.23E-11	6.83E-11	1.59E-11	1.33E-16	8.00E-11	7.89E-02	5.13E+05
1::GLUP:1:0:0->GLUD:0:0:0=8::U2DD:0:2:1->U2PD:1:2:1	5.80E-11	6.83E-11	1.03E-11	1.33E-16	4.27E-07	1.52E-05	5.13E+05
7::RIO2:1:0:0->RRHP:2:1:0=8::U2PD:1:2:1->U1DD:0:1:1	4.43E-10	5.55E-10	1.13E-10	1.08E-15	1.21E-06	5.13E+05	1.14E-04

Table G.17: Calculated fluxes $\left[\frac{M}{s}\right]$, steady-state concentrations $[M]$ and rate constants $\left[\frac{1}{s}\right]$ for model V-II.2 - Part 3
"->": Transition between two states
"=": separation between two sites, if two sites are involved and no pool.

#LABEL	Netto Flux	Forward Flux	Backward Flux	SSconcA	SSconcB	Forward Rates	Backward Rates
7::RRH1:1:1:0->RRHT:0:1:0	4.83E-10	2.59E-06	2.59E-06	2.49E-06	5.05E-12	5.13E+05	1.38E+00
7::RRHT:0:1:0->RRH2:1:1:0	7.03E-10	2.59E-06	2.59E-06	5.05E-12	5.20E-06	5.13E+05	5.21E-01
5::HemRed:0:1:0->HemOx:0:0:0=8::U1PP:2:1:1->U2PP:2:2:1	1.31E-08	1.58E-08	2.76E-09	3.09E-14	5.09E-01	3.98E-09	5.13E+05
1::GLUD:0:0:0->GLUP:1:0:0=8::U1PP:2:1:1->U1PD:1:1:1	1.07E-07	3.66E-07	2.59E-07	7.13E-13	1.31E-04	5.13E+05	1.94E-02
1::GLUP:1:0:0->GLUD:0:0:0=8::U1DP:1:1:1->U1PP:2:1:1	1.20E-07	4.86E-07	3.66E-07	3.09E-04	7.13E-13	5.13E+05	5.56E-04
7::RIO2:1:0:0->RRHP:2:1:0=8::U2DP:1:2:1->U1DD:0:1:1	2.88E-06	3.14E-06	2.67E-07	6.13E-12	1.21E-06	5.13E+05	3.07E-01
3::HSP:2:0:0->HSD:1:0:0=9::U1DD:0:1:1->U1PD:1:1:1	1.57E-05	1.86E-04	1.70E-04	3.21E-07	3.61E-10	3.32E+01	5.13E+05
3::HSP:2:0:0->HSD:1:0:0=9::U1DD:0:1:1->U1DP:1:1:1	1.62E-05	1.74E-04	1.58E-04	3.21E-07	3.08E-10	6.81E+01	5.13E+05
C10->C00=9::U2PP:2:2:1->EMPTY	2.85E-05	1.57E+00	1.57E+00	3.06E-06	2.41E-03	4.79E+03	5.13E+05
Q10->Q00=9::U2PP:2:2:1->EMPTY	5.18E-05	8.11E-01	8.11E-01	1.58E-06	1.21E-03	4.81E+03	5.13E+05
2::ASPP:1:0:0->ASPD:0:0:0=9::U1DD:0:1:1->U1DP:1:1:1	7.49E-05	2.17E-03	2.09E-03	3.31E-07	4.09E-09	1.16E+03	5.13E+05
3::HSP:2:0:0->HSD:1:0:0=9::U2DP:1:2:1->U2PP:2:2:1	1.24E-04	8.31E-03	8.18E-03	1.62E-08	1.68E-06	5.13E+05	1.16E+05
3::HSP:2:0:0->HSE:1:0:0=9::U2DP:1:2:1->U2PP:2:2:1	1.45E-04	8.31E-03	8.16E-03	1.62E-08	4.94E-04	5.13E+05	1.33E+03
Q01->Q11=9::EMPTY->U2PP:2:2:1	1.52E-04	8.61E+00	8.61E+00	1.29E-02	1.68E-05	4.59E+03	5.13E+05
9::U1DD:0:1:1->U1DP:1:1:1	2.60E-04	4.11E-03	3.85E-03	3.32E-07	3.29E-08	2.29E+01	5.13E+05
9::U2DP:1:2:1->U2PP:2:2:1	3.31E-04	9.32E-03	8.99E-03	1.82E-08	6.35E-04	5.13E+05	7.06E+04
2::ASPP:1:0:0->ASPD:0:0:0=9::U2DP:1:2:1->U2PP:2:2:1	3.46E-04	9.32E-03	8.97E-03	1.82E-08	2.08E-04	5.13E+05	3.28E+02
3::HSP:2:0:0->HSD:1:0:0=9::U2PD:1:2:1->U2PP:2:2:1	3.46E-04	2.37E-01	2.37E-01	4.80E-07	1.68E-06	2.32E+05	5.13E+05
9::U1DD:0:1:1->U1PD:1:1:1	4.00E-04	4.86E-03	4.46E-03	3.32E-07	9.76E-08	2.17E+01	5.13E+05
3::HSD:1:0:0->HSP:2:0:0	5.03E-04	1.53E+04	1.53E+04	2.05E-01	3.05E-01	4.90E+02	5.13E+05
3::HSP:2:0:0->HSE:1:0:0=9::U1DD:0:1:1->U1DP:1:1:1	5.95E-04	1.46E-02	1.40E-02	3.21E-07	3.01E-08	2.28E+03	5.13E+05
2::ASPP:1:0:0->ASPD:0:0:0=9::U2PD:1:2:1->U2PP:2:2:1	6.22E-04	2.47E-01	2.46E-01	4.81E-07	2.08E-04	5.13E+05	3.20E+03
3::HSP:2:0:0->HSE:1:0:0=9::U2PD:1:2:1->U2PP:2:2:1	6.69E-04	2.46E-01	2.46E-01	4.80E-07	4.94E-04	5.13E+05	1.30E+04
9::U2PD:1:2:1->U2PP:2:2:1	6.71E-04	2.47E-01	2.46E-01	4.84E-07	6.35E-04	3.79E+05	5.13E+05
3::HSP:2:0:0->HSE:1:0:0=9::U1DD:0:1:1->U1PD:1:1:1	8.04E-04	2.02E-02	1.94E-02	3.21E-07	7.54E-08	1.62E+03	5.13E+05
4::HemRed:0:1:0->HemOx:0:0:0=9::U1DP:1:1:1->U2DP:1:2:1	9.46E-04	2.06E-03	1.11E-03	3.13E-08	5.92E-09	5.13E+05	1.35E+05
2::ASPP:1:0:0->ASPD:0:0:0=9::U1DD:0:1:1->U1PD:1:1:1	1.09E-03	1.61E-02	1.50E-02	3.31E-07	5.70E-08	1.20E+04	5.13E+05
7::RIO2:1:0:0->RRHP:2:1:0=8::U1PD:1:1:1->U0DD:0:0:1	1.69E-03	1.69E-03	4.04E-11	3.29E-09	1.70E-05	5.13E+05	3.67E-06
2::ASPD:0:0:0->ASPP:1:0:0	2.13E-03	8.12E+04	8.12E+04	3.96E-01	6.04E-01	2.04E+02	5.13E+05
3::HSE:1:0:0->HSP:2:0:0	2.21E-03	7.40E+04	7.40E+04	4.91E-01	3.05E-01	1.22E+04	5.13E+05
4::HemRed:0:1:0->HemOx:0:0:0=9::U1PD:1:1:1->U2PD:1:2:1	2.31E-03	4.79E-03	2.48E-03	8.75E-08	4.96E-08	5.13E+05	2.51E+04
4::HemRed:0:1:0->HemOx:0:0:0=9::U0DD:0:0:1->U1DD:0:1:1	3.26E-03	3.16E-02	2.84E-02	5.04E-01	5.53E-08	2.94E-01	5.13E+05
C11->C01=9::U2PP:2:2:1->EMPTY	3.33E-03	3.15E+02	3.15E+02	6.14E-04	4.53E-01	4.91E+03	5.13E+05
Q00->Q10=9::EMPTY->U0DD:0:0:1	5.68E-03	1.91E+02	1.91E+02	1.21E-03	1.28E-03	5.13E+05	1.35E+05
1::GLUP:1:0:0->GLUD:0:0:0	6.51E-03	8.78E+04	8.78E+04	8.21E-01	1.79E-01	6.01E+04	5.13E+05
4::HemOx:0:0:0->HemRed:0:1:0=5::HemRed:0:1:0->HemOx:0:0:0	6.51E-03	1.26E+04	1.26E+04	2.47E-02	4.85E-01	5.13E+05	2.43E+01
7::RIO1:1:0:0->RIOP:2:0:0	2.18E-02	2.36E+04	2.36E+04	4.60E-02	7.30E-01	5.13E+05	4.36E+04
6::HemOx:0:0:0->HemRed:0:1:0=7::RRH1:1:1:0->RIO1:1:0:0	2.18E-02	1.07E+00	1.05E+00	2.08E-06	9.49E-03	5.13E+05	1.15E+02
7::RRHP:2:1:0->RRH1:1:1:0	2.18E-02	1.30E+00	1.28E+00	1.65E-03	2.49E-06	5.13E+05	8.32E+02
7::RIO2:1:0:0->RRHP:2:1:0=8::U1DP:1:1:1->U0DD:0:0:1	3.70E-02	3.70E-02	2.39E-10	7.22E-08	1.70E-05	5.13E+05	2.86E-05
6::HemOx:0:0:0->HemRed:0:1:0=7::RRH2:1:1:0->RIO2:1:0:0	4.71E-02	2.29E+00	2.25E+00	4.47E-06	3.35E-02	5.13E+05	7.01E+01
7::RRHP:2:1:0->RRH2:1:1:0	4.71E-02	2.71E+00	2.67E+00	1.65E-03	5.20E-06	5.13E+05	1.41E+03
C00->C10=9::EMPTY->U0DD:0:0:1	5.31E-02	3.73E+02	3.73E+02	2.41E-03	2.48E-03	5.13E+05	1.35E+05
Q01->Q11=9::EMPTY->U0DD:0:0:1	1.35E-01	2.03E+03	2.03E+03	1.29E-02	1.41E-02	5.13E+05	1.42E+05
C11->C01=9::U0DD:0:0:1->EMPTY	1.90E-01	7.23E+04	7.23E+04	5.12E-01	4.53E-01	5.13E+05	1.34E+05
C00->C01=8::EMPTY->U2PP:2:2:1	5.30E-01	1.24E+03	1.24E+03	2.41E-03	4.50E-01	5.13E+05	2.29E+03
C10->C11=8::EMPTY->U2PP:2:2:1	9.63E-01	1.28E+03	1.27E+03	2.49E-03	5.09E-01	5.13E+05	2.10E+03
Q01->Q00=8::U0DD:0:0:1->EMPTY	1.05E+00	8.29E+01	8.18E+01	4.71E-04	1.21E-03	5.13E+05	2.99E+05
Q11->Q10=8::U0DD:0:0:1->EMPTY	1.23E+00	9.47E+01	9.34E+01	5.30E-04	1.29E-03	5.13E+05	1.98E+05
1::GLUD:0:0:0->GLUP:1:0:0=8::U1DP:1:1:1->U1DD:0:1:1	2.45E+00	3.29E+00	8.43E-01	6.41E-06	3.36E-05	5.13E+05	9.31E+04
1::GLUP:1:0:0->GLUD:0:0:0=8::U2DP:1:2:1->U2PP:2:2:1	2.74E+00	3.76E+00	1.02E+00	7.32E-06	1.74E-01	1.88E+00	5.13E+05
5::HemRed:0:1:0->HemOx:0:0:0=8::U1DP:1:1:1->U2DP:1:2:1	2.74E+00	5.26E+00	2.52E+00	6.43E-05	7.03E-06	5.13E+05	8.31E+03
Q01->C01	4.11E+00	6.61E+03	6.60E+03	1.29E-02	4.53E-01	3.77E+04	5.13E+05
C00->Q00	4.25E+00	5.69E+02	5.65E+02	2.41E-03	1.21E-03	2.94E+04	5.13E+05
C10->Q10	4.74E+00	6.05E+02	6.01E+02	2.49E-03	1.29E-03	4.65E+04	5.13E+05
C01->C00=8::U0DD:0:0:1->EMPTY	4.83E+00	6.13E+02	6.08E+02	2.90E-03	2.41E-03	5.13E+05	3.58E+05
Q11->C11	4.88E+00	7.21E+03	7.20E+03	1.41E-02	5.13E-01	8.29E+04	5.13E+05

Table G.18: Calculated fluxes $\left[\frac{M}{s}\right]$, steady-state concentrations $[M]$ and rate constants $\left[\frac{1}{s}\right]$ for model V-II.2 - Part 4
"->": Transition between two states
"=": separation between two sites, if two sites are involved and no pool.

#LABEL	Netto Flux	Forward Flux	Backward Flux	SSconcA	SSconcB	Forward Rates	Backward Rates
7::RIO2:1:0:0->RRHP:2:1:0=8::U2PP:2:2:1->U1DP:1:1:1	5.22E+00	9.91E+00	4.68E+00	2.04E-04	9.13E-06	1.75E+03	5.13E+05
Q00->Q01=8::EMPTY->U2PP:2:2:1	5.29E+00	5.18E+02	5.13E+02	1.21E-03	1.24E-02	5.13E+05	1.00E+04
C11->C10=8::U0DD:0:0:1->EMPTY	5.65E+00	6.55E+02	6.49E+02	3.33E-03	2.49E-03	5.13E+05	3.79E+05
Q10->Q11=8::EMPTY->U2PP:2:2:1	5.97E+00	5.49E+02	5.43E+02	1.29E-03	1.35E-02	5.13E+05	1.06E+04
1::GLUP:1:0:0->GLUD:0:0:0=8::U2PD:1:2:1->U2PP:2:2:1	9.97E+00	4.40E+01	3.40E+01	8.58E-05	1.74E-01	6.17E+01	5.13E+05
5::HemRed:0:1:0->HemOx:0:0:0=8::U1PD:1:1:1->U2PD:1:2:1	9.97E+00	1.29E+01	2.92E+00	6.45E-05	6.69E-05	2.59E+05	5.13E+05
1::GLUD:0:0:0->GLUP:1:0:0=8::U1PD:1:1:1->U1DD:0:1:1	1.03E+01	1.88E+01	8.54E+00	6.24E-05	3.36E-05	5.13E+05	4.58E+05
5::HemOx:0:0:0->HemRed:0:1:0=8::U1DD:0:1:1->U0DD:0:0:1	1.27E+01	1.27E+01	2.09E-03	2.48E-05	4.08E-03	5.13E+05	4.14E-02
7::RIO2:1:0:0->RRHP:2:1:0=8::U2PP:2:2:1->U1PD:1:1:1	2.02E+01	6.36E+01	4.33E+01	2.04E-04	1.08E-04	5.13E+05	1.15E+05
6::HemOx:0:0:0->HemRed:0:1:0=7::RRHP:2:1:0->RIOP:2:0:0	2.54E+01	6.74E+02	6.48E+02	1.31E-03	1.76E-01	5.13E+05	3.77E+03
7::RIOP:2:0:0->RIO2:1:0:0	2.55E+01	9.90E+04	9.90E+04	7.30E-01	1.93E-01	5.13E+05	1.22E+05
6::HemRed:0:1:0->HemOx:0:0:0	2.55E+01	1.16E+05	1.16E+05	2.26E-01	7.75E-01	1.92E+05	5.13E+05

ACKNOWLEDGEMENTS

Dankbarkeit ist manchmal ein Band, oft aber eine Fessel.
— Johann Wolfgang von Goethe —

EIDESSTATTLICHE VERSICHERUNG

Hiermit versichere ich an Eides statt, dass ich die vorliegende Arbeit selbstständig verfasst und keine anderen als die von mir angegebenen Quellen und Hilfsmittel verwendet habe.

Weiterhin erkläre ich, dass ich die Hilfe von gewerblichen Promotionsberatern bzw. –vermittlern oder ähnlichen Dienstleistern weder bisher in Anspruch genommen habe, noch künftig in Anspruch nehmen werde.

Zusätzlich erkläre ich hiermit, dass ich keinerlei frühere Promotionsversuche unternommen habe.

Bayreuth, 25.1.2024

Jan Zoller